



**Bayerische Julius-
Maximilians-Universität
Würzburg**

Fakultät für Chemie und Pharmazie

**Theoretical Characterization and
Optimization of Photochemical
Alkoxy Radical Precursors**

Dissertationsschrift zur Erlangung
des akademischen Grades

Dr. rer. nat.

der Universität Würzburg

vorgelegt von

Mario Arnone

Würzburg, 2007

Eingereicht am:
bei der Fakultät für Chemie und Pharmazie

1. Gutachter:
2. Gutachter:
der Dissertation

1. Prüfer:
2. Prüfer:
3. Prüfer:
des Öffentlichen Promotionskolloquiums

Tag des Öffentlichen Promotionskolloquiums:
Doktorurkunde ausgehändigt am:

Meiner Familie

Vorwort

Diese Arbeit wurde von Oktober 2001 bis März 2007 unter der Leitung von Prof. Dr. Bernd Engels im Institut für Organische Chemie der Bayrischen Julius-Maximilians-Universität Würzburg angefertigt. Teile der im Rahmen dieser Arbeit beschriebenen Ergebnisse sind Gegenstand von vier Publikationen^[1-4] sowie einiger Posterpräsentationen.

Zuerst möchte ich meinem Chef Bernd Engels für die wissenschaftlichen und finanziellen Möglichkeiten danken, die er mir zur Verfügung gestellt hat, um die Forschungsarbeiten, die zur Anfertigung dieser Arbeit notwendig waren, durchzuführen. In den vergangenen Jahren meiner Arbeit in seiner Gruppe hat er mir durch seine Betreuung und zahlreiche Diskussionen über meine Ergebnisse einen fundierten Einblick in das wissenschaftliche Arbeiten gegeben. Zusätzlich sorgte er durch seine lockere Art und zahlreiche „nichtwissenschaftliche“ Unternehmungen für ein angenehmes Arbeitsklima.

Ein weiterer Dank gilt meinen Kollegen, mit denen ich die letzten Jahre zusammen gearbeitet habe. Besonders mit Christian, Sebastian und Milena war während der Arbeitszeit und auch darüber hinaus bei Unternehmungen, wie AK Ausflüge oder Tagungen immer für Stimmung und gute Laune gesorgt.

Vielen Dank an meine Eltern die mir während der Zeit meiner Promotion, wie schon während meines ganzen Chemiestudiums, immer zur Seite standen, auch in schwiereigeren Zeiten für mich da waren und mich unterstützten. Ihnen und meinen Brüdern verdanke ich, dass ich nicht alleine durch die Promotionszeit gehen mußte und vor allem am Wochenende immer die nötige Ablenkung und Erholung finden konnte. In der letzten Zeit hat mir neben meiner Familie auch meine Freundin Mona sowie ihre Tochter Tanja, durch unseren Kontakt sehr viel Freude, Kraft und Ausdauer für meine Arbeit gegeben.

Dass es mir auch außerhalb der Uni nicht langweilig wurde, verdanke ich neben den schon erwähnten Kollegen hauptsächlich meinem langjährigen Freund und früheren Mitbewohner Uwe. Mit ihm konnte ich immer Spaß haben und bei einer Caipirinha auch über meine Probleme reden. Meine gute Freundin Barbara, die ich durch ihr Pharmaziestudium in Freiburg begleiten durfte, hat bei unseren vielen Gesprächen und Lerntreffen immer ein offenes Ohr für mich und meine wissenschaftliche Arbeit gehabt. Ohne diese beiden Personen wären die letzten Jahre um einiges trister verlaufen.

Diese Arbeit ist durch eine Kooperation mit der experimentellen Arbeitsgruppe von Prof. Dr. Jens Hartung entstanden. Ihm gilt mein Dank für das zur Verfügung stellen experimenteller Daten sowie zahlreicher fruchtbarer wissenschaftlicher Diskussionen im Rahmen

unserer Zusammenarbeit. Nina Schneiders und Andreas Groß, aus seiner Arbeitsgruppe in Kaiserslautern danke ich für das nachträgliche Synthetisieren sowie die Aufnahme der UV/vis Spektren von **4me5h-OH** und **4me5h-OMe**, damit ich diese in meine Arbeit aufnehmen konnte.

Contents

1	Introduction	1
1.1	Goals of this Work	4
2	Generation and Application of Alkoxy Radicals	7
2.1	Possibilities to generate Alkoxy Radicals	8
2.1.1	The Photochemical Approaches	9
2.2	The Applications of Alkoxy Radicals	13
2.2.1	Stereoselective Organic Synthesis	15
2.2.2	Bioorganic Studies	17
3	Theoretical Basics	21
3.1	Electronically Excited States and Spectroscopy	21
3.1.1	Types of Excited States	22
3.1.2	UV/vis-Spectroscopy	24
3.1.3	CD-Spectroscopy	26
3.1.4	The Simulation of Experimental Spectra from Theoretical Data	26
3.2	Quantum Chemical Methods to describe Excited States	28
3.2.1	Time-Dependent - Density Functional Theory	30
3.2.2	The Complete Active Space (CAS) Approach	37

4	The Electronic Spectra of the known Precursors	49
4.1	Theoretical Details	52
4.2	Equilibrium Structures of the Parent Compounds	54
4.3	Validation of the Theoretical Approaches	58
4.3.1	The <i>N</i> -Methoxy Compounds	58
4.3.2	The <i>N</i> -Hydroxy Compounds	62
4.3.3	Conclusion	64
4.4	Interpretation of the UV/vis Spectra	65
4.4.1	The Pyridinethione Compounds	65
4.4.2	The Thiazolethione Compounds	68
4.4.3	Experimentally known <i>N</i> -substituted Thiazolethiones	71
5	The Photochemical Alkoxy Radical Liberation	75
5.1	Theoretical Details	77
5.2	The N,O Bond Homolysis	78
5.2.1	<i>N</i> -(Methoxy)-Thiazole-2(3 <i>H</i>)-thione (2a-OMe)	78
5.2.2	Single Reference Approaches	83
5.2.3	<i>N</i> -(Methoxy)-Pyridine-2(1 <i>H</i>)-thione (1a-OMe)	84
5.2.4	A generalized Model for the Reactivity.	87
5.2.5	<i>N</i> -(Methoxy)-Pyridine-2(1 <i>H</i>)-one (1b-OMe)	89
6	Substituent Effects on the UV/vis Spectra	91
6.1	Theoretical Details	93
6.2	Substituents on the Thiazolethione Heterocycle	95
6.3	Substituents on the Pyridinethione Heterocycle	100

6.3.1	Electron Withdrawing Fluorine Substituents	100
6.3.2	Validation of the TD-DFT Approach	103
6.3.3	Electron Rich Methoxyl Substituents	106
6.3.4	Comparison between the Fluorine and the Methoxyl Substituents. . .	113
6.3.5	NO ₂ Substituents that can conjugate with the π -Electrons	113
7	Design of New Precursor Systems	115
7.1	Computational Details	118
7.2	The Screening Step	119
7.3	The Bond Dissociation Paths	123
7.3.1	<i>N</i> -(Methoxy)-(1,3)Dihydro-Pyrrole-2-thione (3a)	124
7.3.2	<i>N</i> -(Methoxy)-(1,3)Dihydro-[1,3]Azaphosphole-2-thione (6a)	126
7.3.3	<i>P</i> -(Methoxy)-(1,3)Dihydro-[1,3]Oxaphosphole-2-thione (5c)	130
7.4	Conclusion	131
8	Summary	133
9	Zusammenfassung	143

Chapter 1

Introduction

Alkoxy radicals are a very important class of compounds in different fields of organic chemistry.^[5,6] They are applied in the bioorganic chemistry to investigate the oxidative capacity of these reactive compounds in the oxidative stress.^[7-13] In organic synthesis those compounds serve as valuable reagents.^[14-18] The generation of such oxygen centered radicals, however, is often only possible with the aid of very unstable precursor systems or under special conditions like the presence of strong oxidants. For the application in bioorganic studies or fine organic synthesis however, “milder” sources of alkoxy radicals are recommended. Photochemically generated $\bullet\text{O-R}$ radicals starting from a homolytic N,O bond cleavage in heterocyclic thiohydroxamic-*O*-esters fulfill this condition^[19] (see figure 1.1).

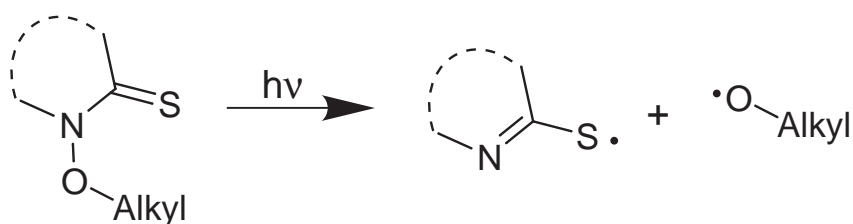


Figure 1.1: A schematical representation of the photochemical generation of alkoxy radicals starting from cyclic thiohydroxamic-*O*-esters

In the modern alkoxy radical chemistry two kinds of precursor systems on the basis of thiohydroxamic-*O*-esters are applied. The first compounds are the *N*-(alkoxy)-pyridine-2(1*H*)-thiones (**1a-OR**). They serve as clean source of alkoxy radicals when irradiated with near UV light. However, the synthesis and storage of these molecules is complicated due to a strong daylight sensitivity.^[20,21]

To avoid these problems, precursor systems on the basis of the thiazolethione heterocycle were developed. Those systems exhibit no daylight sensitivity and also liberate alkoxy

radicals under photochemical conditions. A problem of these newer precursor compounds is the reactivity of the photoproducts after the initial photo process. When applied without proper radical trapping reagents, the irradiation of *N*-(alkoxy)-thiazole-2(3*H*)-thiones (**2a-OR**) yields often many unwanted side products besides the desired alkoxy radicals.^[21–23]

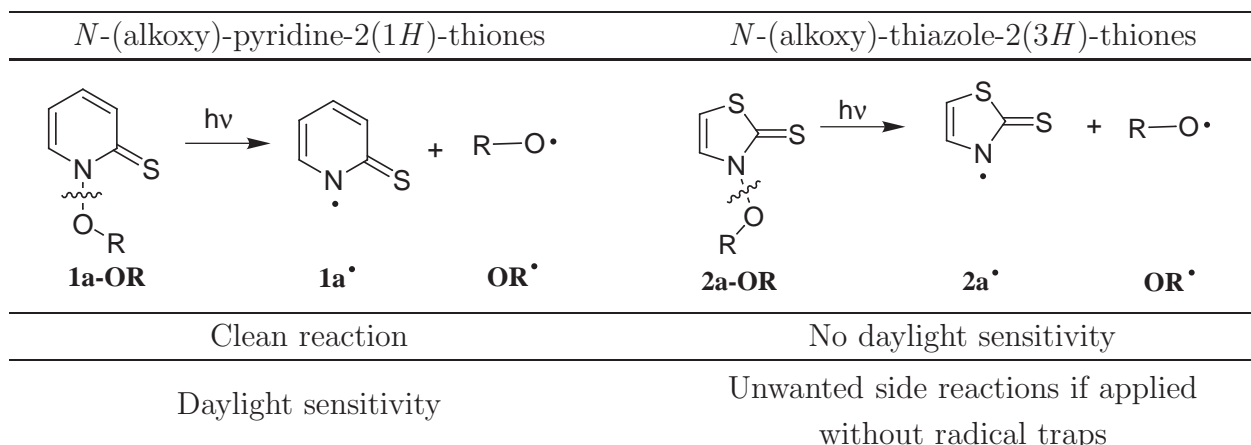


Figure 1.2: The advantages and disadvantages of the two applied heterocyclic alkoxy radical precursors on thiohydroxamic-*O*-ester basis. The left side shows the properties of the *N*-(alkoxy)-pyridine-2(1*H*)-thione (**1a-OR**) precursors, while the corresponding facts of the *N*-(alkoxy)-thiazole-2(3*H*)-thiones (**2a-OR**) are listed on the right hand side.

For the application in the bioorganic chemistry or in organic synthesis the initiation wave length of a photochemical reagent is often an important factor. The photo process that yields the alkoxy radicals in the experiments on the oxidative capacity of these compounds is initiated by a laser pulse with a wave length of about 350 nm.^[9] This experimental condition is only partly fulfilled by both applied precursor molecules.

In the scope of this work quantum chemical investigations should help to understand the photochemical behavior of the two heterocyclic compounds. The differences in this behavior should be discovered and explained. With this knowledge then it was tried to optimize and adapt the known precursor systems to experimental conditions and to suggest new compounds, that should also be applicable as photochemical alkoxy radical precursors.

To achieve these goals various methodical considerations have to be made. At first vertical electronic excitation spectra of various “larger” organic compounds have to be computed. This can be done by the aid of time-dependent density functional theory^[24–26] (TD-DFT). The general accuracy of this approach and the problem of the strong dependency on the choice of the functional made it necessary to validate this method by a comparison with the experiment and higher level computations like the complete active space (CAS) approach^[27–29] together with a perturbational estimation^[30,31] (PT2) of dynamic correlation effects (CASPT2). The CASPT2 calculations could only be done on “small” parent com-

pounds which served as model substances for the real molecules.

Next to vertical excitation spectra also the description of a homolytic bond dissociation process in the ground state and especially in different excited states of various molecules has to be investigated. This automatically leads to several demands on the applied quantum chemical methodology. Not only the dissociation of a closed shell molecule into a biradical species makes the application of unrestricted ansätze necessary. The strong influence of electron correlation effects requires the use of a multi configurational wave function. CASPT2 served as a tool for the theoretical description of the N,O bond cleavage in the investigated molecules in the ground and electronically excited states.

The first two chapters of this work deal with the background of alkoxy radical chemistry, UV/vis spectroscopy and give a description of the theoretical methods that have been used in the presented quantum chemical investigations. In chapter 2 the generation and applications of alkoxy radicals in organic chemistry are outlined. A special focus is on the photochemical generation of these oxygen centered radicals with the aid of the precursor molecules on the basis of the thiohydroxamic-*O*-esters^[19-23] (subsection 2.1.1) and their application in stereoselective organic synthesis^[15,18] (subsection 2.2.1) and in bioorganic experiments^[9,10,12] (subsection 2.2.2). The subject of the first part of chapter 3 is the physical background of the absorption of light^[32] and of UV/vis spectroscopy.^[33,34] In the second section of this chapter the quantum chemical methodology for the description of electronically excited states is introduced.^[35,36] In this framework especially the time-dependent - density functional theory approach^[24-26] (subsection 3.2.1) and the multi configurational complete active space^[27] (CAS) ansatz (subsection 3.2.2) are explained in more detail.

In the chapters 4, 5, 6 and 7 the results of the investigations on the photophysics and photochemistry of the alkoxy radical formation are presented. These chapters all begin with a brief introduction into the respective subject of research, followed by a description of the applied quantum chemical methodology to obtain the desired information. The results of these calculations are discussed in detail. The presented results have also been published in four publications.^[1-4]

1.1 Goals of this Work

The quantum chemical investigations in the frame of this work should help to understand the underlying photophysics and photochemistry of the alkoxy radical generation from thiohydroxamic-*O*-esters. With this knowledge an optimization of the precursor systems should be done. To achieve these goals the work is divided in four main parts.

The first step in understanding the differences of the two heterocyclic precursor systems *N*-(alkoxy)-pyridine-2(1*H*)-thiones (**1a-OR**) and *N*-(alkoxy)-thiazole-2(3*H*)-thiones (**2a-OR**) is to find a quantum chemical approach for the theoretical description of the ground state and the vertical excitation spectra of experimentally known precursor molecules (see chapter 4). This could be done in a combined experimental and theoretical study. Calculated ground state structures of the parent compounds *N*-(methoxy)-pyridine-2(1*H*)-thione **1a-OMe** and *N*-(methoxy)-thiazole-2(3*H*)-thione (**2a-OMe**) have to be compared with X-ray diffraction structures of the corresponding synthesized and crystallized molecules^[21, 37–39] to find an efficient way to obtain appropriate ground state structures of the compounds of interest.

The comparison of measured UV/vis spectra of *N*-(methoxy)-pyridine-2(1*H*)-thione (**1a-OMe**) and *N*-(methoxy)-4-methylthiazole-2(3*H*)-thione (**4me5h-OMe**) with quantum chemically calculated excitation energies gives the possibility to assign the photochemically active UV/vis band. The problems of the time-dependent DFT approach with the description of vertical excitations can be evaluated by a comparison of the TD-DFT excitation spectra with the experiment and higher level multistate^[40] (MS)-CASPT2 calculations. Further validations of TD-DFT with the aid of MS-CASPT2 calculations and an approach where the CC2 model^[41] is combined with the RI approximation^[42, 43] (RI-CC2) should help to find a proper functional basis sets as theoretical approach for the efficient calculation of vertical excitation spectra. This validation of the applied functional, by a comparison with the experiment and, especially in the case of “new”, experimentally unknown compounds, with higher level CASPT2 calculations should always be done.

To understand the differences between the two experimentally applied heterocyclic alkoxy radical precursors not only the knowledge about their vertical excitation spectra is necessary. Since both photochemical precursors show different reactivities in radical chain reactions (clean alkoxy radical liberation in the case of *N*-(alkoxy)-pyridine-2(1*H*)-thiones *vs.* unwanted side products in the case of *N*-(alkoxy)-thiazole-2(3*H*)-thiones) the photochemical alkoxy radical liberation process has to be understood (see chapter 5). Therefore the homolytic N,O bond dissociation process of the two parent compounds *N*-(methoxy)-pyridine-2(1*H*)-thione (**1a-OMe**) and *N*-(methoxy)-thiazole-2(3*H*)-thione (**2a-OMe**) has

to be investigated in detail. This has to be done in the ground state and in the first electronically excited states. To do this a different quantum chemical methodology has to be chosen. Here the DFT approach only can give access to the structures of the molecules their ground state and on the lowest triplet surface. A proper description of the bond dissociation process in excited states is only possible with the aid of the multi configurational CASPT2 approach. For these calculations the choice of the active space is a crucial point. An analysis of the orbitals that are involved in the photochemical activation process and in the resulting alkoxy radical liberation has to be performed to obtain a suitable active space. The calculated N,O bond dissociation paths of both heterocyclic precursor systems than have to be compared. From the different shapes of the potential surfaces that describe this photo process a model for the reactivity of photochemical alkoxy radical precursors should be developed. This model can additionally be tested and proved on the *N*-(methoxy)-pyridine-2(1*H*)-one (**1b-OMe**) molecule, an applied alkoxy radical precursor on the basis of heterocyclic hydroxamic-acid-*O*-esters. A comparison of the photochemical reaction paths obtained from the CASPT2 calculations with potential surfaces calculated on TD-DFT or RI-CC2 level should be able to show the already expected failure of single reference ansätze for this purpose.

After understanding the differences of the applied photochemical precursors an optimization of their properties can be done. Chapter 6 and 7 show two different approaches that are tried in the scope of this work.

One possibility to adapt the precursor molecules to the desired photochemical conditions (no daylight sensitivity, clean reactions, excitation wave length at about 350 nm), would be a shift in the initial excitation wave length of the photo process. This would mean that the *N*-(alkoxy)-pyridine-2(1*H*)-thione (**1a-OR**) compounds loose their sensitivity to unfiltered daylight. Also an “adjustability” of the initial photochemical wave length of both compounds, and with that a possibility to addapt them to various experimental requirements, could be possible. The desired shifts in the photochemical excitation energy can be achieved by substituent effects on the electronic spectra. A combined theoretical and experimental research to shift the initiation wave length of the precursors on the basis of the thiazole heterocycle to the desired experimental value of about 350 nm is possible. Since the precursors on the basis of the pyridinethione heterocycle seem to be a “cleaner” alkoxy radical source a shift of their photochemical initiation wave length towards shorter wave length would be advantageous for their stability against daylight and experimental handling. So far no experiments on effects of substituents on the pyridine heterocycle, on the UV/vis spectra of *N*-(alkoxy)-pyridine-2(1*H*)-thione (**1a-OR**) compounds are made. With the aid of the in chapter 4 established quantum chemical methodology (TD-DFT and validation with CASPT2) theoretical investigations on such effects of substituents with dif-

ferent electronic character (electron poor, electron rich, conjugation with the π -electrons), on the electronic excitations of *N*-(methoxy)-pyridine-2(1*H*)-thione (**1a-OMe**) are possible. The different effects should be understood and the development of an incremental system for the additivity of these effects is desired. These calculations also suggested multiple substitution patterns that should help to adapt the initiation wave length of the photo process in the pyridinethione compounds to various experimental requirements.

From the results of the calculations on the photochemical bond dissociation process (chapter 5) a second possibility to obtain optimized photochemical alkoxy radical precursors can be obtained. Since quantum chemistry is not limited to experimental restrictions the known heterocyclic precursors can be modified systematically to obtain new possible parent compounds that show photochemical activity with respect to an alkoxy radical liberation. Next to the “type” of heterocycle also the thiohydroxamic acid functionality that characterizes the precursor molecules can be varied. To identify the promising precursor systems a screening of the lower electronic excitations of all possible systems has to be performed. For promising systems (initiation wave length between the two known molecules *N*-(methoxy)-pyridine-2(1*H*)-thione (**1a-OMe**) and *N*-(methoxy)-thiazole-2(3*H*)-thione (**2a-OMe**) the influence of a polar solvent is estimated by a continuum model. To check the reliability of the TD-DFT, the excitation energies between the ground state (S_0) and the first three singlet excited states have to be recalculated with the CASPT2 method. If CASPT2 confirmed the TD-DFT prediction the N,O or P,O dissociation paths, respectively, of the S_0 , the T_1 and the first two singlet excited states can be computed. An analysis of these paths according to the established model for the reactivity of such compounds in photochemical alkoxy radical liberation processes (compare chapter 5) gives information about the reactivity of the resulting radical fragments. This study may identify new promising photochemical alkoxy radical precursor systems that should possess attractive properties for their application in organic synthesis or bioorganic studies.

Chapter 2

Generation and Application of Alkoxy Radicals

Alkoxy radicals are a reactive oxygen species that are found in many different chemical contexts. In the atmospheric chemistry for example a photolytic or radical induced decomposition of environmental chemicals like methane^[44] leads to alkoxy radicals (see figure 2.1).^[45]

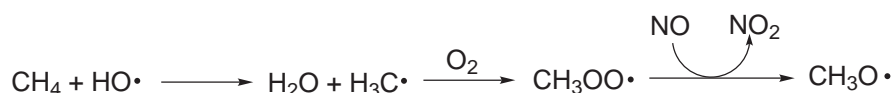


Figure 2.1: The formation of alkoxy radicals in the atmosphere

A formation of alkoxy radicals due to an irradiation of fatty acids on human skin was also found recently.^[46]

In living cells alkoxy radicals are a product of bio activation processes in the metabolism of foreign substances. Also some enzymes like galactose oxidase^[47,48] or ribonucleotide reductase^[49,50] require the oxygen centered tyrosyl radical to perform their tasks.

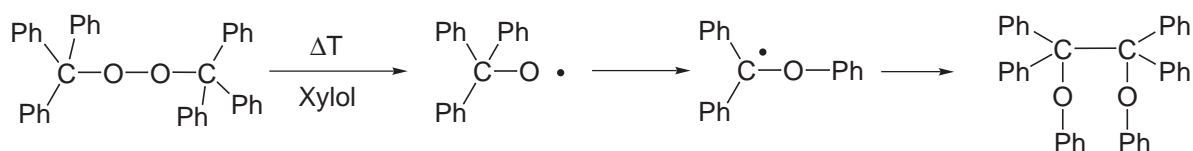


Figure 2.2: The formation of tetraphenyldiphenoxyethane from bistrisphenylmethylperoxide

In the organic chemistry the first aspects of alkoxy radical chemistry dated from the beginning of the 20th century. Wieland described them as intermediates that were nec-

essary to explain the formation of tetraphenyldiphenoxyethane from a heated sample of bistriphenylmethylperoxide (see figure 2.2).^[51]

The basic structural element of alkoxy radicals is an oxygen atom attached to the sp^3 carbon atom of an organic substituent. The simplest member of this family of compounds is the methoxy radical $CH_3-O\cdot$. This molecule possesses C_{3v} symmetry and its electronic ground state represents a degenerated 2E state. This degeneracy is lifted due to the Jahn Teller distortion.^[52-54] This leads to a ground state in C_S symmetry with a $^2A'$ electronic configuration and a second $^2A''$ configuration that lies only 37 cm^{-1} above.^[52] This electronic structure is also found for the higher homologue where the lower symmetry comes directly from the organic alkyl substituent. For these molecules the gap between the two states is about 300 cm^{-1} .^[53,54]

2.1 Possibilities to generate Alkoxy Radicals

Alkoxy radicals are formed by the homolytic cleavage of an oxygen-heteroatom, oxygen-oxygen or oxygen-carbon bond. Precursor systems can be distinguished by the way the O,R; O,O or O,X bond is cleaved.^[5] In the first and largest group of precursors this process is initiated thermally or by irradiation. Alkoxy radical precursors that have their origin in the esterification of an alcohol with an inorganic acid can be sorted in this group of precursors. Here a strong O,H bond is converted into a weak oxygen-nitrogen, oxygen-halogen or oxygen-sulfur bond. Also the liberation of alkoxy radicals from peroxides and organic perethers, that are formed by autoxidation with O_2 , is initiated thermally. In the alkoxy radical precursors on the basis of heterocyclic thiohydroxamic-O-esters, which are the subject of this work, the weak N,O bond is homolyzed both thermally and photochemically.

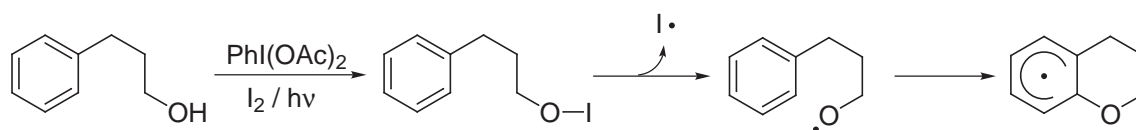


Figure 2.3: An example for the generation of an alkoxy radical by oxidation with $PhI(OAc)_2/I_2$ ^[55]

A second way to liberate alkoxy radicals is the reaction of an alcohol with a strong oxidant (see fig. 2.3) like $Pb(OAc)_4$,^[56] $Ag_2S_2O_8$ ^[57] or I_2/HgO .^[58] The application of this type of precursors in organic synthesis or bioorganic studies, however, is limited by the fact that many other functional groups could also be oxidized by the oxidant.

The third type of precursors utilizes the rearrangement of oxygen containing carbon

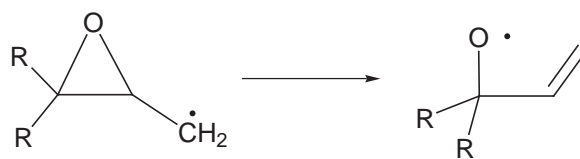


Figure 2.4: Rearrangement of an epoxymethylene radical to an alkoxy radical

centered radicals. In this context the ring opening reaction of the strained epoxymethylene radical can be mentioned (see figure 2.4).^[14]

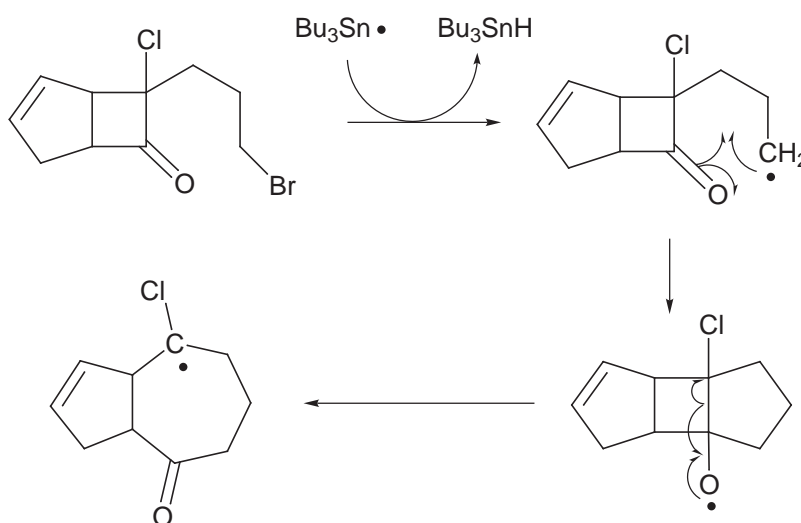


Figure 2.5: The generation and application of an alkoxy radical in a ring expansion reaction.^[59]

An intramolecular addition of a carbon centered radical to a carbonyl group can lead to alkoxy radicals too. For example the attack of the bicyclic radical in figure 2.5, generated by a bromine abstraction with $\text{Bu}_3\text{Sn}^\bullet$, on the cyclobutanone carbonyl group leads to an alkoxy radical. This can undergo a rearrangement reaction that gives the possibility for a ring expansion.^[59]

2.1.1 The Photochemical Approaches

Since most of the alkoxy radical precursors mentioned in chapter 2.1 are chemically very unstable (organic perethers, inorganic esters) or require special conditions (strong oxidants, strained oxygen containing carbon-radicals), they are not useful for mechanistic, synthetic or bioorganic studies. Good precursors should be easy to synthesize and to handle, in combination with an efficient liberation of the radicals.

For the generation of carbon centered radicals the “Barton-esters” provide precursors

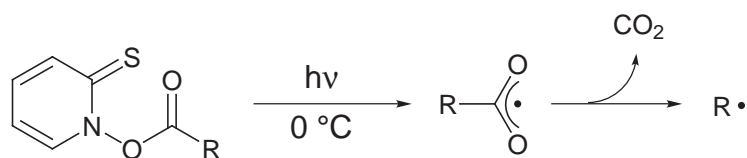


Figure 2.6: A schematic representation of the formation of a carbon centered radical through a photochemical reaction of a “Barton-ester”.

that fulfill the criteria mentioned above. Barton *et. al.*^[22,60,61] showed that it is possible to generate carbon centered radicals photochemically by irradiation of *N*-(acyloxy)-pyridine-2(1*H*)-thiones and a subsequent decarboxylation (see figure 2.6).

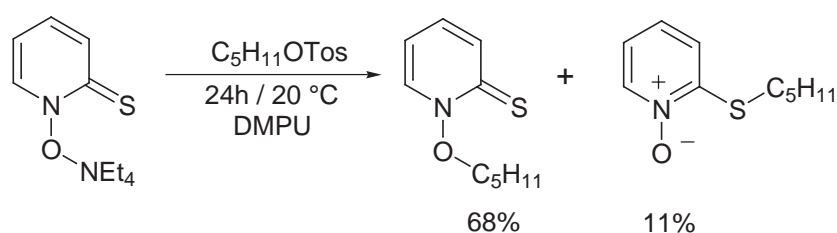


Figure 2.7: Synthesis of the alkoxy radical precursor *N*-(*n*-pentyl)-pyridine-2(1*H*)-thione by an alkylation of *N*-(hydroxy)-pyridine-2(1*H*)-thione tetrabutylammonium salt with *n*-pentyltosylate.

Beckwith and Hay discovered that the *N*-alkoxy derivatives of *N*-(hydroxy)-pyridine-2(1*H*)-thione show a similar reactivity and are able to liberate alkoxy radicals under mild conditions.^[19] They also showed that it is possible to synthesize these precursor molecules from easily available reactants.^[20] The group of Hartung improved this synthesis and was able to obtain the *N*-(alkoxy)-pyridine-2(1*H*)-thiones in good yields^[21] (see figure 2.7).

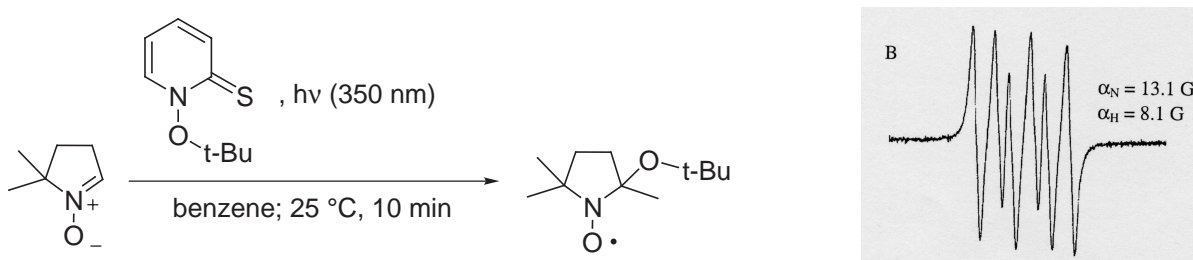


Figure 2.8: The photolysis reaction of the *N*-(*tert*-butoxy)-pyridine-2(1*H*)-thione molecule in the presence of 5,5'-dimethyl-pyrrole-*N*-oxide (DMPO) and the ESR spectra of the DMPO *tert*-butoxy radical trapping adducts.

The obtained *N*-(alkoxy)-pyridine-2(1*H*)-thiones (**1a-OR**) are light sensitive yellow compounds, that sometimes can only be isolated as oils. When exposed to unfiltered day light they decompose due to a broad absorption band at about 360 nm. Only if the blue

part of the light is filtered out these compounds are stable. The evidence for the liberation of alkoxy radicals upon irradiation of the pyridinethione compounds is made by esr spectroscopy. If *N*-(alkoxy)-pyridinethione compounds are irradiated with UV light in the presence of 5,5'-dimethyl-pyrrole-*N*-oxide (DMPO), characteristic esr signals for alkoxy radical adducts to DMPO are found (see figure 2.8).^[12]

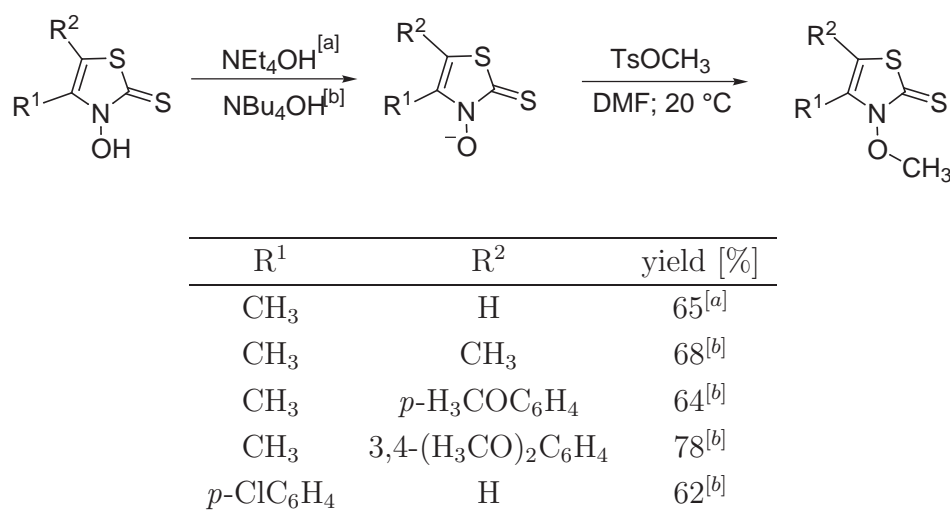
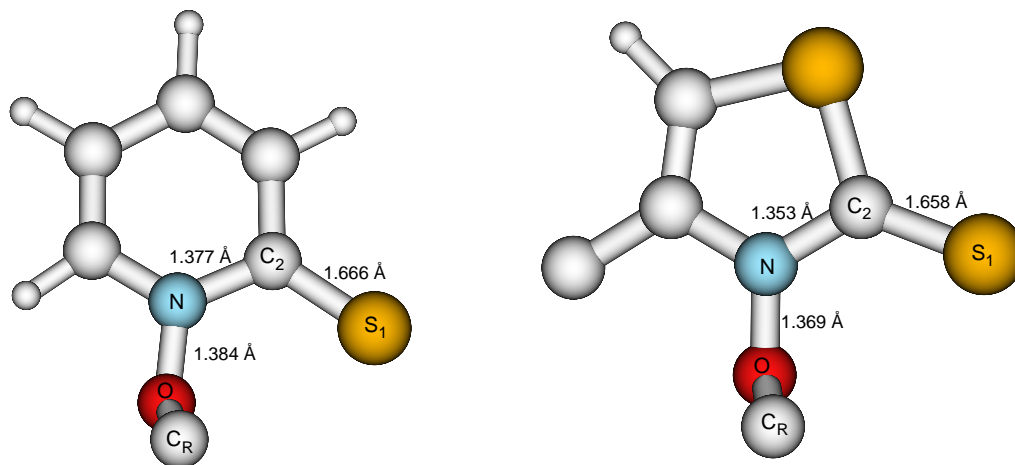


Figure 2.9: The synthesis of the alkoxy radical precursors on the basis of the thiazolethione heterocycle.

To eliminate the synthetic problems (light sensitive molecules, oils) the group of Hartung developed another precursor system on the basis of the thiazolethione heterocycle. Various C⁴ and C⁵ substituted *N*-(hydroxy)-thiazole-2(3*H*)-thiones (**2a-OH**) for example were treated with tetraethylammonium hydroxide (formation of NEt₄ salts) or tetrabutylammonium hydroxide (synthesis of NBu₄ derivatives) to furnish the corresponding tetraalkylammonium salts. They were selectively *O*-methylated using methyl *p*-toluenesulfonate to yield the corresponding *N*-(methoxy)-thiazole-2(3*H*)-thiones^[21–23] (derivates of **2a-OMe** see figure 2.9). This synthesis of *N*-(alkoxy)-thiazole-2(3*H*)-thiones, from the corresponding tetrabutyl ammonium salts, by alkylation leads to white crystalline products. Due to an absorption at about 320 nm these compounds are stable with respect to daylight. Their reactivity in photochemical radical liberation chain reactions is similar to the reactivity of the pyridinethione compounds. Though the photolysis of the thiazolethione precursors leads to unwanted side products, if the reaction is performed without efficient radical trapping reagents.

X-ray studies showed that the structure of the thiohydroxamic acid ester functionality of both kinds of heterocyclic precursors is very similar^[23,37] (see figure 2.10). The C,S double bond and the C,N and N,O single bonds in the thiazolethione compound are slightly shorter but identical in their character. The *O*-alkyl group is bend out of the plane of the

heterocycle by about 80° to 100° . For the *N*-(hydroxy) compound of the precursor molecules on the basis of the pyridinethione heterocycle (**1a-OH**) an intramolecular hydrogen bond between the thiohydroxamic acid proton and the thiocarbonyl sulfur atom is found by X-ray crystallography. The solid state structure of *N*-(hydroxy)-4-methylthiazole-2(3*H*)-thione (**4me5h-OH**) in contrast consists of hydrogen bridged dimers.



angle	pyridine	thiazole	angle	pyridine	thiazole
\angle N-C ₂ -S	122.5°	117.8°	\angle C ₂ -N-O	—	120.7°
\angle N-O-C _R	112.4°	112.4°	\angle C ₂ -N-O-C _R	99.9°	81.7°

Figure 2.10: X-ray structural parameters for the thiohydroxamic acid ester functionality of both heterocyclic alkoxy radical precursors.

2.2 The Applications of Alkoxy Radicals

Alkoxy radicals are able to perform various kinds of elementary chemical reactions.

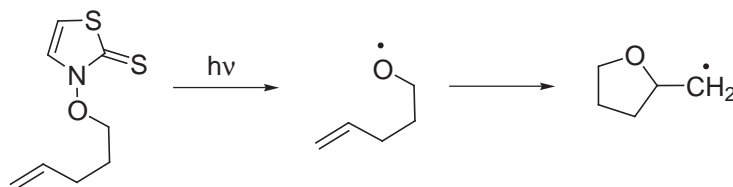


Figure 2.11: A possibility for the synthesis of the furan heterocycle applying an intramolecular addition of the oxygen centered radical to the C,C double bond.

They can add to carbon-carbon^[62] or carbon-heteroatom^[63] double bonds. The resulting radical intermediates can be trapped directly to stable products or can perform further radical reactions. An intramolecular addition to a C,C double bond is the key step in the formation of substituted furanes (see figure 2.11). This type of reaction applying the alkoxy radical precursors on the basis of heterocyclic thiohydroxamic acid O-esters is discussed in more detail in chapter 2.2.1.

reaction	E_a^a	ΔH_f^a	reaction	E_a^a	ΔH_f^a
	12	-97		65	-18
	32	-100		87	8


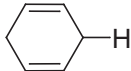
^aall values in kJ mol^{-1}

Table 2.1: Calculated activation energies (E_a) and reaction enthalpies (ΔH_f) for ring opening reactions of alkoxy radicals.^[64]

Homolytic β -C,C bond cleavages in alkoxy radicals are also synthetically useful reactions since carbonyl compounds and carbon centered radicals are formed.^[65] In organic synthesis most of these β -C,C bond cleavages start from cyclic structures. The thermodynamics of these ring opening reactions correlates with the strain of the cyclic structure. Calculated reaction enthalpies (ΔH_f) and activation energies (E_a) for the ring opening reaction of the very strained cyclopropyloxy- or cyclobutyloxy-radical are much lower than for the less strained cyclopentyloxy or the nearly strain free cyclohexoxy radical (see table 2.1).^[64]

Furthermore intramolecular rearrangement reactions are found for alkoxy radicals.

Typically these reactions are 1,2 shifts, especially involving a phenyl group. The first described example of this kind of reaction is the second step in the formation of tetraphenyldiphenoxyethane from bistriphenylmethylperoxide^[51] (see figure 2.2).

R-H	BDE ^a	rate constant ^b
	94.5 ^[66]	$8.6 \cdot 10^5$
	73.0 ^[67]	$6.8 \cdot 10^7$
BU ₃ Sn-H	73.7 ^[67]	$5.0 \cdot 10^8$

^ain kcal mol⁻¹

^bin M⁻¹ s⁻¹

Table 2.2: Bimolecular rate constants^[68] for hydrogen abstraction reactions by the *tert*-butyloxy radical and the corresponding C,H bond dissociation energies (BDE).

Alkoxy radicals can perform homolytic abstraction reactions. Due to the large presence of C,H bonds in organic compounds and solvents most of these reactions involve a hydrogen atom transfer. The rate constants of these reactions correlate directly with the C,H bond strength of the bond to be cleaved (compare table 2.2). For example a C,H bond in cyclopentane (BDE = 94.5 kcal mol⁻¹) is cleaved 100 times slower than the C,H bond in 1,4-cyclohexadiene (BDE = 73 kcal mol⁻¹). For the also very weak Sn,H bond in BU₃SnH even a further increase of the rate constant by a factor of 10 is found.^[68]

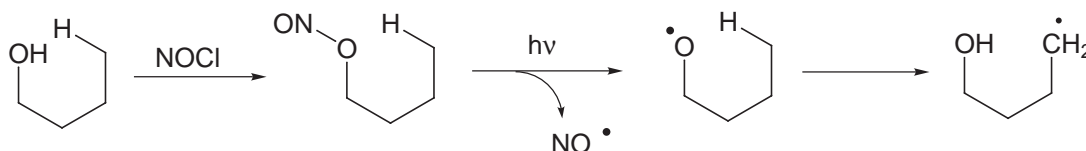


Figure 2.12: Schematic presentation of the 1,5 hydrogen abstraction of an alkoxy radical generated via the photolysis of a nitrite ester (“Barton reaction”).

The most favorable intramolecular hydrogen abstraction is a 1,5 H-shift. It is clearly preferred over the 1,2; 1,3; 1,4 and 1,6 hydrogen abstraction. This highly regioselective 1,5 H-atom abstraction is a key step in the “barton reaction”. Here a nitrite ester is photolyzed, and the resulting alkoxy radical abstracts a H-atom from the δ -carbon (see figure 2.12). This reaction sequence can be applied to generate carbon radicals from unactivated C,H bonds.

Such H-abstraction reactions by alkoxy radicals can also occur in various bio molecules like DNA and RNA. These potentially mutagenic reactions are also investigated with the aid

of the alkoxy radical precursors on the basis of heterocyclic thiohydroxamic-acid-*O*-esters. These studies are presented in chapter 2.2.2.

2.2.1 Stereoselective Organic Synthesis

To apply radicals in organic synthesis three things have to be considered. The radicals should be liberated under conditions that are favorable for the further reactions. Since free radicals are a highly reactive chemical species, detailed information about their reactivity is needed. Also a possible low “effective concentration” in the reaction mixture is wanted. The latter demand is fulfilled by applying efficient radical chain reactions. With the development of the alkoxy radical precursors on the basis of heterocyclic thiohydroxamic-*O*-esters an efficient source for alkoxy radicals – generated under mild conditions – is available. Many mechanistic studies on the various possible reactions of oxygen centered radicals were performed (see chapter 2.2 and the literature cited therein).

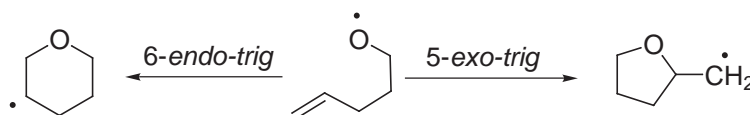


Figure 2.13: The two possibilities for a 4-penten-1-oxyl radical to form oxygen containing heterocycles by an intramolecular cyclization.

As shown in figure 2.13 an intramolecular addition of an oxygen centered radical to a double bond leads to oxygen containing heterocycles. Mechanistic studies in the working group of Hartung applying the pyridinethione radical precursors have shown that a 4-penten-1-oxyl radical can cyclize in two ways. A *6-endo-trig* cyclization leads to a pyran ring while a *5-exo-trig* attack will yields a substituted furan heterocycle. Both cyclization reactions are allowed according to the Baldwin rules^[69] but the *5-exo-trig* process is about 100 times faster than the *6-endo-trig* reaction.^[15] This leads to a 98 : 2 ratio of the furan product if the reaction is performed kinetically controlled.

If substituted 4-penten-1-oxyl radicals are applied multiply substituted 2-methylfuranes can be obtained. Further mechanistic studies were performed with the aid of phenyl substituted *N*-(4-pentenyl-1-oxy)-pyridine-2-(1*H*)-thiones. The stereochemistry of the *5-exo-trig* cyclization showed a high diastereoselectivity. If the 4-pentene-1-oxy residue has a phenyl substituent in position C¹ the majority of the obtained furanes are 2,5 trans substituted. A phenyl group at position two of the radical precursors pentene chain leads to a 88 : 12 ratio in favor of the 2,4 cis disubstituted heterocycle. If the allyl position of the 4-penten-1-oxyl radicals is substituted with a phenyl group the 2,3 disubstituted 2-methylfuranes

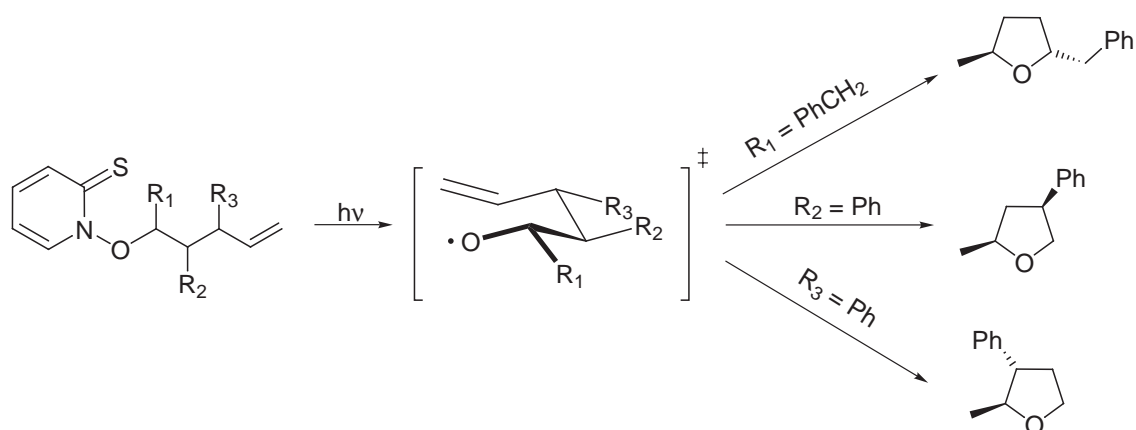


Figure 2.14: A transition state model to explain the diastereoselectivity of the 5-*exo-trig* cyclization of substituted 4-penten-1-oxyl radicals.^[15]

mostly show a *trans* configuration. This could be explained by the transition state for the 5-*exo-trig* cyclization shown in figure 2.14.

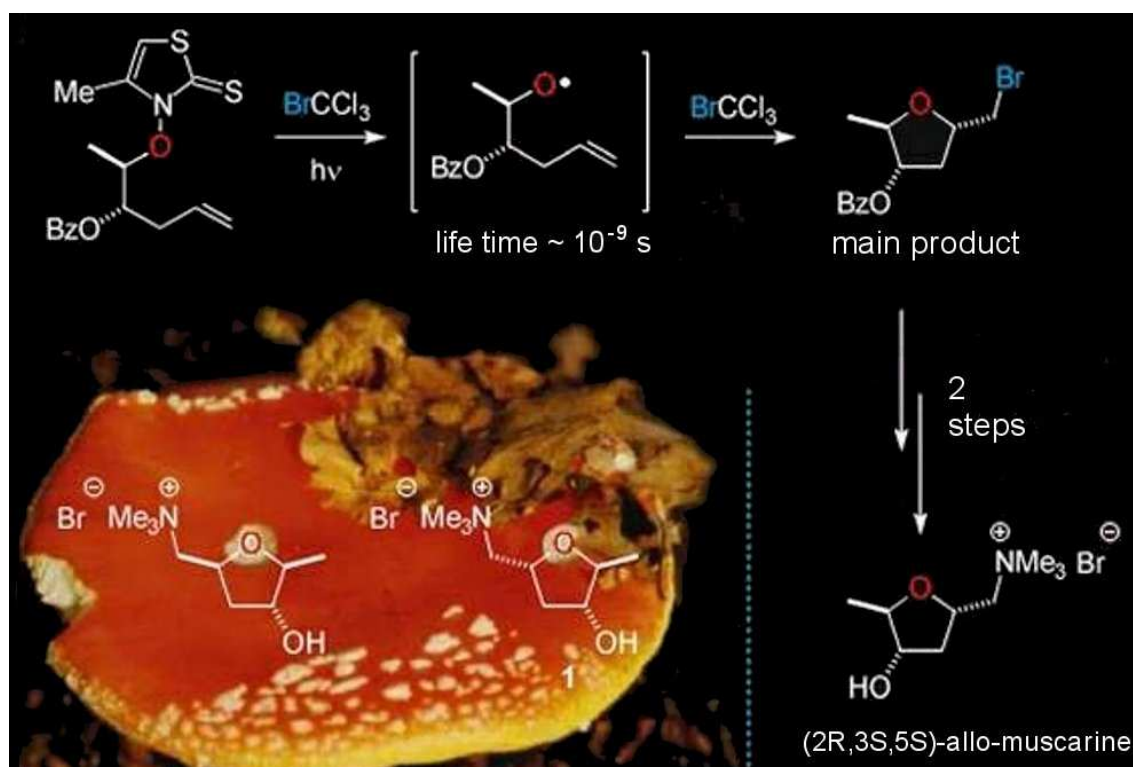


Figure 2.15: The synthesis route towards the natural compound (2*S*,3*R*,5*R*)-*allo*-muscarine starting from an alkoxy radical precursor on the basis of the thiazolethione compounds.^[18]

This knowledge about the stereochemistry of the cyclization of substituted 4-penten-1-oxyl radicals to furanes gave the possibility for the stereoselective synthesis of natural products. The (2*S*,3*R*,5*R*)-*allo*-muscarine a drug of the fly agaric *Amanita muscaria*, represents

an 1,3,5 trisubstituted furan heterocycle. Irradiation of *N*-(2,3-*anti*-3-benzyloxy-5-hexene-2-oxy)-4-methylthiazole-2(3*H*)-thione in the presence of the radical trap BrCCl₃ leads to the 3-benzyloxy-5-hexene-2-oxyl radical. This very short living molecule reacts highly diastereoselectiv in a 5-*exo-trig* cyclization. The obtained main product *cis*-3-benzyloxy-5-bromomethyl-*trans*-2-methyltetrahydrofuran can be transformed in two steps to (2*R*,3*S*,5*S*)-*allo*-muscarine the enantiomer of the wanted natural compound.^[18]

2.2.2 Bioorganic Studies

In vivo damages of the DNA and RNA by highly reactive oxygen derivatives are considered as important factors in aging,^[70–72] inflammation^[73] and especially mutagenesis and cancerogenesis.^[74,75] Compounds assumed to be involved in this oxidative stress are the hydroxyl radical ($\bullet\text{O-H}$), peroxy radicals^[76] ($\bullet\text{OO-R}$) and also alkoxy radicals ($\bullet\text{O-R}$). Those reactive oxygen radicals are produced in cells under physiological conditions during the oxygen metabolism and other redox reactions, which are of vital importance for biological functions.^[12] The hydroxyl radical $\bullet\text{O-H}$ for example is formed during the hydrogen peroxide (H_2O_2) metabolism by a Fe(II) induced H_2O_2 decomposition (*Fenton*-reaction)^[77] or a reaction of H_2O_2 in the presence of the superoxide radical anion $\text{O}_2^{\bullet-}$ (*Haber-Weiss*-reaction).^[78]

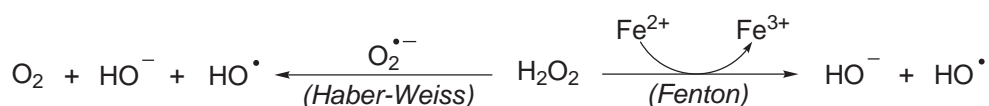


Figure 2.16: The formation of hydroxyl radicals in the *Fenton*- (right side) and the *Haber-Weiss*-reaction (left side).

For the hydroxyl radical various mechanisms for the damage of DNA and RNA are known. It attacks the DNA by hydrogen abstraction in the sugar backbone or by addition to the purin- and pyrimidine bases.^[74,79–85] The hydrogen abstractions on the DNA ribose molecules are randomized and the resulting 2'-desoxyribose radicals can eliminate a phosphate group. This leads to DNA strand breaks.^[83–85] Also all four DNA bases are attacked in a similar rate by the $\bullet\text{OH}$ radical.^[85] 2'-desoxyguanosine for example is attacked mostly at the positions C₄ and C₈.^[83–85] The C₄ addition product eliminates water and rearranges to diamino-[2- β -D-(desoxyerythropentofuranoylse)-4-amino]-5-oxazolone. The C₈ adduct will be oxidized to formamidopyrimidine.^[81] The other bases also are oxidized and damaged in similar ways.

Alkoxy radicals can also be generated under physiological conditions.^[86] This happens through carbon centered radicals, that are byproducts of the metabolism of foreign

substances. Those radicals add in a nearly diffusion controlled rate O_2 to form peroxy radicals.^[87,88]

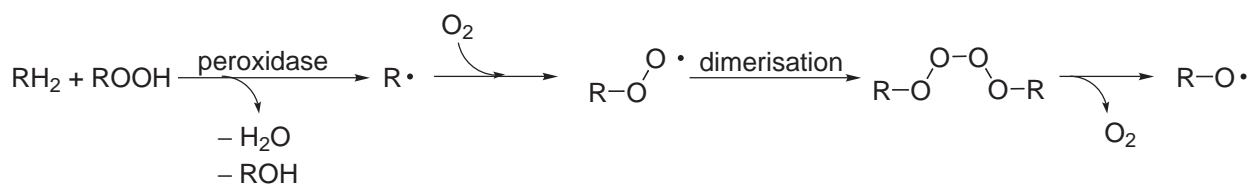
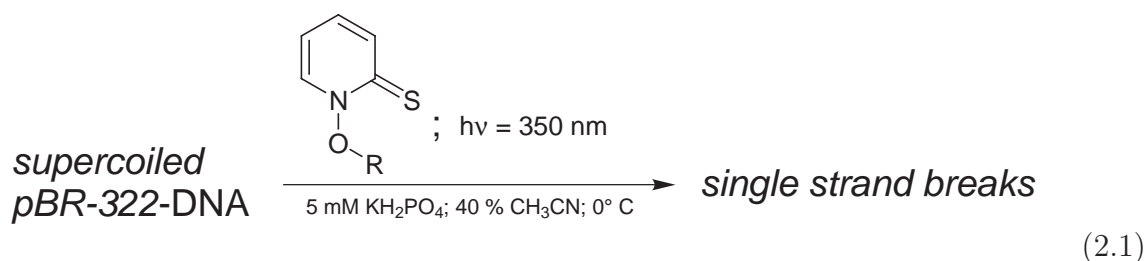


Figure 2.17: A possible way for the in vivo generation of alkoxy radicals.

The peroxy radicals decompose in a bimolecular mechanism involving a very short living tetroxide.^[89] A discussed way of the decomposition of this tetroxide is the liberation of alkoxy radicals and O_2 .^[90]

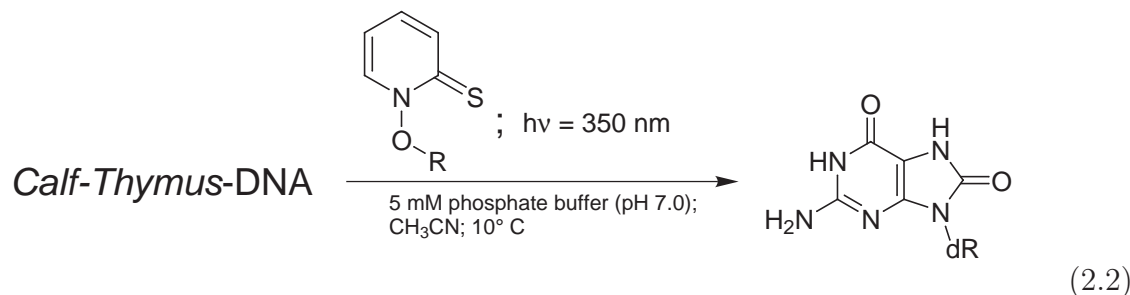
Since the reactive oxygen radicals are formed constantly the organism developed various ways to defeat himself. Next to enzymes, nonenzymatic antioxidants like the vitamins A (β -carotene), C (ascorbic acid) and E (α -tocopherol) are well known “oxygen traps”. Also glutathione serves as hydrogen donor to radicals.^[86] However, if the reactive oxygen species are formed in an uncontrolled rate and the defense mechanisms are surcharged, an oxidation of bio molecules like DNA and RNA can occur. This in vivo damage of the cells is called oxidative stress.^[75]

The mode of action of the hydroxyl radical in this oxidative stress on a molecular scale is under intense investigations.^[74,79–82] To get similar information about the damage mechanisms of alkoxy radicals, precursor systems are necessary that are able to liberate these radicals under physiological conditions. Since *N*-(hydroxy)-pyridine-2(1*H*)-thione (**1a-OH**) is already applied as photochemical OH-radical source^[91–93] in experiments on oxidative DNA damages, in the group of Adam, the *N*-alkoxy derivatives were applied as photochemical alkoxy radical precursors.^[9,10,12] These precursor systems, various *N*-(alkoxy)-pyridine-2(1*H*)-thiones, were synthesized according to the reaction scheme shown in figure 2.7.

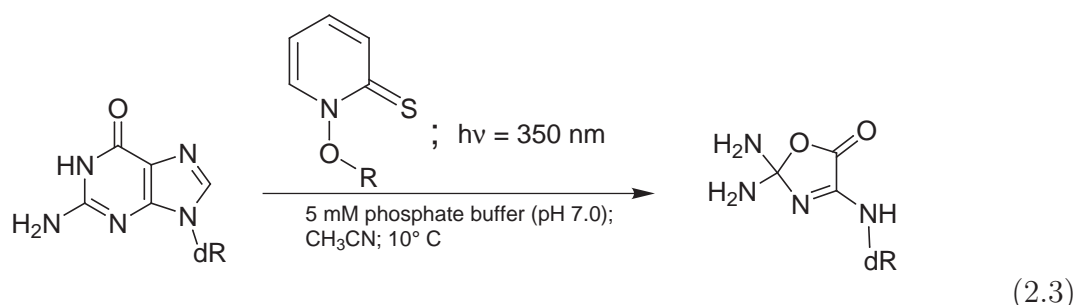


To investigate the ability of alkoxy radicals to enforce DNA strand breaks the alkoxy radical precursors on pyridinethione basis are irradiated ($h\nu = 350 \text{ nm}$) under physiological conditions in the presence of supercoiled pBR-332-DNA (equation 2.1). Strand breaks

detected by gel electrophoresis were found five minutes after the irradiation. This indicates that the strand breaking and therefore the single strands origin from the released alkoxy radicals. Also a significant reduction of observed broken DNA fragments, if the reaction was performed in the presence of the radical trapping reagent *tert*-butanol, is an evidence for this findings.^[12]



A second experiment that indicates a strand breaking potential of alkoxy radicals is the irradiation of the alkoxy radical precursors in the presence of calf-thymus DNA (equation 2.2). The observed oxidation product 7,8-dihydro-8-oxo-2'-desoxyguanosine, after the irradiation with 350 nm, is a clear sign for the DNA oxidation. Since preirradiated *N*-(alkoxy)-pyridine-2(1*H*)-thiones or the presence of the radical trapping reagent di-*tert*butylcresole leads to a significant lower yield of the oxidation product, only the liberated alkoxy radicals should be responsible for the DNA oxidation.^[9]



To check if the alkoxy radicals are able to initiate an oxidation of the DNA bases guanine an irradiation of different *N*-(alkoxy)-pyridine-2(1*H*)-thiones under physiological conditions in the presence of 2'-desoxyguanosine was performed (equation 2.3). The detected oxazolone indicates an oxidation mechanism similar to the one for the OH radicals. Like in the previously described experiments on DNA oxidation and strand breaking the presence of radical trapping reagents significantly lowers the yield of the oxidation product.^[9]

Chapter 3

Theoretical Basics

For the investigations of electronic absorption spectra and photochemical processes the theoretical description of electronically excited states is necessary. Modern quantum chemistry offers various methods for the calculation of these states.^[35,36] Since this work is about theoretical investigations on photochemical radical precursors the first part of this chapter should give a short introduction into the theory of excited states and the spectroscopy^[33] (see section 3.1). A description of the various quantum chemical methods that are able to calculate excited states is given in section 3.2. In this context especially the time-dependent - density functional theory^[24-26] (TD-DFT) which is capable to describe electronic excitations in “large” organic molecules is delineated in detail in chapter 3.2.1. The complete active space^[27] (CAS) approach, that is able to take multireference effects into account, which are often necessary to describe photochemical bond dissociation processes, is briefly introduced in chapter 3.2.2.

3.1 Electronically Excited States and Spectroscopy

In its ground state all electrons of a molecule are in the lowest energy levels. In the orbital picture for a closed shell molecule this is achieved by putting all electrons pairwise in the orbitals with the lowest energies. In an electronically excited state one or more electrons are in a higher level. This can be described, in the scope of the orbital picture, by taking one or more electrons from occupied orbitals and putting them into virtual ones. The choice of the electrons and the virtual orbitals determine the type of excited state that is constructed.

Transitions between the ground state and an excited state can be induced by absorption of electromagnetic radiation in the visible or the UV range. The energy of an excited

state and the probability to reach it after an absorption can be measured by the means of UV/vis-spectroscopy.^[33,34] If the excitation experiment is done with circularly polarized light also the interaction with the magnetic contribution to the electromagnetic field can be investigated. This is applied in the circular dichroism (CD) spectroscopy^[94] and gives information about the stereochemistry of the compounds.

3.1.1 Types of Excited States

The electronic structure of the ground state of most organic molecules can be described with a wave function where the lowest orbitals are doubly occupied (see figure 3.1). In this closed shell case the molecular orbitals that are lowest in energy represent the core orbitals. For elements from the second row of the periodic table the 1s electrons are occupying these orbitals. The next higher orbitals are the valence orbitals. In the LCAO formalism these orbitals represent the bonding molecular orbitals like the σ -bond frame and the π -orbitals. Also orbitals that can be interpreted as lone pairs are in this orbital energy region. The HOMO-LUMO gap marks the border between the occupied orbitals and the virtual ones. The lower lying virtual orbitals mostly represent the antibonding molecular orbitals. Another type of virtual orbitals are the Rydberg orbitals. Rydberg orbitals are orbitals with a much larger spatial extent than the molecule. They have a shape like atomic orbitals.

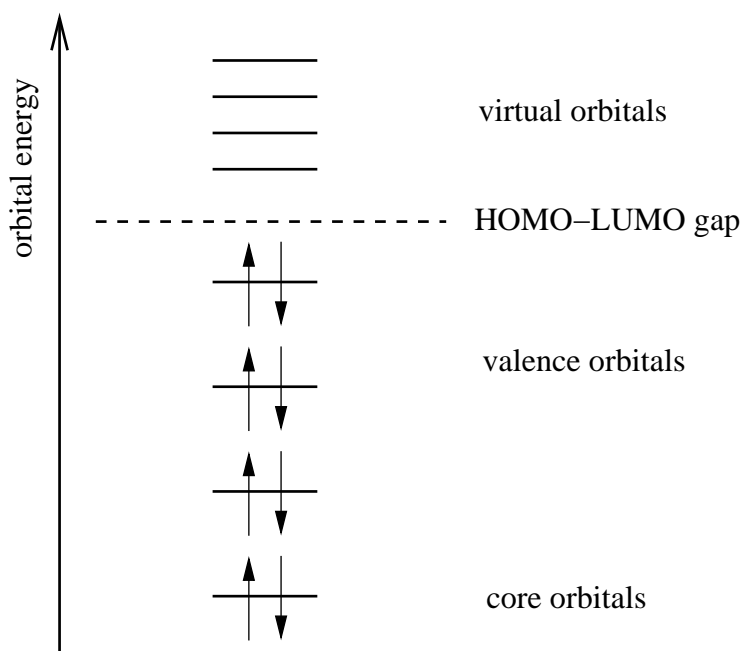


Figure 3.1: Schematic representation of the molecular orbitals of a closed shell organic molecule

Starting from this orbital scheme of a closed shell molecule the various types of excited

states can be described. A first characterization can be done by looking at the orbitals that are involved in the excitations.^[33,35]

- Valence excited states arise from excitations of electrons from the valence orbitals into the antibonding orbitals. For organic molecules these are the usual excitations that take place by irradiation with light in the visible or UV region.
- Rydberg states are obtained by exciting valence electrons into the Rydberg orbitals. These states are normally quenched when the irradiation of the molecules is done in solvent.
- If the energy of the radiation is very high core excited states can be formed, where an electron from the core orbitals is excited to a virtual one. This process often involves fragmentation or ionization of the molecules

Another differentiation of excited states can be made by the spatial locations of the orbitals involved in the excitation process. If an electron is transferred between two orbitals that are spatially close together this is called a local excitation. If the starting orbital and the final orbital are spatially separated a charge transfer occurs. This often happens if a molecule contains two separated π -electron systems or similar structural elements.

The multiplicity of the excited states is also a possibility to classify them. A normal UV/vis induced excitation starting from a closed shell molecule leads to a singlet excitation. The spin of the excited electron is not changed during the process and the multiplicity of the excited state still is one. The excited state could be called a low spin excited state. If the spin of the excited electron is flipped during or after the excitation process, the resulting excited state is a triplet state with a multiplicity of three. If spin-orbit effects are neglected this inter-spin crossing is not possible by normal absorption of light, and thus singlet triplet excitations are forbidden. A molecule can, however, be enforced in its triplet state by triplet sensitizers like naphthalene.^[95,96]

By considering the possibility of a theoretical description of excited states further classifications are possible. In this case the necessary theoretical approach to describe the electronic structure of the excited state characterizes it.

The ground state of a closed shell organic molecule can normally be described with a single determinate. Single reference approaches are sufficient to describe such molecules. If these approaches are also sufficient for the description of the electronic distribution of the excited state it can be seen as single reference excited state. If the electronic structure of the excited state is more complex and a linear combination of more determinants

is required to describe it a multireference approach is necessary. These states are called multiconfigurational excited states.^[35]

To describe the wave function of an excited state the electrons of the ground state can be put in virtual orbitals to generate excited determinants. If only a single electron is moved to create the excited state wave function this state is a singly excited state. If the excitation of more electrons is necessary to generate excited determinants the corresponding state is a multiply excited state.

3.1.2 UV/vis-Spectroscopy

One experimental way to generate electronically excited states is the irradiation of molecules with light in the ultraviolet (UV) or visible (vis) region of the electromagnetic spectrum. Light is an electromagnetic wave which can be described as an oscillating electric field (\mathcal{E}).^[32,33] Perpendicular to this field a magnetic field (\mathbf{H}) oscillates at the same frequency. The wave front is propagating with the speed of light ($c = 3 \cdot 10^8 \text{ m sec}^{-1}$). The electric field is able to exert forces on charged particles like nuclei and electrons. The magnetic field component can also exert forces on magnetic dipoles like nuclear or electron spins. Due to the oscillation the generated force fields \mathcal{E} and \mathbf{H} are time-dependent. The time-dependent magnitude of \mathcal{E} is given in equation 3.1.

$$\mathcal{E} = \mathcal{E}_0 \cos 2\pi\nu t \quad (3.1)$$

Here \mathcal{E}_0 is a fixed value of the electric field and ν is the frequency of the wave. This oscillating electric field can induce oscillations in other dipoles like the electrons in the field of the positive nuclei. During this process energy is exchanged between the oscillating electric field and the electrons. Due to the quantized nature of the electronic states only electromagnetic radiation that fulfills the condition $\Delta E = h\nu$ interacts with the electrons. ΔE is the energy gap between two possible electronic states and ν is the frequency of the radiation and the induced oscillating dipole. Since the oscillation of the electrons between the nuclei in a molecule normally possesses a frequency of 10^{-15} to $10^{-16} \text{ sec}^{-1}$ the resonance case falls in the wave length range of 200 to 700 nm. The absorption of light in this region of the spectra sets the electrons in molecules into oscillation.^[33,96]

The total force that works on an electron in the electromagnetic field of a light wave can be expressed according to equation 3.2.

$$\mathbf{F} = e\mathcal{E} + \frac{e[\mathbf{H}\mathcal{V}]}{c} \quad (3.2)$$

In this equation \mathbf{F} is the total force on the electron and $e\mathcal{E}$ is the electrical part of it. The magnetic part $\frac{e[\mathbf{H}\mathcal{V}]}{c}$ of the force also contains the speed of the electron \mathcal{V} . This speed normally is much smaller than c and so the magnetical part of the force can be neglected.

The electric force moves the electron from its unperturbed place in the molecule to a new position. The distance δr the electron is moved depends on the polarizability α of the molecule.

$$\alpha = \frac{e\delta r}{\mathcal{E}} = \frac{\mu_i}{\mathcal{E}} \quad (3.3)$$

The charge e of an electron and the difference between the old and the new position of the electron δr represent the transition dipole moment μ_i . The existence of a finite transition dipole moment is a necessary condition for the absorption of light.

A connection between the transition dipole moment and the extinction coefficient ϵ , the experimental quantity for the intensity of an absorption, is made with the concept of the oscillator strength. The oscillator strength f of an electron that can oscillate free in the framework of a positive nucleus is set to unity. f is related to the extinction coefficient by equation 3.4

$$f \equiv 4.3 \cdot 10^{-9} \int \epsilon d\bar{\nu} \quad (3.4)$$

The integral $\int \epsilon d\bar{\nu}$ corresponds to the area under the curve when the molecular extinction coefficient is plotted against the wavenumber of the absorbed light. $\bar{\nu}$ is the energy (in cm^{-1}) of the absorption. The oscillator strength is also proportional to the square of the transition dipole moment.

$$f \propto \mu_i^2 = \langle e\mathbf{r} \rangle^2 \quad (3.5)$$

If μ_i is expressed as $\langle e\mathbf{r} \rangle$, where \mathbf{r} is the length of the induced dipole the only missing thing is the constant of proportionality between these two quantities. Quantitatively the relationship between μ_i and f can be formulated according to equation 3.6.

$$f = \left(\frac{8\pi m_e}{3he^2} \right) \bar{\nu} \mu_i^2 \quad (3.6)$$

f only depends on the transition dipole moment and the transition energy. The mass of the electron m_e , the charge e and Planck's constant h are constant. Equation 3.6 makes it possible to calculate the oscillator strength from a known transition dipole moment.

$$f = \left(\frac{8\pi m_e}{3he^2} \right) \bar{\nu} \langle \Psi_i | \hat{\mu}_i | \Psi_f \rangle^2 \quad (3.7)$$

In the quantum mechanical description f can be expressed as the expectation value of the transition dipole moment μ_i with the initial and final state of the excitation. So the

oscillator strength can be calculated on a quantum mechanical level by applying equation 3.7. In formula 3.7 Ψ_i and Ψ_f represent the wave function of the initial state i and the final state f of the electronic excitation. $\bar{\nu}$ is the quantum chemically obtained excitation energy. A more detailed description of the theoretical methods to obtain the wave functions Ψ_i and Ψ_f and $\bar{\nu}$ is given in the next section.

3.1.3 CD-Spectroscopy

After introducing the total force that works on an electron in the electromagnetic field of a light wave (see eq. 3.2) it was said that the magnetic part $\frac{e[\mathbf{H}\nu]}{c}$ can be neglected. This is only correct for the interaction of nonpolarized light with molecules. If circularly polarized light is used, the magnetic component of the radiation field of right (+) circularly polarized light interacts different with the orbital angular momentum of the electrons than the magnetic component of left (-) circularly polarized light. This leads to two different extinction coefficients ϵ_+ and ϵ_- . This effect is called circular dichroism.^[94,97]

Experimentally this difference is measured in the circular dichroism (CD) spectroscopy. Here the difference $\Delta\epsilon = (\epsilon_+ - \epsilon_-)$ is plotted against the excitation energy or the wave length of the absorbed light. Similar to the oscillator strength f a quantity that is proportional to the area under a CD curve can be defined. In CD spectroscopy the integral under the $\Delta\epsilon$ curve is proportional to the rotatory strength \mathbf{R} .

$$\mathbf{R} \propto \int \Delta\epsilon d\bar{\nu} \quad (3.8)$$

Theoretically the rotatory strength \mathbf{R} can be expressed as the scalar product of the expectation values of the initial and final wave function with the electric and the magnetic transition dipole moment.

$$\mathbf{R} = \bar{\nu} \langle \Psi_i | \hat{\mu} | \Psi_f \rangle \times \langle \Psi_i | \hat{m} | \Psi_f \rangle \quad (3.9)$$

The dipole moments μ_i and m are obtained from the electronic densities of the initial state Ψ_i and the final state Ψ_f respectively.

3.1.4 The Simulation of Experimental Spectra from Theoretical Data

Starting from the concept of oscillator- (f) or rotatory strength (\mathbf{R}) the yield of a quantum chemical calculation on electronic excitations is a line spectrum. Here the excitation energy

(ν or λ) is plotted against f or \mathbf{R} (compare figure 3.2). However, a comparison of such line spectra with an experimentally obtained one is limited.^[35] Usually measured electronic excitation bands are no sharp lines but are broadened by various mechanisms.^[33]

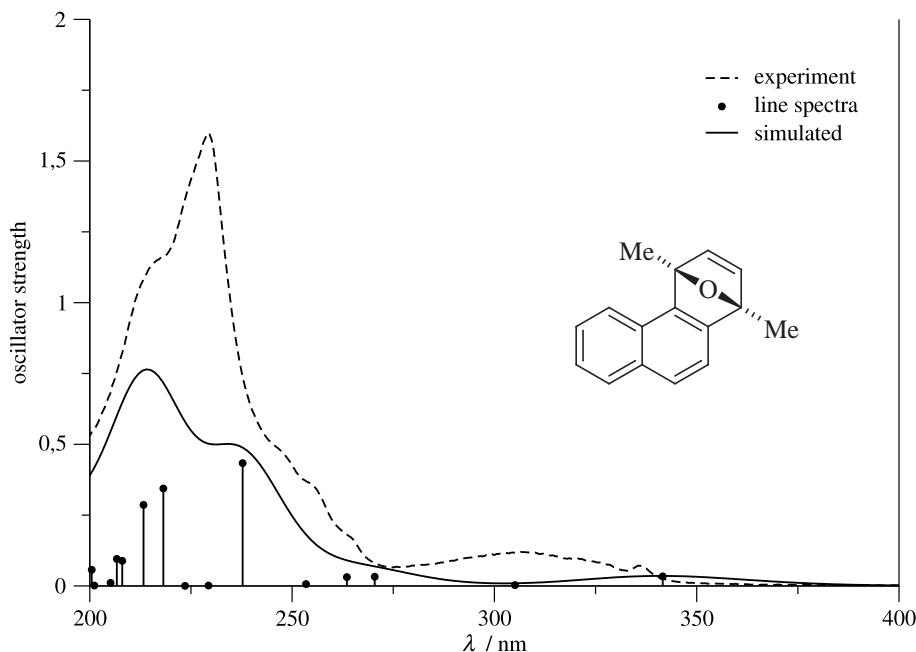


Figure 3.2: An example of a theoretically calculated line spectra (vertical lines) and the corresponding experimentally measured UV/vis spectra in comparison (dashed line). Also the simulated UV/vis spectra, obtained by an overlay of gaussian functions, is shown (full line).

The first factor that leads to broadened absorption bands is the lifetime of the excited state. Electronically excited states have a lifetime of usually only about 10 ns. That corresponds to a natural line width of approximately $\Delta E = 5 \cdot 10^{-4} \text{ cm}^{-1}$ ($\approx 10^{-8} \text{ eV}$). In the region of UV/vis absorptions this value, however, is negligible in comparison to other broadening mechanisms.

The various vibrational levels of the electronic states lead to broadened bands. In the Franck-Condon picture an electronic excitation starts from the vibrational ground state ω_0 of the electronic ground state. The transition dipole moment to vibrationally excited states of the final state of an electronic excitation depends on the Franck-Condon (FC) integrals $\langle \omega'_{ex} | \omega_0 \rangle$. Here the overlap of the vibrational wave function ω'_{ex} of the excited state with the one of the ground state determines the final intensity of the absorption band. Since the FC-integrals $\langle \omega'_{ex} | \omega_0 \rangle$ are not vanishing for several vibrational states ω'_{ex} of the final state of the electronic excitation not only one sharp absorption line but a broadened band is observed. The presence of a solvent in the UV/vis experiment leads to a further broadening of the absorption bands.

To get a simple possibility to compare the theoretically obtained line spectra with experimentally measured ones the simulation of the spectra with the aid of “shape functions” is possible.^[35,94]

$$\Delta\epsilon(E) = \frac{1}{\sqrt{2\pi\sigma}} \sum_i^a \lambda_i R_i e^{-\left[\frac{E-\lambda_i}{2\sigma}\right]^2} \quad (3.10)$$

To take the vibrational and solvent induced broadening of the absorption bands into account the line spectrum is superimposed with gaussian functions (see eq. 3.10). They are weighted by the absorption energy and the oscillator strength f of the corresponding calculated excitation. In the case of the simulation of a CD spectrum rotatory strength (\mathbf{R}) weighted gaussian functions are summed up. The usual estimation for the full width at half maximum σ of the gaussian functions lies in the region of 0.1 to 0.4 eV for a normal UV/vis band.

3.2 Quantum Chemical Methods to describe Excited States

Modern quantum chemistry in combination with the fast developments in computer hardware offers a variety of *ab-initio* methods to calculate electronically excited states of molecules of a “chemically relevant” size. The choice of the applied approach for the calculation of excited states depends on various factors.^[35,36] As already briefly mentioned in chapter 3.1 the wave function of the ground or excited state of a molecule can either be dominated by one determinant (single reference case) or has to be constructed by a linear combination of more configurations (multi reference case). A proper description of excited states often requires the application of multi reference (MR) ansätze, since the electronic structure of such states is more complex than the one of the ground state. Also photochemical processes often involve intermediates, whose wave functions can only be described appropriately by multi reference approaches. The theoretical methods that are capable to deal with MR effects are multi reference configuration interaction (MR-CI) approaches,^[98] complete active space (CAS) calculations^[28,29] or MR perturbational methods like the CASPT2^[30,31] or the MR-Møller-Plesset ansatz in the framework of the DIESEL CI program.^[99] A problem in the application of those MR ansätze is their high demand in computer power and CPU time. This limits the use of these very accurate methods (Δ_{exp} CASPT2 excitation energies < 0.2 eV^[100]) to the description of only small to medium sized molecules. For investigations on some photochemical processes, like the photolytical bond dissociation in the alkoxy radical precursors, however, the use of MR methods is unavoidable. The complete active space (CAS) ansatz, that was applied in the frame of this work, is therefore the subject of

subsection 3.2.2.

The ground state wave function of an usual organic molecule is normally dominated by only one Slater determinant. If this also holds for the excited states of these systems, calculations on electronic excited states can be performed by applying single reference methods. These approaches can further be divided in two categories.

The most obvious single reference ansatz to calculate an excited state is the configuration interaction (CI) approach.^[98,101] In this case the energies and properties of the excited state are obtained variationally. A single reference CI wave function is constructed as a linear combination of the normal Hartree Fock (HF) ground state determinants ψ_{HF} and further determinants. These correspond to excitations of electrons from the occupied orbitals (a, b) to virtual basis functions (r, s).

$$|\Phi_{CI}\rangle = c_0|\psi_{HF}\rangle + \sum_{a,r} c_a^r|\psi_a^r\rangle + \sum_{ab,rs} c_{ab}^{rs}|\psi_{ab}^{rs}\rangle + \dots + \sum_j c_j|\psi_j\rangle \quad (3.11)$$

This approach is shown in equation 3.11. Here c_0 is the expansion coefficient of the HF ground state wave function ψ_{HF} . c_a^r determines the fraction of the singly excited determinants ψ_a^r in the CI wave function Φ_{CI} . The double excitations are weighted with c_{ab}^{rs} and so on. The CI energy is minimized with respect to these coefficients provided that the whole CI wave function is normalized. This leads to a set of linear equations (eq. 3.12) that has to be solved.

$$c_i(E_i - E_{CI}) + \sum_{\substack{\text{all excitation levels} \\ j \neq i}} c_j \langle \psi_i | \hat{H} | \psi_j \rangle = 0 \quad (3.12)$$

By diagonalizing the so obtained Hamiltonian matrix (eq. 3.13) the eigenvalues (energies) of the excited states can be calculated.

$$\begin{pmatrix} E_0 - E_{CI} & \langle \psi_0 | \hat{H} | \psi_a^r \rangle & \langle \psi_0 | \hat{H} | \psi_{ab}^{rs} \rangle & \cdots & \langle \psi_0 | \hat{H} | \psi_j \rangle \\ \langle \psi_a^r | \hat{H} | \psi_0 \rangle & E_1 - E_{CI} & \langle \psi_a^r | \hat{H} | \psi_{ab}^{rs} \rangle & \cdots & \langle \psi_a^r | \hat{H} | \psi_j \rangle \\ \langle \psi_{ab}^{rs} | \hat{H} | \psi_0 \rangle & \langle \psi_{ab}^{rs} | \hat{H} | \psi_a^r \rangle & E_2 - E_{CI} & \cdots & \langle \psi_{ab}^{rs} | \hat{H} | \psi_j \rangle \\ \vdots & \vdots & \vdots & \ddots & \vdots \\ \langle \psi_j | \hat{H} | \psi_0 \rangle & \langle \psi_j | \hat{H} | \psi_a^r \rangle & \langle \psi_j | \hat{H} | \psi_{ab}^{rs} \rangle & \cdots & E_i - E_{CI} \end{pmatrix} + \begin{pmatrix} c_0 \\ c_a^r \\ c_{ab}^{rs} \\ \vdots \\ c_j \end{pmatrix} = \begin{pmatrix} 0 \\ 0 \\ 0 \\ \vdots \\ 0 \end{pmatrix} \quad (3.13)$$

Since this Hamiltonian matrix becomes very large if more and more excitation levels i and j are included, truncated CI methods were developed. For the calculation and simulation of UV/vis spectra only the CI-singles (CIS) is applied routinely.^[35,36,102] Here only the HF ground state and singly excited determinants ψ_a^r are considered for the CI wave function. The computational demand of such a CIS calculation is not much higher than for

the corresponding HF calculation. However, due to the lack of dynamic electron correlation effects, the accuracy of this approach is also only in the same region like the accuracy of a HF ground state calculation.^[35]

A second single reference access route to excited state energies and properties is the time-dependent (TD) response approach. In this case a time-dependent external perturbation (*e.g.* μ of an external radiation field) acts on the ground state wave function. Some properties like the frequency dependent polarizability ($\alpha(\omega)$) exhibit poles if the frequency of the time-dependent perturbation corresponds to an electronic excitation energy.^[35] By applying proper response functions the time-dependent response ansatz became the basis of various quantum chemical methods for the description of electronically excited states. Next to a time-dependent HF variant also the equation of motion coupled cluster (EOM-CC) ansatz^[103] is a linear response approach. The most widely used TD approach however, is the time-dependent - density functional theory (TD-DFT).^[24-26] Also in the framework of the investigations on the electronic spectra of the photochemical alkoxy radical precursors, the TD-DFT approach was the only sufficient method to obtain informations on the UV/vis spectra of a large amount of different bigger organic molecules. Therefore section 3.2.1 deals in more detail with the theoretical basis of the linear response approach and its application in the TD-DFT.

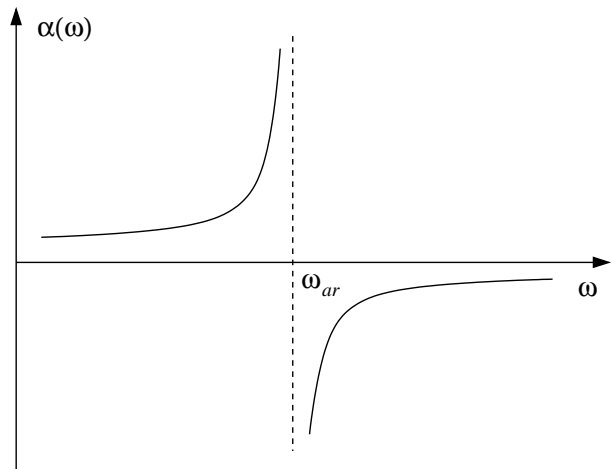
3.2.1 Time-Dependent - Density Functional Theory

In contrast to the Hartree Fock approach where the electron structure of a molecule is described by finding the best orbitals in a given basis set, density functional theory (DFT) starts from the electron density of a system.^[98,101,104] It is assumed that the real electron density corresponds to a reference density of non interacting particles that move in an effective local single particle potential $v_0(\vec{r})$ (Kohn-Sham potential). The Hohenberg Kohn (HK) theorem states that there is a one to one correspondence between the wave function and the electron density. The wave function and each quantum mechanical observable can be expressed as a functional of the electron density. With the introduction of the Kohn-Sham orbitals as basis of the reference density, and the correct functional, DFT is a variational, exact many body theory for ground state properties of molecules. To obtain informations about excited states a time-dependent variant of the density functional theory (TD-DFT) was developed.^[24-26]

The basis of this theory is the linear response of a property of the ground state of a molecule on a time-dependent perturbation.^[105] For the purpose of calculating electronically excited states the most important time-dependent perturbation is the electric dipole part μ

of a radiation field. A property that responds on μ is the frequency dependent polarizability $\alpha(\omega)$.

$$\alpha(\omega) = \sum_{a,r} \frac{f_{0ar}}{\omega_{ar}^2 - \omega^2} \quad (3.14)$$



Equation 3.14 shows the sum-over states formula for $\alpha(\omega)$. f_{0ar} is the oscillator strength of the electronic excitation $a \rightarrow r$. If the frequency ω of the time-dependent perturbation matches the excitation frequency ω_{ar} of the system this equation exhibits a pole. The calculation of excitation energies and excited state properties can therefore be reduced to the search for poles in proper linear response functions like $\alpha(\omega)$.

For the TD variant of density functional theory the concept of the Kohn-Sham (KS) potential has to be expanded to a time-dependent potential.^[24–26] Therefore the external potential $v_{ext}(\vec{r}, t)$ is assumed according to equation 3.15

$$v_{ext}(\vec{r}, t) = \begin{cases} v_0(\vec{r}) & ; t \leq t_0 \\ v_0(\vec{r}) + v_1(\vec{r}, t) & ; t > t_0 \end{cases} \quad (3.15)$$

At the time $t \leq t_0$ the external potential $v_{ext}(\vec{r}, t)$ corresponds to the normal ground state potential $v_0(\vec{r})$. At all later times $t > t_0$ the external potential is a sum of $v_0(\vec{r})$ and a time-dependent perturbation $v_1(\vec{r}, t)$. According to the HK theorem the static ground state is determined uniquely by the density $\rho_0(\vec{r})$. This holds also for the time-dependent density $\rho(\vec{r}, t)$ which can be expressed as a functional of the external potential $v_{ext}(\vec{r}, t)$.

$$\rho(\vec{r}, t) = \rho[v_{ext}](\vec{r}, t) \quad (3.16)$$

Runge and Gross^[26] had proven that there is an unique one to one correspondence between the time-dependent densities and the time-dependent potentials. The external potential $v_{ext}(\vec{r}, t)$ therefore also can be expressed as a functional of the time-dependent density.

$$v_{ext}(\vec{r}, t) = v_{ext}[\rho](\vec{r}, t) \quad (3.17)$$

For small perturbations $v_1(\vec{r}, t)$ the density $\rho(\vec{r}, t)$ at a time $t > t_0$ can be expanded in a Taylor series, which can be broken after the second term.

$$\rho(\vec{r}, t) = \rho_0(\vec{r}) + \rho_1(\vec{r}, t) + \rho_2(\vec{r}, t) + \dots \quad (3.18)$$

$\rho_0(\vec{r})$ is the static ground state density. $\rho_1(\vec{r}, t)$ represents the linear (first order) response of the density ρ to the perturbation $v_1(\vec{r}, t)$ and is given by

$$\rho_1(\vec{r}, t) = \int dt' \int d^3 r' \chi(\vec{r}, \vec{r}', (t - t')) v_1(\vec{r}', t') \quad (3.19)$$

$\chi(\vec{r}, \vec{r}', (t - t'))$ is the density-density response function. It characterizes the response of the density $\rho(\vec{r}, t)$ of the system at the time t to the external perturbation $v_1(\vec{r}, t)$

$$\chi(\vec{r}, \vec{r}', (t - t')) = \left. \frac{\delta \rho [v_{ext}] (\vec{r}, t)}{\delta v_{ext}(\vec{r}', t')} \right|_{v_{ext}[\rho_0]} \quad (3.20)$$

According to the Runge-Gross theorem each external time-dependent potential $v_{ext}(\vec{r}, t)$ determines a density $\rho [v_{ext}(\vec{r}, t)]$, that determines a new potential $v_s [\rho [v_{ext}(\vec{r}, t)]]$.

$$v_s(\vec{r}, t) = v_{ext}(\vec{r}, t) + \int d^3 r' \frac{\rho(\vec{r}', t)}{|\vec{r} - \vec{r}'|} + v_{xc}(\vec{r}, t) \quad (3.21)$$

This time-dependent Kohn-Sham potential v_s yields a time-dependent electron density of noninteracting KS particles, that corresponds to a real time-dependent density of Coulomb interacting particles in the external time-dependent potential $v_{ext}(\vec{r}, t)$. In this TD-Kohn-Sham potential the term $\int d^3 r' \frac{\rho(\vec{r}', t)}{|\vec{r} - \vec{r}'|}$ is the time-dependent Hartree potential. $v_{xc}(\vec{r}, t)$ corresponds to the time-dependent exchange correlation potential. Inserting the KS potential v_s into equation 3.20 the density response function χ_s of the KS density can be obtained.

$$\chi_s(\vec{r}, \vec{r}', (t - t')) = \left. \frac{\delta \rho [v_s] (\vec{r}, t)}{\delta v_s(\vec{r}', t')} \right|_{v_s[\rho_0]} \quad (3.22)$$

The mathematical functional chain rule gives a link between the KS response function and its “real” counterpart χ . With the functional derivative of v_s with respect to the external potential v_{ext} the response function χ can be expressed as

$$\chi(\vec{r}, \vec{r}', (t - t')) = \int d^3 x \int d\tau \left. \frac{\delta \rho(\vec{r}, t)}{\delta v_s(\vec{x}, \tau)} \frac{\delta v_s(\vec{x}, \tau)}{\delta v_{ext}(\vec{r}', t')} \right|_{\rho_0} \quad (3.23)$$

Applying the functional chain rule a second time the functional derivative of v_s with respect to v_{ext} can be calculated.

$$\left. \frac{\delta v_s(\vec{r}, t)}{\delta v_{ext}(\vec{r}', t')} \right|_{\rho_0} = \delta(\vec{r} - \vec{r}') \delta(t - t') + \int d^3 x \int d\tau \left(\frac{\delta(t - \tau)}{|\vec{r} - \vec{x}|} + \frac{v_{xc}(\vec{r}, t)}{\delta \rho(\vec{x}, \tau)} \right) \frac{\delta \rho(\vec{x}, t)}{\delta v_{ext}(\vec{r}', t')} \quad (3.24)$$

Inserting the functional derivative 3.24 into the expression 3.23 of the “real” response function $\chi(\vec{r}, \vec{r}', (t - t'))$, and applying the definitions of χ_s (3.22) and χ (3.20), the relation between χ and χ_s is found.

$$\begin{aligned} \chi(\vec{r}, \vec{r}', (t - t')) &= \chi_s(\vec{r}, \vec{r}', (t - t')) + \int d^3x \int d\tau \int d^3x' \int d\tau' \chi_s(\vec{r}, \vec{r}', (t - t')) \\ &\quad \left(\frac{\delta(\tau - \tau')}{|\vec{x} - \vec{x}'|} + f_{xc}[\rho_0](\vec{x}, \vec{x}', (\tau - \tau')) \right) \chi(\vec{x}, \vec{r}', (\tau' - t')) \end{aligned} \quad (3.25)$$

$f_{xc}[\rho_0](\vec{x}, \vec{x}', (\tau - \tau'))$ is the so called time-dependent exchange-correlation kernel (TD-*xc* kernel).

$$f_{xc}[\rho_0](\vec{x}, \vec{x}', (\tau - \tau')) := \left. \frac{\delta v_{xc}[\rho](\vec{r}, t)}{\delta \rho(\vec{r}', t')} \right|_{\rho_0} \quad (3.26)$$

f_{xc} is a functional of the initial density ρ_0 and represents a functional derivative of the time-dependent *xc* potential v_{xc} with respect to the density ρ .

To obtain the TD Kohn-Sham equations for the linear density response, equation 3.24 has to be multiplied by the time-dependent perturbation $v_1(\vec{r}', t)$ and integrated over \vec{r}' and t' .

$$\rho_1(\vec{r}, t) = \int dt' \int d^3x' \chi_s(\vec{r}, \vec{r}', (t - t')) v_{s,1}(\vec{r}', t') \quad (3.27)$$

In equation 3.27 $v_{s,1}(\vec{r}', t')$ represents the effective time-dependent perturbation that yields the linear density response of noninteracting KS particles. This corresponds to the exact linear density response $\rho_1(\vec{r}, t)$ of an interacting system to the time-dependent perturbation $v_1(\vec{r}, t)$.

$$v_{s,1}(\vec{r}', t') = v_1(\vec{r}, t) + \int d^3r' \frac{\rho_1(\vec{r}', t)}{|\vec{r} - \vec{r}'|} + \int d^3r' \int dt' f_{xc}[\rho_0](\vec{r}, \vec{r}', (t - t')) \rho_1(\vec{r}', t') \quad (3.28)$$

To obtain the exact frequency dependent linear density response equations 3.27 and 3.28 have to be combined and the Fourier transformation has to be taken.

$$\rho_1(\vec{r}; \omega) = \int d^3r' \chi_s(\vec{r}, \vec{r}'; \omega) \left[v_1(\vec{r}'; \omega) + \int d^3x \left(\frac{1}{|\vec{r}' - \vec{x}|} + f_{xc}[\rho_0](\vec{r}', \vec{x}; \omega) \right) \rho_1(\vec{x}; \omega) \right] \quad (3.29)$$

In this equation the Kohn-Sham response function χ_s can be expressed in terms of the static unperturbed KS orbitals.

$$\chi_s(\vec{r}, \vec{r}'; \omega) = 2 \sum_{j,k} (n_k - n_j) \frac{\varphi_k^*(\vec{r}) \varphi_j(\vec{r}) \varphi_j^*(\vec{r}') \varphi_k^*(\vec{r}')}{\omega - \omega_{jk} - i\delta} \quad (3.30)$$

Here n_k and n_j are the occupation numbers (0 or 1) of the KS orbitals and the summation runs over both occupied and unoccupied orbitals including the continuum states. This response function exhibits poles at the Kohn-Sham orbital energy differences $\omega_{jk} = (\epsilon_j - \epsilon_k)$. Since the true excitation energies Ω of a system are normally not identical with the KS orbital energy differences ω_{jk} equation 3.29 has to be rewritten.^[106,107]

$$\int d^3 r' \chi_s(\vec{r}, \vec{r}'; \omega) = \int d^3 x \left[\delta(\vec{r} - \vec{x}) - \int d^3 r' \chi_s(\vec{r}, \vec{r}'; \omega) \left(\frac{1}{|\vec{r}' - \vec{x}|} + f_{xc}[\rho_0](\vec{r}', \vec{x}; \omega) \right) \right] \rho_1(\vec{x}; \omega) v_1(\vec{r}'; \omega) \quad (3.31)$$

In this reordered equation the left hand side that contains the KS response function χ_s stays finite if the frequency ω corresponds to a true excitation energy Ω . The “exact” density response ρ_1 on the right hand side of equation 3.32 in contrast exhibits a pole at the true excitation energy $\omega = \Omega$. The eigenvalues of $(\int d^3 x)$ must vanish which is equal to the condition that the eigenvalues $\lambda(\omega)$ in

$$\int d^3 r \int d^3 r' \chi_s(\vec{x}, \vec{r}; \omega) \left(\frac{1}{|\vec{r} - \vec{r}'|} + f_{xc}[\rho_0](\vec{r}, \vec{r}'; \omega) \right) \zeta(\vec{r}' \omega) = \lambda(\omega) \zeta(\vec{x} \omega) \quad (3.32)$$

must satisfy the condition $\lambda(\Omega) = 1$. This is an exact condition to determine the excitation energies of a system. In practical applications not the full spectrum of the frequency dependencies of the functions in 3.32 is wanted. To calculate only some excitation energies the single pole approximation (SPA) is made.^[106,108] Here every function in 3.32 is expanded in a mathematical series around a single Kohn Sham orbital excitation ω_{jk} . For the time-dependent exchange correlation kernel f_{xc} this expansion at the single particle KS orbital excitation $k \rightarrow j$ is shown in equation 3.33

$$f_{xc}[\rho_0](\vec{r}, \vec{r}'; \omega) = f_{xc}[\rho_0](\vec{r}, \vec{r}'; \omega_{j,k}) + \left. \frac{df_{xc}[\rho_0](\vec{r}, \vec{r}'; \omega)}{d\omega} \right|_{\omega_{j,k}} (\omega - \omega_{j,k}) + \dots \quad (3.33)$$

The single particle approximation only holds if the differences between the true excitation energy Ω and the KS orbital energy difference ω_{jk} is smaller than the energy differences between two states Ω_1 and Ω_2 of the system. Together with the SPA of the functions the eigenvalue problem 3.32 is expanded in the basis of the complete set of Kohn-Sham orbitals. A non-Hermitian eigenvalue problem is obtained, that has to be solved for ω .

$$\begin{pmatrix} A & B \\ B & A \end{pmatrix} \begin{pmatrix} X \\ Y \end{pmatrix} = \omega \begin{pmatrix} 1 & 0 \\ 0 & -1 \end{pmatrix} \begin{pmatrix} X \\ Y \end{pmatrix} \quad (3.34)$$

X and Y represent the solution vectors for a single particle excitation $a \rightarrow r$ (X) and the deexcitation $r \rightarrow a$ (Y) respectively. The matrix elements A and B contain the orbital

energy differences and the Coulomb and exchange integrals over the KS orbitals.

$$A_{ar,bs} = \delta_{ab}\delta_{rs}(\epsilon_r - \epsilon_a) + (ar|bs) + (ar|f_{xc}|bs) \quad (3.35)$$

$$B_{ar,bs} = (ar|sb) + (ar|f_{xc}|sb) \quad (3.36)$$

Due to the fact that in the time-dependent xc kernel the exact Coulomb interaction is replaced by a response integral, containing an approximated local exchange correlation functional v_{xc} , TD-DFT has problems to describe some kinds of excited states.^[36,107,109–114] The xc potentials of the applied approximated functionals shows a wrong long range behavior. The true potential has a $1/R$ fall-off for the distance R between two charges, while the potentials in the density functionals decay faster due to the locality of the Local Density Approximation^[101,115] (LDA) or the Generalized Gradient Approximation^[101,116] (GGA). Because of this wrong fall off behavior, excited states, where the electron is excited over a long spatial distance, are described incorrectly. This error is especially dramatic for Rydberg states, whose error in the TD-DFT excitation energies can be a few electron volts and their calculated potential energy surfaces show a wrong curvature.^[36,107,114] Also excitations in long range π -electron systems,^[36,109,112,113] between two separated molecules or other electronic transitions that involve a larger spatial charge transfer (CT) are often drastically underestimated.^[36,110,111] This can be understood by looking at the matrix elements A (eq. 3.35) and B (eq. 3.36) in the eigenvalue problem 3.34. If an electron is transferred from an occupied orbital a (*e.g.* the highest occupied molecular orbital (HOMO)) to a virtual orbital r (*e.g.* the lowest unoccupied molecular orbital (LUMO)) that have only a sparse or no overlap, all two electron integrals in 3.35 and 3.36 vanish. The excitation energy in this case is given only by the Kohn-Sham orbital energy difference $\epsilon_r - \epsilon_a$ of the contributing orbitals. In the Hartree-Fock scheme the orbital energy difference between well separated HOMOs and LUMOs is a rough approximation for a charge transfer excitation energy. This holds because according to Koopman’s theorem^[117] the orbital energy of the HOMO corresponds to the ionization potential IP of a molecule and the LUMO energy is the electron affinity EA. In contrast to HF in the DFT approach also the virtual orbitals are evaluated in the correct n -electron potential. Therefore the virtual orbitals are more strongly bound and the excitation energies of charge transfer (CT) excitations are underestimated. This problem can partly be solved if hybrid functionals like the B3LYP^[118,119] or the PBE0^[120,121] functional are applied. Here some parts of A and B contain the “exact” HF Coulomb and exchange potential with the correct $1/R$ long range behavior.

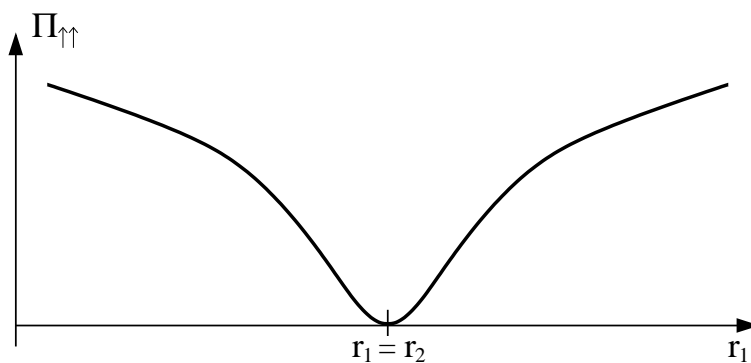
In spite of the known and understood problems of TD-DFT with charge transfer or Rydberg states, this approach became the most widely used quantum chemical methods for the investigation of electronically excited states of medium and larger sized molecules. Especially for valence excited states in ordinary organic molecules TD-DFT yields excitation

energies with an typical error of 0.1 to 0.3 eV in comparison to the experimental excitation energies.^[35] This is in the same region as the values of high-level correlated methods like EOM-CCSD and CASPT2. The advantage over those methods is the comparably low computational effort of the TD-DFT approach. Additional computation time can be saved by applying the resolution of identity (RI) approximation^[122,123] for the evaluation of the “Coulomb-like” integrals in B (eq. 3.36). This decreases the time for the calculations by a factor of 3 to 8, depending on the molecular and basis set size.^[124] Especially for large basis sets this approximation is very useful since the computational cost of the two electron integral evaluation grows with n^4 in the normal scheme but only with n^3 if the RI approximation can be applied. The error in the excitation energies that is introduced by this approximation is marginal since the errors in the ground and excited states are subtracted out.

Nowadays TD-DFT is a standard method in computational chemistry that is implemented in various quantum chemical program packages like the TURBOMOLE^[125] or GAUSSIAN03.^[126] However, TD-DFT should not be seen as a “black box” method for the calculation of excited states. Since the “correct” exchange correlation functional is not known, the approximated functionals in the frame of the LDA or GGA lead to a strong dependency of the obtained results on the choice of the functional. The pure density functionals like the BLYP^[119,127] or PW91^[128] often underestimate the excitation energies. The reason for this are the more strongly bound virtual KS orbitals and the wrong long range fall off behavior of the approximated Coulomb potentials. Due to this dependency on the functionals a comparison of the obtained TD-DFT results (excitation energies, oscillator strength) with higher level *ab-initio* methods like the CASPT2 or experimental spectra is recommended.^[35] In the frame of this work small “parent” compounds (*N*-(methoxy)-pyridine-2(1*H*)-thione (**1a-OMe**), *N*-(methoxy)-thiazole-2(3*H*)-thione (**2a-OMe**)) were applied as model systems for a comparison of the TD-DFT results with CASPT2 calculations. This strategy, together with a comparison of the results obtained with various functionals with experimental UV/vis spectra, showed a dependency of the TD-DFT spectra on the choice of the functional for even different electronic excitations (compare chapter 4). The spectroscopically visible $\pi \rightarrow \pi^*$ transition for example is described correctly with the BLYP functional in the case of *N*-(methoxy)-thiazole-2(3*H*)-thione while all other excitations in this compound and the spectra of *N*-(methoxy)-pyridine-2(1*H*)-thione is obtained more correctly with the B3LYP functional.^[2]

3.2.2 The Complete Active Space (CAS) Approach

In the first part of section 3.2 electronically excited states were subdivided in single reference and multireference cases. For closed shell organic molecules with their, in energy well separated excited states, those states can be described with time-dependent single determinant ansätze like TD-DFT or the RI-CC2^[41–43] approach. However, if the excited states come close to each other in energy or a bond is lengthened or broken in a photochemical process these single reference ansätze break down. The reason for this behavior of one Slater determinant approaches like the Hartree Fock (HF) ansatz is the lack of some parts of the electron correlation.^[98,101] The HF method describes each electron in the averaged field of all other electrons. This, however, neglects the instantaneous repulsive interactions between the electrons. The electrons avoid each other *i.e.* their motions are correlated. The probability to find an electron next to another becomes smaller.



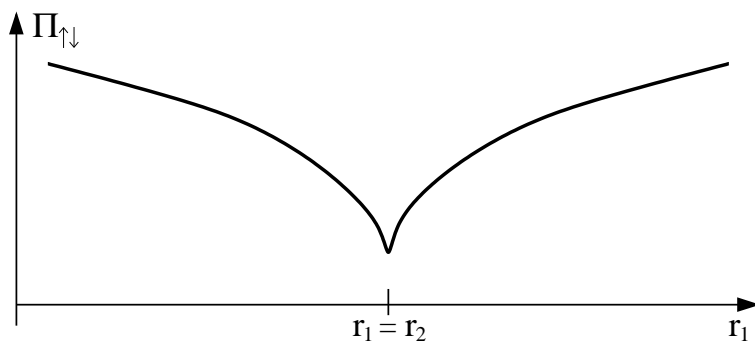
$$\Pi_{\uparrow\uparrow} = \frac{1}{2} dr_1 dr_2 \{ |\phi_1(r_1)|^2 |\phi_2(r_2)|^2 + |\phi_1(r_2)|^2 |\phi_2(r_1)|^2 \} - 2(\phi_1(r_1)\phi_2(r_2) + \phi_1(r_2)\phi_2(r_1))$$

Figure 3.3: Schematical representation of the pair density $\Pi_{\uparrow\uparrow}$ of two electrons with the same spin.

The first effect that leads to correlated motions of the electrons is the Pauli repulsion. Two electrons with the same spin can not occupy the same spatial region. The pair density $\Pi_{\uparrow\uparrow}$ of two electrons with the same spin exhibits the so called Fermi hole, *i.e.* is zero if the coordinates r_1 and r_2 of the electrons are equal (compare figure 3.3).

Due to their negative charge also electrons with different spins avoid each other. The pair density $\Pi_{\uparrow\downarrow}$ of two electrons with different spins however, is not zero if $r_1 = r_2$ (compare figure 3.4).

The correlation effects that are neglected in the HF approach lead to a systematical error of the Hartree Fock energy. The energy difference ΔE between the lowest non relativistic



$$\Pi_{\uparrow\downarrow} = \frac{1}{2} dr_1 dr_2 \{ |\phi_1(r_1)|^2 |\phi_2(r_2)|^2 + |\phi_1(r_2)|^2 |\phi_2(r_1)|^2 \}$$

Figure 3.4: Schematic representation of the pair density $\Pi_{\uparrow\downarrow}$ of two electrons with opposite spin.

energy E_{exact} and the best HF energy $E_{HF-limit}$ is called correlation energy E_{corr} .

$$E_{corr} = E_{HF-limit} - E_{exact} \quad (3.37)$$

The correlation energy is only one percent of the total energy of a system but this is still bigger than the usual bond energy between two atoms in a molecule.^[98]

From the theoretical point of view the electron correlation can be subdivided in two parts. If the gap between the occupied and the virtual orbitals is very small and the electrons can alternatively occupy other orbitals than in the closed shell HF wave function, a multi configuration (MC) ansatz, like the multi-configurational self consistent field (MC-SCF) approach, is necessary. The part of the correlation energy that is covered by such an approach is the so called near degeneracy correlation or static correlation. Static correlation is also important for the description of excited states since several singly excited states starting from a closed shell HF wave function are often close in energy. This problem of single reference approaches is even more dramatic if a photolytic bond dissociation process is under investigation. Already for a bond dissociation in the ground state the restricted closed shell HF ansatz (RHF) leads to wrong dissociation energies and potentials. For the excited state potential energy surfaces of such a process single reference approaches like TD-DFT or the RI-CC2 approach fail completely.

The second part of the correlation energy comes from the instantaneous interaction of the electrons that is not covered by the average HF potential. This part is called the dynamic correlation and is usually estimated by perturbative methods.

The plainest way to take correlation effects into account is the already in section 3.2 described configuration interaction (CI) approach. The inclusion of excited determinants

to the wave function leads to slightly modified charge distributions. This offers the system more degrees of freedom and electron correlation effects are covered. The problem of this approach, however, is that the orbitals are not modified and optimized during the CI procedure. During a bond dissociation process the orbitals of a molecule often undergo a dramatical change in their shapes. To obtain accurate bond dissociation energies and potentials in the ground and excited states a variational procedure that involves both, the optimization of CI coefficients of different configurations and the optimization of the orbitals, is required. An approach that fulfills this criterion is the multi-configurational self consistent field (MC-SCF) method.

A MC-SCF wave function can be constructed as a linear combination of different electron configurations expressed as Slater determinants.^[27,98,101]

$$\Psi_{MC-SCF} = \sum_m c_m \left| \underbrace{(\sum_i c_i \phi_i)}_{\psi_m} \right\rangle \quad (3.38)$$

The aim of a MC-SCF procedure is to optimize the CI expansion coefficients c_m of the configurations ψ_m as well as the orbital coefficients c_i of the orbital basis ϕ_i simultaneously. To do this the electronic energy of a system is considered as a function of the variational parameters c_m and c_i . Iterative methods are used to find stationary points on this multi-dimensional (in c_i and c_m) energy surface. The electronic energy of a system is expressed as the expectation value of the electronic Hamiltonian

$$E = \langle \Psi | \hat{H} | \Psi \rangle = \langle \Psi | \hat{F} | \Psi \rangle + \langle \Psi | \frac{1}{r_{12}} | \Psi \rangle \quad (3.39)$$

The electronic Hamiltonian \hat{H} is a sum of one electron operators \hat{F} like the kinetic energy of the electrons and the electron-nuclear attraction, and the two electron, electron-electron repulsion operator $1/r_{12}$.

The minimization of the electronic energy with respect to the variational parameters c_m and c_i can be done more easily if the formalisms of second quantization are introduced.^[27,98] Second quantization starts not with the electrons but with a full basis set of orthonormal spin orbitals. Single Slater determinants (configurations) are described by an occupation number vector $|m_1, m_2, m_3, \dots, m_{2n}\rangle$ that indicates if a basis function (spin orbital) is occupied ($m_i = 1$) or not ($m_i = 0$). The complete set of determinants with all possible occupation number vectors defines the Fock space.

The annihilation operator \hat{a}_i and the creation operator \hat{a}_i^\dagger are defined.

$$\hat{a}_i |m_1, m_2, \dots, m_i, \dots, m_{2n}\rangle = m_i (-1)^{p_i} |m_1, m_2, \dots, 0_i, \dots, m_{2n}\rangle \quad (3.40)$$

The annihilation operator \hat{a}_i (eq. 3.40) acts on the elements m_k of the occupation number vector in the way that it sets the occupation number m_i at the position i to zero. This is

equivalent to the removal (annihilation) of an electron from the corresponding spin orbital. If m_i is already 0 the annihilation has no effect.

$$\hat{a}_i^\dagger |m_1, m_2, \dots, m_i, \dots, m_{2n}\rangle = (1 - m_i)(-1)^{p_i} |m_1, m_2, \dots, 1_i, \dots, m_{2n}\rangle \quad (3.41)$$

The creation operator \hat{a}_i^\dagger in contrast adds (creates) an electron to the corresponding orbital i by setting m_i to 1. Like for \hat{a}_i the creation \hat{a}_i^\dagger has no effect if the occupation number m_i is already 1. The term $(-1)^{p_i}$ is responsible to retain the antisymmetry of the Slater determinants.

Another operator that is defined in second quantization is the single excitation operator.

$$\hat{a}_i^\dagger \hat{a}_j |m_1, m_2, \dots, 0_i, \dots, 1_j, \dots, m_{2n}\rangle = (-1)^{p_j - p_i} |m_1, m_2, \dots, 1_i, \dots, 0_j, \dots, m_{2n}\rangle \quad (3.42)$$

which excites an electron from orbital j to orbital i . In terms of occupation number vectors this corresponds to the annihilation (\hat{a}_j) of an electron in the orbital m_j followed by the creation (\hat{a}_i^\dagger) of the electron in orbital m_i . Since the electronic Hamiltonian \hat{H} in equation 3.39 contains no spin dependent operators it is possible to use spin summed excitation operators \hat{E}_{ij} for the further treatment of the MC-SCF problem.

$$\hat{E}_{ij} = \hat{a}_{i\alpha}^\dagger \hat{a}_{j\alpha} + \hat{a}_{i\beta}^\dagger \hat{a}_{j\beta} \quad (3.43)$$

The indices i and j in 3.43 refer to the n molecular orbitals (MOs) which can have the occupation number 0, 1 and 2. If \hat{E}_{ij} acts on a Slater determinant where j is not occupied zero is produced. The same result is obtained if the molecular orbital i is doubly occupied and $i \neq j$. For i equal to j an “excitation” from the MO i to itself is described and \hat{E}_{ij} becomes 2. In general it can be said that the action of the excitation operator \hat{E}_{ij} on a configuration expressed in molecular orbitals $|m\rangle$ results an occupation number vector n_i with the values 0, 1 and 2.

$$\hat{E}_{ii}^\dagger |m\rangle = n_i |m\rangle \quad (3.44)$$

With the aid of the second quantization operators every quantum mechanical operator can be expressed in the space spanned by all Slater determinants generated in a given basis set. An one electron operator \hat{F} in second quantitation is expressed as

$$\hat{F} = \sum_{i,j} f_{ij} \hat{a}_i^\dagger \hat{a}_j \quad (3.45)$$

where f_{ij} is the matrix with the values of the operator in the spin orbital basis.

$$f_{ij} = \int \phi_i^*(x) \hat{F}(x) \phi_j(x) dx \quad (3.46)$$

For the spin independent one electron operators in \hat{H} the terms in 3.45 can be summed pair-wise over the spin quantum number. Now it is possible to formulate an one electron operator \hat{F} in terms of the excitation operators \hat{E}_{ij} .

$$\hat{F} = \sum_{i,j} f_{ij} \hat{E}_{ij} \quad (3.47)$$

were the sum runs over the molecular orbitals and the integrals in f_{ij} are in the MO basis. The expectation value of the excitation operator \hat{E}_{ij} in a multi-configurational system $\Psi_{MC} = \sum_m c_m |\psi_m\rangle$ (compare equation 3.38) is the first order reduced density matrix which contains the expansion coefficients c_m for the configurations ψ_m in Ψ_{MC}

$$D_{ij} = \langle \Psi_{MC} | \hat{E}_{ij} | \Psi_{MC} \rangle = \sum_{m,n} c_m^* c_n D_{ij}^{mn} \quad (3.48)$$

With the relations 3.47 and 3.48 the expectation values of one electron operators \hat{F} in the multi-configurational system Ψ_{MC} in the molecular orbital basis is given as

$$\langle \Psi_{MC} | \hat{F} | \Psi_{MC} \rangle = \sum_{i,j} f_{ij} D_{ij} \quad (3.49)$$

In second quantization two electron operators \hat{G} are expressed in the spin orbital basis as

$$\hat{G} = \sum_{i,j,k,l} g_{ijkl} \hat{a}_i^\dagger \hat{a}_k^\dagger \hat{a}_l \hat{a}_j \quad (3.50)$$

with g_{ijkl} as the two electron integrals in this basis. The only two electron operator in the MC-SCF treatment is the $1/r_{12}$ operator for the electron-electron repulsion. This operator is spin independent and equation 3.50 can be summed over the spin variables. With the use of symmetry properties of the two electron integrals g_{ijkl} and anti-commutator relations for the creation and annihilation operators, \hat{G} can be expressed in the MO basis in terms of excitation operators.

$$\hat{G} = \sum_{i,j,k,l} g_{ijkl} (\hat{E}_{ij} \hat{E}_{kl} - \delta_{jk} \hat{E}_{il}) \quad (3.51)$$

where the integrals g_{ijkl} in the molecular orbital basis φ_i have the form

$$g_{ijkl} = \int \varphi_i^*(r_1) \varphi_j(r_1) \frac{1}{r_{12}} \varphi_k^*(r_2) \varphi_l(r_2) dr_1 dr_2 \quad (3.52)$$

With the aid of 3.51 the second order density matrix P_{ijkl} for the MC wave function can be obtained, like for the first order density matrix in equation 3.48, in the notation of second quantization

$$P_{ijkl} = \sum_{m,n} c_m^* c_n P_{ijkl}^{mn} \quad (3.53)$$

For Ψ_{MC} the expectation value of the $1/r_{12}$ operator in the MO basis is given as

$$\langle \Psi_{MC} | \frac{1}{r_{1,2}} | \Psi_{MC} \rangle = \sum_{ijkl} g_{ijkl} P_{ijkl} \quad (3.54)$$

The equations 3.47 and 3.51 give the possibility to express the electronic Hamiltonian operator \hat{H} in the operator basis constructed from the excitation operators \hat{E}_{ij}

$$\hat{H} = \sum_{i,j} f_{ij} \hat{E}_{ij} + \frac{1}{2} \sum_{i,j,k,l} g_{ijkl} (\hat{E}_{ij} \hat{E}_{kl} - \delta_{jk} \hat{E}_{il}) \quad (3.55)$$

f_{ij} are the one electron integrals containing the kinetic energy and the electron-nuclear attraction and g_{ijkl} are the integrals over $1/r_{12}$ shown in equation 3.52. One important fact of second quantization that is seen in equation 3.55 is, that the number of electrons does not appear in the definition of the operators. This information is found completely in the Slater determinant basis. With the expectation values of the one electron operators (eq. 3.49) and the $1/r_{12}$ operator (eq. 3.54) the electronic energy of a system, as the expectation value of the electronic Hamiltonian 3.55 for a multi-configurational wave function expanded in Slater determinants, can be obtained according to

$$E = \langle \Psi_{MC} | \hat{H} | \Psi_{MC} \rangle = \sum_{ij} f_{ij} D_{ij} + \sum_{ijkl} g_{ijkl} P_{ijkl} \quad (3.56)$$

In this expression the information about the molecular orbitals (coefficients c_i in 3.38) is contained completely within the one- and two-electron integrals f_{ij} and g_{ijkl} . The density matrices D_{ij} and P_{ijkl} contain the information about the CI expansion coefficients c_m .

Now that an expression for the total energy is found the minimization with respect to the optimization parameters c_i and c_m has to be done. The most prominent method for the solution of a multidimensional optimization problem is the second order Newton-Raphson (NR) procedure.^[27,98] Second order approaches for a multidimensional optimization problem expand the energy to the first and second derivative. In the NR methods the energy as a function of the optimization vector \mathbf{p} is expanded up to the second order around a point p_0 in a Taylor series.

$$E(\mathbf{p}) = E(0) + \sum_i \underbrace{\left(\frac{\partial E}{\partial p_i} \right)_0}_{\mathbf{g}} p_i + \frac{1}{2} \sum_{i,j} p_i \underbrace{\left(\frac{\partial^2 E}{\partial p_i \partial p_j} \right)_0}_{\mathbf{H}} p_j + \dots \quad (3.57)$$

$E(0)$ is the starting point for the energy and can arbitrary set to 0. The first derivative of the energy ∂E with respect to the variational parameters p_i is the gradient vector \mathbf{g} while the second derivative corresponds to the Hessian matrix \mathbf{H} . To find stationary points on the multidimensional energy surface the gradient in equation 3.57 has to be zero. This

leads to a system of linear equations that has to be solved iteratively. This Newton-Raphson procedure is nowadays implemented in the usual MC-SCF programs like the complete active space self consistent field (CASSCF) module of MOLCAS.^[129]

In the CASSCF module of MOLCAS a second optimization method is implemented. This so called Super-CI (SCI) approach tries to find the optimal MC wave function by annihilating the singly excited configurations.^[27,29] According to the generalized Brillouin theorem^[130] there is no interaction between the optimized multi-configurational reference state $|\psi_0\rangle$ and singly excited states $|\psi_q^p\rangle = \hat{E}_{pq}|\psi_0\rangle$. A Super-CI wave function expanded in the reference state and the singly excited states can be constructed.

$$|\Psi_{SCI}\rangle = |\psi_0\rangle + \sum_{p>q} t_q^p |\psi_q^p\rangle \quad (3.58)$$

In the Super-CI method stationary points now are found by minimizing the expansion coefficients t_q^p of the singly excited configurations $|\psi_q^p\rangle$ with respect to the original variation parameters c_i and c_m contained in the reference state $|\psi_0\rangle$.

The most important problem in a multi-configurational calculation is to find a proper multi reference starting wave function for the solution of the MC-SCF equations. For a single determinant approach it is easy to provide a starting point by specifying a molecular geometry, the number of electrons and an appropriate basis set for the atomic orbitals.^[27,98,101] In the multi-configurational case this could not be done so easily. Since the MC wave function Ψ_{MC} is constructed as a linear combination of several electronic configurations ψ_m (compare eq. 3.38) an a priori knowledge of the electronic structure is necessary.^[27] This is possible for normal bonding situations in molecules where for example the resonance structures of Lewis formulas give the correct “chemical” idea for the important configurations. For transition states of reactions or excited states, however, normally the electronic structure is not known before and an adequate MC-SCF wave function can not be provided. To solve this problem the complete active space (CAS) method was developed.

The CAS approach normally starts from a closed shell HF ground state wave function.^[27,98,101] For the complete active space procedure the HF orbitals are subdivided in different subsets (compare figure 3.5). The lowest molecular orbitals (MOs) are the inactive orbitals. They are kept doubly occupied in all configurations in the CAS wave function. To save additional computational resources the core orbitals, like the 1s orbitals of second row elements, can additionally set frozen, that means they are not varied during the MC-SCF procedure. The active orbitals normally contain the highest occupied orbitals and the lowest virtual ones of the HF ground state. From these orbitals the configurations ψ_m of the CAS wave function are constructed by a full CI in this active orbital space. The external orbitals span the rest of the orbital space, defined from the chosen AO basis sets. This CAS

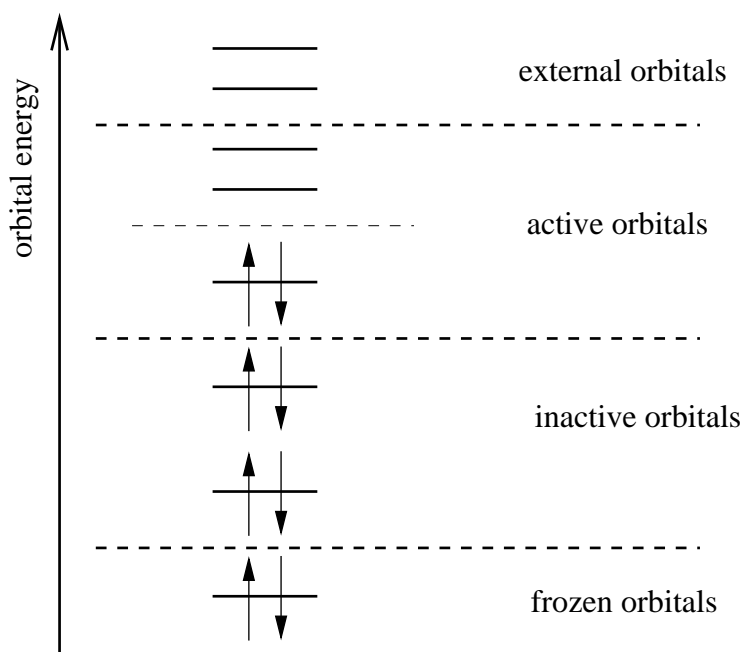


Figure 3.5: The partitioning of the orbital space in the complete active space (CAS) treatment.

approach to a MC wave function partly solves the problem of the a priori knowledge of the necessary configurations. Instead of deciding which configuration ψ_m has to be taken into account, “only” the relevant orbitals for a given chemical problem have to be chosen. For the investigations on the photochemical N,O bond homolysis of the *N*-(alkoxy)-pyridine-2(*1H*)-thiones (**1a-OR**) and the *N*-(alkoxy)-thiazole-2(*3H*)-thiones (**2a-OR**) for example the eight highest occupied MOs and the four lowest virtual Hartree Fock orbitals have to span the active space to obtain the correct dissociation paths in the ground state and the first two singlet excited states.

A problem of the CAS approach to a multi-configurational wave function however, is the fast growing size of the full CI expansion in the active space.^[27] This limits the application of the CASSCF procedure to active spaces with about 10 to 12 orbitals. Mere if only a few electrons have to be correlated in the active space this orbital limit can be exceeded.

With the CASSCF approach^[28,29] it is possible to obtain proper wave functions for the investigation of photochemical processes where multi-configurational effects are important and the shapes of the orbitals vary to a large amount in different excited states. Transition probabilities like transition moments or the oscillator strength can be calculated as the transition matrix element of the operator between two electronic states. In the frame of the MOLCAS program this is done with the the restricted active space state interaction^[131] (RASSI) module. Although the values for transition densities and other state interaction

properties are obtained quite accurately with the CASSCF approach, the values for the excitation energies often show an error of 1 - 2 eV. The reason for this are the dynamic correlation effects, that are often different in the ground and the various excited states. For a HF ground state wave function such effects are usually estimated by the aid of second order Møller-Plesset perturbation theory^[98,101] (MP2). To apply the CASSCF approach on the problem of calculating electronic excitation energies in an exact way a multi reference MP2 approach, with the CAS wave function as multi-configurational basis, was developed.^[30,31]

In single reference MP2 theory the Hamiltonian \hat{H}_{MP2} is divided in the unperturbed operator \hat{H}_0 that corresponds to the Fock operator \hat{F} , and the perturbation \hat{V} which is the difference between the complete Hamiltonian \hat{H} and \hat{H}_0 .

$$\hat{H}_{MP2} = \underbrace{\sum_p \epsilon_p \hat{E}_{pp}}_{\hat{F}=\hat{H}_0} + \underbrace{(\hat{H} - \hat{H}_0)}_{\lambda\hat{V}} \quad (3.59)$$

The wave function Ψ and the energy expectation value E can now be expanded in Taylor series

$$\Psi = \Psi_0 + \lambda\Psi_1 + \lambda^2\Psi_2 + \dots \quad (3.60)$$

$$E = E_0 + \lambda E_1 + \lambda^2 E_2 + \dots \quad (3.61)$$

The energy E_0 of the unperturbed system Ψ_0 has to be an eigenfunction of \hat{H}_0 ($\hat{H}_0|\Psi_0\rangle = E_0|\Psi_0\rangle$). In the Møller-Plesset case this is realized with the Fock operator \hat{F} as \hat{H}_0 . Therefore E_0 is the sum for the orbital energies ϵ_p of the occupied orbitals.

$$E_0 = \langle\Psi_0|\hat{H}_0|\Psi_0\rangle = \langle\Psi_0|\hat{F}|\Psi_0\rangle = \sum_p \epsilon_p \quad (3.62)$$

The first order energy E_1 is obtained as the expectation value of the perturbation \hat{V} in the basis of the zero order wave function Ψ_0 .

$$E_1 = \langle\Psi_0|\hat{V}|\Psi_0\rangle \quad (3.63)$$

From the definition of the MP2 Hamiltonian \hat{H}_{MP2} in 3.59 it follows directly that the sum of the zero order and the first order energy is the HF ground state energy.

$$E_{HF} = \sum_p \epsilon_p + \langle\Psi_0|\hat{V}|\Psi_0\rangle \quad (3.64)$$

The doubly counted electron electron repulsion in the Fock operator $\hat{F} = \hat{H}_0$ is corrected by the expectation value of the perturbation operator \hat{V} in the basis of the unperturbed wave function Ψ_0 . The desired dynamic correlation effects are taken into account with the second order and higher perturbation energies.

The second order perturbation energy E_2 is obtained as the expectation value of the perturbation \hat{V} between the unperturbed wave function Ψ_0 and the first order wave function Ψ_1 .

$$E_2 = \langle \Psi_0 | \hat{V} | \Psi_1 \rangle \quad (3.65)$$

To calculate this expectation value the first order wave function Ψ_1 has to be expanded in the complete set of all configurations generated in the chosen MO basis except the HF determinant Ψ_0 itself.

$$\Psi_1 = \sum_i c_i \Psi_0^{(i)} \quad (3.66)$$

The first order expansion coefficients c_i of the determinants $\Psi_0^{(i)}$ that correspond to all possible excited states with respect to the HF ground state are obtained by solving the equation

$$(\hat{H}_0 - E_0) | \Psi_1 \rangle = (E_1 - \hat{V}) | \Psi_0 \rangle \quad (3.67)$$

The coefficients c_i contain the interactions between all configurations $\Psi_0^{(i)}$ and the HF ground state wave function Ψ_0

$$c_i = \frac{\langle \Psi_0^{(i)} | \hat{V} | \Psi_0 \rangle}{E_0 - E_0^{(i)}} \quad (3.68)$$

The denominator of equation 3.68 contain the difference of the zero order energy E_0 (sum of all occupied orbital energies in the HF determinant) and the energies of the configurations $E_0^{(i)}$ as sum of the orbital energies of the occupied orbitals in the determinants $\Psi_0^{(i)}$. In the MP2 case not all excited determinants $\Psi_0^{(i)}$ with respect to the HF ground state have to be considered. Since \hat{V} is a two electron operator third or higher order excitations have no contributions to $\langle \Psi_0^{(i)} | \hat{V} | \Psi_0 \rangle$. Due to the Brillouin theorem also the singly excited determinants Ψ_a^r have no interactions with the HF ground state Ψ_0 . For the first order wave function therefore only the doubly excited determinants Ψ_{ab}^{rs} have to be taken into account. Inserting the so obtained first order wave function 3.66, with the coefficients 3.68, in the second order energy expression 3.65, the second order MP2 energy is obtained.

$$E_2 = \langle \Psi_0 | \hat{V} | \sum_i c_i \Psi_0^{(i)} \rangle = \sum_i \frac{\langle \Psi_0 | \hat{V} | \Psi_{ab}^{rs} \rangle \langle \Psi_{ab}^{rs} | \hat{V} | \Psi_0 \rangle}{E_0 - E_{ab}^{rs}} \quad (3.69)$$

Due to the intermediate normalization $\langle \Psi_{ges} | \Psi_0 \rangle = 0$ and the fact that the perturbation wave functions Ψ_i are orthonormal to Ψ_0 ($\langle \Psi_i | \Psi_0 \rangle = \delta_{i0}$) the perturbation operator \hat{V} can be replaced by the Hamiltonian \hat{H} . The denominator of 3.69 is, according to Koopman's theorem, the energy difference between the occupied orbitals a and b and the virtual orbitals r and s .

$$E_2 = \sum_i \frac{\langle \Psi_0 | \hat{H} | \Psi_{ab}^{rs} \rangle \langle \Psi_{ab}^{rs} | \hat{H} | \Psi_0 \rangle}{\epsilon_a + \epsilon_b - \epsilon_r - \epsilon_s} \quad (3.70)$$

The complete single configuration MP2 energy of a molecular system can now be obtained as a sum of the HF ground state energy and the second order perturbation energy.

$$E_{MP2} = E_{HF} + \sum_i \frac{\langle \Psi_0 | \hat{H} | \Psi_{ab}^{rs} \rangle \langle \Psi_{ab}^{rs} | \hat{H} | \Psi_0 \rangle}{\epsilon_a + \epsilon_b - \epsilon_r - \epsilon_s} \quad (3.71)$$

For the here discussed multi-configurational MP2 method the CASSCF wave function serves as reference function $|\psi_0\rangle$.

$$|\Psi_{CASSCF}\rangle = |\psi_0\rangle \quad (3.72)$$

The complete configurational space $|\psi_{complete}\rangle$ ($\Psi_0^{(i)}$ in equation 3.66 for the single reference case) that is used to expand the first order wave function can be divided in four parts.^[27,30,31]

$$|\psi_{complete}\rangle = |\psi_0\rangle + |\psi_K\rangle + |\psi_{SD}\rangle + |\psi_X\rangle \quad (3.73)$$

Next to the reference configuration $|\psi_0\rangle$, the configurational space $|\psi_K\rangle$, including all other possible configurations generated in the active space (all CAS full CI configurations), can be defined. These configurations are orthogonal to $|\psi_0\rangle$ if optimized CASSCF orbitals are used. The configurational space $|\psi_{SD}\rangle$ contains all configurations that are obtained by single and double excitations with respect to $|\psi_0\rangle$.

$$|\psi_{SD}\rangle = \sum_{pq} \hat{E}_{pq} |\psi_0\rangle + \sum_{pq \geq rs} \hat{E}_{pq} \hat{E}_{rs} |\psi_0\rangle \quad (3.74)$$

The indices q and s refer to occupied orbitals (inactive or active orbitals) whereas the indices p and r correspond to virtual orbitals from the active or external space. If all four orbitals p , q , r and s are in the active space the generated configuration belongs to $|\psi_K\rangle$. In $|\psi_X\rangle$ the remaining configurations that are created by higher order excitations are included. Those do not interact with the reference function $|\psi_0\rangle$.

For the perturbational treatment the complete Hamiltonian has to be divided in an unperturbed Hamiltonian \hat{H}_0 , that has to be an eigenfunction of $|\psi_0\rangle$, and the perturbation \hat{V} . With the orthogonality properties of the optimized CASSCF orbitals only configurations from the $|\psi_{SD}\rangle$ space interact with the reference function via the total Hamiltonian. The unperturbed Hamiltonian therefore is constructed in a way that also only configurations from the $|\psi_{SD}\rangle$ space contribute to the necessary expansion of the first order wave function (equation 3.66 in the single reference case).

$$\Psi_1 = \sum_j c_j |\psi_{SD}^{(j)}\rangle = \sum_{pq} c_q^p \hat{E}_{pq} |\psi_0\rangle + \sum_{pq \geq rs} c_{qs}^{pr} \hat{E}_{pq} \hat{E}_{rs} |\psi_0\rangle \quad (3.75)$$

The expansion coefficients are then obtained by solving a set of linear equations

$$\sum_j c_j \langle \psi_{SD}^{(i)} | \hat{H}_0 - \underbrace{(\langle \psi_0 | \hat{H}_0 | \psi_0 \rangle)}_{E_0} | \psi_{SD}^{(j)} \rangle = - \langle \psi_{SD}^{(i)} | \hat{H} | \psi_0 \rangle \quad (3.76)$$

The right hand side of this equation $\langle \psi_{SD}^{(i)} | \hat{H} | \psi_0 \rangle$ represents the interactions between the $|\psi_{SD}\rangle$ space and the reference function $|\psi_0\rangle$. The solution of equation 3.76 however, is not so easy like in the single reference case (compare equation 3.67) because the basis ψ_{SD} is not linear independent. The coefficients c_j of the first order wave function expansion in the $|\psi_{SD}\rangle$ space now are used to calculate the second order energy contribution E_2 .

$$E_2 = \langle \psi_0 | \hat{H} | (\sum_j c_j |\psi_{SD}^{(j)}\rangle) \rangle \quad (3.77)$$

The complete CASPT2 energy can now be obtained, like in the single reference MP2 case, as the sum of the CASSCF energy E_{CASSCF} and the second order perturbative correction E_2 .

$$E_{CASPT2} = E_{CASSCF} + \langle \psi_0 | \hat{H} | (\sum_j c_j |\psi_{SD}^{(j)}\rangle) \rangle \quad (3.78)$$

This perturbative correction E_2 estimates the dynamic correlation effects that are not contained in the CASSCF energy.

For the calculation of excitation energies in a multi-configurational system where the states strongly interact the use of a “state averaged” CASSCF wave function as reference state $|\psi_0\rangle$ is possible. This leads to the multi state (MS) CASPT2 variant.^[40] In this work the MS-CASPT2 energies were used as theoretical reference values for the validation of the computational less demanding single reference TD-DFT method.

Chapter 4

The Electronic Spectra of the known Precursors

UV/Vis photolysis of heterocyclic thiohydroxamic-*O*-esters and their *N*-hydroxy analogues provide oxygen-centered radicals^[5] for an application in photobiological,^[7,8,11–13] mechanistic,^[91,132] and synthetic studies.^[16–18] Since light quanta of comparatively low energy suffice in order to induce the N,O homolysis, it is likely that the primary photophysical event upon UV/vis excitation of *N*-(alkoxy)-pyridine-2(1*H*)-thiones^[15,19] (**1a-OR**) and *N*-(alkoxy)-thiazole-2(3*H*)-thiones,^[133] (**2a-OR**) and the corresponding acids is associated with an excitation of the thiocarbonyl chromophore^[134] rather than an electronic transition within the orbitals of the heterocyclic part or the N,O bond itself.^[135] According to fundamentals of thiocarbonyl photochemistry^[136,137] and photophysics,^[138–141] the two energetic lowest and hence photochemically relevant electronic excitations between singlet potential energy surfaces in aliphatic and aromatic thiocarbonyl compounds originate from symmetry-forbidden $n \rightarrow \pi^*$ excitations in the visible to near IR region and symmetry-allowed $\pi \rightarrow \pi^*$ transitions in the near UV region. Substituting an amino or a thiyyl group for an alkyl substituent in thioketones causes thiocarbonyl $\pi \rightarrow \pi^*$ transitions to be red-shifted and C=S $n \rightarrow \pi^*$ transitions to be blue-shifted.^[142] The spectroscopic influence of a nitrogen bound hydroxylaminyl substituent, conjugated π -systems, or additional heteroatoms bound to the thiocarbonyl chromophore have until today not been investigated in detail. This lack in information, prevents a satisfying interpretation of electronic transitions in UV/vis-spectra of the heterocyclic thiohydroxamate-derived *O*-radical precursors. However, without detailed informations about these spectroscopic properties an optimization of these important precursor molecules is not possible. So the first step of this work is a combined experimental and theoretical study on the UV/vis-spectra of selected heterocyclic thiones.

Modern computational chemistry offers a considerable diversity of methods for calculating electronically excited states and with this the possibility to describe UV/vis spectra. The multireference configuration interaction method (MRCI)^[35,98] and an approach which combines the complete active space ansatz (CASSCF)^[28,29] for the wave function to account for the near-degeneracy effects, with a perturbational treatment in second order to include dynamical correlation (CASPT2^[30,31]), are known for the prediction of very accurate vertical excitation energies and are well suited to describe photochemical reactions. However, they are very time consuming and demand quite a big amount of hardware resources. TD-DFT approaches are much faster and less demanding, but the achieved accuracies are considerably lower. For example TD-DFT in combination with the commonly applied exchange correlation (*xc*) functionals are known to possess problems to describe charge transfer transitions or Rydberg states precisely^[36,109–111,114] (compare subsection 3.2.1). Fabian and coworkers have demonstrated that the TD-DFT approach in association with a hybrid functional is able to describe electronic excitations involving the thiocarbonyl chromophore^[142] being one of the chromophores of *N*-(alkoxy)-pyridine-2(1*H*)-thiones (**1a-OR**) and *N*-(alkoxy)-thiazole-2(3*H*)-thiones (**2a-OR**). The effects of substituents at the thiocarbonyl carbon atom on the energetic positions of the $n \rightarrow \pi^*$ and the $\pi \rightarrow \pi^*$ excitation were reproduced with an excellent precision. Even if a considerable intramolecular charge transfer from a donor group to the thiocarbonyl acceptor group occurs, the transition energies are not that erratic as in the case of other intramolecular charge transfer transitions. Another approach to calculate excitation energies is the CC2 model.^[41] It represents an approximation of the Coupled Cluster method including single and double excitation (CCSD) and gives excitation energies for single excitations correct through second order in the electron fluctuation potential. If the wave function of the excited state is dominated by single replacements out of the reference determinant CC2 gives vertical excitation energies typically correct within $\Delta E \leq 0.3$ eV^[143,144] but sometimes an accuracy of even 0.1 eV is found.^[145] Combining the CC2 model with the RI approximation^[122,123] (RI-CC2) the CC2 model gets quite efficient^[42,43] and can be employed for rather large molecules. Besides its efficiency it has the advantage that it describes charge-transfer states correctly.

The first aim of this chapter is to find theoretical approaches that are adequate in order to reproduce the structure and the experimental UV/vis spectral characteristics of known pyridine-2(1*H*)-thione and of thiazole-2(3*H*)-thione alkoxy radical precursors. The TD-DFT approach in combination with various functionals, the RI-CC2 method, and the CASPT2 approach are tested for this purpose.

A comparison of the obtained theoretical excitation energies between those different approaches and with experimentally recorded UV/vis spectra served as a validation of the applied functionals for the TD-DFT approach. This is necessary since TD-DFT is the only quantum chemical approach that is able to calculate electronic excitation spectra of many

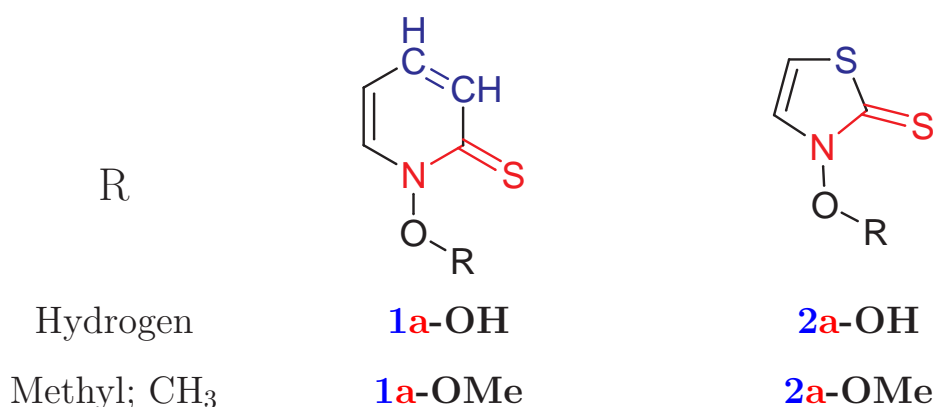


Figure 4.1: The enumeration scheme for the parent compounds of the alkoxy radical precursors on the basis of the pyridine-2(1*H*)-thione and thiazole-2(3*H*)-thione heterocycle. The blue atoms (**number**) represent the type of heterocycle while the red atoms (**letter**) define the type of functional group.

different larger organic molecules in an efficient and fast way. The so obtained knowledge about theoretical possibilities to describe the electronic transitions in heterocyclic thiohydroxamic compounds serves as tool for the interpretation of substituent effects on the UV/vis spectra of the pyridine and thiazole compounds (Chapter 6) and also for the prediction of spectroscopic properties of new compounds (Chapter 7). After this validation step the assignment of the experimental observed UV/vis bands of the known *N*-(hydroxy)-pyridine-2(1*H*)-thione (**1a-OH**), *N*-(methoxy)-pyridine-2(1*H*)-thione (**1a-OMe**) and the corresponding thiazole-2(3*H*)-thiones (**2a-OH** and **2a-OMe**) to electronic transitions was performed.

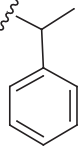
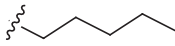
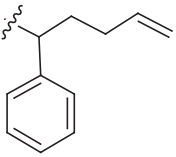
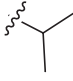
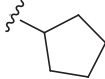
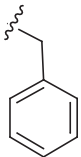
R	name	R	name
Methyl, CH ₃	4me5h		1phenylethyl
	npentyl		1phenyl4pentenyl
	ipropyl		
	cpentyl		
	benzyl		

Figure 4.2: The name scheme for the various calculated *N*-alkoxy esters (**4me5h-OR**) of *N*-(hydroxy)-4-methylthiazole-2(3*H*)-thione (**4me5h-OH**).

To apply the alkoxy radical precursors on the basis of the thiazolethione heterocycle in

mechanistic and synthetic studies of the cyclization of substituted 4-penten-1-oxyl radicals to furanes a knowledge of the effects of various types of alkoxy substituents at the thiazole nitrogen atom on the electronic spectra of these photochemical precursor molecules is necessary. The last part of this chapter therefore deals with a combined theoretical and experimental study on such effects. Primary, secondary and benzylic O-esters of *N*-(hydroxy)-4-methylthiazole-2(3*H*)-thione (**4me5h-OH**) were prepared and their UV/vis spectra were measured. Theoretical simulations of the electronic spectra gave detailed information about the effects of *N*-alkoxy substituents in the UV/vis properties of the *N*-(alkoxy)-thiazole-2(3*H*)thiones (**2a-OR**).

4.1 Theoretical Details

All DFT, TD-DFT and RI-CC2 calculations were performed with the TURBOMOLE program package^[125] while CASSCF^[28,29] and CASPT2^[30,31] computations were performed with the MOLCAS program.^[129]

All vertical excitation energies were computed for theoretically determined ground state structures. They were obtained with the BLYP/SVP approach^[119,127,147,148] applying the resolution of identity (RI) approximation.^[122,123] This approximation is included since it is often the only practical tool if many and large molecules shall be screened. To study resulting errors, vertical excitation energies for the parent compounds **1a-OH**, **1a-OMe**, **2a-OH** and **2a-OMe** were also computed for ground state structures obtained with the RI-MP2/cc-pVTZ approach.^[149–151] CASSCF computations for calculating vertical excitation energies were done with different active spaces. For the PT2 computations the G3 approach^[152] for the fock matrix, and the multi-state variant (MS-CASPT2)^[40] were used. For these computations the cc-pVTZ basis sets^[150,151] were applied on all atoms except of the hydrogen atoms and the methoxy carbon atom in *N*-(methoxy)-pyridine-2(1*H*)-thione **1a-OMe**. These atoms had to be described with the cc-pVDZ basis sets^[150,151] due to software and hardware limitations. CAS computations in which the cc-pVTZ basis sets were enlarged by diffuse functions (2s,2p, table 4.1 for an example) failed due to hardware limitations. Their influence has been estimated by computations employing the smaller TZVP basis with and without one diffuse sp set (table 4.1). This approximation seems to be valid since all approaches showed nearly the same influence of the diffuse functions. Oscillator strengths within the CAS approach were obtained with the restricted active space state interaction program^[131] (RASSI) together with the 12/12 CAS space. In these computations the cc-pVDZ basis sets were used due to limitations in the computer resources. For time-dependent density functional theory (TD-DFT) methods and the RI-CC2 ansatz TZVP^[153]

	TZVP-dif		cc-pVTZ-dif	
	exponent ζ	coefficient χ	exponent ζ	coefficient χ
Sulfur	(14s/15s9p/10p1d)	[5s/6s4p/5p1d]	(41s/43s16p/18p2d1f)	[7s/9s4p/6p2d1f]
	7s		13s	
	⋮	⋮	⋮	⋮
	3s		13s	
	⋮	⋮	⋮	⋮
	2s		13s	
	⋮	⋮	⋮	⋮
	1s		1s	
	0.40541030112	1.0000000000	0.77670000000	1.0000000000
	1s		1s	
	0.14550651059	1.0000000000	0.13220000000	1.0000000000
	1s		1s	
	0.07	1.0000000000	0.06500000000	1.0000000000
	6p		1s	
	⋮	⋮	0.03000000000	1.0000000000
	1p		7p	
	0.83882201296	1.0000000000	⋮	⋮
	1p		7p	
	0.31288746900	1.0000000000	⋮	⋮
	1p		1p	
	0.10770109004	1.0000000000	0.86880000000	1.0000000000
	1p		1p	
	0.050000000000	1.0000000000	0.10980000000	1.0000000000
	1d		1p	
	0.55000000000	1.0000000000	0.05500000000	1.0000000000
	aux-TZVP-dif		1p	
	1s		0.02500000000	1.0000000000
	0.1354	1.00	1d	
	1p		0.26900000000	1.0000000000
	0.1469	1.00	1d	
	1d		0.81900000000	1.0000000000
	0.1292	1.00	1f	
	1f		0.55700000000	1.0000000000
	0.3000	1.00		
	1f			
	0.0960	1.00		
	1g			
	0.3500	1.00		

Table 4.1: An example for the augmentation of the TZVP and cc-pVTZ basis sets with diffuse functions (red entries) for the sulfur atoms. The diffuse functions^[146] that were augmented to the auxiliary basis sets of the TURBOMOLE^[125] to perform RI-TD-DFT and RI-CC2 calculations are also shown.

and cc-pVTZ^[150,151] basis sets (together with the matching auxiliary basis sets^[123,149] in case of RI calculations) were applied. Additionally, the influence of diffuse functions was tested. The TZVP basis sets were supplemented with one diffuse s and one diffuse p function. To the cc-pVTZ basis two diffuse s and two diffuse p functions were added (for an example compare table 4.1). Within TD-DFT the BLYP,^[119,127] the B3LYP,^[118] the BHLYP,^[154] and the PBE0^[120,121] functionals were applied. For BLYP calculations, the RI approximation in the time-dependent formalism (RI TD-DFT)^[124] was used. For RI computations with diffuse functions the auxiliary basis sets were modified according to the literature^[146] (table 4.1, entry aux-TZVP-dif for an example).

The assignment of the electronic excitations was done on the TD-B3LYP/TZVP//RI-BLYP/SVP level of theory. The corresponding B3LYP orbitals are characterized according to the shape of a density plot obtained with the MOLDEN^[155] program.

4.2 Equilibrium Structures of the Parent Compounds

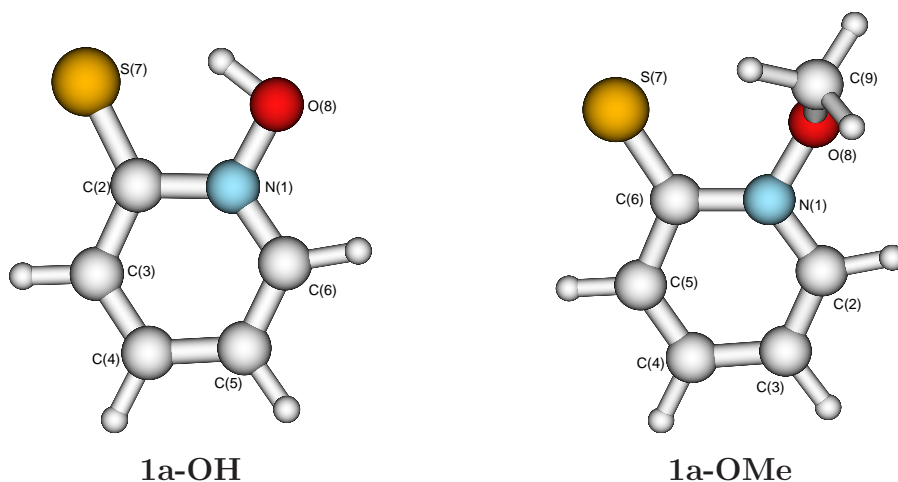
The computed equilibrium structures of the parent compounds of the precursors on the basis of the pyridine heterocycle *N*-(hydroxy)-pyridine-2(1*H*)-thione (**1a-OH**) and *N*-(methoxy)-pyridine-2(1*H*)-thione (**1a-OMe**) are compared to a X-ray structure of the corresponding molecule (free acid **1a-OH**)^a, respectively with the measured solid state structure of *N*-*trans*-(*tert*-butyl-cyclohexyl)-4-oxy derivative^b since **1a-OMe** could not be crystallized until today.

The RI-MP2/cc-pVTZ ground state structures (right values in table 4.2) are slightly more compact than the one obtained with RI-BLYP/SVP (left values in table 4.2), *e.g.* all bond distances decrease by about 0.02 Å.

The heterocyclic core of the pyridinethione compounds is best described as a distorted planar hexagon with alternating bond lengths. The sequence of shorter (*e.g.* C³-C⁴; C⁵-C⁶) and longer bonds (*e.g.* C⁴-C⁵) is in nice agreement with the distances obtained from the X-ray crystallographic analysis. The same is found for the N,O and the C,S distances. The calculated angles N¹-C²-C³ are the smallest and the adjacent angles C²-N¹-C⁶ the largest within the six-membered rings. The acidic OH proton of the hydroxyl derivate (**1a-OH**)

^aSelected geometrical parameter for *N*-(hydroxy)-pyridine-2(1*H*)-thione (**1a-OH**) (X-ray diffraction): N³-C² = 1.367(3) Å, C²-C³ = 1.400(4) Å, C³-C⁴ = 1.349(4) Å, C⁴-C⁵ = 1.372(5) Å, C⁵-C⁶ = 1.344(4) Å, N¹-O⁸ = 1.377(3) Å, C²-S⁷ = 1.684(2) Å, C²-N¹-C⁶ = 125.5(2)°, C³-C²-N¹ = 113.5(2)°, C²-C³-C⁴ = 122.1°, C³-C⁴-C⁵ = 120.8°.^[21]

^bSelected geometrical parameter for *N*-[*trans*-(*tert*-butylcyclohexyl)-4-oxy]-pyridine-2(1*H*)-thione (X-ray diffraction): C²-C³ = 1.411(6) Å, C³-C⁴ = 1.338(6) Å, C⁴-C⁵ = 1.392(7) Å, C⁵-C⁶ = 1.344(6) Å, C³-C²-N¹ = 112.4(4)°, C²-N¹-C⁶ = 125.3(3)°, C²-N¹-O⁸-C⁹ = 99.9(3)°.^[37]

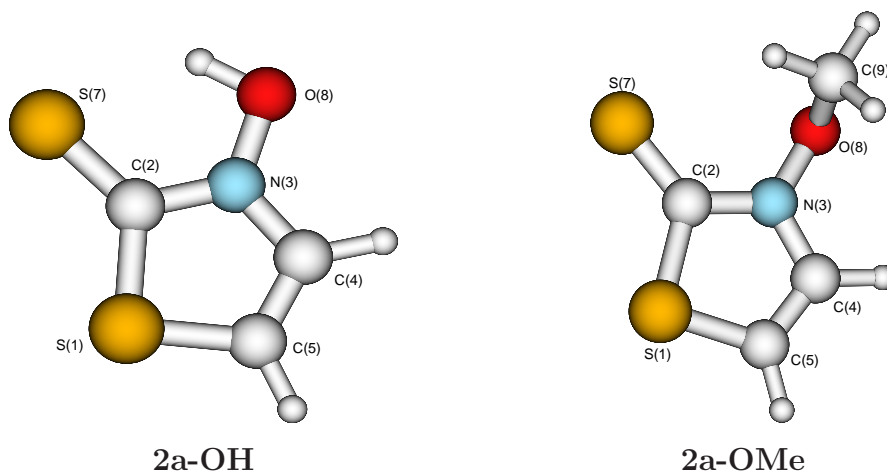


Parameter	1a-OH	1a-OMe
N ¹ -C ² [Å]	1.415 / 1.382	1.421 / 1.390
C ² -C ³ [Å]	1.433 / 1.417	1.450 / 1.432
C ³ -C ⁴ [Å]	1.392 / 1.378	1.389 / 1.371
C ⁴ -C ⁵ [Å]	1.422 / 1.403	1.431 / 1.410
C ⁵ -C ⁶ [Å]	1.389 / 1.374	1.380 / 1.367
C ⁶ -N ¹ [Å]	1.363 / 1.347	1.375 / 1.358
C ² -S ⁷ [Å]	1.701 / 1.681	1.681 / 1.662
N ¹ -O ⁸ [Å]	1.371 / 1.359	1.400 / 1.379
O ⁸ -R [Å]	1.037 / 1.013 (R = H)	1.451 / 1.438 (R = C ⁹)
C ² -N ¹ -C ⁶ [°]	125.2 / 126.1	125.4 / 126.3
N ¹ -C ² -C ³ [°]	114.0 / 113.6	112.2 / 112.0
C ² -C ³ -C ⁴ [°]	122.0 / 122.2	123.3 / 123.5
C ³ -C ⁴ -C ⁵ [°]	120.4 / 120.0	120.4 / 120.1
N ¹ -O ⁸ -R [°]	99.5 / 99.3 (R = H)	112.1 / 109.1 (R = C ⁹)
S ⁷ -C ² -N ¹ -O ⁸ [°]	0.0 / 0.0	-5.1 / -1.9
C ² -N ¹ -O ⁸ -R [°]	0.0 / 0.0 (R = H)	82.3 / 81.9 (R = C ⁹)

Table 4.2: RI-BLYP/SVP (left values) and RI-MP2/cc-pVTZ (right values) optimized equilibrium structural parameters of *N*-(hydroxy)-pyridine-2(1*H*)-thione (**1a-OH**) and *N*-(methoxy)-pyridine-2(1*H*)-thione (**1a-OMe**).

forms an intramolecular hydrogen bond to the sulphur center of the thiocarbonyl group as it was found in the solid state structure of *N*-(hydroxy)-pyridine-2(1*H*)-thione. In the *O*-methyl ester no hydrogen bond can be formed and the methoxy substituent is rotated out of the heterocyclic plane in *N*-(methoxy)-pyridine-2(1*H*)-thione (**1a-OMe**) (C²-N¹-O⁸-C⁹ = 82.3° / 81.9°). This also correlates well with the X-ray data from the corresponding

substructure of the *trans*-*N*-*tert*-butylcyclohexyl-4-oxy derivative.



Parameter	2a-OH	2a-OMe
S ¹ -C ² [Å]	1.788 / 1.735	1.811 / 1.753
C ² -N ³ [Å]	1.380 / 1.351	1.392 / 1.371
N ³ -C ⁴ [Å]	1.386 / 1.367	1.396 / 1.375
C ⁴ -C ⁵ [Å]	1.368 / 1.358	1.362 / 1.354
C ⁵ -S ¹ [Å]	1.766 / 1.726	1.768 / 1.730
C ² -S ⁷ [Å]	1.678 / 1.664	1.658 / 1.648
N ³ -O ⁸ [Å]	1.380 / 1.360	1.392 / 1.371
O ⁸ -R [Å]	1.012 / 0.996 (R = H)	1.452 / 1.440 [R = C ⁹]
C ² -N ³ -C ⁴ [°]	118.5 / 118.6	118.6 / 118.5
S ¹ -C ² -N ³ [°]	106.4 / 106.7	105.1 / 105.6
C ⁵ -S ¹ -C ² [°]	92.0 / 92.7	92.8 / 93.4
N ³ -C ⁴ -C ⁵ [°]	112.0 / 111.2	112.8 / 111.9
N ³ -O ⁸ -R [°]	100.0 / 99.4 (R = H)	111.9 / 109.2 [R = C ⁹]
S ⁷ -C ² -N ³ -O ⁸ [°]	0.0 / 0.0	-6.8 / -3.1
C ² -N ³ -O ⁸ -R [°]	0.1 / 0.0 (R = H)	82.5 / 80.7 [R = C ⁹]

Table 4.3: RI-BLYP/SVP (left values) and RI-MP2/cc-pVTZ (right values) optimized equilibrium structural parameters of *N*-(hydroxy)-thiazole-2(3*H*)-thione (**2a-OH**) and *N*-(methoxy)-thiazole-2(3*H*)-thione (**2a-OMe**).

The parent compounds of the precursors on the basis of the thiazole heterocycle *N*-(hydroxy)-thiazole-2(3*H*)-thione (**2a-OH**) and *N*-(methoxy)-thiazole-2(3*H*)-thione (**2a-OMe**) have hitherto not been synthesized experimentally. Therefore the X-ray structure of the 4-methylthiazole-2(3*H*)-thione (**4me5h**) derivatives (*N*-(hydroxy)^c and *N*-(1-ethoxycarbonylpropyl)-

^cSelected geometrical parameter for *N*-(hydroxy)-4-methylthiazole-2(3*H*)-thione (**4me5h-OH**) (X-ray

2-oxy ester^d) have been selected for a comparison with the calculated structures of **2a-OH** and **2a-OMe** (table 4.3).

For the thiazolethione compounds also the RI-MP2/cc-pVTZ ground state structures (table 4.3 right values) are described more compact than the ones obtained with the DFT approach (table 4.3 left values). Especially the carbon sulfur single bonds in the heterocycles are shortened by 0.04 to 0.05 Å.

The match between computed bond lengths and angles within the thiohydroxaic group and within the heterocyclic ring agree reasonably with the geometrical parameter obtained from an X-ray analysis of *N*-(hydroxy)-4-methylthiazole-2(3*H*)-thione^c and its *N*-[(1-ethoxycarbonylpropyl)-2-oxy] ester^d. For the C,S single bonds the compacter RI-MP2/cc-pVTZ structures give a better reproduction of the measured solid state bond length. The acidic hydrogen atom is – like for the corresponding pyridine derivate **1a-OH** – part of an intramolecular hydrogen bond in the calculated structure of **2a-OH**. The experimental solid state structure of the compared 4-methyl derivate in contrast consists of hydrogen bond bridged dimers.

diffraction): S¹-C² = 1.715(10) Å, C²-N³ = 1.330(12) Å, N³-C⁴ = 1.392(12) Å, C⁴-C⁵ = 1.342(14) Å, C⁵-S¹ = 1.712(10) Å, C²-S⁷ = 1.687(10) Å, N³-O⁸ = 1.380(10) Å, C²-N³-C⁴ = 118.1(8)°, S¹-C²-N³ = 107.9(7)°, C⁵-S¹-C² = 92.2(5)°, N³-C⁴-C⁵ = 109.5(8)°.^[38]

^dSelected geometrical parameter for *N*-[(1-ethoxycarbonylpropyl)-2-oxy]-4-methylthiazole-2(3*H*)-thione (X-ray diffraction): S¹-C² = 1.724(2) Å, C²-N³ = 1.352(2) Å, N³-C⁴ = 1.399(2) Å, C⁴-C⁵ = 1.332(3) Å, C⁵-S¹ = 1.724(2) Å, C²-S⁷ = 1.658(2) Å, N³-O⁸ = 1.385(2) Å, C²-N³-C⁴ = 117.8(1)°, S¹-C²-N³ = 107.0(1)°, C⁵-S¹-C² = 92.50(8)°, N³-C⁴-C⁵ = 110.2(2)°.^[39]

4.3 Validation of the Theoretical Approaches

4.3.1 The *N*-Methoxy Compounds

<i>N</i> -(methoxy)-pyridine-2(1 <i>H</i>)-thione (1a-OMe)						
State	(12/12) CAS ^a			other CAS ^b		
	CASSCF	CASPT2	MS-CASPT2	(4/4)	(8/8)	(16/12)
S ₁	2.72 / 3.30	2.89 / 2.95	2.97 / 3.03	2.88	2.90	2.87
S ₂	3.45 / 3.82	3.09 / 3.08	3.27 / 3.24	3.14	3.32	3.04
S ₃	3.90 / 4.49	3.71 / 3.67	3.80 / 3.77	4.12	3.76	
<i>N</i> -(methoxy)-thiazole-2(3 <i>H</i>)-thione (2a-OMe)						
State	(12/12) CAS ^a			other CAS ^b		
	CASSCF	CASPT2	MS-CASPT2	(4/4)	(8/8)	(16/12)
S ₁	3.77 / 3.62	3.54 / 3.51	3.63 / 3.63	3.17	3.92	3.55
S ₂	4.80 / 4.85	3.68 / 3.66	3.86 / 3.90	3.88	3.99	3.83
S ₃	5.00 / 5.05	4.42 / 4.51	4.52 / 4.63	5.07	4.53	

^aThe ground state structures were determined with RI-BLYP/SVP (left values) and with RI-MP2/cc-pVTZ (right values), respectively. The right values also include the influence of diffuse functions (TZVP computations, see text).

^bThe MS-CASPT2 values are given, the ground state structures were determined with RI-BLYP/SVP.

Table 4.4: Complete active space results for the vertical excitation energies [eV] of the *N*-methoxy compounds **1a-OMe** and **2a-OMe**.

The results of complete active space computations for vertical electronic excitations of *N*-(methoxy)-pyridine-2(1*H*)-thione (**1a-OMe**) and *N*-(methoxy)-thiazole-2(3*H*)-thione (**2a-OMe**) using a complete active space correlating 12 electrons in the six highest occupied and six lowest virtual orbitals [(12/12) CAS] are summarized in the left part of table 4.4. The corresponding ground state structures are the previously discussed RI-BLYP/SVP (left values) and RI-MP2/cc-pVTZ structures (right values). Since CAS computations in which the cc-pVTZ basis sets were enlarged by diffuse functions (2s,2p, table 4.1 for an example) failed due to hardware limitations the values obtained on the RI-MP2 structures also contain an estimation of diffuse functions. This was done by CAS calculations with the smaller TZVP basis sets with and without the augmentation with one diffuse s and one diffuse p function (augmentation scheme compare table 4.1 left column).

The results shown in the left part of table 4.4 underline the importance of the use of second order perturbation theory in order to obtain reliable excitation energies. The differences between the normal (G3 ansatz for the Fock matrix) and the multistate (MS) variant are

generally ≤ 0.1 eV. For the S_2 state of thiones **1a-OMe** and **2a-OMe**, a difference of 0.2 eV is found, indicating some mixing. For **1a-OMe** the CASPT2 or MS-CASPT2 values change less than 0.1 eV if the vertical excitation energies are computed for the RI-MP2/cc-pVTZ ground state structures and if the influence of diffuse functions is included. For the S_1 and S_2 states of **2a-OMe** the RI-MP2/cc-pVTZ ground state structure leads to slightly higher excitation energies (< 0.1 eV). The vertical excitation energy to the S_3 state increases by about 0.3 eV.

In the right part of table 4.4 the MS-CASPT2 excitation energies obtained with different active spaces are shown. Here smaller (4/4) and (8/8) spaces and the (16/12) complete active space were tested. The space that correlates 16 electrons in the eight highest occupied and four lowest virtual orbitals is necessary to describe the photochemically induced dissociation processes (compare chapter 5). The smaller spaces allow a faster computation of the excitation energies. A complete active space that contains four electrons and four orbitals is, as expected, not sufficient to get reliable excitation energies. For the pyridinethione compound **1a-OMe** already the correlation of eight electrons in eight orbitals seems to be adequate for the description of the vertical excitations to the first three singlet states (compared to the (12/12) CASPT2 values). For the thiazolethione heterocycle, especially for the description of the S_1 state, the large (12/12) active space is required. Slightly lower excitation energies (0.1 eV), were obtained upon the use of a (16/12) instead of a (12/12) space.

The predictions of time-dependent density functional theory (TD-DFT) applied with various functionals and of the RI-CC2 method for the *N*-(methoxy) substituted pyridine-2(1*H*)-thione (**1a-OMe**) and the corresponding thiazole-2(3*H*)-thione **2a-OMe** are summarized in table 4.5. As for table 4.4 the left values are the predictions obtained in combination with the RI-BLYP/SVP ground state structures. The excitation energies were computed with TZVP basis set. For the right values the RI-MP2/cc-pVTZ ground state structures and the cc-pVTZ basis sets augmented with diffuse basis functions (see table 4.1) were employed to obtain the excitation energies. The corresponding (12/12) MS-CASPT2 values are given for comparison (compare table 4.4).

For all methods the deviations in the excitation energies between both approaches (applied equilibrium structure and basis set size) are less than 0.1 eV. For all states of **1a-OMe** and for the S_1 and S_2 state of **2a-OMe** this results since all changes (change in basis set and structures, inclusion of diffuse basis functions) do not effect the excitation energies considerably (< 0.1 eV). For the S_3 state of **2a-OMe**, however, the small deviations results since structural and basis set effects cancel each other to some extend. The change in the structure lead to higher excitation energies of about 0.15–0.25 eV while a decrease of about 0.15–0.2 eV results from the inclusion of diffuse functions. The influence of the additional

<i>N</i> -(methoxy)-pyridine-2(1 <i>H</i>)-thione (1a-OMe) ^a						
State	CASPT2 ^b	BLYP	B3LYP	BHLYP	PBE0	RI-CC2
S ₁	2.97 / 3.03	2.24 / 2.28 ^c	2.77 / 2.83	3.32 / 3.41	2.91 / 2.98	3.13 / 3.18
S ₂	3.27 / 3.24	2.96 / 2.98	3.33 / 3.35	3.79 / 3.83	3.45 / 3.48	3.60 / 3.62
S ₃	3.80 / 3.77	3.04 / 3.05	3.58 / 3.55	4.61 / 4.55	3.76 / 3.73	4.02 / 3.93
<i>N</i> -(methoxy)-thiazole-2(3 <i>H</i>)-thione (2a-OMe) ^d						
State	CASPT2 ^b	BLYP	B3LYP	BHLYP	PBE0	RI-CC2
S ₁	3.63 / 3.63	3.27 / 3.24 ^c	3.48 / 3.50	3.74 / 3.81	3.57 / 3.61	3.74 / 3.76
S ₂	3.86 / 3.90	3.84 / 3.81	4.16 / 4.11	4.46 / 4.41	4.26 / 4.22	4.19 / 4.13
S ₃	4.52 / 4.63	3.96 / 3.99	4.40 / 4.44	4.96 / 4.99	4.54 / 4.61	4.73 / 4.73

^aThe experimental spectrum (in ethanol) shows two broad bands with maxima at 3.45 eV and 4.31 eV.

^bThe values correspond to the (12/12) MS-CASPT2 results summarized in table 4.4.

^cLeft values: ground state structures determined with RI-BLYP/SVP, excitation energies computed with the TZVP basis sets. Right values: ground state structures determined with RI-MP2/cc-pVTZ, excitation energies computed with the cc-pVTZ basis sets augmented with diffuse functions (compare table 4.1).

^dThe experimental spectrum of *N*-(methoxy)-4-methylthiazole-2(3*H*)-thione (**4me5h-OMe** in methanol), *i.e.* the 4-methyl derivative of thione **2a-OMe**, shows a broad band with a maximum at 3.87 eV.

Table 4.5: Excitation energies [eV] for the methoxy compounds **1a-OMe** and **2a-OMe** obtained with various approaches.

diffuse (sp)-basis (cc-pVTZ vs. TZVP) is small (< 0.1 eV) as expected.

MS-CASPT2 and RI-CC2 mostly agree within the expected uncertainties of both approaches. For the S₂ states of **1a-OMe** RI-CC2 predicts a higher excitations by about 0.4 eV while the deviation for the other states under consideration is 0.2 eV or less. The agreement between the MS-CASPT2 method and the various TD-DFT approaches depends strongly on the functional chosen for the TD-DFT approach and the state under consideration. The BHLYP functional generally strongly overestimates the excitation energies (0.5–0.6 eV with respect to MS-CASPT2), except of the S₁ state of **2a-OMe**, for which it agrees within a precision of 0.1 eV to the MS.CASPT2 results. The BLYP functional on the other hand considerably underestimates all excitation energies (up to 0.8 eV). Only the predicted energy location of the S₂ state of *N*-(methoxy)-thiazole-2(3*H*)-thione (**2a-OMe**) is in excellent agreement with the MS-CASPT2 result. This agreement may originate from a cancellation of errors, since all other functionals overestimate this excitation energy considerably. The PBE0 functional agrees nicely with MS-CASPT2. Except for the S₂ states of both molecules, the deviations with respect to the MS-CASPT2 values are less than 0.1 eV. For both S₂ states the deviations are 0.2 eV (for **1a-OMe**) and 0.4 eV (for **2a-OMe**). Besides the PBE0, the B3LYP functional performs reasonable since for S₁ and S₂ states it deviates by only 0.1–0.2 eV from the MS-CASPT2 results. For the S₂ state

of *N*-(methoxy)-pyridine-2(1*H*)-thione (**1a-OMe**) it possesses the best agreement with the MS-CASPT2 excitation energy.

<i>N</i> -(methoxy)-pyridine-2(1 <i>H</i>)-thione (1a-OMe) ^a						
State	RASSI ^b	BLYP	B3LYP	BHLYP	PBE0	RI-CC2
S ₁	0.03	<0.01 ^c	<0.01	0.02	0.01	<0.01
S ₂	9.19	2.51	5.14	12.7	6.09	12.6
S ₃	0.03	0.06	0.06	0.04	0.06	0.04
<i>N</i> -(methoxy)-thiazole-2(3 <i>H</i>)-thione (2a-OMe) ^d						
State	RASSI ^b	BLYP	B3LYP	BHLYP	PBE0	RI-CC2
S ₁	<0.01	0.01 ^c	0.01	0.02	0.01	0.01
S ₂	26.4	5.20	13.3	19.9	15.0	23.9
S ₃	0.03	0.06	0.06	0.07	0.06	0.10

^aThe experimental spectrum (in ethanol) shows two broad bands with maxima at 3.45 eV and 4.31 eV. According to the CASPT2 computations the maxima at 3.45 eV is assigned as the transition to the S₂ state.

^bThe (12/12) space together with the cc-pVDZ basis sets was applied.

^cThe ground state structures were determined with RI-BLYP/SVP, oscillator strength computed with the TZVP basis sets.

^dThe experimental spectrum of *N*-(methoxy)-4-methylthiazole-2(3*H*)-thione (**4me5h-OMe** in methanol), *i.e.* the 4-methyl derivative of thione **2a-OMe**, shows a broad band with a maximum at 3.87 eV which, according to the CASPT2 computations, is assigned as the transition to the S₂ state.

Table 4.6: Computed oscillator strength f [10^{-2} arb. units] for the methoxy compounds **1a-OMe** and **2a-OMe** obtained with the various approaches.

The computed oscillator strengths for transitions in the thiones **1a-OMe** and **2a-OMe** are summarized in table 4.6. All approaches agree that only excitations to the S₂ show non-vanishing transition probabilities in the near UV region.

The experimental spectrum of **1a-OMe** (in ethanol) shows two broad and featureless bands with their maxima at 3.45 eV and 4.31 eV. The experimental spectrum of *N*-(methoxy)-4-methylthiazole-2(3*H*)-thione (**4me5h-OMe**), *i.e.* the 4-methyl derivative of thione **2a-OMe** (in methanol, compare table 4.12), shows a broad band with a maximum at 3.87 eV. For *N*-(methoxy)-thiazole-2(3*H*)-thione **1a-OMe** the predictions of the CASPT2 and RI-CC2 approach for the vertical excitation energy to the UV active S₂ state bracket the experimental maximum of the lowest band (3.45 eV) while the MS-CASPT2 values computed for **2a-OMe** agrees better to the maximum of the band measured for *N*-(methoxy)-4-methylthiazole-2(3*H*)-thione (3.87 eV). The methyl substituent on position 4 is not expected to influence this band in comparison to the parent compound **2a-OMe**. For the agreement of the predictions made by the TD-DFT approach with the experimentally measured spectra the usual functional dependencies are found. Since the BLYP functional predicts the location of the S₂ state of **2a-OMe** in excellent agreement with the CASPT2 result it also

predicts the maximum of the broad UV/vis band in the measured spectra of thiazolethione compounds in a very accurate way. The hybrid functional PBE0 fails in the prediction of the excitation energies for the $S_0 \rightarrow S_2$ transitions. The fact that these transition dominates the experimental UV/vis-spectra, limits the applicability of this functional for the study of spectroscopic effects in heterocyclic thiohydroxamic-*O*-esters to some extent. For the S_2 state energy of *N*-(methoxy)-pyridine-2(1*H*)-thione (**1a-OMe**) the B3LYP functional possesses the best agreement with the maximum of the measured broad band at 3.45 eV.

4.3.2 The *N*-Hydroxy Compounds

<i>N</i> -(hydroxy)-pyridine-2(1 <i>H</i>)-thione (1a-OH) ^a						
State	CASPT2 ^b	BLYP	B3LYP	BHLYP	PBE0	RI-CC2
S ₁	3.17 / 3.28	3.04 / 3.05 ^c	3.44 / 3.48	3.92 / 3.97	3.56 / 3.61	3.63 / 3.71
S ₂	3.55 / 3.75	3.06 / 3.10	3.55 / 3.59	4.15 / 4.23	3.71 / 3.76	3.91 / 3.95
S ₃	4.35 / 4.32	3.74 / 3.73	4.23 / 4.20	4.80 / 4.78	4.41 / 4.37	4.45 / 4.47
<i>N</i> -(hydroxy)-thiazole-2(3 <i>H</i>)-thione (2a-OH) ^d						
State	CASPT2 ^b	BLYP	B3LYP	BHLYP	PBE0	RI-CC2
S ₁	3.92 / 3.88	3.74 / 3.75 ^c	3.99 / 4.05	4.31 / 4.42	4.10 / 4.17	4.21 / 4.21
S ₂	4.08 / 4.14	3.88 / 3.85	4.19 / 4.17	4.49 / 4.48	4.29 / 4.27	4.31 / 4.36
S ₃	4.58 / 5.10	3.99 / 4.00	4.47 / 4.48	5.08 / 5.07	4.61 / 4.66	4.83 / 4.80

^aThe experimental spectrum (in ethanol) shows two broad bands with maxima at 3.57 eV and 4.40 eV.

^b(12/12) MS-CASPT2 Left values: ground state structures were determined with RI-BLYP/SVP, excitation energies were computed with cc-pVTZ basis sets. Right values: ground state structures were determined with RI-MP2/cc-pVTZ, excitation energies were computed with the cc-pVTZ basis. The influence of diffuse functions was estimated with the help of TZVP computations (see text).

^cLeft values: ground state structures determined with RI-BLYP/SVP, excitation energies computed with the TZVP basis sets. Right values: ground state structures determined with RI-MP2/cc-pVTZ, excitation energies computed with the cc-pVTZ basis sets augmented with diffuse functions (compare table 4.1).

^dThe experimental spectrum of *N*-(hydroxy)-4-methylthiazole-2(3*H*)-thione (**4me5h-OH** in methanol), *i.e.* the 4-methyl derivative of thione **2a-OH**, shows a broad band with a maximum at 3.94 eV.

Table 4.7: Excitation energies [eV] for the hydroxy compounds **1a-OH** and **2a-OH** obtained with various approaches.

The calculated excitation energies for the free acids *N*-(hydroxy)-pyridine-2(1*H*)-thione (**1a-OH**) and *N*-(hydroxy)-thiazole-2(3*H*)-thione (**2a-OH**) are summarized in table 4.7. With respect to the influence of the basis set size and the ground state structure the MS-CASPT2 values for **1a-OH** and **2a-OH** possess somewhat stronger dependencies than for **1a-OMe** and **2a-OMe**. Especially for the S_2 state of **1a-OH** and the S_3 state of **2a-OH** the difference between the two approaches is 0.2 eV (S_2 state of **1a-OH**) respectively 0.52 eV

for the S_3 state of **2a-OH**. The time-dependent DFT and the RI-CC2 approach show like for the N -methoxy derivatives of both compounds nearly no dependencies ($\Delta E \leq 0.1$ eV) on the ground state structure and the basis set size.

<i>N</i> -(hydroxy)-pyridine-2(1 <i>H</i>)-thione (1a-OH) ^a						
State	RASSI ^b	BLYP	B3LYP	BHLYP	PBE0	RI-CC2
S_1	10.5	<0.01 ^c	3.95	10.1	4.66	8.86
S_2	0.02	1.91	<0.01	<0.01	<0.01	<0.01
S_3	<0.01	<0.01	<0.01	24.5	<0.01	29.0
<i>N</i> -(hydroxy)-thiazole-2(3 <i>H</i>)-thione (2a-OH) ^d						
State	RASSI ^b	BLYP	B3LYP	BHLYP	PBE0	RI-CC2
S_1	<0.01	0.02 ^c	0.02	0.02	0.02	27.2
S_2	31.3	11.1	17.7	23.4	19.2	0.02
S_3	<0.01	<0.01	0.01	0.02	0.01	0.02

^aThe experimental spectrum (in ethanol) shows two broad bands with maxima at 3.57 eV and 4.40 eV. According to the CASPT2 computations the maxima at 3.57 eV is assigned to the $S_0 \rightarrow S_1$ transition.

^bThe 12/12 CASSCF space together with the cc-pVDZ basis sets was applied.

^cGround state structures determined with RI-BLYP/SVP, oscillator strength computed with the TZVP basis sets.

^dThe experimental spectrum of *N*-(hydroxy)-4-methylthiazole-2(3*H*)-thione (**4me5h-OH** in methanol), *i.e.* the 4-methyl derivative of thione **2a-OH**, shows a broad band with a maximum at 3.94 eV, which, according to the CASPT2 computations, was assigned to the $S_0 \rightarrow S_2$ transition.

Table 4.8: Computed oscillator strength f [10^{-2} arb. units] for the hydroxy compounds **1a-OH** and **2a-OH** obtained with the various approaches.

The oscillator strengths associated with the electronic transitions in **1a-OH** and **2a-OH** are listed in table 4.8. The major structural difference between *N*-(methoxy)-substituted thiones **1a-OMe** and **2a-OMe** and *N*-(hydroxy) compounds **1a-OH** and **2a-OH** originates from an intramolecular hydrogen bond between the hydroxyl group and the thiocarbonyl sulfur atom. All methods except the BLYP functional predict that this interaction leads to an interchange of the S_1 and S_2 states in *N*-(hydroxy)-pyridine-2(1*H*)-thione **1a-OH**, if compared to *N*-(methoxy) derivative **1a-OMe**. Going from *N*-(methoxy)-thiazole-2(3*H*)-thione **2a-OMe** to *N*-(hydroxy)-thiazole-2(3*H*)-thione **2a-OH** only the RI-CC2 approach predicts an interchange of the S_1 and S_2 states. However, for **2a-OH** all methods predict that the energy separation of both states is less than 0.1 eV.

The experimental UV/vis spectra in ethanol of the free acid of the pyridinethione compound (**1a-OH**) shows three broad and featureless bands at $\lambda_{exp} = 350$ (halfwidth $\lambda = 54$ nm), 283, and 218 nm in 1:3:2.6 intensity ratio. The spectra of *N*-(hydroxy)-4-methoxythiazole-2(3*H*)-thione (4-methyl derivate of **2a-OH**), respectively, displays one featureless band with a halfwidth of $\Delta\lambda = 38$ nm ($\lambda_{exp} = 315$ nm) and a shoulder at $\lambda_{exp} = 233$ nm in a ratio of

peak heights of ca. 1.5:1. In contrast to the *N*-methoxy esters of **1a-OH** and **2a-OH** for the *N*-hydroxy compounds the estimation of the MS-CASPT2 approach for the excitation energies to the UV/vis active states (S_1 for **1a-OH** and S_2 for **2a-OH**) is not that exact. The excitation energy to the photoactive S_1 state of **1a-OH** is underestimated by more than 0.3 eV in comparison to the experiment. However, it is important to note that the measured UV/vis band is broad and that the influence of the vibrational structure is unknown.

The RI-CC2 approach overestimates the excitation energies to the photochemically active states of both molecules. The deviation from the experiment is with 0.1–0.3 eV in the usual error borders of this approach.

The various applied functionals in the frame of TD-DFT show, also for the *N*-hydroxy compounds, their usual functional dependencies. In the case of the pyridine compound **1a-OH** the hybrid functionals B3LYP and PBE0 give very accurate results compared to the UV/vis experiment. In the case of *N*-(hydroxy)-thiazole-2(3*H*)-thione **2a-OH** like for the methoxylated compound only the pure BLYP functional gives a comparable excitation energy. The hybrid functionals overestimate this photochemical important excitation by 0.3 to 0.5 eV.

4.3.3 Conclusion

Assuming that the excitations which dominate the low energy spectrum of the investigated photochemical alkoxy radical precursors are mainly dominated by a electronic transition to the S_2 state, a study about the influence of substituents on the absorption spectra of thiazolethione compounds could be performed with the BLYP functional. It predicts the near UV transition into this state correctly and it is so efficient that many large compounds can be investigated quite easily. However, for systems in which other states gain oscillator strength due to substituent effects the BLYP becomes too inaccurate. As pure density functional it could also possess strong problems with the description of charge transfer states. In order to obtain reliable descriptions for other states, from TD-DFT approaches, the hybrid functionals B3LYP or PBE0 should be applied. However, for the thiazolethione compounds the PBE0 functional is less accurate for the S_2 state so TD-DFT in combination with the B3LYP functional is an appropriate approach to investigate the spectroscopical properties of the photochemical alkoxy radical precursors on the basis of the thiazolethione heterocycle. For theoretical studies on the spectroscopic properties of alkoxy radical precursors derived from the pyridine heterocycle TD-DFT calculations applying the B3LYP functional also seem to be the best choice. The excitation energy to the spectroscopic active S_2 state is in an accuracy of $\Delta E_{exp} \leq 0.1$ eV in comparison to the experiment. If considerable charge transfer between the thiocarbonyl chromophore and possible substituents on the

heterocycles is expected the RI-CC2 approach represents an attractive choice. Its use had the advantage that possible charge transfer states would also be adequately treated. For a qualitative assignment of the experimental bands to electronic transitions all methods seem to be appropriate. For the design of new compounds the application of TD-DFT is limited by the strong functional dependency of the results. A validation of the spectroscopic properties obtained with various functionals by a comparison with CASPT2 is always recommended.

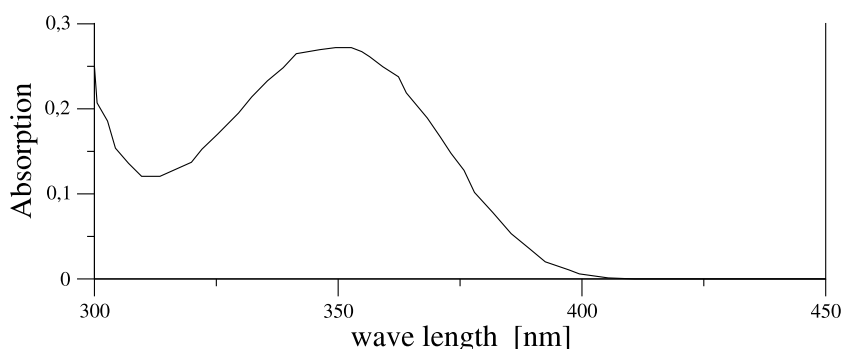
4.4 Interpretation of the UV/vis Spectra

In the previous section of this chapter the TD-DFT approach in combination with various functionals was tested to describe the experimental spectra of the parent compounds of the investigated heterocyclic alkoxy radical precursors. A comparison with the MS-CASPT2 approach yielded the B3LYP functional in combination with the TZVP basis sets on a RI-BLYP/SVP ground state structure as an efficient and accurate methodology. This computational approach is now applied to interpret the measured UV/vis spectra of the parent compounds *N*-(hydroxy/methoxy)-pyridine-2(1*H*)-thione (**1a-OH/OMe**) and *N*-(hydroxy/methoxy)-thiazole-2(3*H*)-thione (**2a-OH/OMe**).

4.4.1 The Pyridinethione Compounds

The nature of the calculated electronic excitations in the pyridinethiones **1a-OH** and **1a-OMe** in the spectral region of $\lambda > 250$ nm are characterized in table 4.9 for the free acid **1a-OH**, and in table 4.10 for the *N*-methoxy ester **1a-OMe**, respectively. The experimental UV/vis spectra of both compounds are also shown.

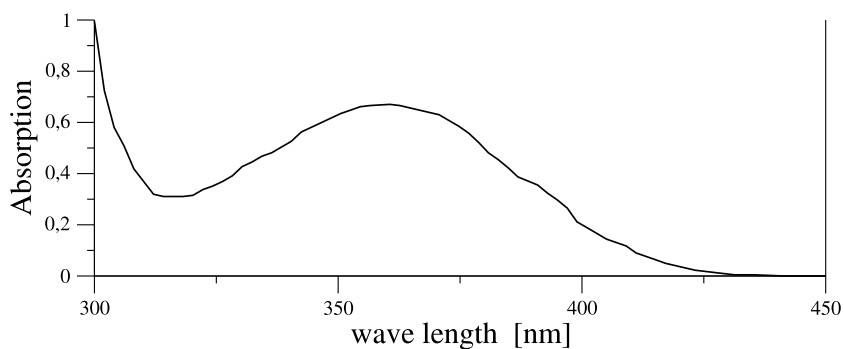
The results from the TD-B3LYP/TZVP//RI-BLYP/SVP computations predict that the electronic excitation spectrum of *N*-(hydroxy)-pyridine-2(1*H*)-thione (**1a-OH**) consists of four major electronic transitions. A transition with an oscillator strength of $f = 0.040$ is located at 361 nm and a stronger one at 278 nm ($f = 0.238$). Two additional excitations with $f < 10^{-3}$ are found at 349 nm and at 293 nm. The calculated excitation spectrum of *N*-(methoxy)-pyridine-2(1*H*)-thione (**1a-OMe**) also consists of four electronic transitions that lead to two stronger [372 nm ($f = 0.051$), 281 nm ($f = 0.272$)] and two very weak UV/vis bands (448 nm, 347 nm, both $f < 10^{-3}$). The characters of the calculated excited states are indicated by the contributing configurations which are also listed in the tables 4.9 and 4.10. The configurations are characterized by the orbital transitions out of the electronic ground state. The importance of a configuration is given by its weight. The characters of



ΔE	f	Character	Weight ^a
361 / 3.44	0.040	$\pi_{CS} \rightarrow \pi_{ring}^*$	0.921
349 / 3.55	$<10^{-3}$	$n_{CS} \rightarrow \pi_{ring}^*$	0.962
293 / 4.23	$<10^{-3}$	$n_{CS} \rightarrow \pi_{CS}^*$	0.958
278 / 4.46	0.238	$\pi_{CS} \rightarrow \pi_{CS}^*$	0.866

^aConfigurations with weights below 0.10 have, for the sake of clarity, not been considered.

Table 4.9: Excitation energies ΔE [nm / eV] and an assignment of the electronic excitations in *N*-(hydroxy)-pyridine-2(1*H*)-thione (**1a-OH**) to orbital transitions. The experimentally measured UV/vis spectra in ethanol is also shown.



ΔE	f	Character	Weight ^a
448 / 2.77	$<10^{-3}$	$n_{CS} \rightarrow \pi_{ring}^*$	0.921
372 / 3.33	0.051	$\pi_{CS} \rightarrow \pi_{ring}^*$	0.852
347 / 3.57	$<10^{-3}$	$n_{CS} \rightarrow \pi_{CS}^*$	0.884
281 / 4.41	0.272	$\pi_{CS} \rightarrow \pi_{CS}^*$	0.811

^aConfigurations with weights below 0.10 have, for the sake of clarity, not been considered.

Table 4.10: Excitation energies ΔE [nm / eV] and an assignment of electronic excitations in *N*-(methoxy)-pyridine-2(1*H*)-thione (**1a-OMe**) to orbital transitions. The experimentally measured UV/vis spectra in ethanol is also shown.

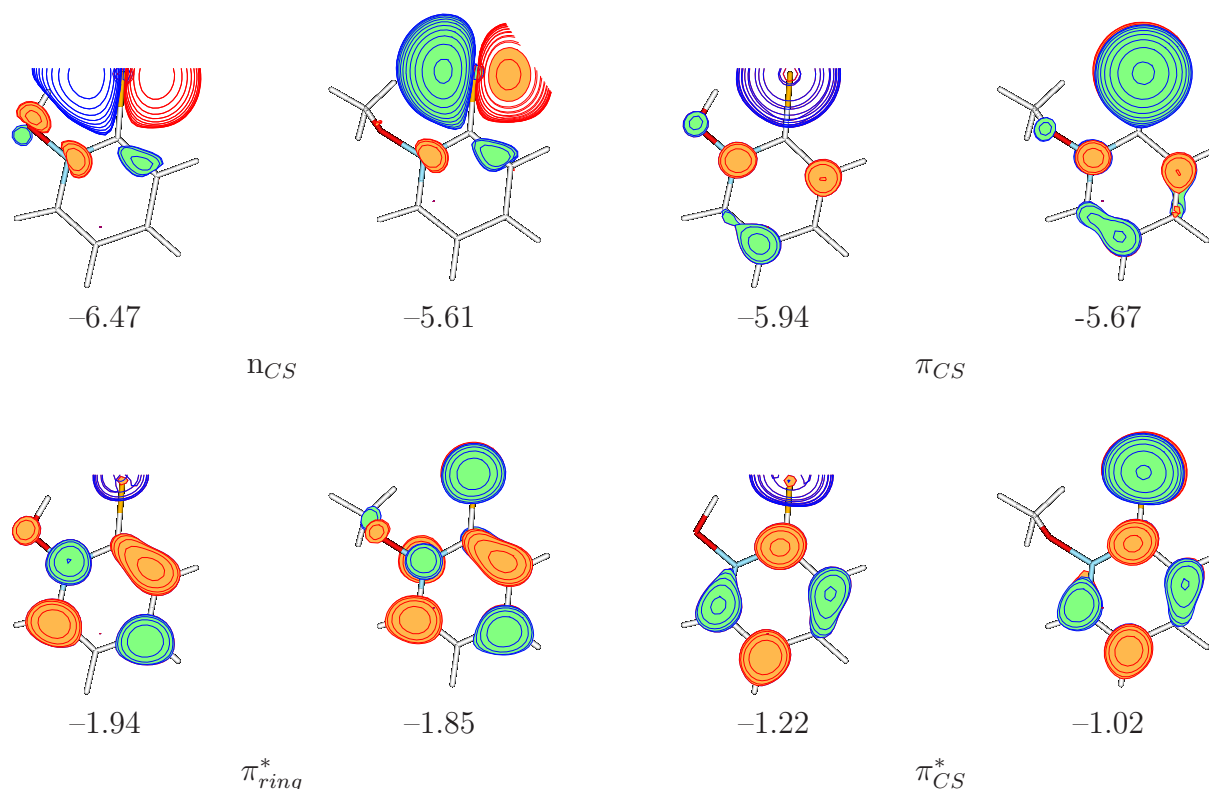


Figure 4.3: Visualization of relevant orbitals for an assignment of the configurations that contribute to the electronic spectra of the pyridine-2(1*H*)-thiones **1a-OH** and **1a-OMe**. The calculated B3LYP orbital energies are given in eV.

the computed states in **1a-OH** and **1a-OMe** are governed by one dominating configuration with weights that range between 0.997 and 0.811. The orbitals that are required for an assignment of these configurations are depicted in figure 4.3

Two occupied and two virtual orbitals are required for an assignment of the most important UV/vis bands of *N*-(methoxy)-pyridine-2(1*H*)-thione **1a-OMe** in the spectral region of $\lambda > 250$ nm. The HOMO₋₁ (π_{CS}), is dominated by contributions from the C=S π -orbital and exhibits further density at C³, C⁴, and C⁶. The HOMO (n_{CS}) of compound **1a-OMe** is largely governed by one of the lone pairs at the sulfur center (n-orbital). The illustration of the MOs of *N*-(methoxy)-pyridine-2(1*H*)-thione (**1a-OMe**) shows a more pronounced delocalization across the thiohydroxamate functionality and the bridging 1,3-butadiene-1,4-diyl entity for the virtual orbitals than for the occupied MOs. The LUMO (π_{ring}^*) shows π^* -type interactions for the thiohydroxamate functionality and contributions at C³, C⁵, and C⁶. The LUMO₊₁ (π_{CS}^*) arises from a combination of the π^* thiocarbonyl orbital and π -type orbitals at C³–C⁶. In *N*-(hydroxy)-pyridine-2(1*H*)-thione (**1a-OH**) the n_{CS} -orbital is significantly more stabilized ($\Delta\varepsilon = -0.86$ eV) in comparison to the methoxy compound than the π_{CS} -orbital ($\Delta\varepsilon = 0.27$ eV) due to the presence of an intramolecular hydrogen bond.

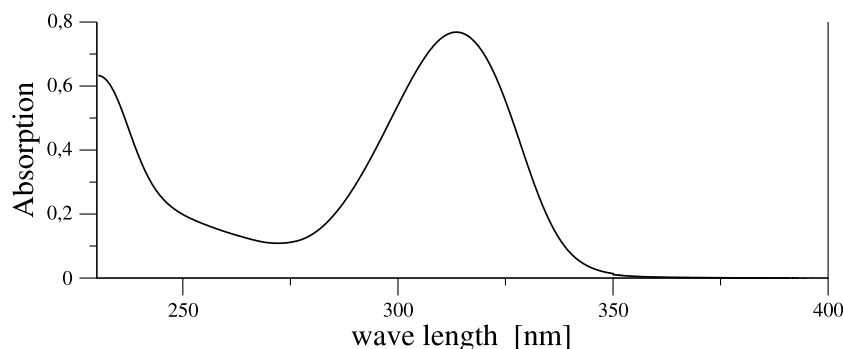
Table 4.9 and 4.10 show that electronic transitions between one of the two highest occupied (n_{CS} , π_{CS}) into one of the two lowest unoccupied orbitals (π_{ring}^* , π_{CS}^*) characterizes the configurations contributing to the excited states in **1a-OH** and **1a-OMe**. The excitation at $\lambda_{calc} = 448$ nm in *N*-(methoxy)-pyridine-2(1*H*)-thione (**1a-OMe**) originates from the $n_{CS} \rightarrow \pi_{ring}^*$ transition. This transition is symmetry-forbidden and therefore possesses vanishing oscillator strength. The next higher band at $\lambda_{calc} = 372$ nm arises from the $\pi_{CS} \rightarrow \pi_{ring}^*$ excitation. This electronic excitation is on the basis of their intensity and spectral location assigned to the measured UV/vis band at 350 nm for **1a-OH**, respectively to the band at 359 nm for **1a-OMe**. The third transition at $\lambda_{calc} = 347$ nm is predominantly due to the $n_{CS} \rightarrow \pi_{CS}^*$ transition. The strongest of the calculated bands is located at $\lambda_{calc} = 281$ nm and comes from a symmetry-allowed $\pi_{CS} \rightarrow \pi_{CS}^*$ transition. The transition to this excited state can be assigned to the strongest measured UV/vis band at 283 nm (**1a-OH**) and 288 nm (**1a-OMe**). The effect of the intramolecular H-bond in *N*-(hydroxy)-pyridine-2(1*H*)-thione (**1a-OH**) causes the $n_{CS} \rightarrow \pi_{ring}^*$ transition to be blue-shifted by 99 nm. The $n_{CS} \rightarrow \pi_{CS}^*$ excitation exhibits a hypsochromic shift to 293 nm, for the same reason. These changes are not observed in the experimental spectrum, since excitations out of n_{CS} are symmetry-forbidden and therefore associated with very weak oscillator strengths. The $\pi \rightarrow \pi^*$ -type transitions in *N*-(hydroxy)-pyridine-2(1*H*)-thione **1a-OH** are not significantly affected by the stabilization of n_{CS} thus leading only to minor blue shifts in comparison to the corresponding excitation in *N*-(methoxy)-pyridine-2(1*H*)-thione **1a-OMe** ($\Delta\lambda = 11$ nm for $\pi_{CS} \rightarrow \pi_{ring}^*$ and 3 nm for $\pi_{CS} \rightarrow \pi_{CS}^*$).

4.4.2 The Thiazolethione Compounds

Table 4.11 and 4.12 show the results of the TD-DFT calculations on the first four electronically excited states in the thiazolethione compounds **2a-OH** and **2a-OMe**. Since these compounds have so far not been synthesized, the correlation between theory and experiment has been achieved by comparing the computed UV/vis spectral characteristics to experimental data of the 4-methylthiazole-2(3*H*)-thiones (**4me5h** compare chapter 6) *i.e.* the 4-methyl derivative of the thiones **2a-OH** and **2a-OMe**.

The experimental spectrum of *N*-(hydroxy)-4-methylthiazole-2(3*H*)-thione (**4me5h-OH**) in methanol displays one featureless band with a halfwidth of $\Delta\lambda = 38$ nm ($\lambda_{exp} = 315$ nm) and a shoulder at $\lambda_{exp} = 233$ nm (halfwidth: $\Delta\lambda = 44$ nm) in a ratio of peak heights of ca. 1.5:1. For *N*-(methoxy)-4-methylthiazole-2(3*H*)-thione one broad absorption band is observed experimentally with a maximum at $\lambda_{exp} = 317$ nm (halfwidth: $\Delta\lambda = 43$ nm).

The TD-DFT computed electronic spectrum of *N*-(hydroxy)-thiazole-2(3*H*)-thione (**2a-**



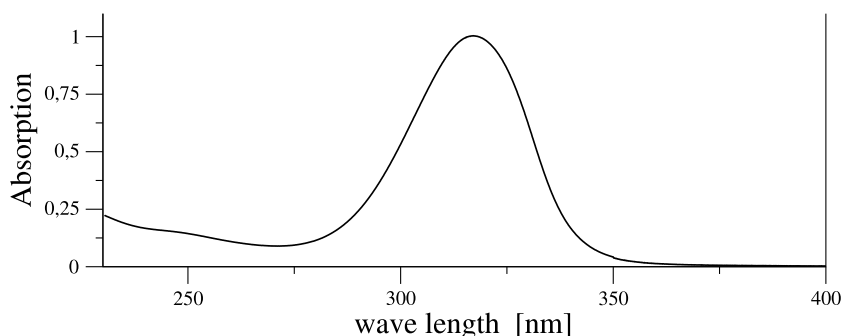
ΔE	f	Character	Weight ^a
311 / 3.99	$<10^{-3}$	$n_{CS} \rightarrow \pi_{SCS}^*$	0.974
296 / 4.19	0.177	$\pi_{SCS}^{non} \rightarrow \pi_{SCS}^*$	0.927
278 / 4.47	$<10^{-3}$	$\pi_{SCS}^{non} \rightarrow LUMO_{+1}$	0.992
247 / 5.01	0.223	$\pi_{SCS}^{non} \rightarrow LUMO_{+2}$	0.800

^aConfigurations with weights below 0.10 have, for the sake of clarity, not been considered.

Table 4.11: Excitation energies ΔE [nm / eV] and an assignment of electronic excitations in *N*-(hydroxy)-thiazole-2(3*H*)-thione (**2a-OH**) to orbital transitions. The experimentally measured UV/vis spectra of the corresponding 4-methylthiazole-2(3*H*)-thione (**4me5h-OH**) in methanol is also shown.

OH) shows two stronger transition [296 nm ($f = 0.177$), 247 nm ($f = 0.223$)] and two excitations with very small oscillator strengths [311, 278 nm ($f < 10^{-3}$ each)]. For *N*-(methoxy)-thiazole-2(3*H*)-thione **2a-OMe**, also two electronic excitations of significant intensity [298 nm ($f = 0.133$) and 256 nm ($f = 0.274$)] and two with oscillator strengths below 10^{-3} (356 and 282 nm) are predicted. The relevant orbitals for an assignment of the computed configurations in the spectra of the thiazolethiones **2a-OH** and **2a-OMe** are shown in figure 4.4.

Two occupied and three unoccupied orbitals are necessary in order to assign the first electronic transitions in *N*-(methoxy)-thiazole-2(3*H*)-thione **2a-OMe**. The $HOMO_{-1}$ (n_{CS}) is dominated by a lone pair from the thiocarbonyl sulfur atom. The HOMO (π_{SCS}^{non}) shows large contributions with opposite orbital phases at the two sulfur atoms. This MO resembles the character of the non-bonding orbital of an allylic system built from the thiocarbonyl group and the sulphur center of the five membered ring. The LUMO (π_{SCS}^*) is similarly dominated by contributions from the S-C=S fragment, this time with identical orbital phases at the two sulfur atoms. It resembles the anti-bonding orbital of the “allylic” system. The $LUMO_{+1}$ and the $LUMO_{+2}$ are strongly delocalized and exhibit complex shapes. In *N*-(hydroxy)-thiazole-2(3*H*)-thione (**2a-OH**), intramolecular hydrogen bonding



ΔE	f	Character	Weight ^a
356 / 3.48	$<10^{-3}$	$n_{CS} \rightarrow \pi_{SCS}^*$	0.978
298 / 4.16	0.133	$\pi_{SCS}^{non} \rightarrow \pi_{SCS}^*$	0.867
282 / 4.40	$<10^{-3}$	$\pi_{SCS}^{non} \rightarrow LUMO_{+1}$	0.780
		$\pi_{SCS}^{non} \rightarrow LUMO_{+2}$	0.210
256 / 4.85	0.274	$n_{CS} \rightarrow LUMO_{+1}$	0.793

^aConfigurations with weights below 0.10 have, for the sake of clarity, not been considered.

Table 4.12: Excitation energies ΔE [nm / eV] and an assignment of electronic excitations in *N*-(methoxy)-thiazole-2(3*H*)-thione (**2a-OMe**) to orbital transitions. The experimentally measured UV/vis spectra of the corresponding 4-methylthiazole-2(3*H*)-thione (**4me5h-OMe**) in methanol is also shown.

between the hydroxyl group and the thiocarbonyl sulfur atom causes a stabilization of the n_{CS} -orbital and a change in its shape, in comparison to the n_{CS} -orbital in *N*-(methoxy)-thiazole-2(3*H*)-thione **2a-OMe**. The remaining four photochemically relevant MOs, *i.e.* π_{SCS}^{non} , π_{SCS}^* , $LUMO_{+1}$, $LUMO_{+2}$, exhibit similar shapes and energies in the free acid **2a-OH** and its methyl ester **2a-OMe**.

The calculated transition at $\lambda_{calc} = 298$ nm of *N*-(methoxy)-thiazole-2(3*H*)-thione (**2a-OMe**) originates from a $\pi_{SCS}^{non} \rightarrow \pi_{SCS}^*$ excitation while the excited state at $\lambda_{calc} = 256$ nm arises due to a $n_{CS} \rightarrow LUMO_{+1}$ excitation. On the basis of their spectral locations and associated intensities, the UV/vis absorption bands at $\lambda_{exp} = 315$ nm for the *N*-(hydroxy)-4-methyl derivate of **2a-OH** and $\lambda_{exp} = 320$ nm for *N*-(methoxy)-4-methylthiazole-2(3*H*)-thione (**4me5h-OMe**) are correlated with excitations that predominantly originate from the $\pi_{SCS}^{non} \rightarrow \pi_{SCS}^*$ transitions.

In addition, two less intense transitions are present in the computed UV/vis spectrum of the thione **2a-OMe**, which originate from a symmetry-forbidden and therefore weak $n_{CS} \rightarrow \pi_{SCS}^*$ excitation ($\lambda = 356$ nm), and a $\pi_{SCS}^{non} \rightarrow LUMO_{+1}/LUMO_{+2}$ transition ($\lambda = 282$ nm). A significant stabilization of the n_{CS} -orbital causes excitations out of this orbital in *N*-(hydroxy)-thiazole-2(3*H*)-thione **2a-OH** to be blue-shifted versus the corre-

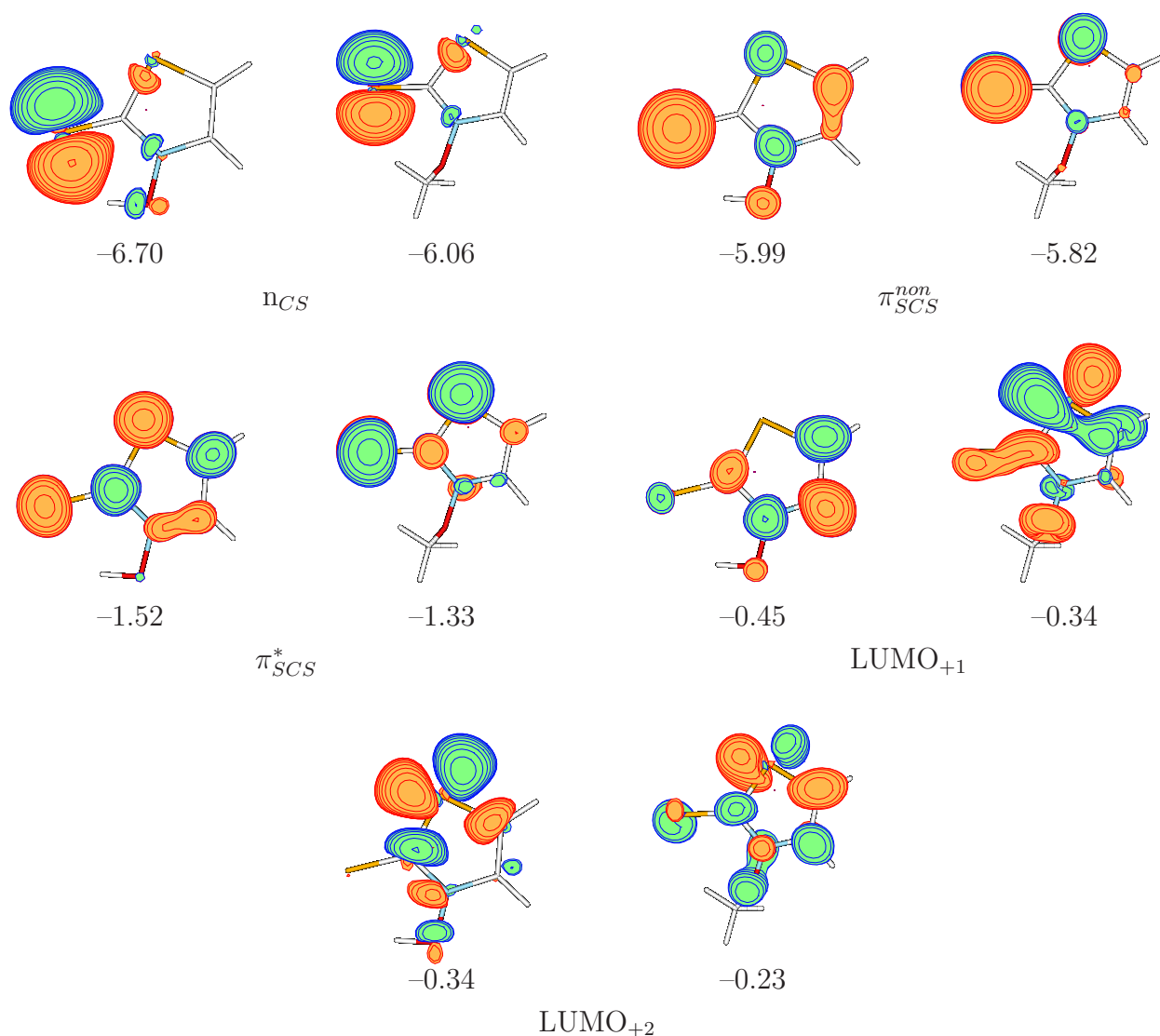


Figure 4.4: Visualization of relevant orbitals for an assignment of the configurations that contribute to the electronic spectra of the thiazole-2(3H)-thiones **2a-OH** and **2a-OMe**. The calculated B3LYP orbital energies are given in eV.

sponding bands in *N*-(methoxy)-thiazole-2(3H)-thione **2a-OMe**. The π_{SCS}^{non} -orbitals in the thiones **2a-OH** and **2a-OMe**, on the other hand, exhibit similar orbital energies thus leading to approximately the same transition energies for both molecules.

4.4.3 Experimentally known *N*-substituted Thiazolethiones

Different alkoxy substituents at the thiazolethione nitrogen atom lead to different oxygen centered radicals when photolyzed. To investigate the influence of such substituents on the spectroscopic properties of thiazole-2(3H)-thiones the electronic spectra of various

primary, secondary and benzylic *O*-esters of *N*-(hydroxy)-4-methylthiazole-2(3*H*)-thione (**4me5h-OH**) were computed. With respect to *N*-(methoxy)-thiazole-2(3*H*)thione (**2a-OMe**) in these compounds the hydrogen at C⁴ is replaced by a methyl group. The influence of this replacement on the spectrum is small (compare chapter 6). Except of the thione with the alkoxy substituent R = CH(C₂H₄CH=CH₂)C₆H₅ (**1phenyl4pentenyl**), all compounds have been previously prepared and therefore allow a concise comparison of the TD-B3LYP/TZVP//RI-BLYP/SVP calculated transition energies with results from experimental electronic spectra.

molecule	$n_{CS} \rightarrow \pi_{SCS}^*$ ^a	$\pi_{SCS}^{non} \rightarrow \pi_{SCS}^*$ ^b	higher energy transitions ^c
4me5h	351 / 3.53	292 / 4.25 (0.159)	276 / 4.50 ; 244 / 5.08
npentyl	354 / 3.51	298 / 4.16 (0.147)	278 / 4.46 ; 250 / 4.95
ipropyl	361 / 3.43	298 / 4.16 (0.142)	278 / 4.45 ; 256 / 4.85
cpentyl	358 / 3.46	297 / 4.17 (0.139)	279 / 4.44 ; 254 / 4.87
benzyl	353 / 3.52	299 / 4.15 (0.115)	300 / 4.13 ; 277 / 4.48 ; 271 / 4.57 268 / 4.63 ; 255 / 4.86
1phenyl-ethyl	358 / 3.46	299 / 4.15 (0.133)	291 / 4.26 ; 271 / 4.58 ; 270 / 4.59 266 / 4.66 ; 256 / 4.85 ; 253 / 4.90
1phenyl-4pentenyl	359 / 3.45	300 / 4.13 (0.126)	291 / 4.26 ; 270 / 4.59 ; 269 / 4.61 266 / 4.66 ; 255 / 4.86 ; 254 / 4.89

^aoscillator strength $f < 10^{-3}$

^boscillator strength f is given in parenthesis

^cTransitions into other orbitals that are computed in the spectral region of 250 – 300 nm. Their oscillator strength f are $< 4 \cdot 10^{-3}$

Table 4.13: TD-B3LYP/TZVP//RI-BLYP/SVP calculated electronic transitions [nm / eV] of various primary, secondary and benzylic *O*-esters **4me5h-OR** of *N*-(hydroxy)-4-methylthiazole-2(3*H*)-thione.

Experimental UV/vis spectra of primary [R = *e.g.* C₅H₁₁ (**npentyl**)] or secondary *O*-esters [R = cyclo-C₅H₉ (**cpentyl**) or CH(CH₃)₂ (**ipropyl**)] of *N*-(hydroxy)-4-methylthiazole-2(3*H*)-thione (**4me5h-OH**) are nearly indistinguishable.

Also the computed effect on the electronic excitation of the thiones **npentyl**, **cpentyl** and **ipropyl** in the spectral range of $\lambda > 250$ nm are small (compare table 4.13). With respect to *N*-(methoxy)-thiazole-2(3*H*)-thione, **2a-OMe**, the bands are shifted by less than 10 nm and also the computed oscillator strengths are nearly unaltered. Their spectra can therefore be interpreted using transitions calculated for **2a-OMe**. If the substituent R encloses a benzene ring like in the compounds **benzyl** (R = CH₂C₆H₅) **1phenylethyl** or **1phenyl4pentenyl** (R = CH(C₂H₄CH=CH₂)C₆H₅) additional bands in the spectral region between 250 nm and 300 nm are computed. However, their intensities vanishes (table 4.13 footnote *c*) which

explains the correspondence of the measured UV/vis spectra of the benzylic *O*-esters with the spectra of the *O*-esters containing only saturated alkyl chains.

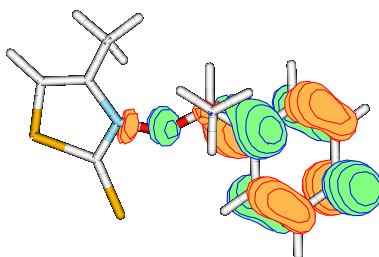


Figure 4.5: The LUMO_{+2} of *N*-(benzyl)-4-methylthiazole-2(3*H*)-thione (**benzyl**) as an example for the π_{sub}^* -orbitals of the aromatic entity of the substituents *R* in benzylic *O*-esters.

These additional excitations originate from transitions out of the π_{SCS}^{non} -orbital into π_{sub}^* -orbitals of the aromatic entity of the ester groups. The corresponding intensities vanish since the relevant orbitals are either located in the thiazole-2(3*H*)-thione moiety or the substituents (compare 4.5 for an example of a π_{sub}^* -orbital). The n_{CS} and the π_{SCS}^{non} -orbitals of the thiazolethione subunit have nearly no intensity at the oxygen center and an aliphatic carbon center within the substituent prevent any delocalization into the aromatic π -system of the benzylic substituents. As a consequence the orbitals are confined to the respective subunits (substituent or thiazole heterocycle) and furthermore no interaction between the subunits cannot occur. This explains why the computed changes within the low lying spectrum that arise due to transitions into low lying virtual orbitals of the substituents possess vanishing oscillator strengths. Computations applying the RI-CC2 model have shown that the computed excitation energies for these charge transfer transitions are underestimated by TD-DFT. RI-CC2 predicts no electronic transitions from the thiazol heterocycle to virtual orbitals of the benzylic substituents in the spectral region of $\lambda > 250$ nm.

Chapter 5

The Photochemical Alkoxy Radical Liberation

In the previous chapter a validation of various quantum chemical approaches for the calculation of electronically excited states of the pyridine-2(1*H*)-thiones **1a-OH** and **1a-OMe** and the corresponding thiazole-2(3*H*)-thiones **2a-OH** and **2a-OMe** was described. The experimentally observed UV/vis bands of these compounds were reproduced using time-dependent density functional theory (TD-DFT) in association with the B3LYP functional. According to a comparison with MS-CASPT2 results this approach is sufficient for this purpose. The experimental spectrum of *N*-(methoxy)-pyridine-2(1*H*)-thione **1a-OMe** in ethanol shows two broad bands in the near UV and visible region of the electromagnetic spectra. On the basis of computed transition energies and oscillator strengths, the lower energy band was assigned to the $S_0 \rightarrow S_2$ excitation ($\pi_{CS} \rightarrow \pi_{ring}^*$). The experimental spectrum of *N*-(methoxy)-4-methylthiazole-2(3*H*)-thione, *i.e.* the 4-methyl derivative of thiazolethione **2a-OMe**, shows one band with a maximum at 3.87 eV, which was correlated with the $S_0 \rightarrow S_2$ transition ($\pi_{SCS}^{non} \rightarrow \pi_{SCS}^*$). In view of the chemistry associated with an electronic excitation of the heterocyclic precursor molecules it is very likely that a population of the S_2 state leads to the succeeding N,O homolysis in derivatives of *N*-(methoxy)-thiazole-2(3*H*)-thione (**2a-OMe**) and *N*-(methoxy)-pyridine-2(1*H*)-thione (**1a-OMe**).

In spite of their ability to liberate alkoxy radicals, *N*-(alkoxy)-pyridine-2(1*H*)-thiones and 4- and 4,5-substituted derivatives of the *N*-(alkoxy)-thiazole-2(3*H*)-thiones behave surprisingly different, if photolyzed in the absence of trapping reagents. *N*-(4-penten-1-oxy)-pyridine-2(1*H*)-thione, undergoes highly efficient rearrangements to provide 2-(2-tetrahydro-furylmethyl-sulfanyl)-pyridines under such conditions. *N*-(4-penten-1-oxy)-thiazole-2(3*H*)-thione, on the other hand, reacts surprisingly sluggish and gives rise to several unwanted side products, if photolyzed in an inert solvent.

Another prominent example of already successfully employed heterocyclic alkoxy radical precursors are the *N*-(alkoxy)-pyridine-2(1*H*)-ones (**1b**). Those molecules on the basis of heterocyclic hydroxamic acid *O*-esters are obtained if the thiocarbonyl sulfur of the pyridinethione compounds is replaced by an oxygen atom. From the isopropyl ester derivative (**1b-OiPr**) for example isopropyl radicals are generated by an irradiation with light with a wave length of 300 nm.^[8] An in-depth investigation of the photochemistry of *N*-(hydroxy)-pyridine-2(1*H*)-one (**1b-OH**) also showed that it represents a much cleaner hydroxyl radical source^[156] than *N*-(hydroxy)-pyridine-2(1*H*)thione (**1a-OH**).

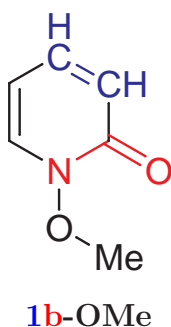


Figure 5.1: The parent compound *N*-(methoxy)-pyridine-2(1*H*)-one (**1b-OMe**) of the already employed alkoxy radical precursors on the basis of the pyridine-2(1*H*)-one heterocycle.

In order to improve the characteristics of a future generation of powerful and versatile photochemical alkoxy radical precursors, it is important to understand the differences in the photophysical and photochemical events associated with near UV/vis excitation of the heterocyclic *O*-esters in general. Therefore, the subject of this chapter is the exploration of the mechanism of the N,O homolysis in the *N*-(methoxy) compounds **1a-OMe** and **2a-OMe** using the multiconfigurational CASPT2 method. The experimental data that is already known for the *N*-(alkoxy)-pyridine-2(1*H*)-ones (derivates of **1b**) opens the possibility to test if the theoretical predictions for the mechanism of the photochemical bond homolysis also holds for a wider range of molecules. So the methoxy ester **1b-OMe** of *N*-(hydroxy)-pyridine-2(1*H*)-one (**1b-OH**) is also included in this study. In addition, it was also tested to what extend the single reference approaches TD-DFT and RI-CC2 are able to describe this photolytic dissociation process.

A detailed analysis of the obtained theoretical results gives the possibility to develop a generalized model for the prediction of the reactivity of heterocyclic precursor molecules in the photochemical alkoxy radical liberation process. This model can be applied in the design of new heterocyclic parent systems for an application in alkoxy radical photochemistry (see Chapter 7).

5.1 Theoretical Details

For the description of the N,O cleavage, all internal degrees of freedom of the molecules were optimized, using DFT on the B3LYP/SVP level of theory, at defined fixed N,O distances. This approach to obtain the structures is valid, since the energy positions of the S_1 and the S_2 state is obviously little influenced by the chosen ground state structures. These calculations were done for the S_0 ground state and the first triplet state (T_1). For calculations on the S_0 structure, a biradical wave function ($\langle S^2 \rangle = 1$) had to be used at a N,O distance of 2.25 Å in order to describe the correct fragmentation channel. In these computations this was achieved with a triplet density matrix as initial guess for the structure optimizations of the S_0 state at long N,O distances. In the following, computations, which involve an optimized structure for the first triplet state, will be abbreviated as $T_1//T_1$, $S_1//T_1$, *etc* (*i.e.* state//optimized structure). Computations, which use the ground state structures, are given as $S_0//S_0$, $T_1//S_0$ *etc*.

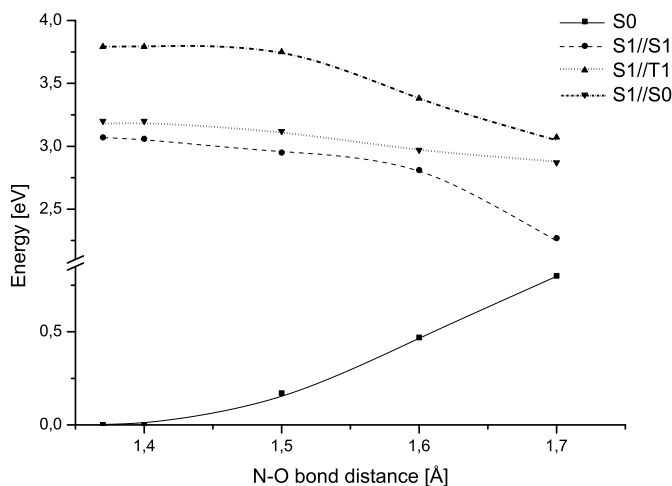


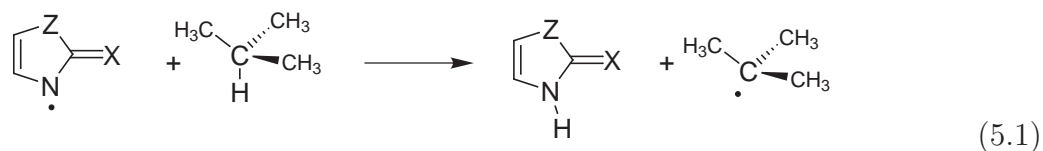
Figure 5.2: A comparison between the $S_1//S_1$, $S_1//T_1$ and $S_1//S_0$ potential curves of *N*-(methoxy)-thiazole-2(3*H*)-thione (**2a-OMe**) obtained on the TD-B3LYP/TZVP level of theory.

The S_1 state was in addition optimized using the TD-DFT gradient^[157] (B3LYP/SVP) that is implemented in TURBOMOLE. However, such optimizations were only possible up to a N,O distance of 1.7 Å. At this bond distance the HOMO-LUMO gap of the B3LYP orbitals considerably decreases. For larger bond distances the wave function of the excited state became instable (degeneration of orbitals) and the computations did not converge. In the region up to 1.7 Å, the $S_1//S_1$ curve for both molecules is slightly lower in energy than the $S_1//T_1$ curve but both are quite parallel (compare figure 5.2). This indicates that

the computed B3LYP/SVP triplet structures represent reasonable approximations for the S_1 states in this study, at least as long as both fragments interact with each other ($R_{N,O} \leq 2.25 \text{ \AA}$).

For CASSCF and CASPT2 calculations, a (16/12) active space is necessary in order to correctly describe the N,O homolysis out of the S_0 , S_1 and S_2 states because during the bond breaking process a strong mixing between these orbitals occurs. With smaller active spaces (*e.g.* with a (12/12) complete active space) a reliable description of this photochemical process in the S_1 and the S_2 state is not possible. Since diffuse functions seem to have little influence on the energy position of the S_1 and the S_2 state (compare section 4.3) Dunning's cc-pVTZ basis sets were used.

For the description of the important states of the non-interacting methoxy radical ($R_{N,O} > 4.0 \text{ \AA}$) the results of Höper *et. al.*^[52] who applied large scale MR-CI calculations were used.



Differences between the behaviour of *N*-(methoxy)-thiazole-2(3*H*)-thione (**2a-OMe**) and *N*-(methoxy)-pyridine-2(1*H*)-thione (**1a-OMe**) could result from differences in the reactivity of the resulting radicals. To estimate the different intrinsic reactivities of the resulting heterocyclic radical fragments ($X=\text{S}, Z=\text{C}_2\text{H}_2 \hat{=} \mathbf{1a}^\bullet$; $X=\text{O}, Z=\text{C}_2\text{H}_2 \hat{=} \mathbf{1b}^\bullet$; $X=\text{S}, Z=\text{S} \hat{=} \mathbf{2a}^\bullet$) and the methoxy radical the isodesmic hydrogen abstraction reactions, corresponding to the example given in equation 5.1, were applied. This was done by computing the reaction energies ΔE ($E_{\text{products}} - E_{\text{educts}}$) of this reaction of isobutane with the radical fragments (**1a** $^\bullet$, **2a** $^\bullet$, **1b** $^\bullet$, **OMe** $^\bullet$) on the B3LYP/TZVP//RI-BLYP/SVP level of theory.

5.2 The N,O Bond Homolysis

5.2.1 *N*-(Methoxy)-Thiazole-2(3*H*)-thione (**2a-OMe**)

The methoxy radical (**OMe** $^\bullet$) and the thiazyl-2-sulfanyl radical (**2a** $^\bullet$) are formed upon near UV excitation of *N*-(methoxy)-thiazole-2(3*H*)-thione **2a-OMe** (equation 5.2).

The potential energy curves associated with the N,O homolysis of *N*-(methoxy)-thiazole-2(3*H*)-thione (**2a-OMe**) starting from different states are depicted in figure 5.3. All curves of the excited states, $T_1//T_1$, $S_1//T_1$, and $S_2//T_1$ are repulsive with respect to the N,O bond thus would lead to a direct homolysis of this connectivity. The T_1 state correlates

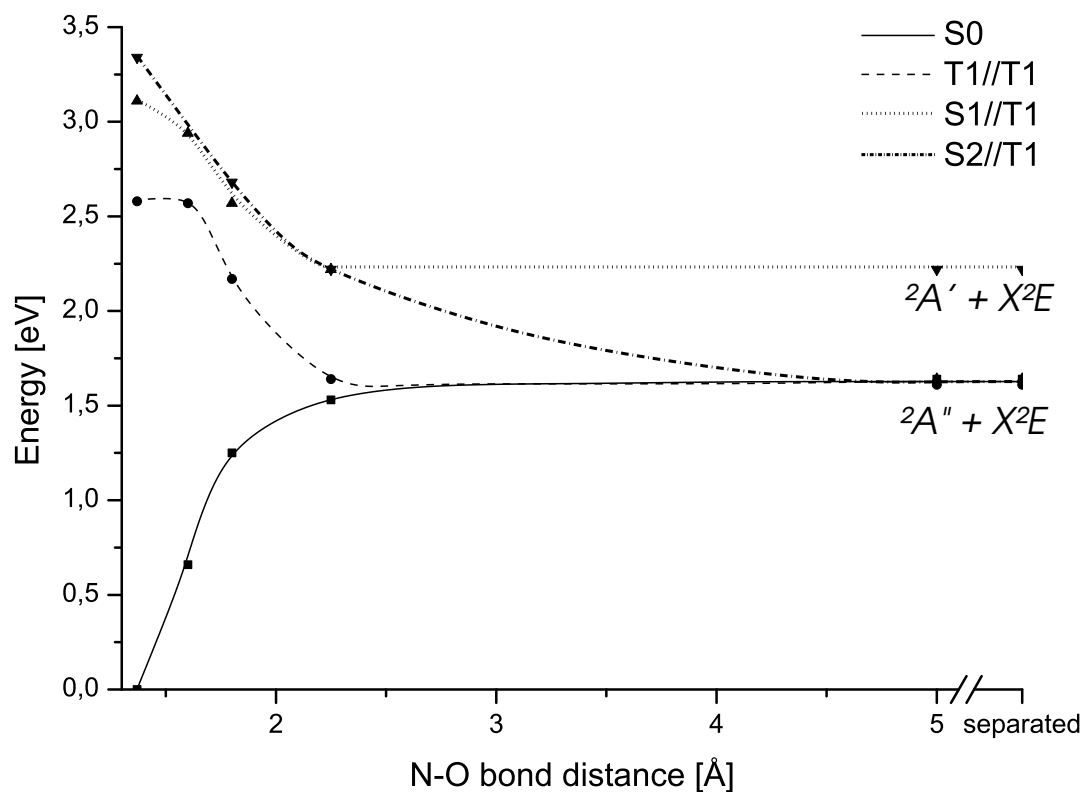
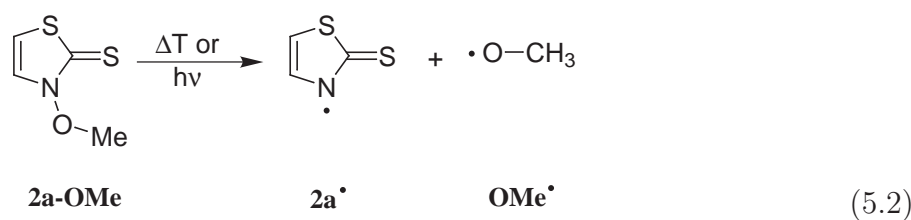


Figure 5.3: Potential curves for the thermal and photolytic N,O homolysis in *N*-(methoxy)-thiazole-2(3*H*)-thione (2a-OMe) obtained with the (16/12) CASPT2 approach.

with the energetic lowest dissociation channel while the S_1 and the S_2 state are connected with the next two higher pathways (figure 5.3).

For a thermally induced cleavage along the S_0 state, the computed dissociation energy is 1.65 eV (159 kJ mol⁻¹)^a. Due to their size consistence with single reference approaches like DFT and CC2 the dissociation energy can be computed as the difference between the equilibrium structures and the sum of the energies of both separated fragments. For the

^aThe S_0 dissociation energies computed on the 16/12 CASPT2/cc-pVTZ//RI-MP2/cc-pVTZ level of theory.

computations employing the CASPT2 approach the dissociation energy has to be computed as difference between the equilibrium structures and a structure with a N,O bond distance of $R_{N,O} = 5 \text{ \AA}$. For this bond distance both fragments show now interactions.

Near UV absorption of *N*-(methoxy)-thiazole-2(3*H*)-thione (**2a-OMe**) will populate primarily the S_2 state and not the S_1 state due to the significant difference in oscillator strengths of the transitions going into these states starting from the S_0 state at the equilibrium structure (table 4.6). A N,O homolysis in **2a-OMe** along the S_2 state would provide the thiazyl-2-sulfanyl radical (**2a•**) in its first excited state (${}^2A'$), while the methoxyl radical (**OMe•**) is formed in its degenerated \tilde{X}^2E ground state. The energetic positioning of this third channel is therefore computed as vertical excitation energy of the thiazyl-2-sulfanyl radical (**2a•**). The corresponding orbitals (see figure 5.4) indicate that in the ${}^2A''$ ground state of **2a•** the unpaired electron is delocalized over the whole heterocycle and the exocyclic sulfur atom (π -orbital). In its first excited state (${}^2A'$) the SOMO of **2a•** represents the n_{CS} -orbital of the thiocarbonyl sulfur atom.



Figure 5.4: The SOMOs (semi occupied molecular orbitals) of the two energetic lowest electronic states of the thiazyl-2-sulfanyl radical (**2a•**).

However, the photochemically induced homolysis of the N,O bond in thione **2a-OMe** along the S_2 potential energy surface is unlikely to occur. The very small energy gap between the $S_2//T_1$ and $S_1//T_1$ potentials at $R_{N,O} = 2.25 \text{ \AA}$ and the shape of both surfaces indicate a crossing of both states. This is also indicated from an analysis of the wave function and the orbitals. However, a final prove was not possible in the scope of these calculations. Even if no conical intersection exists the tiny energy gap would lead to an efficient quenching from the S_2 to the S_1 state. Once the relaxation of the excited molecule into the S_1 state has occurred it can cross into the energetic lower T_1 state because the two states are coupled via spin-orbit interaction. On the other hand, a dissociation starting on the S_1 surface is also feasible because this state is repulsive with respect to the N,O connectivity. Starting from the S_1 level, the methoxyl radical is generated in its first excited state and the thiazyl-2-sulfanyl radical (**2a•**) in its electronic ground state. A cleavage along the T_1 state would

generate both fragments in their electronic ground states.

For the reactivity of the generated radicals it is irrelevant whether the cleavage proceeds along the S_1 or along the T_1 state since both lower channels are connected with the degenerated ground state \tilde{X}^2E of the methoxyl radical (**OMe** \bullet). Due to the Jahn-Teller distortion the \tilde{X}^2E state splits into a $^2A'$ (connected with the homolysis along the T_1 state) and a $^2A''$ (connected with the S_1 state) component. According to extended MR-CI calculations of Höper *et. al.*^[52] the equilibrium structure of the $^2A'$ component lies only about 200 cm^{-1} (0.02 eV) below the C_{3v} structure and only 37 cm^{-1} below the equilibrium structure of the $^2A''$. Due to this near degeneracy and since both channels are strongly coupled via rovibronic effects in both cases a very fast relaxation to the lowest channel (both fragments in their ground state) will take place. As a consequence the arising methoxyl radical is generated in its electronic ground state no matter whether the cleavage proceeds along the S_1 or along the T_1 state. The same arguments are valid for other alkoxy radicals that are formed in photochemically induced reactions from *N*-(alkoxy)-thiazole-2(3*H*)-thiones. For these molecules the degeneracy of the \tilde{X}^2E state is lifted thus leading to small energy gaps between the ground state \tilde{X} and the first excited state \tilde{A} .^[53] For the ethoxyl radical, for example, the experimental adiabatic $\tilde{A} - \tilde{X}$ excitation energy is 355 cm^{-1} (0.04 eV).^[54] For the T conformer of 1-propoxyl radical a value of 320 cm^{-1} (0.04 eV) was measured.^[54] Nevertheless the strong coupling between both low lying states remains.

Variations in the orbitals along the N,O reaction coordinate are shown in figure 5.5. For the equilibrium structure it is seen that the orbitals are primarily located at the heterocyclic core and the thiocarbonyl group. None of the low lying virtual or high lying occupied orbitals possess density at the oxygen atom. Therefore, none of these orbitals reflects an anti-bonding character with respect to the N,O bond. Such orbitals develop if the N,O bond is stretched ($R_{N,O} = 2.25\text{ \AA}$, Figure 5.5). The relatively low lying occupied molecular orbital 32 at a bond distance of $R_{N,O} = 2.25\text{ \AA}$ can be seen as the reason why smaller active spaces (*e.g.* (12/12) CAS) are not sufficient to describe all possible dissociation paths in the S_0 , S_1 and S_2 state.

The reactivity of the radicals set free by this photolytic dissociation can be estimated from their inherent reactivity and the excess energy which is deposited in both fragments due to the photolytic dissociation process. The maximal excess energy is given as the difference between the photoactive $\pi \rightarrow \pi^*$ excitation energy and the thermal dissociation energy of the ground state. The former gives the energy which is deposited in the molecule to initiate the homolytic N,O fragmentation while the latter determines the energy position of the fragments with respect to the starting point of the process. For *N*-(methoxy)-thiazole-2(3*H*)-thione (**2a-OMe**), the S_2 state ($\pi_{SCS}^{non} \rightarrow \pi_{SCS}^*$ transition), which is the starting point for the major route of N,O homolysis, is located 3.86 eV (321 nm) above the S_0 state. Taking

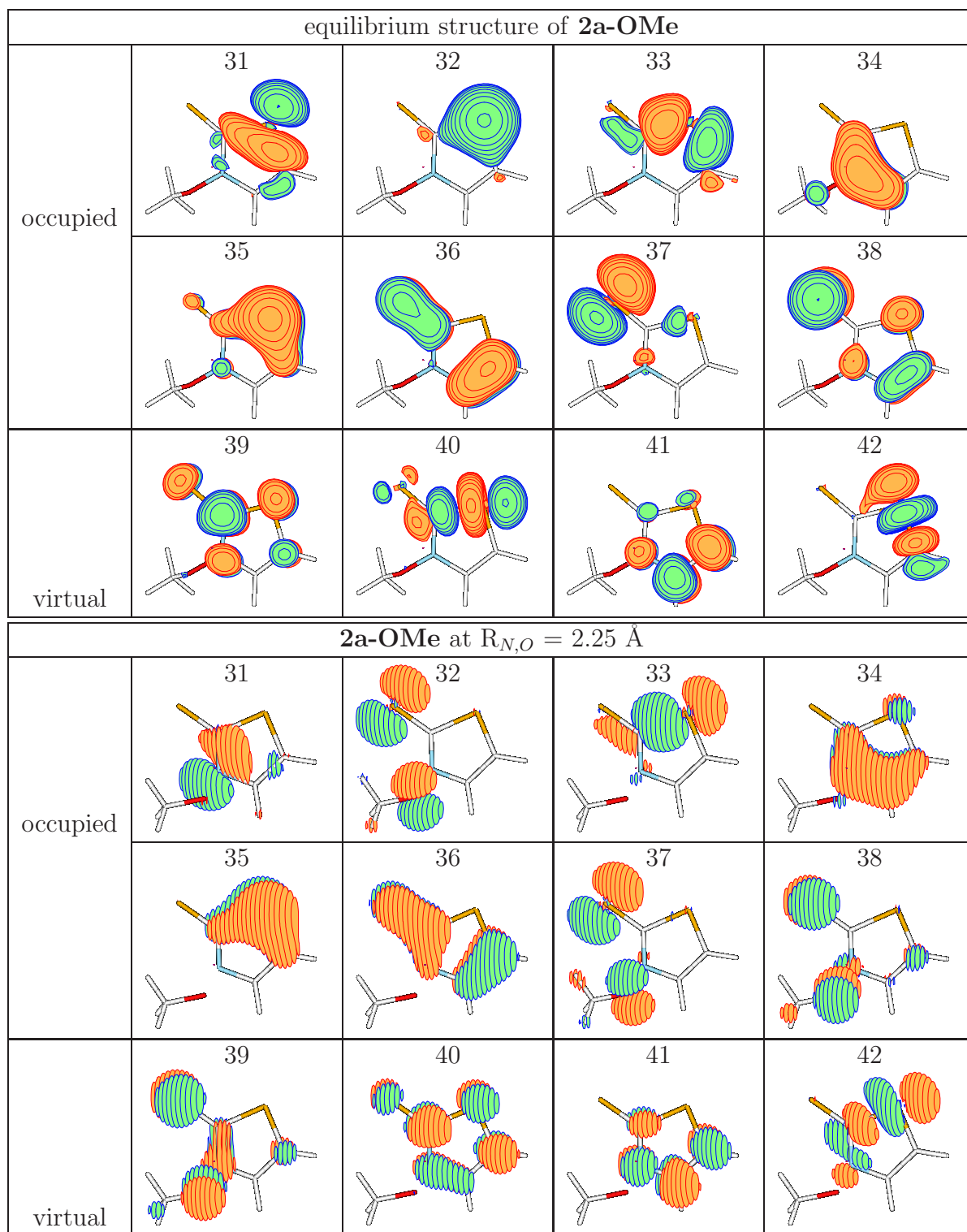


Figure 5.5: The relevant orbitals that have to be taken into the active space for the CASPT2 calculations to describe the photolytic or thermal N,O homolysis in *N*-(methoxy)-thiazole-2(3*H*)-thione (**2a-OMe**).

the computed N,O-dissociation energies of 1.65 eV (159 kJ mol⁻¹) into account, a maximal excess energy of 2.21 eV (213 kJ mol⁻¹) is predicted for the fragments resulting from the thiazolethione **2a-OMe**. The real remaining excess energy can be expected to be much smaller than the maximal excess energy since energy dissipates to other degrees of freedom or the solvent. Estimates show that in a direct dissociation along a repulsive coordinate 50–80 % of the excess energy remains on the fragments.^[158,159] Most of the remaining excess energy is transformed into translation energy. Since the translation energy is distributed according to the conservation of momentum the lighter fragment will gain more translation energy.^[158,159] For **2a-OMe**, only repulsive potential surfaces with respect to the N,O bond in the excited states and a very efficient quenching process from the S₂ to the S₁ state due to a possible conical intersection at R_{N,O} = 2.25 Å is found. This indicates a very fast bond dissociation process and therefore less time for the quenching of excess energy to other degrees of freedom or the solvent.

The intrinsic chemical reactivity of the resulting radical fragments are obtained by computing the reaction energies ΔE ($E_{products} - E_{educts}$) of the isodesmic hydrogen abstraction reaction shown in equation 5.1. The investigated C,H bond in isobutane has a bonding energy of 380 kJ mol⁻¹.^[160] The positive reaction energy of 56 kJ mol⁻¹ indicates that the heterocyclic radical fragment **2a•** resulting from the photochemical dissociation process of **2a-OMe** is not able to abstract the indicated hydrogen of isobutane. The reaction energy for the isodesmic reaction of isobutane with the resulting methoxyl radical (**OMe•**) is about -28 kJ mol⁻¹, underlining its stronger reactivity in comparison to the heterocyclic radical fragment.

5.2.2 Single Reference Approaches

The CASPT2 approach is known to provide very accurate results on excited state properties and photochemical reaction paths but it is too expensive to study the N,O homolysis of systems with large substituents. The single reference approaches TD-DFT and RI-CC2 are less expensive but the question arises whether they are sufficiently accurate. The results obtained with the B3LYP functional and with RI-CC2 are given in figure 5.6. Like the CASPT2 approach, the TD-B3LYP functional predicts repulsive T₁//T₁, S₁//T₁, and S₂//T₁ curves (figure 5.6 left side). With increasing N,O distances, however, the energy gaps between the various states become much larger than predicted by CASPT2. Obviously TD-DFT is not adequate to describe the complicated electronic structure of the S₁//T₁ or S₂//T₁ states for stretched N,O bonds. Although these states are far too high in energy, the energy position of the T₁//T₁ state for **2a-OMe** is in very good agreement with the CASPT2 results. The RI-CC2 approach was found to give quite reliable vertical excitation energies for the

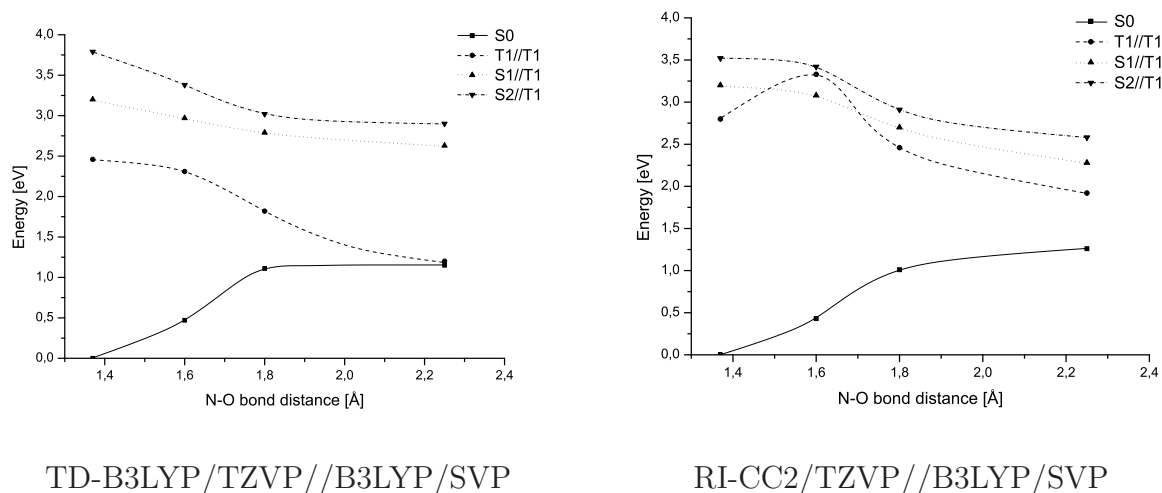


Figure 5.6: Potential curves for the thermal and photolytic N,O homolysis in *N*-(methoxy)-thiazole-2(3*H*)-thione (**2a-OMe**) obtained with the single reference approaches TD-B3LYP/TZVP (left side) and RI-CC2 (right side).

singlet states. Since it represents also a single reference method problems are expected for the description of the photolytic dissociation. This is indeed the case. The computed curves of the S_1 and S_2 states resembles those obtained with the TD-DFT approach. Additionally RI-CC2 also failed to give an adequate description of the $T_1//T_1$ surface.

5.2.3 *N*-(Methoxy)-Pyridine-2(1*H*)-thione (**1a-OMe**)

An UV/vis absorption of *N*-(methoxy)-pyridine-2(1*H*)-thione **1a-OMe** and the subsequent N,O bond homolysis furnishes the methoxyl and the pyridyl-2-sulfanyl radical (**1a \bullet** ; compare equation 5.3).

The computed potential energy curves characterizing the thermally and the photochemically induced N,O homolysis in *N*-(methoxy)-pyridine-2(1*H*)-thione (**1a-OMe**) are displayed in figure 5.7. The properties of the S_2 state is of major interest for the photochemistry of **1a-OMe** since it is the only state that is populated via near UV excitation in a transition starting from the ground state ($\pi_{CS} \rightarrow \pi_{ring}^*$ transition) and exhibits significant oscillator strength.

Relevant orbitals for the equilibrium structure and for $R_{N,O} = 2.25 \text{ \AA}$ are depicted in figure 5.8. As for **2a-OMe** also here quite low lying occupied orbitals (*e.g.* orbital 31) become important in the configurations of the excited states at longer N,O bond distances. Therefore in the case of (**1a-OMe**) also a (16/12) active space is necessary for the CASPT2 computations.

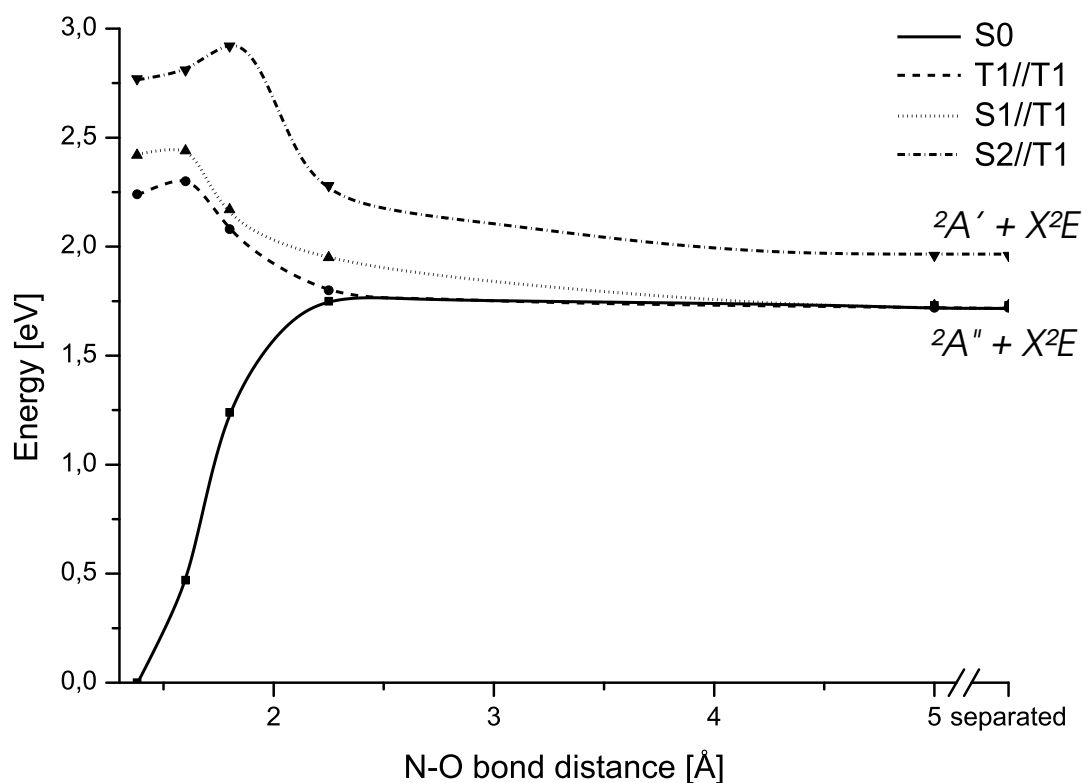
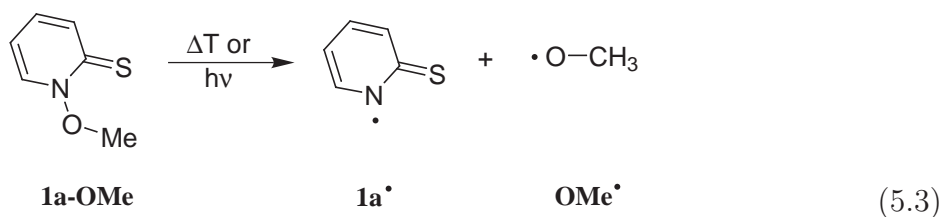


Figure 5.7: Potential curves for the thermal and photolytic N,O homolysis in *N*-(methoxy)-pyridine-2(1*H*)-thione (**1a-OMe**).

For the thermal cleavage along the S_0 ground state, the computed dissociation energy is 1.71 eV (165 kJ mol^{-1}) for *N*-(methoxy)-pyridine-2(1*H*)-thione (**1a-OMe**). This value is in the same energy region than for **2a-OMe**. Like for the thiazole compound **2a-OMe** a direct fragmentation out of the photoactive S_2 state would yield the methoxyl radical in its ground state (\tilde{X}^2E) and the pyridyl-2-sulfanyl radical **1a** $^\bullet$ in its first excited state ($^2A'$). The main difference between both compounds is the shape of the $S_2//T_1$ curve. For the thiazole derivative **2a-OMe**, this curve shows a repulsive shape. For **1a-OMe**, the fragmentation starting from the S_2 state is hindered by a small barrier of about 0.11 eV (11 kJ mol^{-1}). Furthermore, the energy difference between the $S_2//T_1$ and $S_1//T_1$ surfaces

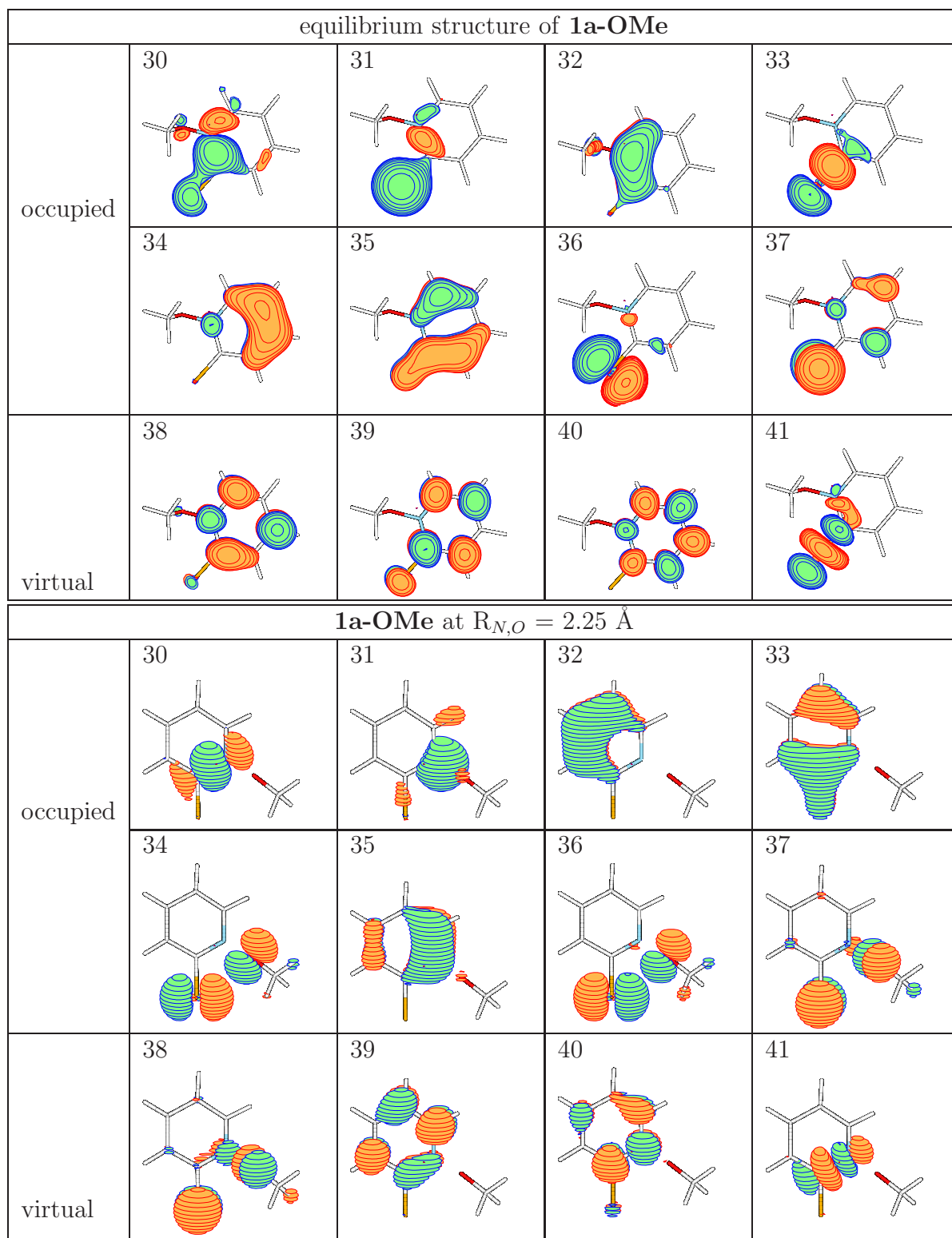


Figure 5.8: The relevant orbitals that have to be taken into the active space for the CASPT2 calculations to describe the photolytic or thermal N,O homolysis in *N*-(methoxy)-pyridine-2(1*H*)-thione (**1a-OMe**).

(0.4–0.6 eV) is larger than for the thiazolethione **2a-OMe** (< 0.1 eV) and the potentials do not at all indicate a conical intersection between both states. The larger energy gap between the $S_2//T_1$ and $S_1//T_1$ could to some extent slow down the relaxation from the S_2 to the S_1 state in the pyridinethione compound **1a-OMe**. However, since a direct fragmentation via the higher energy dissociation channel experiences a small energy barrier, a relaxation into the S_1 state is expected to occur also for this compound, as for example predicted by Kasha's rule.^[161]

Similar to the situation in thiazolethione **2a-OMe**, the $S_1//T_1$ and $T_1//T_1$ curves in pyridinethione **1a-OMe** are within a first approximation parallel. The energy gap for the two curves is, however, considerably smaller (ca. 0.2 eV) than for the thiazole derivative **2a-OMe** (0.6–1.0 eV). As a consequence, it is expected that relaxation from the S_1 state into the T_1 state is more efficient in pyridinethione **1a-OMe**. Since a strong rovibronic coupling between both lowest lying dissociation channels occurs, the radicals that are formed from the dissociation reaction end up in their electronic ground state (${}^2A''$ for **1a•** and \tilde{X}^2E for the methoxyl radical), regardless whether they originate from a N,O homolysis in the S_1 or the T_1 state.

For *N*-(methoxy)-pyridine-2(1*H*)-thione (**1a-OMe**), an $S_0 \rightarrow S_2$ excitation energy of 3.27 eV (379 nm) has been computed. With the computed thermal bond dissociation energy of 1.71 eV (168 kJ mol⁻¹) the maximal possible excess energy for the radical fragments **1a•** and **OMe•** is 1.56 eV (150 kJ mol⁻¹). For **1a-OMe**, the S_2 state exhibits a small barrier and the $S_2 \rightarrow S_1$ relaxation occurs slower since the two potential curves are well separated along the whole N,O reaction coordinate. Assuming that energy dissipation occurs in the time it takes for the S_2 -excited thione **1a-OMe** to relax into the S_1 state and probably also in the T_1 state, the combined excess energy of radical **1a•** and the methoxyl radical can be expected to dissipate very efficient into other degrees of freedom or the solvent.

The intrinsic chemical reactivity of the pyridyl-2-sulfanyl radical fragment (**1a•**) is comparable to the one of **2a•**. This is confirmed by the reaction energy of the hydrogen abstraction reaction (equation 5.1), which is, with 44 kJ mol⁻¹, only 12 kJ mol⁻¹ less endotherm than for the thiazyl-2-sulfanyl fragment **2a•**.

5.2.4 A generalized Model for the Reactivity.

With the values for **1a-OMe** and **2a-OMe** that are summarized in table 5.1 the reason for the different chemistry that follows upon near UV/vis excitation of, *e.g.*, substituted *N*-(4-penten-1-oxy)-pyridine-2(1*H*)-thione and the corresponding *N*-(4-penten-1-oxy)-4-methylthiazole-2(3*H*)-thione in the absence of efficient trapping reagents can be explained. The thermal bond dissociation energy of both molecules and the inherent reac-

molecule	excitation	dissociation	maximal excess	barrier for the	isodesmic
	energy ^a	energy ^b	energy ^b	dissociation ^c	reaction ^d
	eV / nm	eV / kJ mol ⁻¹	eV / kJ mol ⁻¹	eV / kJ mol ⁻¹	kJ mol ⁻¹
1a-OMe	3.27 / 379	1.71 / 165	1.56 / 151	0.11 / 11	44.4
2a-OMe	3.86 / 321	1.65 / 159	2.21 / 213	— / —	56.1
1b-OMe	4.00 / 310	2.20 / 212	1.80 / 174	0.21 / 20	-6.6

^aThe vertical $\pi \rightarrow \pi^*$ excitation energies calculated on the 12/12 CASPT2/cc-pVTZ//RI-MP2/cc-pVTZ level of theory.

^bThe S_0 dissociation energies and the maximal excess energy computed on the 16/12 CASPT2/cc-pVTZ//RI-MP2/cc-pVTZ level of theory.

^cThe highest barrier towards the N,O bond homolysis in the photochemical active state.

^dThe ΔE ($E_{products} - E_{educts}$) values for the isodesmic hydrogen abstraction reaction shown in equation 5.1. The value for the methoxy radical is $\Delta E = -27.9$ kJ mol⁻¹.

Table 5.1: Summary of the data for the description of the photolytic radical liberation process and the chemical behavior of the radical fragments.

tivity of the fragments are computed to be quite similar and do not explain the experimentally found differences. But the maximal excess energy given in the fourth column of table 5.1 reveals a big difference. A photochemical N,O homolysis of **2a-OMe** will yield radical fragments (**2a•** and **OMe•**) that contain about 0.6 to 0.7 eV (60–70 kJ mol⁻¹) more excess energy than the fragments released by the photolytic N,O bond cleavage in **1a-OMe**. From a comparison of the potential surfaces shown in figures 5.3 and 5.7 it can be seen that the N,O dissociation process in compound **2a-OMe** should proceed much faster than in the case of **1a-OMe**. This gives the developing radical fragments **1a•** and **OMe•** much more time for the quenching of excess energy to other degrees of freedom and the solvent. So, the difference between the real excess energies of the radicals obtained from a homolysis of the thiazole compounds and the corresponding fragments from pyridine precursors will be even bigger. This different remaining excess energy yields much more reactive radicals in the case of *N*-(methoxy)-thiazole-2(3*H*)-thione (**2a-OMe**) and therefore is mainly responsible for the differences in the chemical behavior of the fragments.

For a general estimation of the reactivity of other heterocyclic compounds in such a photochemical alkoxy radical liberation process the theoretical results for the N,O dissociation mechanism in **1a-OMe** and **2a-OMe** serve as a reference. Radical fragments with a high maximal possible excess energy and bond dissociation potentials reflecting a perfect slide to the fragments with possible conical intersections to reach the ground state should react relative sluggish and with many unwanted side products if photolyzed in the absence of radical trapping reagents. On the other hand if the N,O bond dissociation paths indicate lower maximal excess energies and slower fragmentation processes (*e.g.* slowed down

by barriers and energetic well separated potential surfaces) the precursors should provide alkoxy radicals in clean reactions like the *N*-alkoxy derivatives of **1a-OMe**.

5.2.5 *N*-(Methoxy)-Pyridine-2(1*H*)-one (**1b-OMe**)

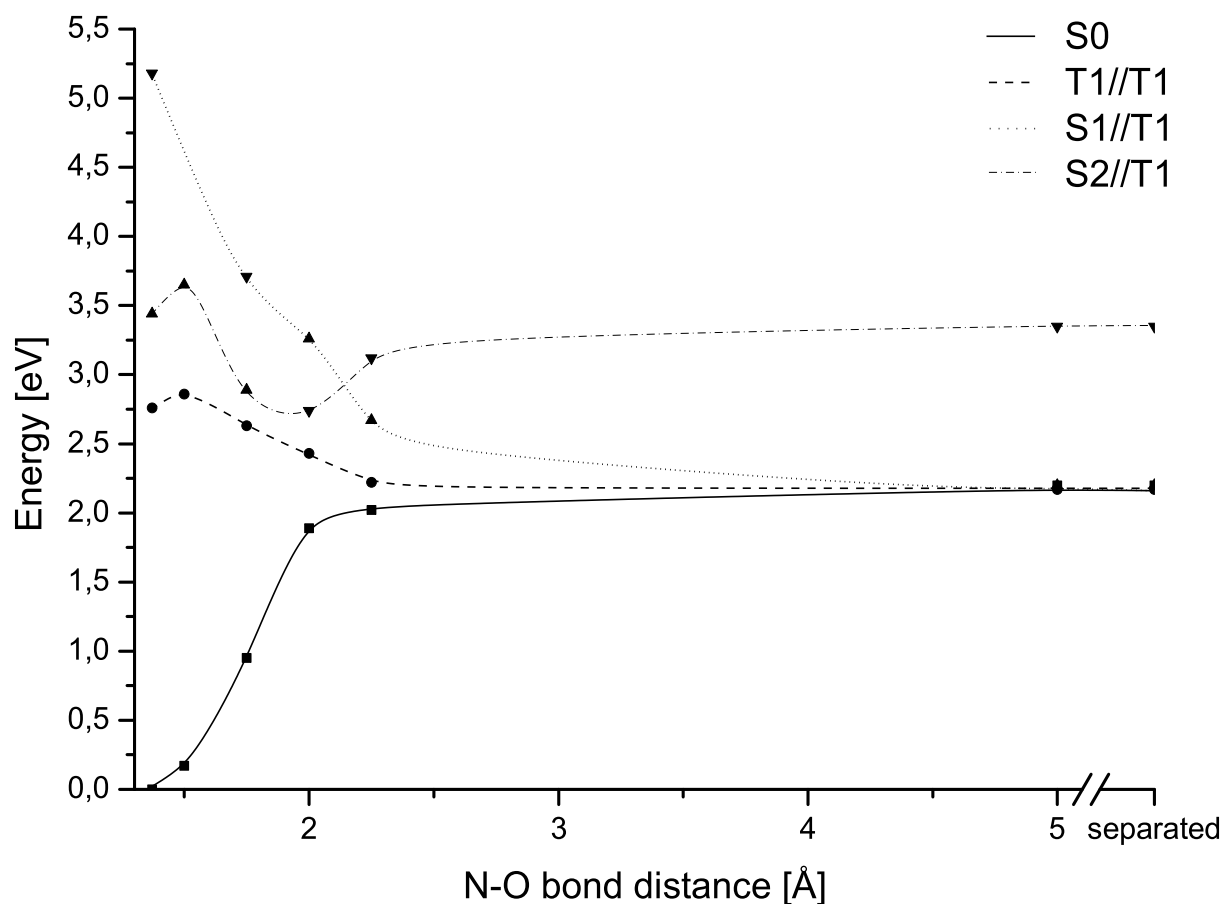
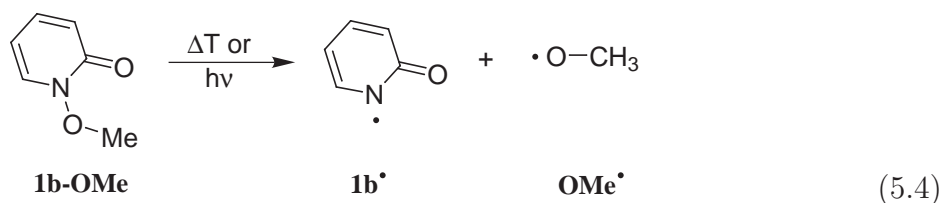


Figure 5.9: Potential curves for the thermal and photolytic N,O homolysis in *N*-(methoxy)-pyridine-2(1*H*)-one (**1b-OMe**).

To check if the developed model for the prediction of the reactivity of photochemical alkoxy radical precursors also holds for a wider range of molecules the experimental data that is already known for the *N*-(alkoxy)-pyridine-2(1*H*)-ones^[8,162,163] served as test case. Those molecules on the basis of the pyridine-2(1*H*)-one heterocycle are applied as “clean”

photochemical alkoxy radical source with an initiation wave length of about 300 nm. The underlying chemical reaction that was investigated theoretically is the homolytic N,O bond dissociation process of *N*-(methoxy)-pyridine-2(1*H*)-one **1b-OMe** shown in equation 5.4. The resulting fragments from the photolytic N,O bond cleavage are the methoxyl radical and the pyridyl-2-oxyl radical (**1b•**).

The potential curves for the thermal and photochemical N,O cleavage in *N*-(methoxy)-pyridine-2(1*H*)-one (**1b-OMe**) are summarized in figure 5.9. In contrast to the thiocarbonyl compounds **1a-OMe** and **2a-OMe** for the hydroxamic acid *O*-ester **1b-OMe** the S_1 state is expected to be populated by an irradiation of the molecule with UV/vis light. From the dissociation energy of the ground state (2.20 eV, 212 kJ mol⁻¹) and the computed vertical $S_0 \rightarrow S_1$ excitation energy (4.00 eV, 310 nm) a maximal excess energy of 1.80 eV (174 kJ mol⁻¹) is obtained, which falls between the values obtained for **1a-OMe** and **2a-OMe**. On the way to the N,O fragmentation along the S_1 potential energy curve the molecule **1b-OMe** will be trapped in a quit deep minimum^b from which it can cross (via spin-orbit coupling) to the triplet surface. Despite the small spin-orbit coupling expected for first row elements the transfer should be efficient since both states come close in energy. From the T_1 state it easily fragments into the desired radicals since the T_1 state is repulsive in that region. Nevertheless due to the time the molecule rests in the minimum of the S_1 state and the singlet triplet transfer occurs, a large amount of excess energy should dissipate to the solvent or other degrees of freedom of the molecule. Due to our model **1b-OMe** should react as **1a-OMe**, which is in perfect agreement with the experiment.

The isodesmic reaction with isobutane (equation 5.1) indicates that the resulting pyridyl-2-oxyl radicals ($\Delta E = -6.6$ kJ mol⁻¹) are considerably more reactive than the pyridyl-2-thionyl radical (**1a•**; $\Delta E = 44.4$ kJ mol⁻¹) which results from the fragmentation of **1a-OMe** or the thiazyl-2-sulfanyl radicals **2a•** ($\Delta E = 56.1$ kJ mol⁻¹). However, comparing the small difference in the reaction energies of the isodesmic reactions with the large difference in the estimated maximal excess energies for the fragments from **1a-OMe** and **2a-OMe** and taking into account that derivatives of **1b-OMe** with longer alkoxy chains serve as clean photochemical source of alkoxy radicals the higher intrinsic reactivity should be less important than the remaining excess energy.

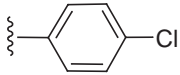
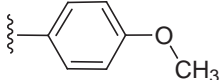
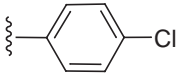
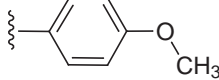
This test on a known and applied hydroxamic acid derivate (**1b-OMe**) indicated that the developed model for the reactivity of heterocyclic photochemical alkoxy radical precursors covers the most important factors to predict the photochemistry of such compounds. This knowledge will be further applied in chapter 7 to perform a computer aided design of completely new promising heterocyclic precursor molecules.

^bThe depth with respect to the dissociation is about 0.2 eV (20 kJ mol⁻¹).

Chapter 6

Substituent Effects on the UV/vis Spectra

In the last two chapters of this work the electronic spectra and the potential energy surfaces for the photolytic N,O bond homolysis of the known and applied precursor systems *N*-(methoxy)-pyridine-2(1*H*)-thione (**1a-OMe**) and *N*-(methoxy)-thiazole-2(3*H*)-thione (**2a-OMe**) were computed and analyzed. MS-CASPT2 computations assigned the spectroscopic visible absorption bands of both compounds to the $S_0 \rightarrow S_2$ transition. These excitations were characterized as the spectroscopic allowed $\pi_{CS} \rightarrow \pi_{ring}^*$ excitation in **1a-OMe** and the $\pi_{SCS}^{non} \rightarrow \pi_{SCS}^*$ transition in **2a-OMe** respectively. The observed higher stabilities of the applied thiazolethione compounds with respect to daylight simply result since their S_2 states are higher in energy than the corresponding states in the likewise applied pyridinethione compounds. An analysis of the theoretically obtained N,O bond dissociation paths for the photochemical alkoxy radical liberation process showed that the higher reactivity of the alkoxy radicals liberated after an irradiation of the thiazole compounds results from the higher maximal excess energy which results from the photolytic fragmentation. Due to the faster N,O dissociation process the excess energy is hardly distributed into vibrational or rotational degrees of freedom of both fragments or the solvent so that two very “hot” fragments are obtained. For *N*-(alkoxy)-pyridine-2(1*H*)-thiones the maximal excess energy of the fragments is lower due to a smaller vertical excitation energy (starting point of the photolytic fragmentation) and a higher dissociation energy of the S_0 state. A dissipation of the excess energy is also much more likely since the S_2 state of the precursor molecules on pyridinethione basis possesses a barrier with respect to the dissociation. Additionally no avoided crossing between S_2 and S_1 is found so that the bond dissociation process is expected to be much slower.

R ⁴	R ⁵	name
H	H	2a-OMe
H	CH ₃	4h5me
CH ₃	H	4me5h
CH ₃	CH ₃	4me5me
CH ₃		4me5pcl
CH ₃		4me5ani
	H	4pcl5h
	H	4ani5h

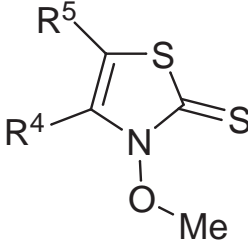


Figure 6.1: The name scheme for the various C⁴ and C⁵ substituted *N*-(methoxy)-thiazole-2(3*H*)-thione alkoxy radical precursors.

For many photobiological experiments on DNA oxidation and strand-breaking processes, precursors that absorb at a wave length of about 350 nm are advantageous. To achieve such properties new 4,5-substituted derivatives of *N*-(methoxy)-thiazole-2(3*H*)-thione (**2a-OMe**) were prepared experimentally to induce a red shift of the $\pi_{SCS}^{non} \rightarrow \pi_{SCS}^*$ excitation wave length to the desired spectral region. Effects of CH₃, *p*-ClC₆H₄ and *p*-H₃COC₆H₄ substituents at the 4 and 5 position on the electronic excitations of these compounds have been investigated in detail in order to lay a profound basis for a future rational design of new alkoxy radical precursors on the basis of the thiazole heterocycle for specialized applications. The electronic excitations of these various 4 and 5 substituted cyclic thiohydroxamic *O*-methyl esters were calculated (TD-DFT) and compared to those of the parent compound **2a-OMe**. The experimental UV/vis-spectra of these new 4 and 5 substituted derivatives of **2a-OMe** than could be interpreted in terms of molecular orbital transitions.

The photochemical N,O bond dissociation of the *N*-(alkoxy)-pyridine-2(1*H*)-thiones (**1a-OR**) leads to a “cleaner” radical liberation process than the fragmentation of the thiazolethione precursors, so the question arises if substituents on the pyridine heterocycle can lead to a blue shift of the photoactive $\pi_{CS} \rightarrow \pi_{ring}^*$ excitation wave length towards shorter wave length to avoid daylight sensitivity. To get informations about the influence of different substituents on the electronic spectra of the pyridine-2(1*H*)-thione compounds the hydrogen atoms of the *N*-(methoxy)-pyridine-2(1*H*)-thione heterocycle (**1a-OMe**) were systematically substituted by fluorine atoms, methoxyl groups or nitro functionalities. Our predictions cannot be checked experimentally, since these substituted pyridine compounds

have not been synthesized until today. The fluorine atoms represent a model for electron withdrawing substituents, while the methoxyl group is an example for an electron rich substituent. The NO_2 group is a model for substituents that are able to conjugate with the π -electron system of the pyridine heterocycle.

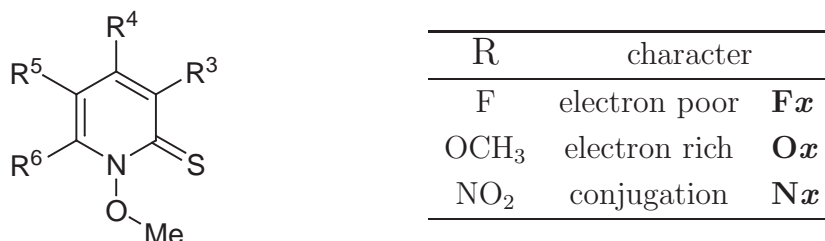


Figure 6.2: The numbering of the substituents on the pyridine heterocycle.

The enumeration scheme for the substituted molecules is shown in figure 6.2. A fluorine substituted heterocycle will be indexed by **F**, the methoxyl derivatives are indicated by an **O** and the nitro compounds are labeled with **N**. The positions of the substituents on the heterocycle are numbered according to figure 6.2, *e.g.* a fluorine substitution on position 3 will be enumerated as **F3**. **O346** describes the *N*-methoxy-3,4,6(trimethoxy)pyridine-2(1*H*)-thione and **N4** abbreviates *N*-methoxy-4-nitropyridine-2(1*H*)-thione, respectively.

The $n_{CS} \rightarrow \pi_{ring}^*$ and the $\pi_{CS} \rightarrow \pi_{ring}^*$ excitations of the substituted molecules were calculated applying the time-dependent density functional theory in combination with the B3LYP functional. This combination is valid for the prediction of the electronic excitations of pyridinethione compounds (compare chapter 4). The fluor systems were also computed employing the CASPT2 approach since the functional dependency of the TD-DFT for the prediction of substituent effects can not be estimated by a comparison with experimental spectra. With the aid of the calculated excitations of the monosubstituted molecules the additivity of the substituent effects on the excitation energies is tested. This leads to an incremental system for the substituent effects which can be applied for larger substituents. The calculated excitation energies of the mono nitro-compounds are applied in this incremental system to estimate the effects of a multiple substitution with NO_2 on the excitation energies of the examined electronic transitions. Additionally, the substituent effects are correlated and explained with shifts in the energetic position of the contributing orbitals.

6.1 Theoretical Details

For the thiazolethione compounds the theoretical results on the electronic transitions and the UV/vis spectral properties are obtained like for the calculations on the parent com-

pound *N*-(methoxy)-thiazole-2(3*H*)-thione (**2a-OMe**) described in Section 4.3. To check if a predicted strong red shift of the photoactive electronic transition in 4 and 5 aryl substituted thiazolethione compounds, that is not seen in the experiment, is not an artefact of the wrong fall off behavior of the applied B3LYP functional, the simulations of the UV/vis spectra of these compounds was also performed applying the RI-CC2//cc-pVTZ approach. This should give correct informations if the substituent effects predicted by TD-DFT are “real” or result only from wrong described CT excitations from the thiazole heterocycle to the aryl substituent.

The spectroscopic properties of all possible fluorine- and methoxyl-pyridinethiones and the mono nitrated molecules were obtained on the TD-B3LYP/TZVP//RI-BLYP/SVP level of theory. This approach was proven to be valid for *N*-(alkoxy)-pyridine-2(1*H*)-thione compounds (Section 4.3).

To establish an incremental system for the substituent effects on the excitation energies of the first two excitations the differences in the excitation energies between the parent compound *N*-(methoxy)-pyridine-2(1*H*)-thione (**1a-OMe**) and the monosubstituted derivatives were calculated. The excitation energies of the multiply substituted fluorine and methoxyl derivatives were estimated applying the increments from the mono substituted compounds.

$$\sigma = \sqrt{\frac{\sum (\Delta E_{calc-inkr})^2}{11}} \quad (6.1)$$

The standard deviation σ (equation 6.1) between the excitation energies obtained from the direct calculations and the incrementally estimated ones is a measure for the quality of the incremental system. Since no experimental data for substituted *N*-(alkoxy)-pyridine-2(1*H*)-thiones is available the energies of the first two excited states of the fluorine compounds were also calculated employing the MS-CASPT2 approach. This was done for the RI-BLYP/SVP structures, and for the monofluorinated molecules (**F3–F6**) and the most promising multiply fluorinated pyridine derivate (with respect to the desired blue shift of the $\pi_{CS} \rightarrow \pi_{ring}^*$ transition), also for RI-MP2/cc-pVTZ structures. For these calculations the cc-pVDZ basis sets had to be applied because with the additional electrons from the fluorine substituents the hardware resources were not sufficient for the triple zeta basis sets. For **1a-OMe** the influence of the rather small cc-pVDZ basis on the calculated excitation energies was estimated by a comparison with the results for the cc-pVTZ basis sets summarized in table 4.5. The predictions of the incremental system are additionally checked on the B3LYP/cc-pVTZ level of theory. TD-DFT with the PBE0 functional and the RI-CC2 approach in combination with Dunning’s correlation consistence triple zeta basis sets have been also applied, since they represent reliable methods for the predictions of the electronic excitation spectra of *N*-(alkoxy)-pyridine-2(1*H*)-thione compounds.

6.2 Substituents on the Thiazolethione Heterocycle

According to observations obtained from the experimentally measured UV/vis spectra of 4 and 5 substituted thiazolethiones it is expected that such a substitution leads to more effects on the UV/vis spectra than *N*-alkoxy substituents (compare subsection 4.4.3). To investigate this influence the first electronic excitations of several 4 and 5 substituted thiazolethione compounds were computed. The electronic transitions up to 250 nm, obtained on RI-BLYP/SVP structures of the molecules, are summarized in table 6.1.

molecule	$n_{CS} \rightarrow \pi_{SCS}^*$ ^a	$\pi_{SCS}^{non} \rightarrow \pi_{SCS}^*$ ^b	additional transitions ^c
4h5me	355 / 3.50	301 / 4.12 (0.164)	288 / 4.31 ; 258 / 4.81
4me5h	357 / 3.48	297 / 4.17 (0.140)	282 / 4.40 ; 255 / 4.86
4me5me	354 / 3.50	299 / 4.15 (0.178)	284 / 4.36 ; 254 / 4.88
4me5pcl	368 / 3.37	343 / 3.62 (0.245)	320 / 3.87 ; 301 / 4.12 ; 293 / 4.23 282 / 4.40 ; 273 / 4.53 ; 254 / 4.89 250 / 4.95
4me5ani	361 / 3.43	325 / 3.82 (0.330)	312 / 3.97 ; 292 / 4.25 ; 282 / 4.40 277 / 4.47 ; 274 / 4.54 ; 258 / 4.80 252 / 4.92
4pcl5h	362 / 3.42	300 / 4.14 (0.145)	335 / 3.70 ; 313 / 3.96 ; 304 / 4.08 277 / 4.48 ; 275 / 4.51 ; 252 / 4.93
4ani5h	358 / 3.46	319 / 3.89 (0.072)	301 / 4.12 ; 298 / 4.17 ; 294 / 4.22 281 / 4.41 ; 270 / 4.59 ; 260 / 4.77

^aoscillator strength $f < 10^{-3}$.

^boscillator strength f [arb. units] is given in parenthesis.

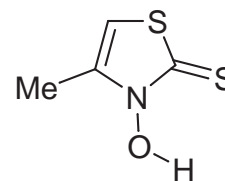
^cTransitions into other orbitals that are computed in the spectral region up to 250 nm.

Table 6.1: Computed electronic excitations (TD-B3LYP/TZVP//RI-BLYP/SVP) in the spectral region up to 250 nm in various C⁴ and C⁵ substituted derivatives of *N*-(methoxy)-thiazole-2(3*H*)-thione.

The calculated spectra of *N*-(hydroxy)-4-methylthiazole-2(3*H*)-thione (**4me5h-OH**) and *N*-methoxy-substituted thione (**4me5h-OMe**) show, as expected, a considerable match to those of the basic structures **2a-OH** and **2a-OMe** (compare chapter 4 tables 4.11 and 4.12). Also the contributing orbitals resemble the ones of the parent compounds. The assignment of electronic transitions (see tables 6.2 and 6.3) can therefore be done with the orbitals for **2a-OH** and **2a-OMe** shown in figure 4.4.

The calculated UV/vis spectra of *N*-(methoxy)-5-methylthiazole-2(3*H*)-thione (**4h5me**) and of the 4,5-dimethyl derivative **4me5me** are qualitatively and quantitatively also com-

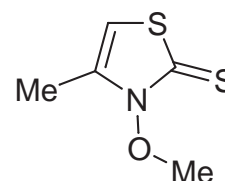
ΔE	f	Character	Weight ^a
307 / 4.04	$<10^{-3}$	$n_{CS} \rightarrow \pi_{SCS}^*$	0.981
294 / 4.22	0.191	$\pi_{SCS}^{non} \rightarrow \pi_{SCS}^*$	0.936
276 / 4.50	$<10^{-3}$	$\pi_{SCS}^{non} \rightarrow LUMO_{+1}$	0.991
244 / 5.08	0.017	$\pi_{SCS}^{non} \rightarrow LUMO_{+2}$	0.781
		$HOMO_{-1} \rightarrow \pi_{SCS}^*$	0.169



^aConfigurations with weights below 0.10 have, for the sake of clarity, not been considered.

Table 6.2: Excitation energies ΔE [nm / eV] and an assignment of electronic excitations in *N*-(hydroxy)-4-methylthiazole-2(3*H*)-thione (**4me5h-OH**) to orbital transitions. The orbitals of **4me5h-OH** are comparable to the one obtained for the parent compounds **2a-OH**.

ΔE	f	Character	Weight ^a
357 / 3.48	$<10^{-3}$	$n_{CS} \rightarrow \pi_{SCS}^*$	0.987
297 / 4.17	0.140	$\pi_{SCS}^{non} \rightarrow \pi_{SCS}^*$	0.866
282 / 4.40	$<10^{-3}$	$\pi_{SCS}^{non} \rightarrow LUMO_{+1}$	0.914
255 / 4.86	0.052	$n_{CS} \rightarrow LUMO_{+1}$	0.884



^aConfigurations with weights below 0.10 have, for the sake of clarity, not been considered.

Table 6.3: Excitation energies ΔE [nm / eV] and an assignment of electronic excitations in *N*-(methoxy)-4-methylthiazole-2(3*H*)-thione (**4me5h-OMe**) to orbital transitions. The orbitals of **4me5h-OMe** are comparable to the one obtained for the parent compounds **2a-OMe**.

parable to that of the basic compound **2a-OMe**.

A *p*-methoxyphenyl (anisyl) substituent located at the C⁵ position causes a bathochromic shift of 15 nm of the lowest energy absorption in the experimental spectrum of the *N*-(methoxy)-4-methyl-5-anisylthiazole-2(3*H*)-thione (**4me5ani**) heterocycle, in comparison to the corresponding bands in 4-methylthiazole-2(3*H*)-thione **4me5h**. Generally the absorption band at the low energy end in the experimental UV/vis spectra of *N*-(methoxy)-thiazole-2(3*H*)-thiones shows a progressive red shift along the series of 4-/5-substituents 4-(*p*-ClC₆H₄)/5-H < 4-(CH₃)/5-H < 4-(CH₃)/5-(CH₃) < 4-(CH₃)/5-(anisyl). This points to a stronger influence of a substituent at the C⁵ position on the excitation energy of the photoactive $\pi_{SCS}^{non} \rightarrow \pi_{SCS}^*$ transition.

In view of the significance of different *O*-alkyl derivatives of **4me5ani** as sources of oxygen-centered radicals in bioorganic studies on DNA damage, the UV/vis spectrum of *N*-(methoxy)-4-methyl-5-(*p*-methoxyphenyl)thiazole-2(3*H*)-thione (**4me5ani**) is investigated

in detail. The spectral information and orbitals, relevant for an assignment of major transitions are provided in table 6.4 and figure 6.3.

ΔE	f	Character	Weight ^a
361 / 3.43	$3 \cdot 10^{-3}$	$n_{CS} \rightarrow \pi_{SCS}^*$	0.819
		$n_{CS} \rightarrow \pi_{sub}^*$	0.149
325 / 3.82	0.330	$\pi_{SCS}^{non} \rightarrow \pi_{SCS}^*$	0.879
312 / 3.97	0.010	$\pi_{SCS}^{non} \rightarrow \pi_{sub}^*$	0.916
292 / 4.25	0.025	$\pi_{SCS}^{non} \rightarrow LUMO_{+2}$	0.834
282 / 4.40	0.016	$n_{CS} \rightarrow LUMO_{+2}$	0.632
		$n_{CS} \rightarrow \pi_{SCS}^*$	0.220
277 / 4.47	0.069	$n_{CS} \rightarrow \pi_{sub}^*$	0.613
		$n_{CS} \rightarrow LUMO_{+2}$	0.152
274 / 4.53	0.020	$\pi_{SCS}^{non} \rightarrow LUMO_{+3}$	0.857
258 / 4.80	0.027	$HOMO_{-2} \rightarrow \pi_{SCS}^*$	0.721
		$n_{CS} \rightarrow LUMO_{+3}$	0.122
252 / 4.92	0.010	$HOMO_{-2} \rightarrow \pi_{sub}^*$	0.720
		$HOMO_{-3} \rightarrow \pi_{SCS}^*$	0.117

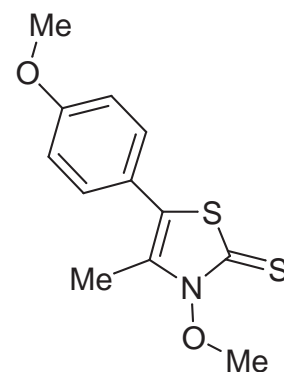


Table 6.4: Excitation energies ΔE [nm / eV] and an assignment of electronic excitations in *N*-(methoxy)-4-methyl-5-(*p*-methoxyphenyl)thiazole-2(3*H*)-thione (**4me5ani**) to orbital transitions.

The experimental UV/vis spectrum of *N*-(methoxy)-4-methyl-5-(*p*-methoxyphenyl)thiazole-2(3*H*)-thione (**4me5ani**) in ethanol exhibits bands at $\lambda = 335$ nm (halfwidth $\Delta\lambda = 45$ nm), 258 nm and 244 nm (4.6:1:2.5 intensity ratio, the latter two shoulders).

Three occupied and three virtual orbitals are relevant in order to assign the calculated electronic spectrum of thione **4me5ani** in the range of $\lambda > 250$ nm. The $HOMO_{-2}$ is delocalized over the whole molecule and may be classified as a combination of a thiazolethione π_{SCS} -orbital and a π -type orbital of the *p*-methoxyphenyl substituent. The $HOMO_{-1}$ is similar in shape than the n_{CS} -orbital in thiazolethione **2a-OMe** but destabilized by 0.22 eV in comparison to the parent compound. The HOMO corresponds to the π_{SCS}^{non} -orbital in **2a-OMe**, but it is destabilized by 0.36 eV and exhibits additional density predominantly located at the ortho- and para-position of the *p*-methoxyphenyl entity in **4me5ani**. The LUMO of **4me5ani** is a combination of the π_{SCS}^* -orbital in **2a-OMe** contributions from a π -like shape along the C^5-C^{ipso} bond and density at the ortho- and para-position of the *p*-methoxyphenyl substituent. The $LUMO_{+1}$ exhibits antibonding π character between the ortho- and meta-position of the *p*-methoxyphenyl entity and can therefore be characterized

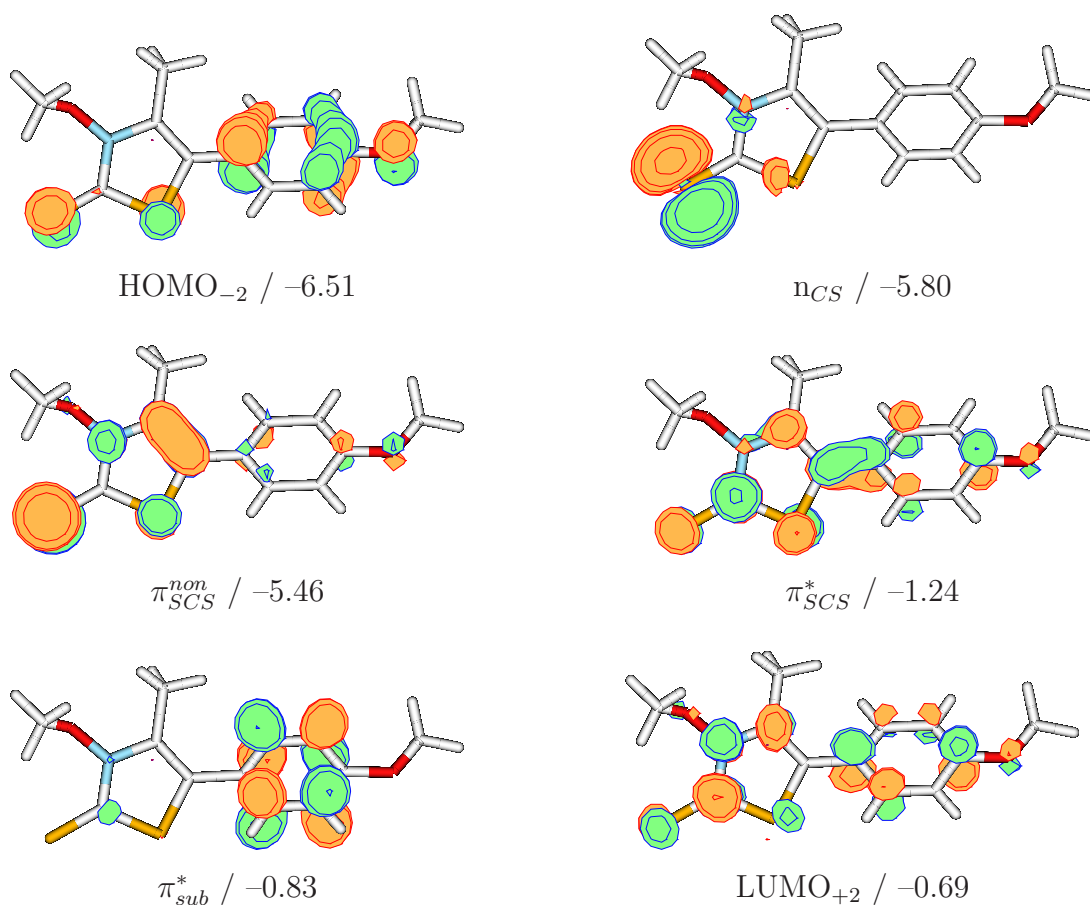


Figure 6.3: Visualization of relevant orbitals for an assignment of the configurations that contribute to the electronic spectra of *N*-(methoxy)-5-(*p*-methoxyphenyl)-4-methylthiazole-2(3*H*)-thione (**4me5ani**) The calculated B3LYP orbital energies are given in eV.

as a π_{sub}^* -orbital. The LUMO_{+2} in **4me5ani** resembles the π_{SCS}^* -orbital of the parent thione **2a-OMe** with additional contributions from orbitals of the *ipso*-, *ortho*- and *para*-carbon atoms of the *p*-methoxyphenyl group. Additional occupied and virtual orbitals besides those outlined above contribute to the calculated UV/Vis spectrum **4me5ani** in the region of $\lambda > 250$ nm. Their orbital shapes shall, however, not be addressed in a similar explicit way due to their complexity.

The first two calculated excitations in the UV/vis spectrum of thiazolethione **4me5ani** up to 250 nm corresponds to the $n_{CS} \rightarrow \pi_{SCS}^*$ and the $\pi_{SCS}^{non} \rightarrow \pi_{SCS}^*$ transition of the parent compound **2a-OMe**. On the basis of spectral intensities and the orbital analysis, the band located at $\lambda_{exp} = 335$ nm for thione **4me5ani** is correlated with the photoactive $\pi_{SCS}^{non} \rightarrow \pi_{SCS}^*$ excitation that initiates the photochemical N,O homolysis. Due to the complex characters of the other excitations in the computed spectral region a clear assignment of the shoulder at 258 nm could not be done. Based on the close structural analogy, a similar

assignment of experimentally observed bands to electronic transitions should be valid for other 5 aryl substituted *N*-(alkoxy)-thiazole-2(3*H*)-thiones like **4me5pcl**.

molecule	TD-B3LYP		RI-CC2	
	excitation energy	$\Delta_{\mathbf{2a-OMe}}$	excitation energy	$\Delta_{\mathbf{2a-OMe}}$
		nm eV		nm eV
2a-OMe	298 / 4.16		300 / 4.14	
4me5h	297 / 4.17	-1 0.01	302 / 4.11	2 -0.03
4h5me	300 / 4.13	2 -0.03	302 / 4.10	2 -0.03
4me5me^a	299 / 4.15	1 -0.01	304 / 4.08	4 -0.06
4me5pcl	343 / 3.62	45 -0.54	317 / 3.91	17 -0.23
4me5ani^a	325 / 3.82	27 -0.34	314 / 3.95	14 -0.19
4pcl5h^a	300 / 4.14	2 -0.02	308 / 4.03	8 -0.10
4ani5h	319 / 3.89	21 -0.27	305 / 4.06	6 -0.08

Table 6.5: The excitation energies [nm / eV] of the $\pi_{SCS}^{non} \rightarrow \pi_{SCS}^*$ transition in the observed C⁴ and C⁵ substituted *N*-(methoxy)-thiazole-2(3*H*)-thione alkoxy radical precursors on the TD-B3LYP/TZVP and the RI-CC2/cc-pVTZ level of theory.

$${}^a\Delta E_{exp}^{4me5me} = 3 \text{ nm}; \Delta E_{exp}^{4me5ani} = 15 \text{ nm}; \Delta E_{exp}^{4pcl5h} = -3 \text{ nm}.$$

The entries for the 4 or 5 aryl substituted thiazolethiones in table 6.1 confirm the experimentally observed trend of a stronger influence of a C⁵ substitution only partly. For a *para*-chlorophenyl substituent in position C⁴ theory also predicts only a small bathochromic shift of about 2 nm for the initial $\pi_{SCS}^{non} \rightarrow \pi_{SCS}^*$ transition in **4pcl5h** with respect to **2a-OMe**. However, for an anisyl substituent in the C⁴ position (**4ani5h**) a red shift of nearly 21 nm is obtained on the TD-B3LYP/TZVP level of theory. Aromatic substituents at C⁵ should induce a red shift of 27 nm in the case of an anisyl substituent (**4me5ani**), and for the the *para*-chlorophenyl substituent (**4me5pcl**) a shift of even 45 nm to longer wave length is predicted in contrast to **2a-OMe**. These calculated surprising strong red shifts of the $\pi_{SCS}^{non} \rightarrow \pi_{SCS}^*$ transition that are not found in the experiment (only 15 nm bathochromic shift in the case of **4me5ani** and nearly no influence in the case of a C⁴ aryl substituent) could be artefacts from the wrong fall off behavior of the applied B3LYP functional. Therefore the relevant electronic excitation of the 4 and 5 substituted *N*-(methoxy) thiazolethiones were recalculated on the RI-CC2/cc-pVTZ level of theory. The obtained excitation energies for the photochemically relevant $\pi_{SCS}^{non} \rightarrow \pi_{SCS}^*$ transition of the various thiazolethiones obtained on the TD-B3LYP/TZVP and the RI-CC2/cc-pVTZ level of theory are summarized in table 6.5. The columns " $\Delta_{\mathbf{2a-OMe}}$ " contain the calculated values for the substituent effect on the excitation energy in comparison to **2a-OMe**. These computations indeed reveal the problem of the B3LYP functional to describe the electronic excitation out of the π_{SCS}^{non} -orbital mainly located on the thiazolethione heterocycle into virtual orbitals that are delocalized over both

conjugated cyclic systems. For the C⁵ aryl substituted heterocycles RI-CC2 confirms the experiment and predicts a bathochromic effect of only 14 nm for the 5 anisyl compound and a slightly stronger red shift of 17 nm for the 5 *p*-chlorophenyl substituted heterocycle. For an aromatic C⁴ substituent nearly no effect on the excitation energy for the photoactive $\pi_{SCS}^{non} \rightarrow \pi_{SCS}^*$ transition was found like in the experiment.

6.3 Substituents on the Pyridinethione Heterocycle

6.3.1 Electron Withdrawing Fluorine Substituents

molecule	$n_{CS} \rightarrow \pi_{ring}^*$			$\pi_{CS} \rightarrow \pi_{ring}^*$		
	ΔE_{calc}	ΔE_{incr}	Δ_{calc}	ΔE_{calc}	ΔE_{incr}	Δ_{calc}
1a-OMe	2.77 / 448			3.33 / 372		
F3^a	2.73 / 454	$\Delta_3 = -0.04$		3.44 / 360	$\Delta_3 = 0.11$	
F4^a	2.91 / 425	$\Delta_4 = 0.15$		3.39 / 366	$\Delta_4 = 0.06$	
F5^a	2.63 / 472	$\Delta_5 = -0.14$		3.17 / 392	$\Delta_5 = -0.16$	
F6^a	2.79 / 444	$\Delta_6 = 0.02$		3.46 / 359	$\Delta_6 = 0.13$	
F34	2.87 / 432	2.88 / 432	0.00	3.49 / 355	3.50 / 354	0.01
F35	2.63 / 472	2.59 / 478	-0.04	3.29 / 376	3.28 / 380	-0.02
F36	2.74 / 452	2.75 / 451	0.01	3.53 / 351	3.57 / 347	0.04
F45	2.79 / 445	2.77 / 449	-0.01	3.27 / 380	3.23 / 385	-0.04
F46	2.93 / 423	2.94 / 422	0.01	3.56 / 349	3.52 / 352	-0.04
F56	2.68 / 463	2.65 / 468	-0.03	3.27 / 379	3.29 / 378	0.02
F345	2.78 / 447	2.73 / 456	-0.04	3.38 / 367	3.34 / 373	-0.04
F346	2.87 / 432	2.90 / 429	0.02	3.62 / 343	3.63 / 340	0.01
F356	2.64 / 469	2.61 / 475	-0.03	3.35 / 370	3.40 / 366	0.05
F456	2.82 / 439	2.80 / 446	-0.03	3.39 / 365	3.35 / 371	-0.04
F3456	2.79 / 445	2.76 / 452	-0.03	3.46 / 358	3.46 / 359	0.00
	$\sigma_{n_{CS} \rightarrow \pi_{ring}^*} = 0.026 \text{ eV}^b$			$\sigma_{\pi_{CS} \rightarrow \pi_{ring}^*} = 0.031 \text{ eV}^b$		

^aFor the monofluorinated derivatives the Δ_x values represent the difference between the excitation energies of **1a-OMe** and **F x** .

^b σ is the standard deviation between the excitation energies obtained from the direct calculations and the incrementally estimated ones.

Table 6.6: Comparison of the TD-B3LYP excitation energies for the possible substitution patterns of the fluorinepyridines with the excitation energies obtained from the incremental system. All excitation energies are in eV / nm.

Since *N*-(methoxy)-pyridine-2(1*H*)-thione (**1a-OMe**) exhibits a strong sensitivity to daylight due to a broad absorption band at about 360 nm the desired substituent effects on the spectra of the pyridine compounds would be a blueshift of the visible $\pi_{CS} \rightarrow \pi_{ring}^*$ excitation. To achieve this goal at first electron withdrawing fluorine substituents are introduced.

The calculated excitation energies for all possible fluorine derivates of *N*-(methoxy)-pyridine-2(1*H*)-thione (**1a-OMe**) are summarized in table 6.6. The columns labeled ΔE_{calc} contain the values that were obtained by directly calculating the excitation energies of the multiple substituted molecules. The values of the column ΔE_{incr} are obtained by adding the differences in excitation energies between **1a-OMe** and the monosubstituted derivates to the calculated energies of **1a-OMe**.

$$\Delta E_{incr} = \Delta E_{\mathbf{1a-OMe}} + \sum_x \underbrace{(\Delta E_{\mathbf{Fx}} - \Delta E_{\mathbf{1a-OMe}})}_{\Delta_x} \quad (6.2)$$

The Δ_{calc} values give the difference between the directly calculated excitation energies and the values obtained via the incremental system.

$$\Delta_{calc} = \Delta E_{calc} - \Delta E_{incr} \quad (6.3)$$

The first three columns of table 6.6 show the calculated values for the spectroscopic forbidden $n_{CS} \rightarrow \pi_{ring}^*$ excitation. A fluorination at C⁴ increases the $n_{CS} \rightarrow \pi_{ring}^*$ excitation energy about 0.15 eV, while a substitution at C⁵ leads to a shift of 0.14 eV towards lower excitation energies. The TD-B3LYP calculations predict nearly no effects of a fluorination at C³ or C⁶ on the $n_{CS} \rightarrow \pi_{ring}^*$ excitation energy. A comparison between the mono- and the poly-substituted systems shows that these substituent effects are additive. The differences between the directly calculated energies and the excitation energies obtained through the incremental system are smaller than 0.05 eV and the standard deviation $\sigma_{n \rightarrow \pi^*}$ (see equation 6.1) is only 0.026 eV.

In the second set of columns in table 6.6 the calculated values for the spectroscopic visible $\pi_{CS} \rightarrow \pi_{ring}^*$ excitation are listed, which represents the initial excitation for the photochemical N,O bond homolysis. Therefore this excitation represents the possibility to tune the photo sensibility of these compounds. A fluorination at C⁵ decreases the excitation energy about 0.16 eV which corresponds to a red shift of about 20 nm. The substitution of the hydrogen atoms by fluorine at the other positions in the pyridine ring increases the value for the excitation energy. The biggest hypsochromic effects with 12 nm and 13 nm are found for **F3** and **F6** respectively. Like for the $n_{CS} \rightarrow \pi_{ring}^*$ excitation energies the effects of the fluorination on the $\pi_{CS} \rightarrow \pi_{ring}^*$ transition are additive. The largest deviation from the directly calculated values is 0.05 eV and the standard deviation $\sigma_{\pi \rightarrow \pi^*}$ is 0.031 eV. A multiple fluorination on the positions C³, C⁴ and C⁶ would give access to derivates of

N-(methoxy)-pyridine-2(1*H*)-thione (**1a-OMe**) which exhibit stronger blue shifts in their excitation wave lengths. In the trifluorinated molecule (**F346**) the excitation energy is shifted to 3.63 eV / 343 nm *i. e.* a hypsochromic shift of about 30 nm with respect to the parent compound **1a-OMe** is obtained according to the TD-B3LYP computations.

molecule	π_{CS} -orbital		n_{CS} -orbital		π_{ring}^* -orbital	
	E_{calc}	E_{incr}	E_{calc}	E_{incr}	E_{calc}	E_{incr}
1a-OMe	-5.67		-5.61		-1.85	
F3^a	-5.83	$\Delta_3 = -0.16$	-5.78	$\Delta_3 = -0.17$	-2.01	$\Delta_3 = -0.16$
F4^a	-5.88	$\Delta_4 = -0.21$	-5.80	$\Delta_4 = -0.19$	-1.91	$\Delta_4 = -0.06$
F5^a	-5.80	$\Delta_5 = -0.13$	-5.77	$\Delta_5 = -0.16$	-2.18	$\Delta_5 = -0.33$
F6^a	-5.84	$\Delta_6 = -0.17$	-5.80	$\Delta_6 = -0.19$	-1.97	$\Delta_6 = -0.12$
F34	-6.03	-6.04	-5.98	-5.97	-2.07	-2.07
F35	-5.95	-5.96	-5.98	-5.94	-2.32	-2.34
F36	-5.98	-6.00	-6.00	-5.97	-2.17	-2.13
F45	-6.01	-6.01	-5.98	-5.96	-2.21	-2.24
F46	-6.05	-6.05	-5.99	-5.99	-2.00	-2.03
F56	-5.94	-5.97	-5.97	-5.96	-2.28	-2.30
F345	-6.17	-6.17	-6.14	-6.13	-2.36	-2.40
F346	-6.19	-6.21	-6.16	-6.16	-2.20	-2.19
F356	-6.10	-6.13	-6.16	-6.13	-2.46	-2.46
F456	-6.16	-6.18	-6.14	-6.15	-2.30	-2.36
F3456	-6.29	-6.34	-6.33	-6.32	-2.36	-2.52
	$\sigma_{\pi_{CS}} = 0.023 \text{ eV}^b$		$\sigma_{n_{CS}} = 0.020 \text{ eV}^b$		$\sigma_{\pi_{ring}^*} = 0.056 \text{ eV}^b$	

^aFor the monofluorinated derivatives the Δ_x values represent the difference between the orbital energies of **1a-OMe** and **F x** .

^b σ is the standard deviation between the orbital energies obtained from the direct calculations and the incrementally estimated ones.

Table 6.7: Comparison of the directly calculated orbital energies [in eV] for the possible substitution patterns of the fluorinepyridines with the orbital energies obtained from the incremental system.

To get deeper information about the effects of the fluorination the energies of the n_{CS} -, the π_{CS} - and the π_{ring}^* -orbital were also investigated in detail (B3LYP/TZVP orbital energies see table 6.7). A fluorination of the heterocycle leads to a stabilization of these orbitals. The n_{CS} -orbital is decreased in energy uniformly, independent from the position of the fluorination. The π_{CS} -orbital is especially stabilized in molecule **F4** while a C⁵ fluorination leads only to a small decrease in energy of this orbital. The virtual π_{ring}^* -orbital exhibits the strongest stabilization in molecule **F5**. The substituent effects on the orbital energies

are also additive and can be estimated with the aid of the energies of the mono substituted derivatives. The standard deviations for the incrementally obtained orbital energies are $\sigma_{n_{CS}} = 0.020$ eV, $\sigma_{\pi_{CS}} = 0.023$ eV and $\sigma_{\pi_{ring}^*} = 0.056$ eV.

Since the n_{CS} -orbital is lowered uniformly in energy the $n_{CS} \rightarrow \pi_{ring}^*$ excitation energy is mainly influenced by the energetic position of the π_{ring}^* -orbital. A correlation of the substituent effects on the orbital energy differences with the effects on the electronic excitations is possible. The strong stabilization of the virtual π_{ring}^* -orbital by a fluorination on C⁵ directly reflects in the decrease of the $n_{CS} \rightarrow \pi_{ring}^*$ excitation energy in all 5-fluorine derivatives of **1a-OMe**.

A comparison of the substituent effects calculated via the excitation energies

$$\Delta E_{subst} = E_{n \rightarrow \pi^* / (\mathbf{F} \mathbf{x})} - E_{n \rightarrow \pi^* / (\mathbf{1a-OMe})} \quad (6.4)$$

with the obtained substituent effects from the orbital energy differences

$$\Delta E_{\Delta \varepsilon} = E_{n-\pi^* / (\mathbf{F} \mathbf{x})} - E_{n-\pi^* / (\mathbf{1a-OMe})} \quad (6.5)$$

gives a standard deviation of only $\sigma_{\Delta n-\pi^*} = 0.071$ eV.

For the $\pi_{CS} \rightarrow \pi_{ring}^*$ excitation the substituent effects on the excitation energies are not reflected that well in the orbital energy differences. The decrease of the excitation energy in the case of a fluorination at C⁵ is found in the corresponding orbital energy differences whereas the increase of the excitation energy in the case of a fluorination at C³ and C⁶ is not seen in the $\pi_{CS} - \pi_{ring}^*$ -orbital energy differences. For this transition the standard deviation between the directly calculated substituent effects and the effects found from the orbital energy differences is $\sigma_{\Delta \pi-\pi^*} = 0.106$ eV.

6.3.2 Validation of the TD-DFT Approach

To check the reliability of the TD-B3LYP method for the description of the substituent effects the first two excitations of all possible *N*-(methoxy)-fluorinepyridine-2(1*H*)-thione derivatives were recalculated on the CASPT2/cc-pVDZ level of theory. To estimate the effect of this rather small basis sets on the calculated energies of the excited states the obtained values for *N*-(methoxy)-pyridine-2(1*H*)-thione (**1a-OMe**) can be compared with the values for the triple zeta basis set in subsection 4.3.1 in table 4.4. If the multi-state variant of the CASPT2 approach (MS-CASPT2) and the G3 approach for the fock matrix is used the calculated excitation energies for the first two states only differ by about 0.05 eV.

In table 6.8 the CASPT2 excitation energies of the $n_{CS} \rightarrow \pi_{ring}^*$ and the $\pi_{CS} \rightarrow \pi_{ring}^*$ transition for **1a-OMe** and all possible fluorinated pyridinethiones are listed. Like for the

molecule	$n_{CS} \rightarrow \pi_{ring}^*$			$\pi_{CS} \rightarrow \pi_{ring}^*$		
	ΔE_{calc}	ΔE_{incr}	Δ_{calc}	ΔE_{calc}	ΔE_{incr}	Δ_{calc}
1a-OMe	3.00 / 413			3.24 / 383		
F3^a	2.87 / 432	$\Delta_3 = -0.13$		3.26 / 380	$\Delta_3 = 0.02$	
F4^a	3.14 / 395	$\Delta_4 = 0.13$		3.31 / 375	$\Delta_4 = 0.07$	
F5^a	2.82 / 439	$\Delta_5 = -0.18$		3.05 / 407	$\Delta_5 = -0.19$	
F6^a	2.98 / 416	$\Delta_6 = -0.02$		3.30 / 376	$\Delta_6 = 0.06$	
F34	3.01 / 412	3.00 / 415	-0.01	3.33 / 372	3.33 / 372	0.00
F35	2.77 / 448	2.69 / 458	-0.08	3.14 / 395	3.07 / 405	-0.07
F36	2.87 / 432	2.85 / 435	-0.02	3.35 / 370	3.32 / 373	-0.03
F45	3.02 / 411	2.96 / 422	-0.06	3.19 / 389	3.12 / 399	-0.07
F46	3.13 / 396	3.12 / 398	-0.02	3.45 / 360	3.37 / 367	-0.08
F56	2.87 / 433	2.81 / 442	-0.06	3.08 / 402	3.11 / 400	0.02
F345	2.92 / 425	2.82 / 441	-0.09	3.24 / 383	3.14 / 396	-0.10
F346	2.99 / 414	2.98 / 418	-0.01	3.39 / 366	3.39 / 365	0.00
F356	2.75 / 452	2.67 / 461	-0.08	3.16 / 393	3.13 / 397	-0.03
F456	3.02 / 410	2.94 / 424	-0.09	3.29 / 377	3.18 / 392	-0.11
F3456	2.91 / 426	2.80 / 444	-0.11	3.27 / 379	3.20 / 389	-0.07
		$\sigma_{n \rightarrow \pi^*} = 0.066 \text{ eV}^b$			$\sigma_{\pi \rightarrow \pi^*} = 0.064 \text{ eV}^b$	

^aFor the monofluorinated derivatives the Δ_x values represent the difference between the excitation energies of **1a-OMe** and **F x** .

^b σ is the standard deviation between the excitation energies obtained from the direct calculations and the incrementally estimated ones.

Table 6.8: Comparison of the CASPT2//cc-pVDZ excitation energies for the possible substitution patterns of the fluorinepyridines with the excitation energies obtained from the incremental system. All excitation energies are in eV / nm.

TD-DFT results the columns labeled ΔE_{calc} contain the directly obtained excitation energies whereas the columns labeled ΔE_{incr} contain the values for the excitation energies of the multiply fluorinated systems estimated with the aid of the values for the monofluorinated systems.

Generally the CASPT2 calculations confirm the estimated substituent effects on the investigated electronic excitations predicted by TD-B3LYP for a C⁴, C⁵ and C⁶ fluorination. A fluorination at C⁵ leads to a decrease of the excitation energies of the $n_{CS} \rightarrow \pi_{ring}^*$ and the $\pi_{CS} \rightarrow \pi_{ring}^*$ excitation by 0.2 eV. A C⁴ fluorination increases the $n_{CS} \rightarrow \pi_{ring}^*$ excitation energy by 0.13 eV and the value for the $\pi_{CS} \rightarrow \pi_{ring}^*$ transition by 0.07 eV. For a C⁶ fluorination nearly no effect on the $n_{CS} \rightarrow \pi_{ring}^*$ transition was computed by CASPT2. The absolute value of the effect of a C⁶ fluorination on the $\pi_{CS} \rightarrow \pi_{ring}^*$ excitation obtained by

CASPT2 ($\Delta_6 = 0.06$ eV) is only half the magnitude than the value obtained with the TD-B3LYP method. For the 3-fluorine pyridinethione **F3** both methods also disagree. While time-dependent B3LYP predicts nearly no substituent effect on the $n_{CS} \rightarrow \pi_{ring}^*$ transition CASPT2 computes an effect for this transition that is nearly as big as for a C⁵ fluorination. For the spectroscopic important $\pi_{CS} \rightarrow \pi_{ring}^*$ excitation in contrast TD-DFT predicts a much bigger effect than CASPT2.

Like for the TD-DFT calculations the CASPT2 increments are additive. The excitation energies for multiple fluorinated pyridinethiones estimated via the incremental system, however, do not agree that nice with the directly calculated values as in the case of the TD-DFT results. The maximal deviation from the directly calculated excitation energies for the $n_{CS} \rightarrow \pi_{ring}^*$ transition is about 0.1 eV and the standard deviation $\sigma_{n \rightarrow \pi^*}$ is 0.066 eV. The incremental values for the $\pi_{CS} \rightarrow \pi_{ring}^*$ excitation energies have, with the standard deviation of $\sigma_{\pi \rightarrow \pi^*} = 0.064$ eV and a maximal deviation of 0.11 eV, the same correlation to the directly obtained values as for the $n_{CS} \rightarrow \pi_{ring}^*$ excitation.

$n_{CS} \rightarrow \pi_{ring}^*$					
method	F3	F4	F5	F6	F346 ^a
B3LYP ^b	-0.01	0.18	-0.16	0.06	0.18 / 0.22
PBE0 ^b	-0.03	0.19	-0.16	0.04	0.15 / 0.20
RI-CC2 ^b	-0.06	0.18	-0.14	0.00	0.08 / 0.13
CASPT2 ^c	-0.12	0.15	-0.18	0.00	0.04 / 0.03
$\pi_{CS} \rightarrow \pi_{ring}^*$					
method	(F3)	(F4)	(F5)	(F6)	F346 ^a
B3LYP ^b	0.15	0.07	-0.20	0.18	0.39 / 0.40
PBE0 ^b	0.14	0.09	-0.21	0.17	0.38 / 0.40
RI-CC2 ^b	0.09	0.14	-0.22	0.09	0.27 / 0.33
CASPT2 ^c	0.05	0.09	-0.22	0.10	0.23 / 0.25

^aThe left value given for (**F346**) shows the substituent effects obtained through the direct calculation of the molecule while the right value corresponds to the incrementally estimated substituent effects.

^bThe cc-pVTZ basis sets were used.

^cThe cc-pVDZ basis sets were used due to hardware and software limitations.

Table 6.9: Comparison of the increments (in eV) for fluorine substituent on the pyridinethione heterocycle obtained with different methods on the RI-MP2/cc-pVTZ structure.

The influence of the calculated ground state structure, the level of theory and the basis sets on the predictions of the incremental system is additionally checked. This was done for the monofluorinated molecules and for *N*-(methoxy)-3,4,6-trifluorinepyridine-2(1*H*)-thione (**F346**) since it exhibits the biggest desired hypsochromic shift for the $\pi_{CS} \rightarrow \pi_{ring}^*$ excita-

tion wave length. In table 6.9 the values of the increments for the substituent effects in the possible monofluorinated pyridinethiones obtained with various methods and the directly calculated and the incrementally estimated values for the substituent effects on the excitation energies in molecule **F346** are given. A comparison of the values in the lines B3LYP and CASPT2 with the corresponding numbers in tables 6.6 and 6.8 shows the small influence of the structure on the predictions of the substituent effects. For the TD-DFT calculations the difference between the increments obtained on the RI-BLYP and the RI-MP2 structure is smaller than 0.1 eV. This difference falls in the range of the usual uncertainties of the TD-DFT method. In the case of the CASPT2 increments the difference between the two structures is, with a value of < 0.05 eV for the mono fluorinated systems, even smaller. The lines labeled B3LYP and PBE0 show that the incremental system itself is not that dependent on the choice of the functional than the absolute values of the excitation energies (compare section 4.3). The values of the increments for the mono fluorinated molecules do not differ more than 0.02 eV between the two functionals. A comparison with the substituent effects predicted by the RI-CC2 method shows the same trends like the other approaches in the cases of a C⁴ or C⁵ fluorination. For **F6** the RI-CC2 calculations confirms the predictions made by CASPT2. This could be an evidence that the TD-DFT overestimates the influence of a fluorine substituent at C⁶. In the case of the fluorination at C³ the RI-CC2 values for the substituent effects on the excitation energies lie in between the predictions of the CASPT2 and the TD-DFT values. For the most promising multi-fluorinated pyridine derivate **F346** CASPT2 predicts a blue shift of only 24 nm (0.25 eV). This shift is also confirmed by the RI-CC2 approach.

6.3.3 Electron Rich Methoxyl Substituents

To compare the effects of the electron withdrawing fluorine substituents with electron rich substituents the hydrogen atoms of the pyridine heterocycle were also systematically substituted by methoxyl groups.

The results from the TD-B3LYP calculations on the first two excitations of the various possible methoxypyridinethiones are summarized in table 6.10. A first analysis of the values for the multiple substituted methoxyl derivates obtained via the incremental system shows a bad agreement with the directly calculated values. The maximal difference between the directly obtained values and the incremental values is 0.24 eV for the $n_{CS} \rightarrow \pi_{ring}^*$ transition and nearly 0.5 eV for the $\pi_{CS} \rightarrow \pi_{ring}^*$ transition. The standard deviations are $\sigma_{n \rightarrow \pi^*} = 0.119$ eV and $\sigma_{\pi \rightarrow \pi^*} = 0.249$ eV. The estimation of the orbital energies of the n_{CS} -, the π_{CS} - and the π_{ring}^* -orbital with the aid of the increments leads to a even worse agreement with the direct obtained values. Here the standard deviations are $\sigma_{n_{CS}} = 0.209$ eV for the

molecule	$n_{CS} \rightarrow \pi_{ring}^*$			$\pi_{CS} \rightarrow \pi_{ring}^*$		
	ΔE_{calc}	ΔE_{incr}	Δ_{calc}	ΔE_{calc}	ΔE_{incr}	Δ_{calc}
1a-OMe	2.77 / 448			3.33 / 372		
O3^a	2.76 / 449	$\Delta_3 = 0.00$		3.54 / 350	$\Delta_3 = 0.21$	
O4^a	3.08 / 403	$\Delta_4 = 0.31$		3.52 / 353	$\Delta_4 = 0.19$	
O5^a	2.68 / 463	$\Delta_5 = -0.09$		3.20 / 388	$\Delta_5 = -0.13$	
O6^a	2.82 / 439	$\Delta_6 = 0.05$		3.49 / 355	$\Delta_6 = 0.16$	
O34	2.89 / 430	3.07 / 404	0.19	3.42 / 363	3.73 / 331	0.31
O35	2.74 / 452	2.67 / 464	-0.07	3.32 / 374	3.41 / 366	0.09
O36	2.83 / 439	2.82 / 440	-0.01	3.51 / 354	3.70 / 333	0.20
O45	2.87 / 432	2.98 / 418	0.12	3.26 / 380	3.38 / 368	0.12
O46	3.03 / 409	3.13 / 395	0.10	3.52 / 352	3.68 / 335	0.15
O56	2.73 / 454	2.73 / 455	0.00	3.13 / 397	3.36 / 370	0.23
O345	2.83 / 438	2.98 / 419	0.15	3.42 / 363	3.59 / 346	0.18
O346	2.89 / 429	3.13 / 395	0.24	3.53 / 352	3.89 / 313	0.36
O356	2.77 / 448	2.73 / 456	-0.04	3.31 / 375	3.57 / 348	0.26
O456	3.02 / 410	3.04 / 410	0.01	3.47 / 357	3.55 / 351	0.07
O3456	2.92 / 425	3.03 / 411	0.11	3.30 / 376	3.76 / 329	0.46
	$\sigma_{n_{CS} \rightarrow \pi_{CS}^*} = 0.119 \text{ eV}^b$			$\sigma_{\pi_{CS} \rightarrow \pi_{CS}^*} = 0.249 \text{ eV}^b$		

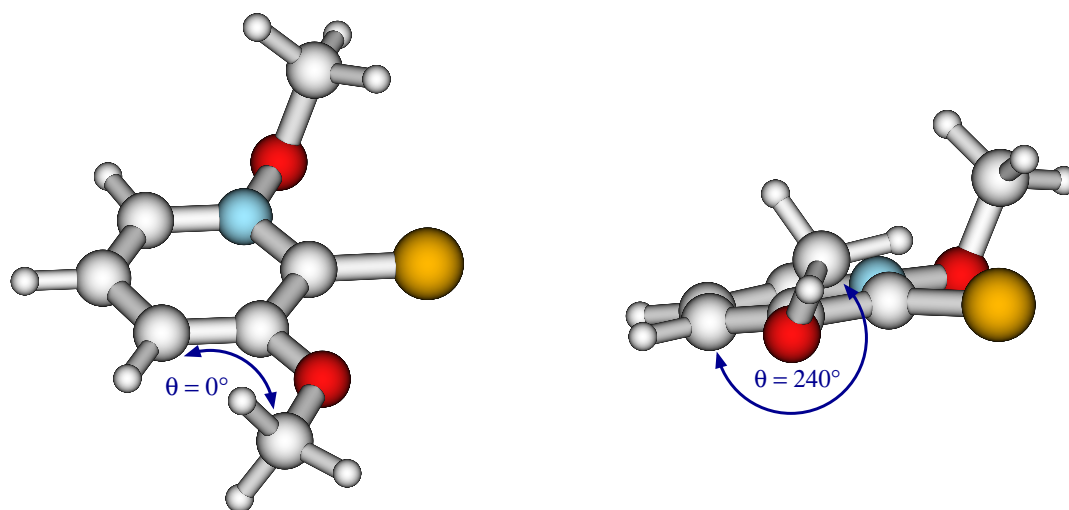
^aFor the mono methoxyl derivatives the Δ_x values represent the difference between the excitation energies of **1a-OMe** and **Ox**.

^b σ is the standard deviation between the excitation energies obtained from the direct calculations and the incrementally estimated ones.

Table 6.10: Comparison of the TD-B3LYP excitation energies for the possible substitution patterns of the methoxypyridines with the excitation energies obtained from the incremental system. All excitation energies are in eV / nm.

n_{CS} -orbital and $\sigma_{\pi_{CS}} = 0.226 \text{ eV}$ for the π_{CS} -orbital. For the virtual π_{ring}^* -orbital the value of $\sigma_{\pi_{ring}^*}$ is 0.272 eV . The reason for this failure of the incremental system is the orientation of the methoxyl groups in the multiply substituted pyridinethiones. Due to their steric demands not all of the methoxyl groups are in their optimal orientation.

In table 6.11 the dihedral angle between the pyridine heterocycle and the methoxyl substituents of the methoxylated molecules are listed. This angle is defined that for $\theta = 0^\circ$ the methoxyl group lies in the plane of the pyridine ring and the CH_3 group is pointing away from the thiocarbonyl group. The observed rotation takes place counterclockwise around the *C^{ipso}*-O bond. For **O3** the dihedral angle θ is 0° due to the steric demands of the thiocarbonyl group. For the same reason the *N*-(methoxyl) group directs the methoxyl group at C^6 to a



molecule	C ³	C ⁴	C ⁵	C ⁶	molecule	C ³	C ⁴	C ⁵	C ⁶
O3	0	—	—	—	O46	—	0	—	180
O4	—	180	—	—	O56	—	—	180	180
O5	—	—	0	—	O345	0	0	0	—
O6	—	—	—	180	O346	0	0	—	180
O34	0	0	—	—	O356	240	—	290	100
O35	240	—	0	—	O456	—	180	120	100
O36	240	—	—	180	O3456	100	0	290	100
O45	—	0	0	—					

Table 6.11: The calculated dihedral angle θ between the pyridine ring and the methoxyl groups as they occur in the methoxylated compounds.

dihedral angle θ of 180° . For **O4** and **O5** a value for θ of 180° respectively 0° was found. In the multiply substituted molecules some of the methoxyl groups are pointing out of the plane of the ring due to steric hindrance. To obtain information about the influence of the orientation of the methoxyl groups on the electronic excitations the rotation profile for the rotation around the $C^{ipso}-O$ bond of the four mono substituted pyridine derivatives were calculated (compare figure 6.4).

For a methoxyl group at C⁴ or C⁵ the arrangements with the methoxyl group in the plane of the ring are the optimal structures while for $\theta = 90^\circ$ the rotation profile exhibits a maximum. For the molecules **O3** and **O6** the rotation profiles have a more complex shape. Due to the steric demand of the thiocarbonyl sulfur atom for **O3** the orientation with $\theta = 180^\circ$ is a maximum on the potential surface for the rotation. At an dihedral angle θ of 120° and 240° a local minimum is found. This orientation for the methoxyl group is found in some of the multiply substituted molecules with a methoxyl group at C³. The

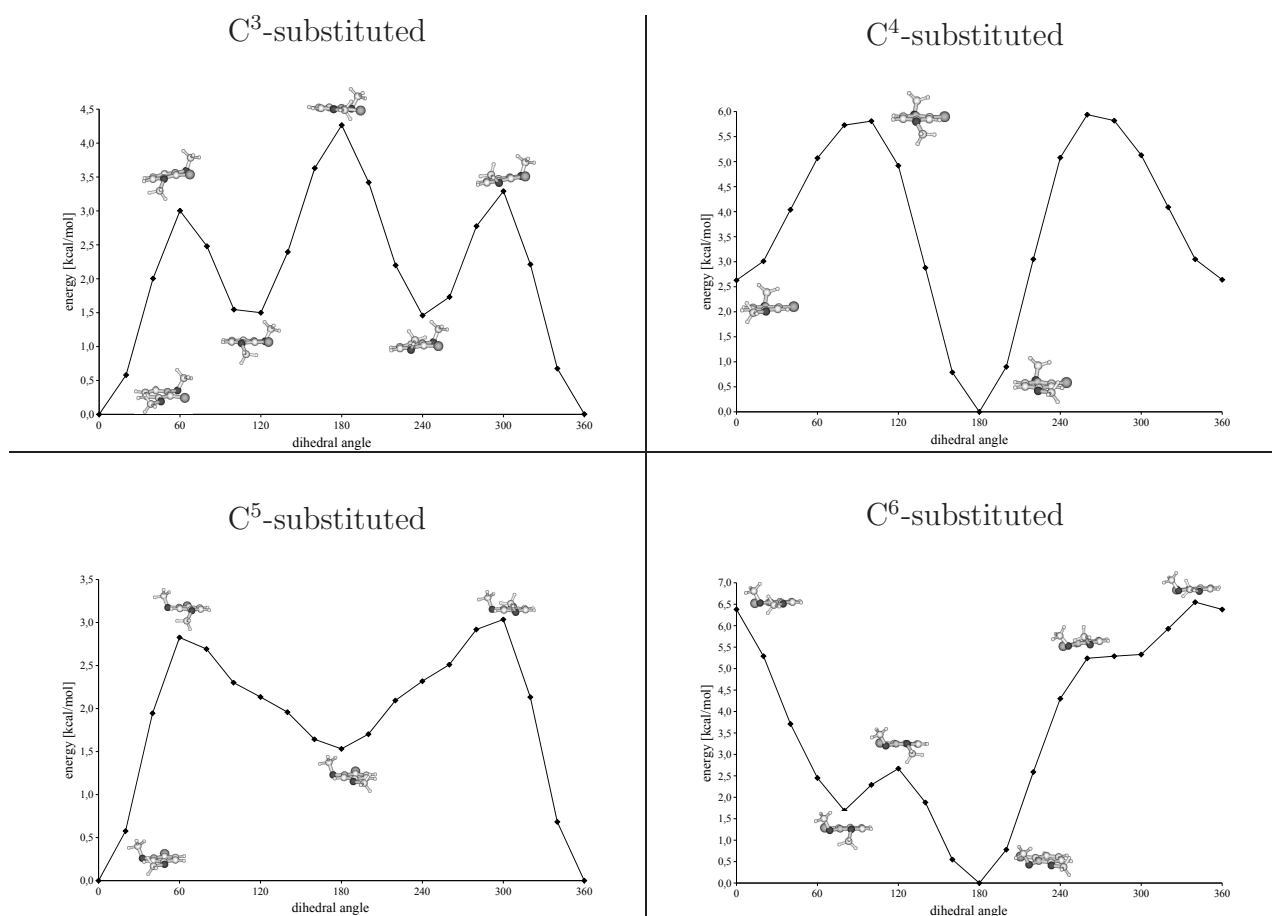


Figure 6.4: The rotation profiles for the rotation around the C^{ipso} -O bond of the four mono substituted pyridine derivatives.

minimum structure of **O6** exhibits a dihedral angle of $\theta = 180^\circ$. The $\theta = 0^\circ$ orientation is a maximum because of the steric hindrance of the methoxyl group attached to the pyridine nitrogen atom. At a dihedral angle of about 80° a second minimum is found. In the multiply substituted systems this orientation of the methoxyl substituent at C^6 is chosen if also the C^5 position is substituted with a methoxyl group. Since the rotation around the C^{ipso} -O bond influences the orbital energies of the n_{CS} - the π_{CS} - and the π_{ring}^* -orbital the excitation energies for the $n_{CS} \rightarrow \pi_{ring}^*$ and for the $\pi_{CS} \rightarrow \pi_{ring}^*$ transition also depend on the orientation of the methoxyl groups.

In table 6.12 the increments for the methoxyl substituents in their orientation as they occur in the multiply substituted pyridine derivatives (compare tab. 6.11) are listed. An attachment of a methoxyl group at C^3 or C^6 has nearly no influence on the $n_{CS} \rightarrow \pi_{ring}^*$ excitation energy. This is independent from a rotation around the C^{ipso} -O bond. A methoxyl group at C^4 increases the excitation energy of this transition. If the dihedral angle θ between the ring and the methoxyl group is 0° the excitation is shifted about 0.2 eV and if the angle $\theta = 180^\circ$ the value for the excitation energy even increases by 0.3 eV. A methoxylation at

θ^a	$n_{CS} \rightarrow \pi_{ring}^*$		$\pi_{CS} \rightarrow \pi_{ring}^*$	
	ΔE_{calc}	Δ_x	ΔE_{calc}	Δ_x
C ³ substituted				
0	2.77 / 448	0.00	3.54 / 350	0.21
100	2.79 / 445	0.02	3.40 / 365	0.07
240	2.81 / 442	0.04	3.43 / 361	0.10
C ⁴ substituted				
0	2.95 / 420	0.18	3.29 / 377	-0.04
180	3.08 / 403	0.31	3.52 / 353	0.19
C ⁵ substituted				
0	2.68 / 463	-0.09	3.20 / 388	-0.13
120	2.68 / 462	-0.08	3.18 / 390	-0.15
180	2.63 / 472	-0.14	3.02 / 411	-0.31
290	2.71 / 458	-0.06	3.21 / 386	-0.12
C ⁶ substituted				
100	2.77 / 448	0.00	3.35 / 370	0.03
180	2.82 / 439	0.05	3.49 / 355	0.16

^aThe orientations of the methoxyl group as they occur in the multiply methoxylated pyridinethione derivatives (compare tab. 6.11) are shown.

Table 6.12: The excitation energies [eV / nm] and the obtained increments (in eV) for different orientations of the methoxyl group.

C⁵ of the heterocycle has the opposite effect. This substituent decreases the $n_{CS} \rightarrow \pi_{ring}^*$ excitation energy by 0.06 to 0.14 eV.

The $\pi_{CS} \rightarrow \pi_{ring}^*$ excitation energy depends more on the orientation of the substituents. A methoxyl group at C³ increases this excitation energy. The effect is maximal if the methoxyl group is in its minimum orientation with $\theta = 0^\circ$. For this orientation the excitation energy is increased by 0.21 eV. At the other orientations of the methoxyl group this shift is only about 0.1 eV. For molecule **O4** a orientation with $\theta = 0^\circ$ leads to a slight decrease of the excitation energy. For $\theta = 180^\circ$ a shift of 0.2 eV to higher energies is found. Since in the monosubstituted molecules a free rotation around the C^{*ipso*}-O bond is possible a broadened absorption band should occur in the UV/vis spectra. This band would exhibit a maximum that is shifted about 0.1 eV to higher energy in comparison to molecule **1a-OMe**. Like for the fluorinated molecule **F5** a methoxyl substituent at position C⁵ decreases the $\pi_{CS} \rightarrow \pi_{ring}^*$ excitation energy. This effect is maximal if the dihedral angle θ is 180° . The excitation energy is decreased by 0.31 eV. At the other orientations that occur for a C⁵ methoxylated ring the decrease in excitation energy is only about 0.1 to 0.15 eV. In this

case the free rotation should also lead to a broadening of the UV/vis band and to an overall decrease of the excitation energy of about 0.15 to 0.2 eV. A methoxyl substituent at C⁶ in its optimal orientation of $\theta = 180^\circ$ leads to the highest value for the shift of the $\pi_{CS} \rightarrow \pi_{ring}^*$ excitation energy. It is increased by 0.16 eV in comparison to the unsubstituted molecule. For the other orientation that is found in the multiply substituted molecules ($\theta = 100^\circ$) nearly no effect on this electronic transition is found. With the new increments from table 6.12 and the orientations of the methoxyl substituents listed in table 6.11 the excitation energies of the multiply methoxylated pyridines can be estimated.

molecule	$n_{CS} \rightarrow \pi_{ring}^*$			$\pi_{CS} \rightarrow \pi_{ring}^*$			
	ΔE_{calc}	ΔE_{incr}^a	Δ_{calc}	ΔE_{calc}	ΔE_{incr}^a	Δ_{calc}	
O34	2.89 / 430	2.95 / 420	0.06	3.42 / 363	3.50 / 354	0.08	
O35	2.74 / 452	2.71 / 457	-0.03	3.32 / 374	3.30 / 376	-0.02	
O36	2.83 / 439	2.86 / 434	0.03	3.51 / 354	3.60 / 345	0.09	
O45	2.87 / 432	2.86 / 434	-0.01	3.26 / 380	3.16 / 393	-0.11	
O46	3.03 / 409	3.01 / 413	-0.03	3.52 / 352	3.45 / 359	-0.07	
O56	2.73 / 454	2.68 / 462	-0.05	3.13 / 397	3.18 / 390	0.05	
O345	2.83 / 438	2.86 / 434	0.03	3.42 / 363	3.37 / 368	-0.05	
O346	2.89 / 429	3.00 / 413	0.11	3.53 / 352	3.66 / 338	0.14	
O356	2.77 / 448	2.74 / 452	-0.03	3.31 / 375	3.34 / 371	0.04	
O456	3.02 / 410	2.99 / 414	-0.03	3.47 / 357	3.39 / 365	-0.08	
O3456	2.92 / 425	2.91 / 426	-0.01	3.30 / 376	3.27 / 379	-0.03	
		$\sigma_{n \rightarrow \pi^*} = 0.047 \text{ eV}^b$			$\sigma_{\pi \rightarrow \pi^*} = 0.077 \text{ eV}^b$		

^aThe orientations of the substituents as they occur in the multiply substituted molecules (compare tab. 6.12) were used.

^b σ is the standard deviation between the excitation energies obtained from the direct calculations and the incrementally estimated ones.

Table 6.13: Comparison of the TD-B3LYP excitation energies for the multiply substituted methoxypyridines with the excitation energies obtained from the new incremental system. All excitation energies are in eV / nm.

Table 6.13 compares the calculated excitation energies for the $n_{CS} \rightarrow \pi_{ring}^*$ and the $\pi_{CS} \rightarrow \pi_{ring}^*$ transition in the multiply substituted pyridinethione derivatives with the values obtained through the new incremental system.

With the new increments that take the orientation of the methoxyl groups in the multiply substituted systems into account the excitation energies obtained via the incremental system show nearly the same deviation from the directly obtained as for the fluorinepyridines. For the $n_{CS} \rightarrow \pi_{ring}^*$ transition the maximal deviation from the directly calculated excitation energies is also about 0.1 eV. The standard deviation $\sigma_{n \rightarrow \pi^*}$ is 0.047 eV. The new

incremental values for the $\pi_{CS} \rightarrow \pi_{ring}^*$ excitation energies have a standard deviation of $\sigma_{\pi \rightarrow \pi^*} = 0.077$ eV and a maximal deviation of 0.14 eV. These values for the correlation to the directly obtained values are slightly worse than for the $n_{CS} \rightarrow \pi_{ring}^*$ excitation, but still in the range of the accuracy of the TD-DFT.

To obtain information about the correlation of the orbital energy differences with the excitation energies the new incremental system with the optimized orientations of the methoxyl groups is first tested for the prediction of the orbital energies in the multiply substituted molecules. A methoxylation of the heterocyclic part of *N*-(methoxy)-pyridine-2(1*H*)-thione (**1a-OMe**) leads to a increase of the orbital energies of the n_{CS} - the π_{CS} - and the π_{ring}^* -orbitals, independent of the position of the methoxyl group. Only the π_{ring}^* -orbital in *N*-(methoxy)-5-methoxypyridine-2(1*H*)-thione (**O5**) is not affected by the methoxylation. The substituent effects are additive, but as for the excitation energies the steric orientations of the methoxyl groups (compare table 6.11) has to be taken in account. With the matching increments the orbital energies of the multiply substituted pyridinethiones could be determined. The standard deviation between the directly obtained orbital energies and the values calculated with the aid of the increments are $\sigma_n = 0.049$ eV, $\sigma_\pi = 0.080$ eV and $\sigma_{\pi^*} = 0.048$ eV for the virtual π_{ring}^* -orbital.

For the $n_{CS} \rightarrow \pi_{ring}^*$ transition the excitation energies of the molecules correlates very good with the energetic differences of the contributing orbitals. The maximal energy difference between the substituent effects calculated via the excitation energies and the obtained substituent effects from the orbital energy differences is smaller than 0.1 eV. The standard deviation for this difference is only $\sigma_{\Delta n-\pi^*} = 0.049$ eV. The decrease in excitation energy of this transition in the case of a C⁵ methoxylation could be rationalized with the vanishing effect of the methoxyl group at this position on the energy of the π_{ring}^* -orbital. In the case of a methoxylation at C⁴ the π_{ring}^* -orbital experiences the biggest destabilization. This correlates directly with the strongest increase in excitation energy of the $n_{CS} \rightarrow \pi_{ring}^*$ transition. For a methoxyl group at C³ or C⁶ the substituent effects on the n_{CS} - and the π_{ring}^* -orbital are similar. Therefore the overall shifts of the excitation energy in the case of **O3** and **O6** are small. The influence of the methoxyl substituents on the energetic position of the $\pi_{CS} \rightarrow \pi_{ring}^*$ excitation could not be explained easily by the orbital energy differences. The decrease of the excitation energy in the case of a C⁵ methoxylation has the same reason as for the $n_{CS} \rightarrow \pi_{ring}^*$ transition. The π_{CS} -orbital is raised in energy while the π_{ring}^* -orbital is not affected by a methoxyl substituent at position 5. This also holds for the increase of the $\pi_{CS} \rightarrow \pi_{ring}^*$ excitation energy in *N*-(methoxy)-4-methoxypyridine-2(1*H*)-thione (**O4**). Like for the fluorinated pyridinethiones the substituent effects in the C³ and C⁶ substituted molecules **O3** and **O6** could not be explained by the effects on the orbital energy differences. The standard deviation $\sigma_{\Delta\pi-\pi^*}$ is with 0.115 eV also in the same region than for the fluorinated molecules.

6.3.4 Comparison between the Fluorine and the Methoxyl Substituents.

A comparison between the electron withdrawing fluorine substituents and the electron rich methoxyl substituents shows the same effects on the observed electronic excitations. Though the effects that increase the excitation energies are bigger in the case of the methoxyl substituents. As expected the orbital energies of the contributing orbitals are lowered in energy if electron withdrawing fluorine substituents are introduced. The electron rich methoxyl substituents rise these orbital energies. For the $n_{CS} \rightarrow \pi_{ring}^*$ transition the biggest shift to higher excitation energies is achieved with a methoxyl substituent at C⁴. The excitation energy is risen by 0.31 eV. A fluorination at C⁵ leads to the lowest $n_{CS} \rightarrow \pi_{ring}^*$ excitation energy with a shift of -0.14 eV compared with molecule **1a-OMe**. For the UV/vis allowed $\pi_{CS} \rightarrow \pi_{ring}^*$ transition the largest bathochromic effect is achieved by a fluorination or methoxylation at C⁵. The $\pi_{CS} \rightarrow \pi_{ring}^*$ transition is shifted about 20 to 25 nm to longer wave length. This corresponds a decrease in excitation energy of about 0.15 to 0.2 eV. Methoxyl substituents at C³, C⁴ and C⁶ show the strongest hypsochromic effect on the excitation energy. They lead to a increase of the excitation energy of about 0.2 eV or a shift of the absorption wave length of 20 nm to shorter values. A monosubstitution with fluorine at this positions has a smaller effect but for molecule **F346** the additivity of the substituent effects leads to the strongest hypsochromic shifts in all observed molecules.

6.3.5 NO₂ Substituents that can conjugate with the π -Electrons

The last type of substituents that can influence the electronic spectra of the pyridinethione heterocycle are functional groups that are able to conjugate with the π -electron system. An example for this kind of substituents is the nitro group.

molecule	$n_{CS} \rightarrow \pi^{*a}$		$\pi_{CS} \rightarrow \pi^{*a}$	
	ΔE_{calc}	Δ_x	ΔE_{calc}	Δ_x
N3	2.29 / 542	-0.48	2.69 / 461	-0.64
N4	1.89 / 654	-0.87	2.38 / 520	-0.94
N5	2.41 / 515	-0.36	2.98 / 431	-0.35
N6	2.00 / 620	-0.77	2.32 / 534	-1.01

^aDue to the contributions of the nitro substituents the shape of the lowest π^* -orbital differs considerably from the π_{ring}^* -orbitals of the other observed compounds.

Table 6.14: The effects of a NO₂ substituent at the pyridine heterocycle on the first two electronic excitations. All excitation energies are in eV / nm.

Table 6.14 lists the calculated excitation energies and the increments for **1a-OMe** and the mono nitro compounds **N3–N6**. A comparable assignment to the $n_{CS} \rightarrow \pi_{ring}^*$ and the $\pi_{CS} \rightarrow \pi_{ring}^*$ transitions could not be made due to the NO_2 contributions to the π^* -orbitals. Their shapes differ considerably to the shapes of the π_{ring}^* -orbital of **1a-OMe** and the fluorinated and methoxylated pyridine derivatives. This π^* -orbital of the nitrated heterocycles exhibit a strong stabilization due to the conjugation with the NO_2 substituent which leads to a direct decrease of the excitation energies independent of the position of the NO_2 substituent. The strongest decrease in the $n_{CS} \rightarrow \pi^*$ excitation energy is found for a nitration at C^4 and C^6 . This correlates directly with the biggest stabilization effect of the NO_2 substituent on the π^* -orbital. For **N5** the smallest effect on the excitations was found. This results from a rather strong stabilization of the n_{CS} - and the π_{CS} -orbital in comparison to the π^* -orbital. In *N*-(methoxy)-3-nitropyridine-2(1*H*)-thione (**N3**) the NO_2 group is not periplanar with the heterocycle and the conjugation with the π electrons is worse. The result is a smaller redshift of the $n_{CS} \rightarrow \pi^*$ and the $\pi_{CS} \rightarrow \pi^*$ excitation wave length in comparison to **N4** and **N6**. The strong bathochromic effect of the NO_2 group on the spectroscopic active $\pi_{CS} \rightarrow \pi^*$ excitation leads to colored compounds and therefore to an expected strong sensibility to daylight. This excludes the nitro group and other substituents that are able to conjugate with the π electrons from the application as substituents to shift the photoactive $\pi_{CS} \rightarrow \pi_{ring}^*$ excitation of *N*-(alkoxy)-pyridine-2(1*H*)-thione compounds towards shorter wavelength. Nevertheless, if precursors on the basis of the pyridine-2(1*H*)-thione heterocycle with considerably red shifted spectra are wanted, the NO_2 group would be an appropriate substituent.

Chapter 7

Design of New Precursor Systems

To optimize the applied alkoxy radical precursors on the basis of the pyridinethione and the thiazolethione heterocycle in the last chapter a tuning of their initial photochemical excitation energy by introducing substituents on both parent compounds (**1a-OMe**; **2a-OMe**) has been described. This was done in a combined theoretical and experimental study in the case of the thiazolethione compounds. For substituted pyridine-2(*1H*)-thiones no experimental data on their UV/vis spectral properties is available. So the quantum chemical methodology established in chapter 4 for the unsubstituted parent compounds *N*-(methoxy)-pyridine-2(*1H*)-thione (**1a-OMe**) was applied to get information about substituent effects on the excitation energy of the $\pi_{CS} \rightarrow \pi_{ring}^*$ transition. Those computations suggested substitution patterns on the pyridine heterocycle that lead to a hypsochromic shift of the initial wave length.

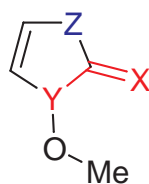
With the detailed knowledge on the N,O fragmentation process in **1a-OMe** and **2a-OMe** the higher reactivity during and after the photochemical alkoxy radical liberation process in the absence of efficient radical traps of the thiazole compounds can be explained. It results since the potential surfaces which determine the photolytic N,O bond cleavage process represent a perfect slide from the S_2 state through a conical intersection into the S_1 and then into the final ground state of the radical fragments. Due to the resulting fast dissociation process the excess energy which results from the photolytic fragmentation is dissipated to the solvent or other degrees of freedom only to small amounts. For *N*-(alkoxy)-pyridine-2(*1H*)-thiones (**1a-OR**) a dissipation of the excess energy is much more likely since their S_2 state possesses a barrier^a with respect to the dissociation. Additionally, no avoided crossing between S_2 and S_1 is found so that also the deexcitation process predicted for example by Kasha's rule can be expected to be much slower. Finally the maximal

^aaccording to computations on the parent compound **1a-OMe** described in subsection 5.2.3.

excess energy of the fragments is also lower. This results from a lower vertical excitation energy and a higher dissociation energy of the S_0 state. This model for the reactivity of photochemical alkoxy radical precursors on the basis of heterocyclic thiohydroxamic *O*-esters was extended and tested also for *N*-(methoxy)-pyridine-2(1*H*)-one (**1b-OMe**). Other *N*-(alkoxy) derivatives are already successfully employed as photochemical alkoxy radical sources. For **1b-OMe** the vertical $S_0 \rightarrow S_1$ transition leads to the photochemically active state, and the radical fragment **1b•** and the methoxyl radical should possess a maximal excess energy of 174 kJ mol^{-1} , which falls between the values obtained for **1a-OMe** and **2a-OMe**. The N,O fragmentation process is expected to be rather slow since in its S_1 state the molecule **1b-OMe** will be trapped in a quite deep minimum from which it can cross (via spin-orbit coupling) to the triplet surface. In the T_1 state it fragments into the desired radicals. Nevertheless due to the time needed for the singlet triplet transfer a large amount of excess energy should dissipate to the solvent or other degrees of freedom. The pyridyl-1-oxyl radical **1b•** was computed to be more reactive than the radical fragments **1a•** and **2a•**. However, since the amount of remaining excess energy is the most important factor for the reactivity **1b-OMe** should serve as a clean alkoxy radical source. This is indeed the case so this test supports that the model for the reactivity indeed captures the most important effects.

This model is now applied in a computer aided design to identify new lead structures for photochemical precursor systems which combine the advantages of the thiazole and the pyridinethione compounds. The dissociation behavior of new precursors should be similar to the behavior of pyridinethione compounds to avoid unwanted side reactions during the radical formation process. On the other hand the excitation wave length which initiates the fragmentation process should lie below the excitation wave length of the pyridinethiones so that no daylight sensitivity occurs. Since for many experiments on DNA oxidation and strand-breaking processes precursors that absorb at a wave length of about 350 nm are advantageous, additionally, the bond breaking process should be initiated by light with the wave length of about 350 nm.

To find new promising lead structures the parent substance of the thiazolethione precursors is modified systematically. The heterocycle is modified by substitution of the thiazole sulfur atom by other units. An enumeration of the various systems is summarized in figure 7.1. The pyrrole (**3**) heterocycle results from substitution of the sulfur with a CH_2 group while the imidazole system (**4**) is obtained if a NH moiety is introduced. An oxygen atom instead of sulfur leads to the oxazole heterocycle (**5**). A substitution of the sulfur by a PH unit generates the phosphazole heterocycle (**6**). Further modifications are obtained by a substitution of the thiocarbonyl group by a carbonyl group. This leads to the hydroxamic acid derivatives of the various heterocycles. Like already used in Chapter 5 the thiohydrox-



Z	heterocycle
CH=CH	pyridine (1)
S	thiazole (2)
CH ₂	pyrrole (3)
NH	imidazole (4)
O	oxazole (5)
PH	phosphazole (6)

X	Y	functional group
S	N	thione (a)
O	N	ketone (b)
S	P	phosphonethione (c)

Figure 7.1: Structural formula and indexing of the systematically modified heterocycles

amic acid derivatives are indexed by **a** while the hydroxamic acid derivatives will be indicated by **b**. Finally the exchange of the hydroxamic acid N atom with phosphorus results in “phosphothiohydroxamic” acid derivatives which will be denoted by **c**.

To identify the promising precursor systems a screening of the lower electronic excitations of all resulting 18 systems was performed with TD-DFT employing the B3LYP approach. This screening gives a first impression of the influences of different functional groups and heterocycles on the UV/vis spectra of these compounds. The calculated excitation wave length of the transition that exhibits strong oscillator strength and shows a $\pi \rightarrow \pi^*$ character^a is taken as a first selection criterion for the promising systems. For these molecules the influence of a polar solvent was estimated by a continuum model. To check the reliability of the TD-B3LYP approach the excitation energies between the ground state (S_0) and the first three singlet excited states of the preselected promising precursor systems were also recalculated with the CASPT2 method. If the CASPT2 confirmed the TD-DFT prediction the N,O or P,O dissociation paths, respectively, of the S_0 , the T_1 and the first two singlet excited states were computed. An analysis of these paths according to the model developed in chapter 5 gives information about the reactivity of the resulting radical fragments. Further informations are obtained by the isodesmic reaction shown in equation 5.1. This information is included, although comparing the small difference in the reaction energies of the isodesmic reactions with the large difference in the estimated maximal excess energies and taking into account that the derivatives of **1b-OMe**^b with longer

^aThis transition is assumed to be the initial electronic excitation for the photochemical bond homolysis process.

^bThe reaction energy of the obtained pyridyl-2-oxyl (**2a[•]**) radical with isobutane is with -6.6 kJ mol^{-1}

alkoxyl chains serve as clean photochemical source of alkoxyl radicals, the higher intrinsic reactivity is less important than the remaining excess energy.

7.1 Computational Details

All vertical excitation energies in the frame of the first screening were computed for theoretically determined ground state structures. Since many compounds needed to be screened for this step the structures were obtained with the RI-BLYP/SVP approach. This approach is sufficient for the screening since for the precursors **1a-OMe** and **2a-OMe** the influence of the structure on the vertical excitation energies was found to be small in comparison to uncertainties arising from the TD-DFT approaches (compare chapter 4). For the screening the vertical excitation energies of the five lowest lying states were obtained with TD-DFT employing the B3LYP functional. In these computations the TZVP basis sets were applied. To check the solvent effects on the excitation energies the COSMO approach with a dielectric constant $\epsilon = 78$ was applied in the frame of the TD-DFT calculations. The characters of the photochemically relevant absorptions were identified through their oscillator strength and the shapes of the contributing orbitals. To validate the TD-DFT approach for the most promising systems the ground state structures were reoptimized (RI-MP2/cc-pVTZ) and the excitation energies were recalculated employing the (12/12) MS-CASPT2/cc-pVTZ approach. For all hydrogen atoms the cc-pVDZ basis sets have to be employed due to software and hardware limitations. For the UV/vis absorption spectra the TD-DFT oscillator strengths were employed. As shown in section 4.3 for **1a-OMe** and **2a-OMe** this approximation is sufficiently accurate for trends.

The calculations for the reaction paths (figures 7.2–7.4) were performed on the CASPT2 level of theory applying the cc-pVTZ basis sets. According to previous calculations (chapter 5) the bond dissociation paths in the S_1 and S_2 states are described reasonable if triplet structures (T_1 structure) are employed, at least as long as both fragments interact with each other. For the description of the N,O cleavage (or P,O cleavage in case of the molecules **c**) all internal degrees of freedom of the molecules were optimized at defined N,O (or P,O) bond distances for the S_0 ground-state and the lowest lying triplet state (T_1) on the B3LYP/SVP level of theory. For the S_0 structures, a biradical wave function ($\langle S^2 \rangle = 1$) was used at large bond distances in order to describe the correct fragmentation channel. In the following, computations, which involve an optimized structure for the first triplet state, will be abbreviated as $T_1//T_1$, $S_1//T_1$, and computations, which use the ground state structures, are given as $S_0//S_0$, $T_1//S_0$. Due to a strong mixing between orbitals for complete active space

considerably higher than the values obtained for the fragments **1a \bullet** and **2a \bullet** .

computations of the cleavage processes, the (16/12) active space was applied like for the already known precursors **1a**^a and **2a**^a. An estimate for the maximal possible excess energies of the resulting radical fragments and the different intrinsic reactivities of the heterocyclic radical fragments was done according to the model described in chapter 5.

7.2 The Screening Step

The excitation energies and oscillator strengths of the spectroscopic visible $\pi \rightarrow \pi^*$ transition, calculated with the TD-B3LYP method within the scope of the screening, of all possible molecules (compare figure 7.1) are summarized in table 7.1. The $\pi \rightarrow \pi^*$ character of these photochemically relevant transition (strong oscillator strength) was identified by the shape of the contributing orbitals.

heterocycle	thione (a)	ketone (b)	phosphonethione (c)
pyridine (1)	3.33 / 373 (0.051)	4.21 / 294 (0.099)	2.81 / 441 (0.082)
thiazole (2)	4.16 / 298 (0.134)	5.18 / 239 (0.067)	3.08 / 403 (0.056)
pyrrole (3)	4.07 / 305 (0.183)	4.82 / 257 (0.072)	3.20 / 387 (0.022)
imidazole (4)	4.90 / 253 (0.200)	5.23 / 237 (0.033)	3.47 / 358 (0.118)
oxazole (5)	4.77 / 260 (0.181)	5.76 / 215 (0.112)	3.57 / 347 (0.082)
phosphazole (6)	3.77 / 329 (0.139)	4.43 / 280 (0.054)	3.18 / 390 (0.024)

Table 7.1: The excitation energies [eV / nm] and oscillator strength f (in arbitrary units) of the $\pi \rightarrow \pi^*$ excitations of all molecules calculated within the scope of the screening with the TD-B3LYP/TZVP method.

This screening reveals the influence of different heteroatoms and functional groups on the UV/vis spectra of these compounds. Taken *N*-(methoxy)-thiazole-2(3*H*)-thione (**2a**) as reference system the influence of the composition of the heterocycle on the energy position of the $\pi \rightarrow \pi^*$ excitation can be seen if the elements of the column labeled “thione (**a**)” of table 7.1 are compared. A C₂H₂ group instead of the sulfur forms the already described and experimentally applied *N*-(methoxy)-pyridine-2(1*H*)-thione (**1a**). Due to the larger π -electron system in the ring the high lying π -orbitals are lifted in energy, whereas the low lying virtual π^* -orbitals are lowered. Therefore the $\pi \rightarrow \pi^*$ excitation is shifted about 75 nm to longer wave length (*approx.* 0.8 eV lesser excitation energy). This effect was already described as the reason for the daylight sensitivity of these compounds. If the sulfur atom of the heterocycle **2a** is replaced by a CH₂ group ($Z = \text{CH}_2$) the pyrrolothione

^aSince this chapter only deals with the *N*-(methoxy) derivatives of the investigated compounds the index -**OMe** is omitted in the following discussion.

heterocycle **3a** is generated. Its visible $\pi \rightarrow \pi^*$ transition is hardly shifted in comparison to **2a** since the corresponding π and π^* -orbitals have the same energy as those of the thiazole compound. Nevertheless the oscillator strength of this excitation increases in comparison to the reference compound. A nitrogen atom (imidazolethione **4a**) or an oxygen atom (oxazolethione **5a**) increases the energy of the virtual π^* -orbitals. This leads to a blueshift of about 50 to 60 nm (ca. 0.6 to 0.75 eV) of the $\pi \rightarrow \pi^*$ excitation. The phosphorus (PH) derivative **6a** of the thiazole heterocycle absorbs with a redshift of about 30 nm (0.4 eV) in comparison to the reference system **2a**.

Additionally, to the modification of Z also the functional group (X and Y in fig. 7.1) can be varied to screen for promising alkoxy radical precursors. A replacement of the thiocarbonyl unit by a carbonyl unit (compounds **b**; column 2 in table 7.1) leads to hydroxamic acid derivatives. As it is well known for other carbonyl and thiocarbonyl systems the π -orbitals of the carbonyl groups are lower in energy (about 0.2 to 0.5 eV) than the π -orbitals of the corresponding thiocarbonyl groups.^[164] The unoccupied π^* -orbitals raise in energy. This leads to a strong blue shift of the $\pi \rightarrow \pi^*$ excitation together with a decrease in oscillator strength.

Finally Y = N was replaced by Y = P (compounds **c**; column 3 in table 7.1). This substitution leads to considerable structural changes since the phosphorus center is sp^3 hybridized while the nitrogen center is sp^2 hybridized. As a consequence the P,O bond is bent out of the plane of the heterocycle by about 120° . Due to the substitution the π - and the π^* -orbitals are both lowered in energy. Since the shifts are larger for the virtual orbitals than for the occupied ones the $\pi \rightarrow \pi^*$ excitation energies of the phosphorus derivatives are redshifted by about 60 to 100 nm.

These different effects of the modified heterocycles and functional groups on the $\pi \rightarrow \pi^*$ excitation energy lead to possible UV/vis absorptions in a energy range of nearly 230 nm (about 3 eV). This corresponds to strong blue (**5b**; 83 nm / 1.60 eV) and red (**1c**; 143 nm / 1.35 eV) shifts with respect to **2a**. On one side the hypsochromic effects of the oxazole heterocycle and the keto group shifts the excitation energy of this transition to 215 nm (5.76 eV) in the case of molecule **5b**. The other extrema of 441 nm (2.81 eV) for the *P*-(methoxy)-phosphininethione (**1c**) results from the bathochromic effects of the bigger delocalized π -system of pyridine and the phosphothiohydroxamic acid group.

Since this systematical design should yield potential precursor systems with an $\pi \rightarrow \pi^*$ excitation energy between the two heterocyclic thiohydroxamic compounds **1a** and **2a** only four of the 18 molecules are chosen as potential interesting systems. For the currently in the experiment applied thiohydroxamic acid group (**a**) the pyrrole (**3a**) ring, with nearly no shift in comparison to **2a**, and the phosphazole (**6a**) heterocycle, with a bathochromic

shift of about 30 nm (-0.39 eV), absorb UV/vis light in the desired energy region. In the other two thiohydroxamic acid heterocycles the hypsochromic effect of the NH-group (**4a**) or the oxygen atom (**5a**) pushes the $\pi \rightarrow \pi^*$ excitation energies towards 250 nm. The hypsochromic effect of the keto group in the compounds **b** in comparison to the thioketo group in the molecules **a** leads to predicted UV/vis excitations below 300 nm for all compounds. The predicted redshift of the phosphothiohydroxamic acid group (**c**) together with the hypsochromic effect in the imidazole and oxazole heterocycle result in predicted excitation energies of 358 nm (3.47 eV) for *P*-(methoxy)-azaphosphole-2-thione (**4c**) and of 347 nm (3.57 eV) for *P*-(methoxy)-oxaphosphole-2-thione (**5c**). These two systems are also further investigated as promising new photochemical precursor molecules.

$n \rightarrow \pi^*$				
molecule	gas phase	$\epsilon=78^a$	Δ_{gas}	
1a	2.77 / 448	3.19 / 388	0.43	-60
2a	3.48 / 356	3.72 / 334	0.24	-23
3a	3.09 / 401	3.42 / 363	0.33	-38
6a	2.82 / 440	3.08 / 402	0.26	-38
1b^b	— / —	— / —	—	—
4c	2.50 / 496	2.71 / 458	0.21	-38
5c	2.47 / 501	2.66 / 466	0.19	-35

$\pi \rightarrow \pi^*$				
molecule	gas phase	$\epsilon=78^a$	Δ_{gas}	
1a	3.33 / 372	3.63 / 342	0.31	-30
2a	4.16 / 298	4.16 / 291	0.10	-7
3a	4.07 / 305	4.15 / 299	0.08	-6
6a	3.77 / 329	3.88 / 319	0.12	-10
1b	4.21 / 294	4.37 / 283	0.16	-11
4c	3.47 / 358	3.40 / 365	-0.07	7
5c	3.57 / 347	3.49 / 355	-0.08	8

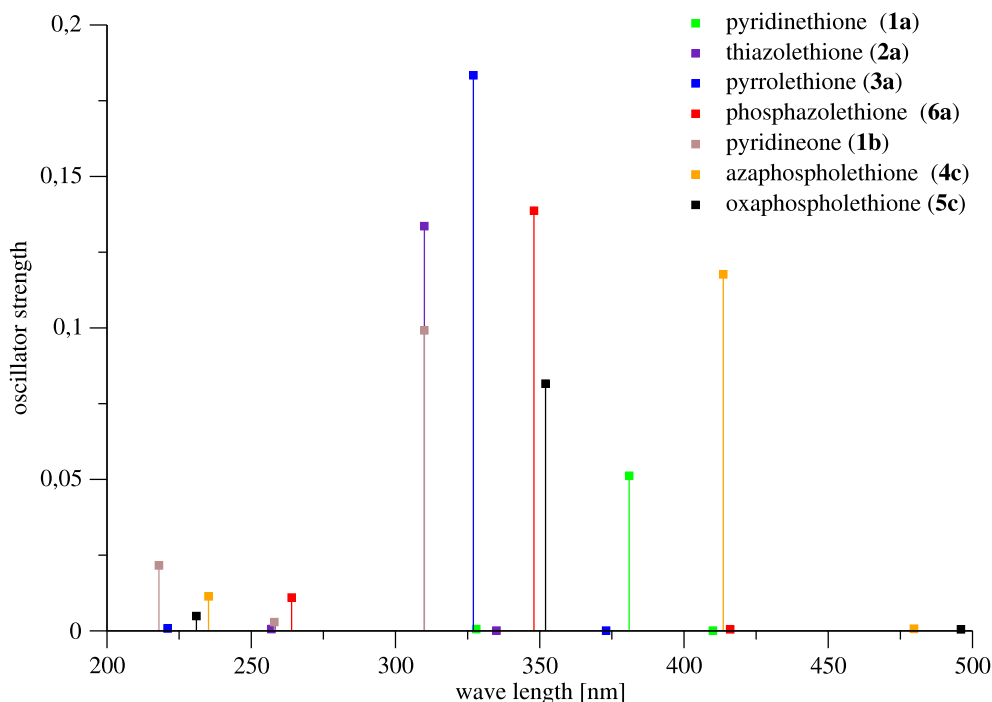
^aThe COSMO model implemented in the TURBOMOLE was used.

^bSince the first electronic excitation is already the $\pi \rightarrow \pi^*$ transition no values for the $n \rightarrow \pi^*$ transition are given.

Table 7.2: Comparison of the TD-B3LYP spectroscopic data of the most promising molecules in gas phase and in solvent. All values are in nm / eV.

Since alkoxy radical precursors are mostly applied in polar solvents the influence of such an environment on the excitation energies of the visible $\pi \rightarrow \pi^*$ excitation the COSMO approach ($\epsilon = 78$) was applied in the framework of TD-DFT (table 7.2). These calculations showed shifts of only 5 to 10 nm which lies within the error bars of the theoretical approach.

For thiazolethione precursor systems the predicted small influence is in line with experimental data.^[1,23] In contrast for pyridinethione **1a** the computations show a strong blue shift (−31 nm), but experimental data to support these predictions seems not to be available. For the $n \rightarrow \pi^*$ transition the influence of a polar solvent is predicted to be much larger. However, these transition are less important due to their vanishing oscillator strengths.



molecule	eV / nm	f
pyridinethione (1a)	3.25 / 381	0.051
thiazolethione (2a)	3.99 / 310	0.134
pyrrolothione (3a)	3.79 / 327	0.183
phosphazothione (6a)	3.57 / 348	0.139
pyridineone (1b)	4.00 / 310	0.099
azaphosphothione (4c)	3.00 / 414	0.118
oxaphosphothione (5c)	3.52 / 352	0.082

Table 7.3: The 12/12 CASPT2/cc-pVTZ//RI-MP2/cc-pVTZ $\pi \rightarrow \pi^*$ excitation energies and the TD-B3LYP/TZVP//RI-BLYP/SVP oscillator strengths from the screening of the promising new precursor molecules and the two reference systems.

The validation of the quantum chemical approaches in chapter 4 showed that the applied TD-DFT method is only valid with the right functional. To get more accurate information about the $\pi \rightarrow \pi^*$ excitation energy of the preselected promising precursor systems the first three excited states were recalculated on the 12/12 CASPT2/cc-pVTZ//RI-MP2/cc-pVTZ

level of theory (compare table 7.3). The values for the photochemically important $\pi \rightarrow \pi^*$ transitions are summarized in table 7.3. Together with the oscillator strengths from the TD-B3LYP calculations line spectra of the selected precursor systems (**3a**, **6a**, **4c**, **5c**) and the applied molecules (**1a**, **2a**, **1b**) can be obtained.

A comparison of the $\pi \rightarrow \pi^*$ excitation energies from table 7.3 with their corresponding values in table 7.1 illustrates the problems with the application of TD-DFT methods. For the reference system pyridinethione (**1a**) and the oxaphosphothione (**5c**) the CASPT2 excitation energies agree very nice ($\Delta E < 0.1$ eV) with the TD-B3LYP values. The calculated DFT $\pi \rightarrow \pi^*$ excitation energies of the molecules **2a**, **3a**, **6a** and **1b** still are of acceptable accuracy ($\Delta E < 0.25$ eV) in the error limits of the TD-DFT methods. Only for the azaphosphothione (**4c**) TD-B3LYP overestimates the $\pi \rightarrow \pi^*$ excitation energy by nearly 0.5 eV (-56 nm). CASPT2 predicts an excitation wave length of 414 nm (3.00 eV). This value however, lies below the desired threshold, the excitation energy of the reference system pyridinethione **1a**. *P*-methoxyazaphosphole-2-thione (**4c**) is excluded from the list of the new promising photochemical alkoxy radical precursors because this excitation energy falls in the region of visible light. **4c** could show an unwanted light sensibility like the reference system **1a**. A second prediction on the UV/vis spectra of the observed molecules could be made with the aid of the line spectra in figure 7.3. According to the calculated oscillator strength *N*-(methoxy)-pyrrole-2-thione (**3a**) should show the UV/vis spectra with the most intense bands of the promising new precursors. The calculated difference in the oscillator strengths of the reference systems **1a** and **2a** have already been observed in our previous calculations and the experiment.

7.3 The Bond Dissociation Paths

In chapter 5 of this work the differences in the chemical behavior of the alkoxy radicals obtained from a photolytic fragmentation of *N*-(methoxy)-pyridine-2(1*H*)-thione (**1a**) and *N*-(methoxy)-thiazole-2(3*H*)-thione (**2a**) were rationalized with the help of the shapes of the potential curves of the $S_0//S_0$, $S_1//T_1$, $S_2//T_1$, and $T_1//T_1$ states. These states and their interactions determine the thermal and photolytic N,O homolysis to the radical fragments. Informations about the maximal excess energy of the fragments and of a possible dissipation into the solvent and other degrees of freedom is obtained from consideration about the time scale of possible cleavage processes. Additionally, to this estimate the intrinsic chemical reactivity of the resulting radical fragments are obtained by computing the reaction energies ΔE ($E_{products} - E_{educts}$) of the isodesmic hydrogen abstraction reaction shown in equation 5.1. However, as it was already pointed out in chapter 5 this should be less important than

molecule	excitation	dissociation	maximal excess	barrier for the	isodesmic
	energy ^a	energy ^b	energy ^b	dissociation ^c	reaction ^d
	eV / nm	eV / kJ mol ⁻¹	eV / kJ mol ⁻¹	eV / kJ mol ⁻¹	kJ mol ⁻¹
3a	3.79 / 327	1.84 / 177	1.95 / 188	< 0.05 / < 5	24.1
6a	3.57 / 348	1.89 / 182	1.68 / 162	0.10 / 10	22.3
5c	3.52 / 352	2.80 / 270	0.72 / 69	no dissociation	—

^aThe vertical $\pi \rightarrow \pi^*$ excitation energies calculated on the 12/12 CASPT2/cc-pVTZ//RI-MP2/cc-pVTZ level of theory.

^bThe S_0 dissociation energies computed on the 16/12 CASPT2/cc-pVTZ//RI-MP2/cc-pVTZ level of theory.

^cThe difference between the initial vertical $\pi \rightarrow \pi^*$ excitation energy (starting point of the fragmentation process) and the dissociation energy of the S_0 state. The 16/12 CASPT2/cc-pVTZ//RI-MP2/cc-pVTZ method was used.

^dThe highest barrier towards the N,O bond homolysis in the photochemical active state.

^eThe ΔE ($E_{products} - E_{educts}$) values for the isodesmic hydrogen abstraction reaction shown in equation 5.1. The value for the methoxyl radical is $\Delta E = -27.9$ kJ mol⁻¹.

Table 7.4: Summary of the data for the description of the photolytical radical liberation process and the chemical behavior of the radical fragments.

the remaining excess energy.

To obtain information about a potential photochemical reactivity of the new promising systems (**3a**, **6a**, **5c**) the N,O dissociation paths (P,O in the case of **5c**) were analyzed to compute the maximal excess energies of the radical fragments and to obtain information about a possible dissipation of this excess energy. The obtained data is summarized in table 7.4 which also contains the highest of possible barriers in the photochemically active state and the reaction energies of the calculated isodesmic reactions of the heterocyclic radical fragments with isobutane. The corresponding potential curves are given in figures 7.2–7.4. In these figures the lines connect those eigenvalues of the Hamilton matrix which possess similar electronic characters (approximated diabatic representation). The symbols themselves indicate the energy order of the eigenvalues (adiabatic approximation). This is made to pronounce possible avoided crossings.

7.3.1 *N*-(Methoxy)-(1,3)Dihydro-Pyrrole-2-thione (**3a**)

The N,O dissociation paths of *N*-(methoxy)-(1,3)dihydro-pyrrole-2-thione (**3a**) for the $S_0//S_0$, $T_1//T_1$, $S_1//T_1$ and the $S_2//T_1$ states are shown in figure 7.2. **3a** has a thermal N,O dissociation energy of 178 kJ mol⁻¹ (1,84 eV). The photochemical process is most probably initiated by an excitation into the S_2 state since only the $S_0 \rightarrow S_2$ transition exhibits a

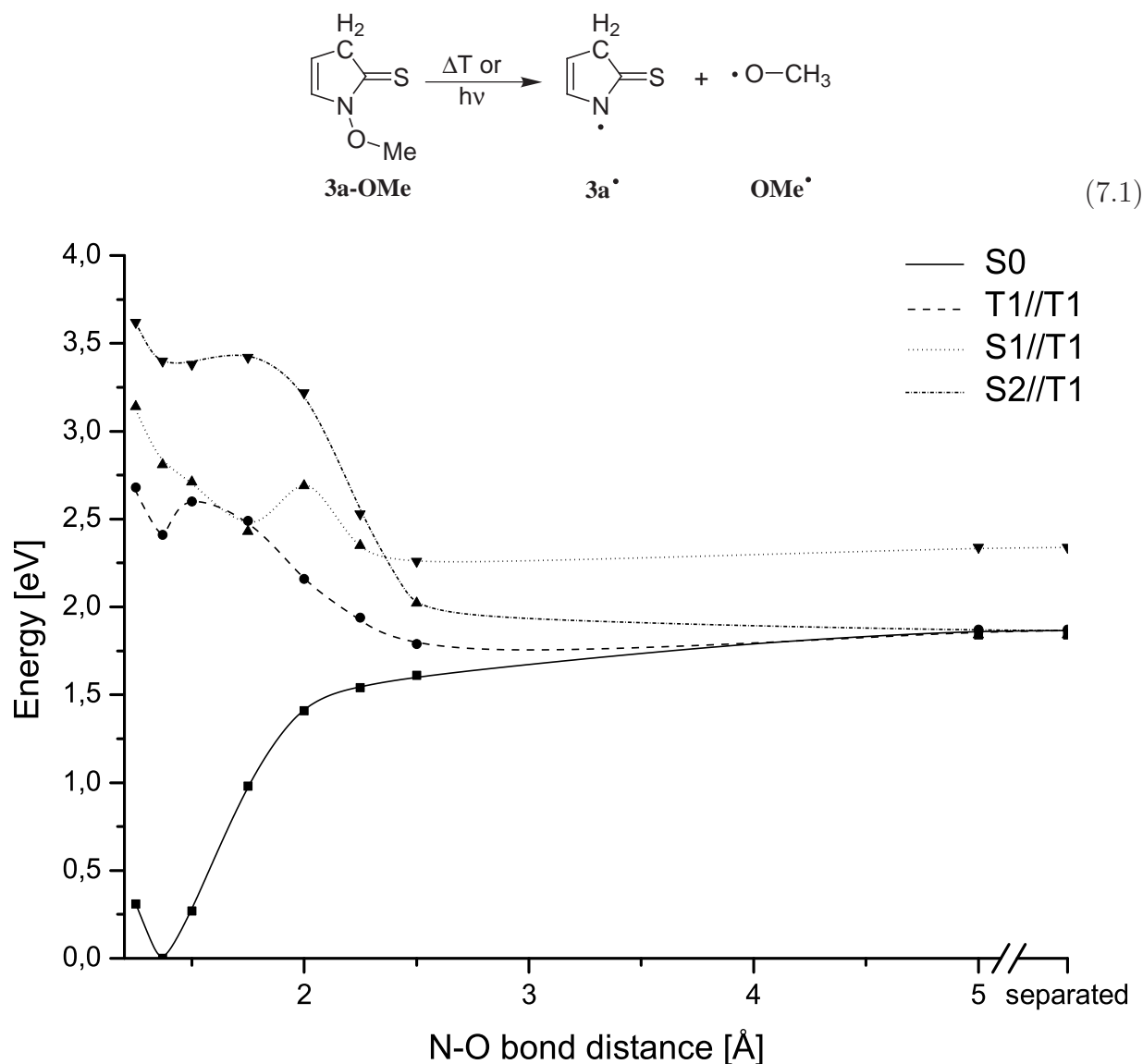


Figure 7.2: The N,O dissociation paths of *N*-(methoxy)-(1,3) dihydro-pyrrole-2-thione (**3a**).

significant oscillator strength (table 7.1). From the difference of the dissociation energy and the vertical excitation energy (3.79 eV) a maximal excess energy of 188 kJ mol⁻¹ is computed for the released radicals in their electronic ground states. This is slightly higher than the corresponding value of **1a** but considerably lower than for **2a**.

The S₂ state possesses only a very small barrier (< 5 kJ mol⁻¹) towards the N,O fragmentation so it can be expected that the N,O bond dissociation takes place after the excitation process. If the barrier is surmounted the transition from the S₂ to the S₁ and with this to the final radical fragments in their ground states (pyrryl-2-sulfanyl radical, methoxyl radical in its degenerated ²E state) will occur quite fast, since at a N,O distance of 2.5 Å the S₂ state crosses with the S₁ state. Due to the fast process a dissipation of the energy to the various

degrees of freedom or the solvent is unlikely. If the barrier towards the dissociation cannot be overcome the S_2 state nevertheless should decay to the S_1 state (Kasha's rule). Due to the flatness of the S_2 potential surface between $R_{N,O} \approx 1.4\text{--}1.8 \text{ \AA}$ at that stage other intramolecular rearrangements cannot be excluded. Since both states are separated by about 0.6 eV at the minimum structure the relaxation to the S_1 will proceed on a longer time scale. If the S_1 state is populated a crossing to the triplet state due to spin-orbit interactions can be expected since the S_1 state also possesses a barrier towards the N,O dissociation and comes very close in energy to the T_1 state at about $R_{N,O} = 1.75 \text{ \AA}$. After this bond distance the T_1 state is repulsive with respect to the fragmentation, *i.e.* the subsequent fragmentation processes should be very rapid. In summary the computations indicate that the chemical behavior of the radical fragments obtained from the irradiation of **3a** should lie between the behavior of the radical fragments obtained from **1a** and **2a**. If the transfer from the S_1 to the T_1 is so slow that the energy gained from the $S_0 \rightarrow S_2$ transition can be dissipated to the environment, the radicals which arise from the fragmentation pathway ($S_2 \rightarrow S_1 \rightarrow T_1 \rightarrow$ fragments) should be even less reactive. The reaction energy ΔE for the isodesmic reaction of the pyrrolyl-2-sulfanyl radical with isobutane is 24.1 kJ mol^{-1} , *i.e.* it possesses a higher intrinsic chemical reactivity than the heterocyclic radical fragments of **1a** and **2a**.

7.3.2 *N*-(Methoxy)-(1,3)Dihydro-[1,3]Azaphosphole-2-thione (**6a**)

The thermal and photochemical paths for the homolytic N,O bond cleavage of *N*-(methoxy)-(1,3)dihydro-[1,3]azaphosphole-2-thione (**6a**) are depicted in figure 7.3. Its dissociation energy in the ground state is with a value of 182 kJ mol^{-1} slightly higher than for **1a** and **2a** but nearly equal to **3a**. The maximal excess energy of the fragments is 162 kJ mol^{-1} , which is only slightly higher than the value computed for **1a** (147 kJ mol^{-1}). It is about 25 kJ mol^{-1} smaller than for the pyrrolothione due to a redshift of 20 nm of the S_2 excitation wave length. For the equilibrium N,O distance of the ground state the photochemically populated S_2 state is located at 3.57 eV (348 nm) and lies about 0.6 eV above the S_1 state. It exhibits a minimum which separates the excited molecule from the N,O dissociation by a barrier of about 10 kJ mol^{-1} (0.1 eV). At $R_{N,O} = 1.75 \text{ \AA}$ the S_2 curve exhibits another minimum possessing a barrier towards the fragmentation of nearly 20 kJ mol^{-1} (0.2 eV). The steep descent starts for bond distances of $R_{N,O} > 2.0 \text{ \AA}$. At about $R_{N,O} = 2.5 \text{ \AA}$ the S_2 state crosses the S_1 state. Consequently, if the barriers are surmounted a dissociation into the radical fragments can be expected. Nevertheless some energy dissipation to the solvent or other degrees of freedom can be expected from the shape of the S_2 state between $R_{N,O} = 1.5 \text{ \AA}$ and 2.25 \AA . The other excited states are also not repulsive with respect to the N,O cleavage. The S_1 state, which might be reached after the $S_2 \rightarrow S_1$ relaxation via

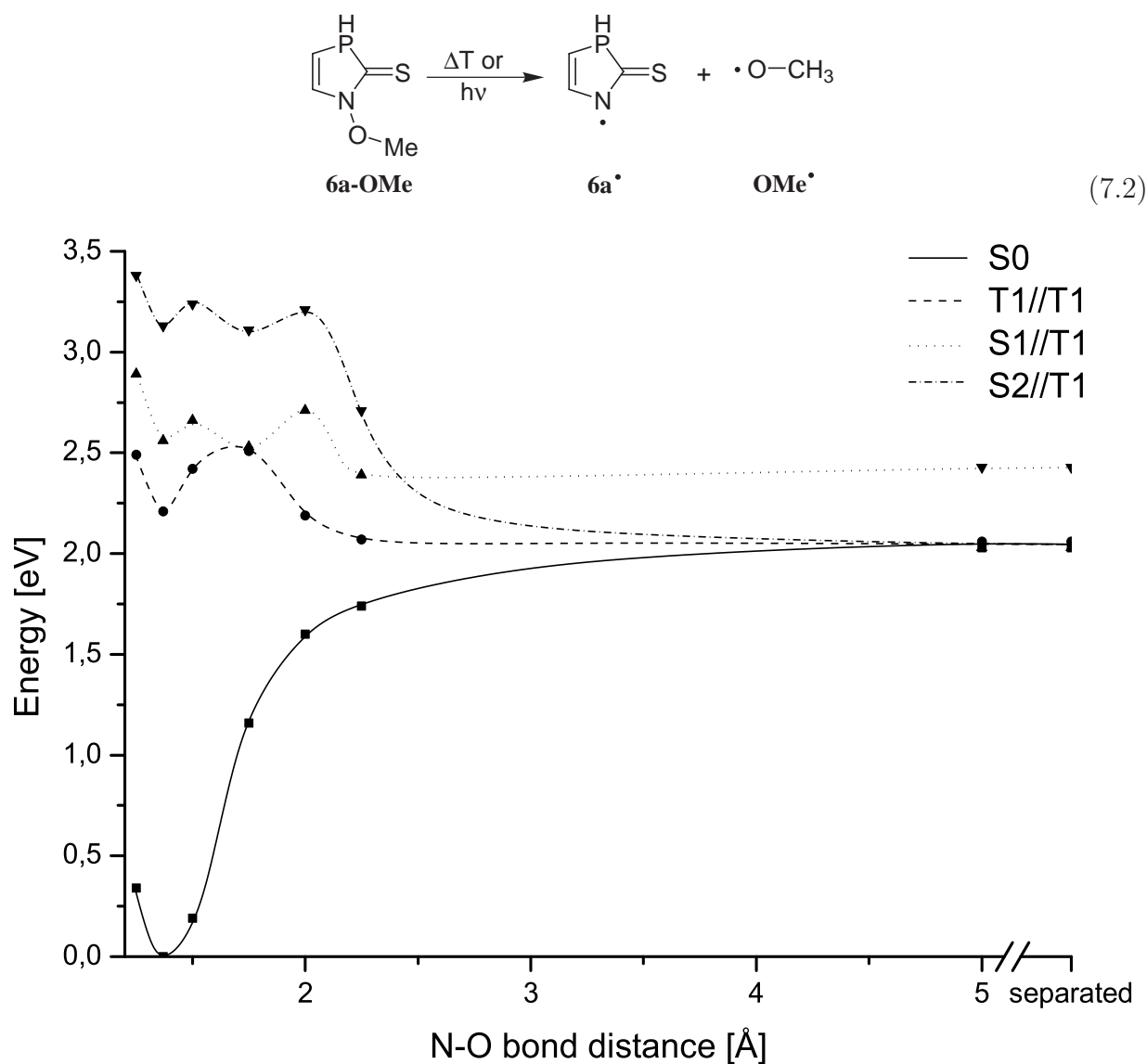
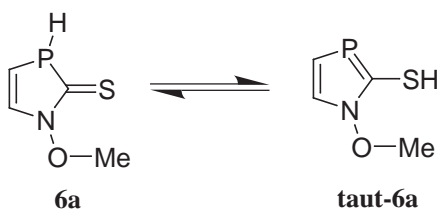


Figure 7.3: The N,O dissociation paths of *N*-(methoxy)-(1,3)dihydro-[1,3]azaphosphole-2-thione (**6a**).

a rovibrational transition, has a small barrier towards the dissociation and the minimum of the T_1 state at $R_{N,O} = 1.75 \text{ \AA}$ even shows a barrier of 0.3 eV (30 kJ mol^{-1}). After the S_1 state is reached the system can migrate to the T_1 state via spin-orbit interaction. With the two third row elements phosphorus and sulfur for **6a** the spin-orbit interaction can be expected to be stronger than for **1a** or **2a**. This transition is also facilitated since both states come very close to each other for $R_{N,O} = 1.75 \text{ \AA}$. If a conversion from the S_1 to the T_1 happens at that point the fragmentation can easily occur since for a N,O bond distance $R_{N,O} > 1.75 \text{ \AA}$ the T_1 state is repulsive with respect to the N,O bond. The nonrepulsive dissociation paths and especially the barrier of the excited singlet states could lead to a

relaxation of the excited molecule to its electronic ground state before the N,O dissociation process starts. If the N,O homolysis however, occurs the radical fragments should lose quite a large amount of excess energy due to the hindered dissociation.

The isodesmic reaction of the heterocyclic [1,3]azaphosphyl-2-sulfanyl radical fragment (**6a**[•]) gives a ΔE value of 22.3 kJ mol⁻¹ showing that it is more reactive than the fragment of **1a**. However, taking into account that the maximal excess energy of the photolytic fragmentation and its dissipation is the dominant effect the radical fragments resulting from a N,O cleavage of **6a** are expected to be about as reactive as those obtained from **1a** due to the expected slow dissociation process. This makes *N*-(methoxy)-(1,3)dihydro-[1,3]azaphosphole-2-thione (**6a**) a very interesting candidate for the application as photochemical alkoxy radical precursor



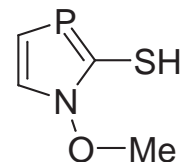
Method	$\Delta(\text{taut-6a} - \mathbf{6a})$
B3LYP/TZVP//RI-BLYP/SVP	-25.6
RI-MP2/cc-pVTZ	-57.2
RICC2/cc-pVTZ//RI-MP2/cc-pVTZ	-45.7
B3LYP/TZVP/ $\epsilon=30$ //RI-BLYP/SVP/ $\epsilon=30$	-16.7
B3LYP/TZVP/ $\epsilon=78$ //RI-BLYP/SVP/ $\epsilon=78$	-16.1

Table 7.5: Energy differences (kJ mol⁻¹) between both tautomeric forms of **6a** calculated with different methods.

A problem however, is, that the phosphazole (**6**) heterocycle possess tautomeric forms which have to be taken in account. The energy difference between the two tautomeric forms was calculated on different levels of theory. All approaches predict the thiol form of **6a** (**taut-6a**) to be lower in energy than the thione form (table 7.5). A polar environment seem to lessen the energy differences but even in water ($\epsilon = 78$) only traces of the thione form will exist. Excitation energies, oscillator strengths and characterizations of the five lowest lying vertical excitations of the thiole form **taut-6a** are summarized in table 7.6. As expected the spectrum does not resemble the one of the thione form. The lowest excitation lies at about 280 nm *i.e.* much higher than the desired range.

Therefore the phosphor has to be methylated (**meth-6a**) to avoid tautomerism and yield the desired properties. To investigate to what extent a methylation of the phosphor center of **6a** influences the energy position of the electronically excited states the three lowest excitation energies of *N*-(methoxy)-3-methylazaphosphole-2-thione (**meth-6a**) were

ΔE [eV / nm]	f	Character ^a	Weight
4.36 / 284	0.015	HOMO \rightarrow LUMO ₊₁	0.682
		HOMO \rightarrow LUMO	0.294
4.80 / 259	0.130	HOMO \rightarrow LUMO	0.568
		HOMO \rightarrow LUMO ₊₁	0.293
4.92 / 252	0.018	HOMO \rightarrow LUMO ₊₂	0.466
		HOMO \rightarrow LUMO ₊₃	0.444
5.19 / 239	0.018	HOMO ₋₁ \rightarrow LUMO	0.353
		HOMO \rightarrow LUMO ₊₃	0.311
		HOMO \rightarrow LUMO ₊₂	0.290

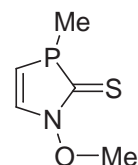
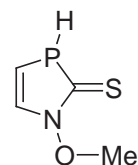


^aThe orbital transitions contributing to the calculated electronic excitation. Contributions with a weight below 0.10 are not shown. A characterization of the orbitals in terms of n , π and π^* was not done since the orbitals possess a complete different character than in compound **6a**.

Table 7.6: TD-B3LYP data for the electronic spectra of the tautomeric form of **6a** (**taut-6a**).

computed (table 7.7). As expected the spectra of **6a** and **meth-6a** are very similar. The $\pi \rightarrow \pi^*$ excitation, which remains the most intensive band, is redshifted by only 5 nm. With the utmost probability the N,O fragmentation paths of **6a** and **meth-6a** will also be very similar. Therefore the calculation of the ones of **meth-6a** was omitted.

6a			
ΔE [eV / nm]	f	Character ^a	Weight
2.82 / 440	$<10^{-3}$	$n \rightarrow \pi^*$	0.901
3.77 / 329	0.139	$\pi^* \rightarrow \pi^*$	0.868
4.79 / 259	0.011	$n \rightarrow$ LUMO ₊₁	0.938
meth-6a			
ΔE [eV / nm]	f	Character ^a	Weight
2.82 / 439	$<10^{-3}$	$n \rightarrow \pi^*$	0.807
3.71 / 334	0.140	$\pi \rightarrow \pi^*$	0.784
4.81 / 258	0.026	$n \rightarrow$ LUMO ₊₁	0.849



^aThe orbital transitions contributing to the calculated electronic excitation. Contributions with a weight below 0.10 are not shown.

Table 7.7: TD-B3LYP data for the electronic spectra of the methylated molecule (**meth-6a**) and **6a**.

7.3.3 *P*-(Methoxy)-(1,3)Dihydro-[1,3]Oxaphosphole-2-thione (**5c**)

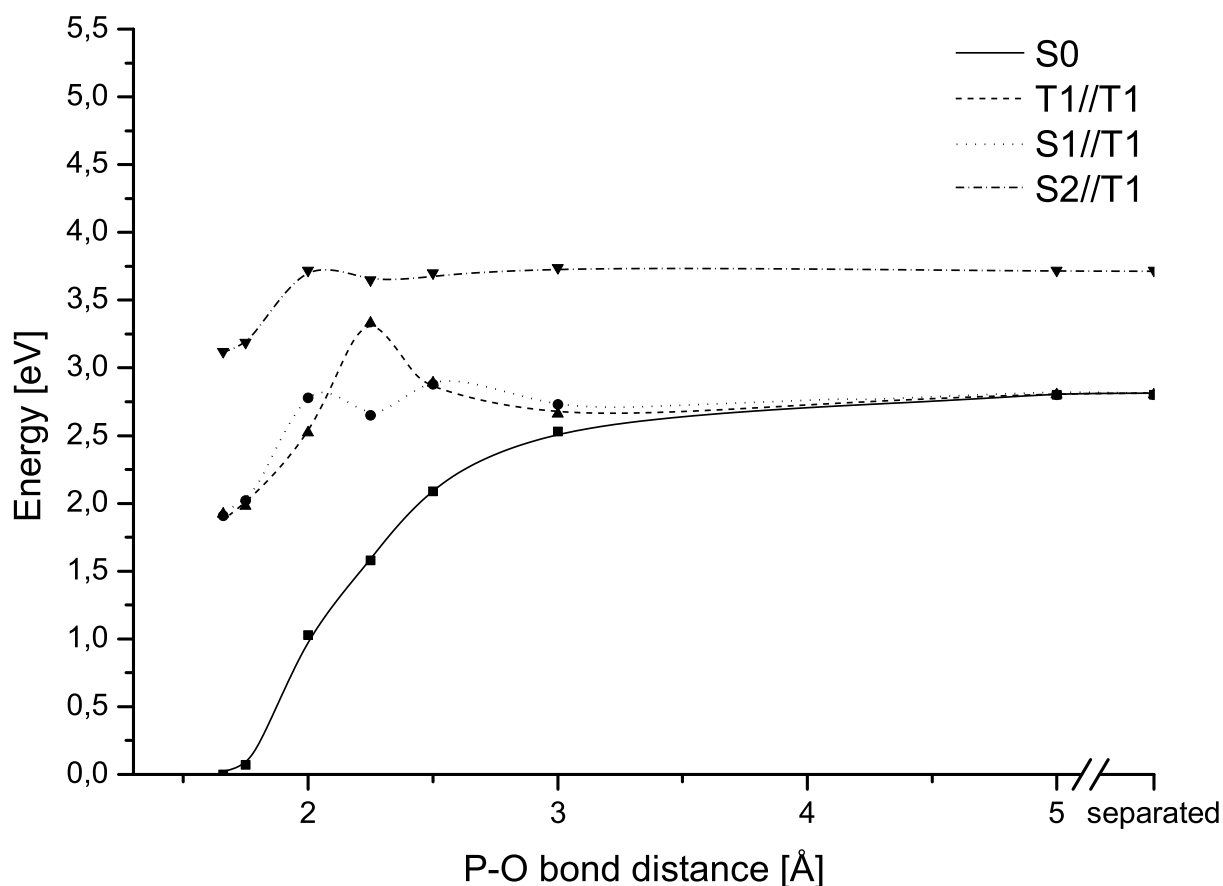
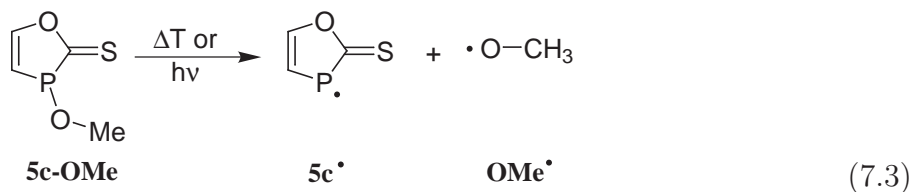


Figure 7.4: The P,O dissociation paths of *P*-(methoxy)-(1,3)dihydro-[1,3]oxaphosphole-2-thione (**5c**).

In the case of *P*-(methoxy)-(1,3)dihydro-[1,3]oxaphosphole-2-thione (**5c**), the bond breaking process involves the P,O bond. The computed paths of the homolytic P,O cleavage in the ground state, the T₁, S₁ and S₂ state that are shown in figure 7.4 possess completely different shapes than those obtained for the other compounds. **5c** has, with a value of 270 kJ mol⁻¹ (2.80 eV), the biggest thermal dissociation energy of the promising precursors. Since the excitation energy into the photochemical active S₂ state is 3.52 eV, the maximal possible excess energy of the radical fragments would be only 69 kJ mol⁻¹. In comparison to the previously observed thiohydroxamic acids **1a**, **2a**, **3a**, **6a** or the hydroxamic acid **1b** in

this case also the S_1 and the T_1 energies at the minimum structure are about 90 kJ mol^{-1} (0.9 eV) below the energy of the separated fragments. The energy of the S_2 state also strongly increases during the P,O bond breaking process. These shapes of the P,O bond dissociation paths (see figure 7.4) clearly indicates that neither a population of the S_1 nor of the S_2 state will lead to a cleavage of the P,O bond. Consequently a fragmentation to an alkoxy radical and an oxaphosphyle radical ($\mathbf{5c^\bullet}$) cannot be expected upon irradiation with UV-light.

7.4 Conclusion

After the investigation of the bond dissociation paths of the new potential promising precursor molecules $\mathbf{3a}$, $\mathbf{6a}$ and $\mathbf{5c}$, the applicability of these molecules for the photochemical radical formation can be evaluated according to the model for the reactivity of such compounds developed in chapter 5. Since the electronic ground state, the T_1 , the S_1 and the S_2 state for oxaphospholethione $\mathbf{5c}$ show a non-repulsive potential with respect to the P,O bond, this molecule should not dissociate after the irradiation with UV/vis light. A molecule excited to the S_2 state should decay to its electronic ground state with no reactions. So the heterocycle $\mathbf{5c}$ is not qualified as a parent system for photochemical alkoxy radical precursors.

N-(methoxy)-(1,3)dihydro-pyrrole-2-thione ($\mathbf{3a}$) and *N*-(methoxy)-(1,3)dihydro-[1,3]azaphosphole-2-thione ($\mathbf{6a}$) show quite similar N,O bond dissociation bathes in the electronic ground state and in the first two excited singlet states. Both molecules have a S_2 state that shows a small barrier for the bond dissociation and is separated in energy from the S_1 state as long as both radical fragments are close to each other. At about 2.5 \AA the S_2 state crosses with the S_1 state. According to Kasha's rule a $S_2 \rightarrow S_1$ relaxation should occur after the photochemical excitation of the molecules. Due to the separation of these two states a loss of excess energy for the uprising radical fragments is possible. The S_1 states of both systems come very close in energy to the T_1 state at a N,O distance of 1.75 \AA . This makes a $S_1 \rightarrow T_1$ transition via spin-orbit interactions possible. This transition is more likely to occur in the case of the phosphazothione $\mathbf{6a}$ due to the presence of two third row elements. The T_1 state of $\mathbf{6a}$ however, shows a barrier for the N,O dissociation at this bond distance. A further loss of excess energy for the phosphazyl-2-sulfanyl ($\mathbf{6a^\bullet}$) and the methoxy radical fragments is possible. Even a reaction back to the undissociated molecule and a relaxation to the electronic ground state could occur. The T_1 state of pyrrolethione $\mathbf{3a}$ has no such barrier for the dissociation. After the spin forbidden $S_1 \rightarrow T_1$ transition the molecule should dissociate into the pyrrol-2-sulfanyl radical ($\mathbf{3a^\bullet}$) and the methoxy radical, both in their electronic ground states. Even if no $S_1 \rightarrow T_1$ transition occurs a dissociation in the S_1 state

to the radical fragments in their ground state is possible. Because of a small barrier in the S_1 state the excess energy of the products should be successfully quenched like in the case of the already applied *N*-(alkoxy)-pyridine-2-thiones. Since the excitation energy to the photochemical active S_2 states of both molecules **3a** and **6a** is hypsochromically shifted about 30 to 50 nm in comparison to **1a** a daylight sensitivity of these molecules should also be excluded. Derivates of *N*-(methoxy)-(1,3)dihydro-[1,3]azaphosphole-2-thione (**6a**), which prevent a tautomerism, and the *N*-(alkoxy) derivates of the (1,3)dihydro-pyrrole-2-thione (**3a-OR**) should be new promising candidates for the application as photochemical alkoxy radical precursors in photobiological, mechanistic and synthetic investigations.

Chapter 8

Summary

Oxygen-centered radicals are important intermediates in photobiological, mechanistic and synthetic studies. The majority of methods for a generation of reactive oxyl radicals relies on homolytic cleavages of O,O bonds in organic peroxides or peresters. Most precursors of this type are, however, labile and thus delicate to handle. Therefore, *O*-alkyl derivatives of *N*-(hydroxy)-pyridine-2(1*H*)-thione (**1a-OH**) and of 4- and 4,5-substituted *N*-(hydroxy)-thiazole-2(3*H*)-thiones (*i.e.* derivatives of **2a-OMe**), have attracted considerable attention as “mild” photochemical source of alkoxy radicals, in the last few years. Since light quanta of comparatively low energy suffice in order to induce N,O homolysis, it is likely that the primary photophysical event upon UV/vis excitation of *N*-(alkoxy)-pyridine-2(1*H*)-thiones and *N*-(alkoxy)-5-(*p*-(methoxyphenyl)-4-methylthiazole-2(3*H*)-thiones, is associated with an excitation of the thiocarbonyl chromophore rather than the olefinic part or the N,O bond itself.

A big disadvantage of the pyridine compounds, is their sensibility to daylight. Due to a broad absorption band around 360 nm a decomposition of the pyridinethiones occurs already when they are exposed to unfiltered daylight. Only if the blue part of the light is filtered out the *N*-(alkoxy)-pyridine-2(1*H*)-thiones are stable. Despite of their similarities^a, *N*-(alkoxy)-pyridine-2(1*H*)-thiones and *N*-(alkoxy)-4-methylthiazole-2(3*H*)-thiones behave surprisingly different, if photolyzed in the absence of trapping reagents. *N*-(4-penten-1-oxy)-pyridine-2(1*H*)-thiones undergo highly efficient radical chain reactions under such conditions. *N*-(4-penten-1-oxy)-thiazole-2(3*H*)-thiones on the other hand, react surprisingly sluggish and give rise to several unwanted side products, if photolyzed. In order to improve the characteristics of a future generations of powerful and versatile alkoxy radical precursor, it is important to understand the differences in photophysical events associated with near UV/vis excitation of cyclic thiohydroxamic acid *O*-esters in general.

^aLiberation of alkoxy radicals under photochemical conditions.

To obtain such knowledge in the frame of this work a “Theoretical Characterization and Optimization of Photochemical Alkoxy Radical Precursors” is performed. Some background information about the generation and application of alkoxy radicals is provided in chapter 2. Electronic excitations and UV/vis spectroscopy together with a description of quantum chemical approaches that are able to calculate such phenomena are outlined in chapter 3. Here especially time-dependent density functional theory and the complete active space approach are described in more detail, since they are mainly applied to obtain the theoretical information in this work. To understand the multireference CAS approach the formalisms of second quantitation are also briefly introduced in subsection 3.2.2

TD-DFT	CASPT2
<ul style="list-style-type: none"> • Single reference approach • Fast and efficient 	<ul style="list-style-type: none"> • Multi reference approach • Very accurate
<ul style="list-style-type: none"> • Strong functional dependency 	<ul style="list-style-type: none"> • High computational demands
<ul style="list-style-type: none"> • Linear response functions • Time-dependent Kohn Sham formalism (Runge & Gross theorem) • Single pole approximation for excited state properties 	<ul style="list-style-type: none"> • Multiconfigurational wave function (static correlation) • Second quantitation • Multireference Møller Plesset perturbation theory (dynamic correlation)

Figure 8.1: A summary of the properties and limits of the two mainly applied quantum chemical approaches in this work.

After the theoretical introductions the first scientific goal of this work is to quantum chemically describe the photochemical properties and differences of the already applied molecules on the basis of heterocyclic thiohydroxamic acid *O*-esters. Chapter 4 deals with computations on the the ground state structures of the parent compounds **1a** and **2a** and especially with the description of the vertical excitation spectra. Therefore a combined theoretical and experimental study on the UV/vis spectral properties of the parent compounds of the alkoxy radical precursors on the basis of the pyridinethione and the thiazolethione heterocycle was performed in cooperation with the working group Hartung. The computed ground state structures of both free acids **1a-OH** and **2a-OH** and the *N*-(methoxy) derivates **1a-OMe** and **2a-OMe** were compared to X-ray structures of crystallized derivates of these compounds. RI-BLYP calculations with the SVP basis sets are sufficient to describe

the important structural features of these heterocyclic compounds. RI-MP2/cc-pVTZ calculations only yielded compacter structures.

In the following validation step CASSCF, CASPT2, TD-DFT in combination with various functionals, and RI-CC2 were tested with respect to their ability to describe the vertical excitations to the first three electronic states of *N*-(methoxy)-pyridine-2(1*H*)-thione (**1a-OMe**) and *N*-(methoxy)-thiazole-2(3*H*)-thione (**2a-OMe**), as well as for the *N*-(hydroxy) derivatives **1a-OH** and **2a-OH**. The complete active space approach in combination with the multistate PT2 ansatz (MS-CASPT2) gives accurate descriptions of the experimental electronic excitation spectra of all compounds. Nearly the same is found for RI-CC2 which in comparison to CASPT2 always predicts slightly higher vertical excitation energies (0.1 to 0.3 eV). The time-dependent DFT results are very sensitive on the choice of the functional and the examined state. The BLYP functional in general underestimates the excitation energies systematically while the BHLYP overestimates them. The Becke three parameter functional (B3LYP) and the PBE0 in most cases give excitation energies in the same region as the CASPT2 computations and the experiment. A validation of TD-DFT results by comparison with experimental data or higher level *ab initio* methods is always recommended.

On the basis of the CASPT2 computations the spectroscopic visible absorption bands of both compounds were assigned to the $S_0 \rightarrow S_2$ transition. In both cases this corresponds to a $\pi \rightarrow \pi^*$ excitation in the thiocarbonyl group of the thiohydroxamic functionality. The calculations characterized the involved orbitals as the π_{CS} - and π_{ring}^* -orbitals in **1a-OMe** and the π_{SCS}^{non} - and π_{SCS}^* -orbitals in **2a-OMe**. The observed higher stabilities of the thiazolethione compounds with respect to daylight simply result since their S_2 states are higher in energy.

In chapter 5 the mechanism of the thermally and the photochemically induced N,O homolysis in *N*-(methoxy)-pyridine-2(1*H*)-thione (**1a-OMe**) and *N*-(methoxy)-thiazole-2(3*H*)-thione (**2a-OMe**) has been studied. In contrast to the vertical excitation spectra for the thermal and the photolytic bond dissociation process, only the CASPT2 method provides reasonable results. The near UV-induced N,O homolysis of thiones **1a-OMe** and **2a-OMe** will start from the S_2 states. In both compounds it is the only state that exhibit significant oscillator strengths, *i.e.* will be populated upon light absorption. A N,O homolysis along the S_2 states potential surfaces would occur with no energy barrier (for **2a-OMe**) or with a small barrier (for **1a-OMe**). This direct dissociation for the S_2 state would furnish excited sulfanyl radicals **1a \cdot** or **2a \cdot** and the methoxyl radical in its electronic ground state. Due to an expected relaxation from the S_2 state to the S_1 state this pathway, however, will not occur. The computed S_2 and the S_1 curves point to a conical intersection between the

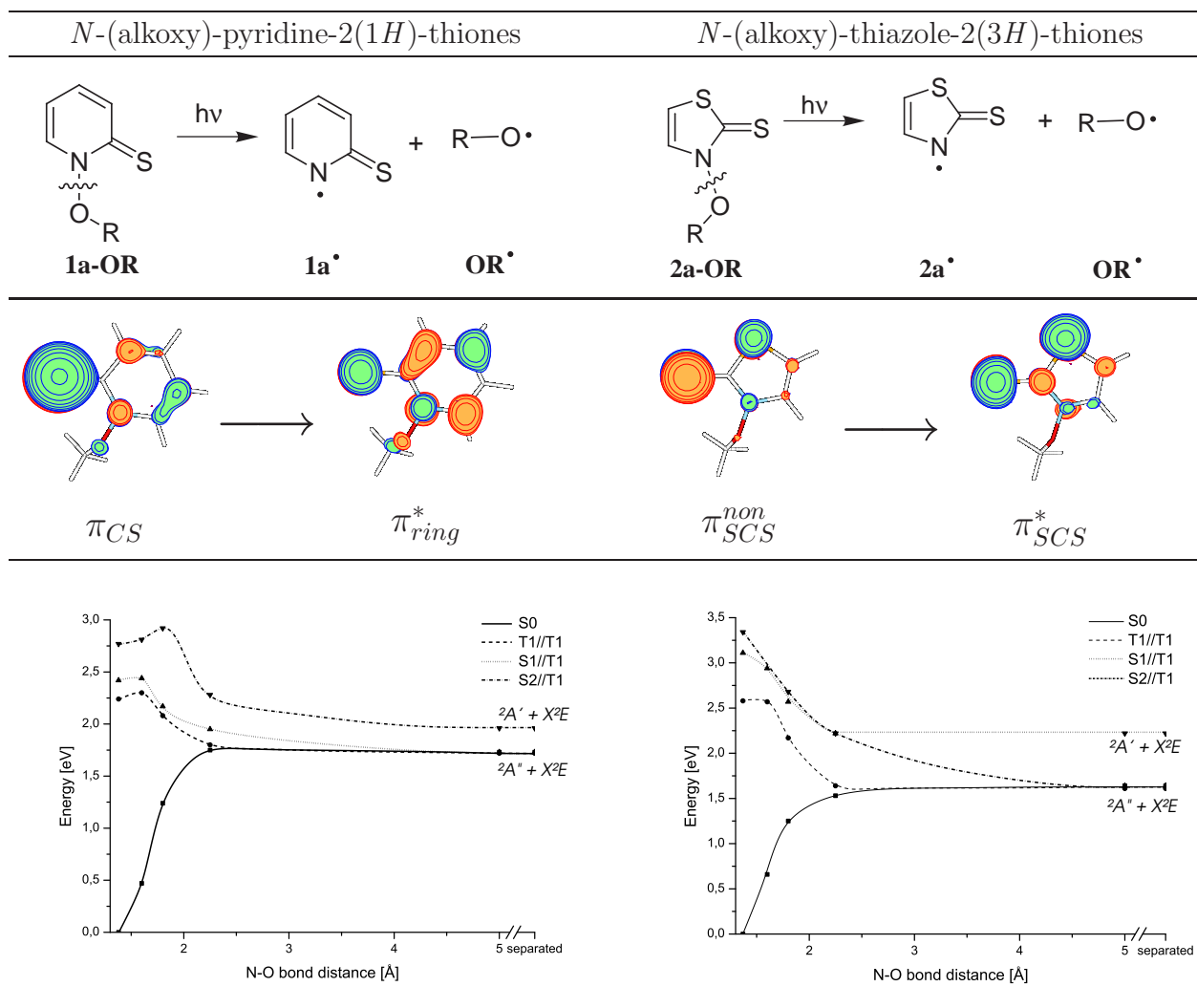


Figure 8.2: A comparison of the obtained photochemical properties of the two applied alkoxy radical precursors *N*-(alkoxy)-pyridine-2(1*H*)-thiones (**1a-OR**; left side) and *N*-(alkoxy)-thiazole-2(3*H*)-thiones (**2a-OR**; right side).

S_1 and the S_2 state which will enable an efficient $S_2 \rightarrow S_1$ relaxation for **2a-OMe**. The potential surfaces of the S_1 and S_2 states of **1a-OMe** do not show such a feature. Because of the hindered dissociation in the S_2 state^b a slower $S_2 \rightarrow S_1$ relaxation should occur as for example predicted by Kasha's rule. For both thiones **1a-OMe** and **2a-OMe**, the S_1 state is repulsive with respect to the N,O bond. Relaxation of S_1 -excited thiones **1a-OMe** and **2a-OMe** into the T_1 state is feasible via spin orbit interaction. The T_1 state leads to the lowest fragmentation channel. For the non-interacting fragments the S_1 and T_1 channel correspond to the 2E groundstate of the methoxy radical. As a consequence the explicit pathway (via S_1 or T_1) is irrelevant for the subsequent chemistry since the relaxation to the ground state of the alkoxy radical will be faster than its chemical reactions.

^bbarrier towards dissociation about 11 kJ mol⁻¹ (0.11 eV).

Due to the resulting faster dissociation process in the case of the thiazolethione compound the excess energy which results from the photochemical activation is dissipated to the solvent or other degrees of freedom only to small amounts. For *N*-(alkoxy)-pyridine-2(1*H*)-thiones a dissipation of the excess energy is much more likely since its S_2 state possesses a barrier with respect to the dissociation. Additionally, no avoided crossing between S_2 and S_1 is found so that also the deexcitation process can be expected to be much slower. Finally the maximal possible excess energy of the fragments obtained from **1a-OMe** is also lower. This results from a lower vertical excitation energy (starting point of the photolytic fragmentation) and a higher thermal dissociation energy of the S_0 state. The latter determines the energy position of the resulting radicals in their ground states. The intrinsic reactivity of the released radical fragments, estimated by isodesmic hydrogen abstraction reactions, was also computed, but it turned out that the most important factor for the reactivity of photochemical alkoxy radical precursors is the maximal possible excess energy and its dissipation to the solvent and other degrees of freedom during the bond dissociation process. This is indeed the case since the radical fragment **1b \bullet** , released by the also already successfully applied precursor system *N*-(methoxy)-pyridine-2(1*H*)-one (**1b-OMe**), possesses a much higher intrinsic reactivity than **1a \bullet** or **2a \bullet** . The N,O bond dissociation paths for **1b-OMe** in contrast exhibit shapes that clearly indicate a rather slow cleavage process. This helps to quench the excess energy, obtained from the photochemical activation, to other degrees of freedom or the solvent. *N*-(alkoxy) derivatives of **1b-OMe** are therefore predicted to be a clean alkoxy radical source like *N*-(methoxy)-pyridine-2(1*H*)-thione (**1a-OMe**), which is indeed already found experimentally.

The computations presented in chapter 4 and 5 yield a model for the theoretical prediction of spectroscopic properties and the photochemical behavior of heterocyclic alkoxy radical precursors. The next goal of this work now is, to apply the obtained knowledge on the possibility to understand the photophysical and photochemical characteristics of such compounds, to optimize their properties or to suggest new compounds that also could be applied in photochemical alkoxy radical chemistry.

Chapter 6 deals with the tuning of the initial excitation wave length of the known pyridine-2(1*H*)-thione and thiazole-2(3*H*)-thione molecules. In a combined theoretical and experimental study various 4 and 5 substituted derivatives of **2a-OMe** were synthesized to record their electronic spectra in order to systematically probe the effect of CH_3 and aryl substituents on the thiazole heterocycle. To assign the experimentally observed UV/vis bands of the substituted thiazole-2(3*H*)-thiones to electronic transitions results from time-dependent density functional theory applying the B3LYP functional together with the TZVP basis sets on RI-BLYP/SVP ground state structures were used. The UV/vis spectra of 4 and 5 substituted *N*-(methoxy)-thiazole-2(3*H*)-thiones can be interpreted like the spectrum

of the parent compound **2a-OMe**. Here also the spectroscopic allowed $\pi_{SCS}^{non} \rightarrow \pi_{SCS}^*$ excitation is responsible for the observed UV/vis band and the photochemical alkoxy radical liberation process. These computations, however, revealed the known problems of TD-DFT with the description of electronic transitions that involve a larger spatial charge transfer. The bathochromic influence of an aryl substituent at the C⁵ position of the thiazolethione heterocycle was overestimated by the applied B3LYP functional due to a considerable charge transfer from the thiocarbonylic π_{SCS}^{non} -orbital to the π_{SCS}^* -orbital which possess density also at the aromatic ring of the C⁵ substituent. RI-CC2 computations in contrast gave the correct reproduction of the experimentally found redshifts of about 15 nm for a 5-*p*-methoxyphenyl (anisyl) substituent.

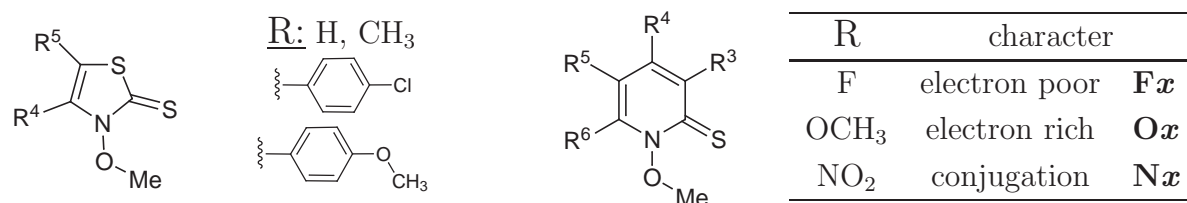


Figure 8.3: The, in chapter 6 of this work, investigated substituents on the two heterocycles that should influence the initial wave length of the photochemical alkoxy radical liberation process

N-(alkoxy)-pyridine-2(1*H*)-thiones (**1a-OR**) are alkoxy radical precursors that are difficult to handle, due to their instability against daylight. Since this instability results from a broad excitation band around 360 nm assigned to the $\pi_{CS} \rightarrow \pi_{ring}^*$ excitation, the second part of chapter 6 deals with the identification of a substitution pattern on the pyridine heterocycle which induces a blue shift of this band to about 350 nm. For this purpose the $\pi \rightarrow \pi^*$ excitations of substituted *N*-(methoxy)-pyridine-2(1*H*)-thiones were computed employing TD-DFT and the CASPT2 approach, since experimental UV/vis spectroscopic data on substituted pyridinethione compounds is not available up today. Fluorine atoms represent a model for electron withdrawing substituents, while the methoxyl group is an example for an electron rich substituent. The NO₂ group is a model for substituents that are able to conjugate with the π -electron system of the pyridine heterocycle.

The computations showed that electron rich and electron poor substituents result the same effects on the electronic excitation spectra. The strongest hypsochromic shift in the case of a monofluorination of the heterocycle is predicted for *N*-(methoxy)-6-fluorinepyridine-2(1*H*)-thione (**F6**) with 11 nm (CASPT2). The substituent effects of the fluorine atoms on the electronic excitations and also on the orbital energies are additive. As a consequence for *N*-(methoxy)-3,4,6-trifluorinepyridine-2(1*H*)-thione (**F346**) a blue shift of 24 nm is predicted. These blue shifts mainly result since the π_{ring}^* -orbitals are less stabilized than the π_{CS} -orbitals. The electron-donating group OMe seems to lead to even stronger blue shifts of

the $\pi_{CS} \rightarrow \pi_{ring}^*$ excitation (*e.g.* 22 nm for *N*-(methoxy)-3-methoxypyridine-2(1*H*)-thione (**O3**)). However, the overall effect will be much smaller since the strong hypsochromic effect is only found if the methoxyl group lies in the plane of the pyridine heterocycle. For an orthogonal orientation the effect is quenched, so that for a freely rotating OMe group the effect will be smaller. For multiple methoxylations no simple additivity is found, since the steric demands of the OMe groups prevent their optimal orientation. The hypsochromic effect of the methoxyl group mainly results since the π_{ring}^* -orbital is more destabilized than the π_{CS} -orbital. As a model for substituents with mesomeric effects the NO₂ group was used. It induces only strong red shifts (*e.g.* 160 nm for *N*-(methoxy)-6-nitropyridine-2(1*H*)-thione (**N6**)), which will be also diminish by the rotation of the NO₂ group as it was found for OMe. The strong bathochromic shifts result since the coupling between both π -systems lead to a new π^* -orbital which is much lower in energy than the π_{ring}^* -orbital of the parent system. An application of substituents that are able to conjugate with the π -electrons of the heterocycle is not able to prevent a daylight sensitivity, but could be used if precursor systems with an initiation wave length in the visible region of the spectra are wanted.

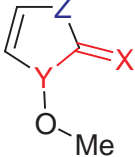
Z	heterocycle		X	Y	functional group
CH=CH	pyridine (1)			S	N
S	thiazole (2)		O	N	ketone (b)
CH ₂	pyrrole (3)		S	P	phosphonethione (c)
NH	imidazole (4)				
O	oxazole (5)				
PH	phosphazole (6)				

Figure 8.4: The systematic modifications of the heterocycle and the functional group to obtain new promising photochemical alkoxy radical precursor molecules.

With the capabilities of computational chemistry it is also possible to identify new lead structures for photochemical precursor systems which combine the advantages of both applied compounds. Chapter 7 describes a computer aided design of new alkoxy radical precursors. Combining the advantages of *N*-(alkoxy)-pyridine-2(1*H*)-thiones and *N*-(alkoxy)-thiazole-2(3*H*)-thiones the radical formation should be initiated by an irradiation with light at about 350 nm, and the amount of side products during the radical formation process should be small even in the absence of radical trapping reagents. To theoretically predict the properties of new test candidates the protocol was employed, which was successful in rationalizing the differences between the properties of **1a-OMe** and **2a-OMe** and was, additionally, tested on *N*-(methoxy)-pyridine-2(1*H*)-one **1b-OMe**. This test supported that this model indeed captures the most important effects.

To find new parent compounds eighteen test candidates were obtained by a system-

atic variation of the parent compound of the thiazolethione precursor. The pyrrole (**3**) heterocycle results from a substitution of the sulfur with a CH₂ group while the imidazole system (**4**) is obtained if a NH moiety is introduced. An oxygen atom instead of sulfur leads to the oxazole heterocycle (**5**). A substitution of the sulfur by a PH unit generates the phosphazole heterocycle (**6**). Further modifications are obtained by a modification of the thiocarbonyl group. The introduction of a carbonyl group leads to the hydroxamic acid (**b**) derivatives of the various heterocycles. Finally the exchange of the hydroxamic acid N atom with phosphorus yields the “phosphothiohydroxamic” acid derivatives **c**.

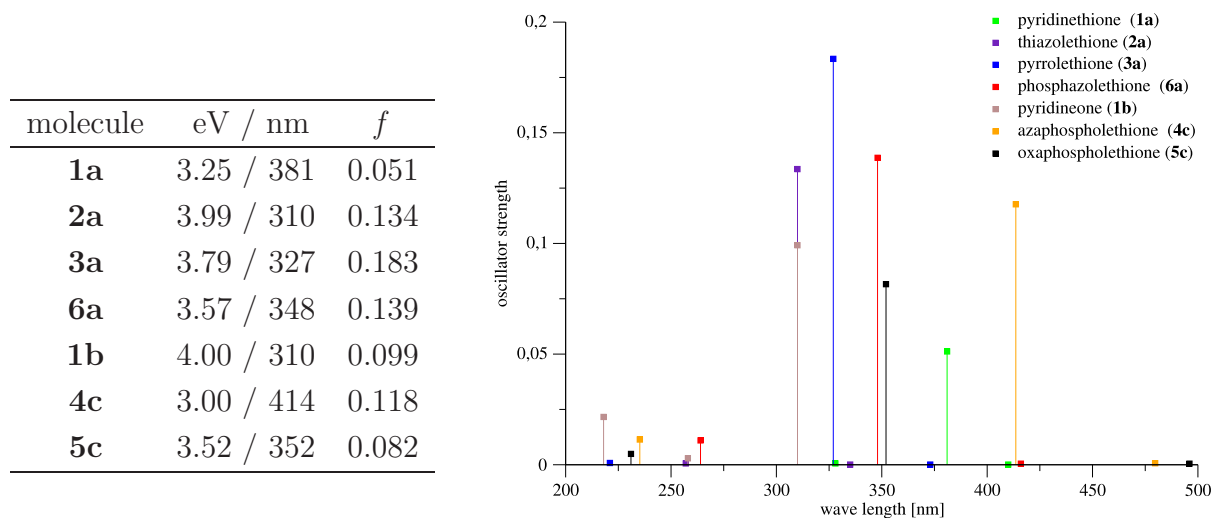


Figure 8.5: The computed CASPT2 electronic excitation spectra of the new promising precursor molecules and the already applied heterocyclic precursor systems.

To identify the promising new precursor systems a screening of the lower electronic excitations of all resulting 18 systems was performed with TD-DFT, employing the B3LYP approach. The influence of a polar solvent was also tested but turned out to be less important for the visible $\pi \rightarrow \pi^*$ excitation of the interesting molecules. For the obtained promising new systems *N*-(methoxy)-(1,3)dihydro-pyrrole-2-thione (**3a**), *N*-(methoxy)-(1,3)dihydro-[1,3]azaphosphole-2-thione (**6a**), *P*-(methoxy)-(1,3)dihydro-[1,3]azaphosphole-2-thione (**4c**) and *P*-(methoxy)-(1,3)dihydro-[1,3]oxaphosphole-2-thione (**5c**) the vertical excitation energies were recalculated on the MS-CASPT2/cc-pVTZ//RI-MP2/cc-pVTZ level to exclude the uncertainties of the TD-DFT approach. This computations once more revealed the problems of TD-DFT. While for the most observed compounds TD-DFT agrees nicely ($\Delta E \leq 0.1$ eV) or reasonable ($\Delta E < 0.25$ eV) with CASPT2, TD-B3LYP overestimated the excitation energy of **4c** by more than 50 nm (-0.5 eV). This excludes **4c** from the list of new promising systems due to an expected daylight sensitivity.

For the remaining three promising systems the N,O or P,O dissociation paths, respectively, of the S₀, the T₁ and the first two singlet excited states were computed. While **5c** is

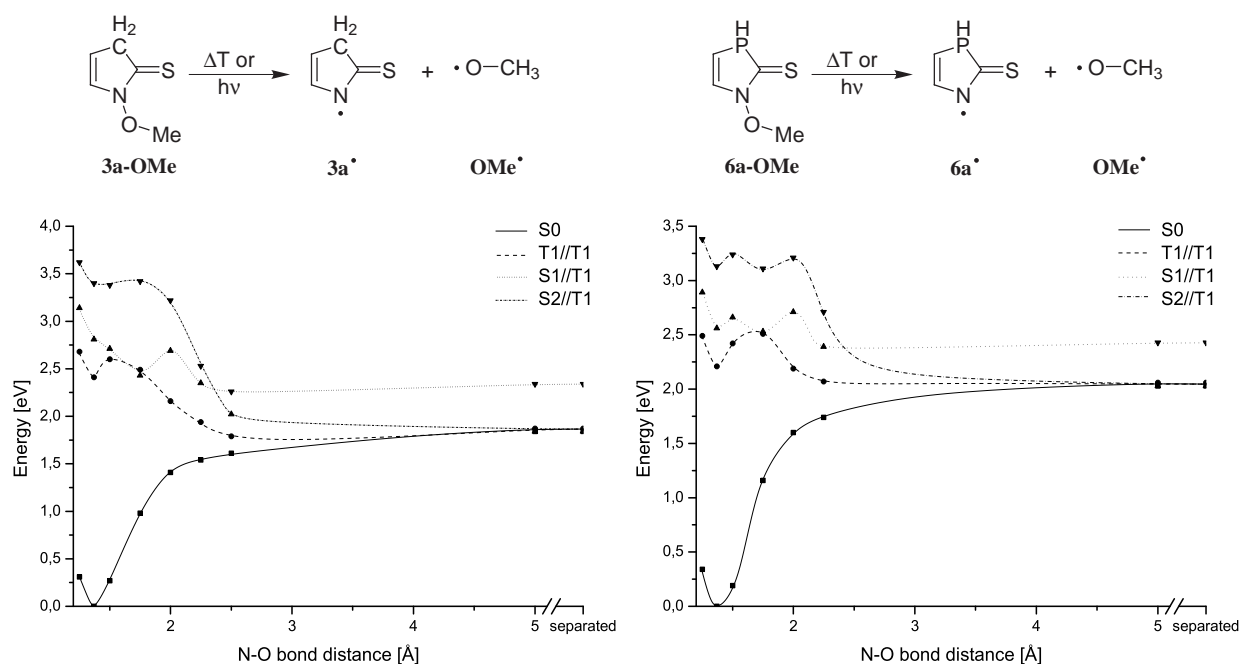


Figure 8.6: The calculated bond dissociation paths in the S_0 , the T_1 and the first two excited singlet excited states for the two promising new photochemical alkoxy radical precursors N -(methoxy)-(1,3)dihydro-pyrrole-2-thione (**3a**) and N -(methoxy)-(1,3)dihydro-[1,3]azaphosphole-2-thione (**6a**).

not able to release alkoxy radicals in a photochemical way^c a methylated^d form **meth-6a** of N -(methoxy)-(1,3)dihydro-[1,3]azaphosphole-2-thione (**6a**) and N -(methoxy)-(1,3)dihydro-pyrrole-2-thione (**3a**) seem to be the most promising candidates. For **meth-6a** the computations predict a strong absorption at about 350 nm while **3a** should absorb at about 330 nm. Due to the amounts of maximal excess energy (188 kJ mol^{-1} for **3a** and 162 kJ mol^{-1} for **6a**) that lies between the two reference compounds **1a-OMe** and **2a-OMe** and the shapes of the potential surfaces of the N,O bond dissociation paths the reactivity of the resulting radical fragments **3a•** and **6a•**, respectively, should resemble more the behavior of the ones obtained from the pyridinethione (**1a**) compounds. Especially for **6a** a large amount of excess energy should be quenched and even a relaxation to the undissociated ground state of the molecule can not be excluded.

^cnone of the computed potential energy surfaces shows a repulsive shape with respect to a P,O bond homolysis.

^dThe methylation of the phosphor center is necessary to prevent tautomerism.

Chapter 9

Zusammenfassung

Sauerstoff zentrierte Radikale sind wichtige Zwischenstufen in photobiologischen, mechanistischen und synthetischen Untersuchungen. Die Mehrzahl der Methoden zur Erzeugung von reaktiven Sauerstoffradikalen gehen von der homolytischen Spaltung der O,O Bindung in organischen Peroxiden oder Perestern aus. Die meisten dieser Vorläufer sind allerdings instabil und deshalb schwer zu handhaben. Deshalb haben *O*-Alkyl Derivate von *N*-(Hydroxy)-Pyridin-2(*1H*)-thion (**1a-OH**) und von 4- und 4,5-substituierten *N*-(Hydroxy)-Thiazol-2(*3H*)-thionen (Derivate von **2a-OMe**) in den letzten Jahren als milde Quelle von Alkoxyradikalen verstärkt Aufmerksamkeit erhalten. Da Licht mit relativ geringer Energie nötig ist, um die N,O Bindungsspaltung auszulösen ist davon auszugehen, dass der erste photophysikalische Vorgang nach der Bestrahlung von *N*-(Alkoxy)-Pyridin-2(*1H*)-thionen und *N*-(Alkoxy)-5-(*p*-Methoxyphenyl)-4-Methylthiazol-2(*3H*)-thionen mit UV Licht einer Anregung im Thiocarbonyl Chromophor entspricht und nicht in den olephinischen π -Systemen oder der N,O Bindung.

Ein großer Nachteil der Pyridinverbindungen ist ihre Tageslichtempfindlichkeit. Wegen einer breiten Absorptionsbande bei ungefähr 360 nm zersetzen sich die Pyridinthione schon bei der Bestrahlung mit ungefiltertem Tageslicht. Nur wenn der blaue Anteil des Lichts herausgefiltert wird sind *N*-(Alkoxy)-Pyridin-2(*1H*)-thione stabil. Neben ihren Gemeinsamkeiten^a verhalten sich *N*-(Alkoxy)-Pyridin-2(*1H*)-thione und *N*-(Alkoxy)-4-Methylthiazol-2(*3H*)-thione sehr unterschiedlich, wenn sie in ohne die Anwesenheit effektiver Radikalfänger Reagenzien photolysiert werden. *N*-(4-Penten-1-oxy)-Pyridin-2(*1H*)-thion reagiert unter diesen Bedingungen in sauberen und sehr effizienten Radikalkettenreaktionen, wogegen das entsprechende *N*-(4-Penten-1-oxy)-Thiazol-2(*3H*)-thion sogar in einem inerten Lösungsmittel ziemlich unkontrollierbar und mit vielen unerwünschten Nebenreaktionen reagiert. Um die

^aPhotochemische Freisetzung von Alkoxyradikalen.

Eigenschaften zukünftiger photochemischer Alkoxyradikal Vorläufer zu verbessern, ist es wichtig, die existierenden Unterschiede in den photophysikalischen Vorgängen, die mit einer UV/vis Anregung cyclischer Thiohydroxamsäure-*O*-estern zusammenhängen, allgemein zu verstehen.

Diese Kenntnisse sollen im Rahmen dieser Arbeit durch eine „Theoretische Charakterisierung und Optimierung photochemischer Alkoxyradikalvorläufer“ erhalten werden. Kapitel 2 behandelt die theoretischen Hintergründe der Erzeugung und Anwendung von Alkoxyradikalen. Elektronische Anregungen, die UV/vis Spektroskopie sowie quantenchemischer Ansätze, die in der Lage sind diese Phänomene zu berechnen, werden in Kapitel 3 dieser Arbeit beschrieben. Hierbei wird insbesondere auf die zeitabhängige Dichtefunktionaltheorie und den „complete active space“ Ansatz eingegangen, da diese beiden Methoden hauptsächlich verwendet wurden, um die theoretischen Informationen im Rahmen dieser Arbeit zu erhalten. Zum Verständniss des Multireferenz CAS Ansatzes wird im Rahmen der Diskussion in Abschnitt 3.2.2 auch auf den Formalismus der zweiten Quantisierung kurz eingegangen.

TD-DFT	CASPT2
<ul style="list-style-type: none"> • Eindeterminanten Ansatz • Schnell und effizient 	<ul style="list-style-type: none"> • Mehrdeterminanten Ansatz • Sehr genau
<ul style="list-style-type: none"> • Starke Funktionalabhängigkeit der Ergebnisse 	<ul style="list-style-type: none"> • Hohe Anforderungen an die Computerressourcen
<ul style="list-style-type: none"> • „Linear response“ Funktionen • Zeitabhängiger Kohn Sham Formalismus (Runge & Gross Theorem) • „Single pole approximation“ zur Berechnung angeregter Zustände 	<ul style="list-style-type: none"> • Multiconfigurationale Wellenfunktion (statische Korrelation) • Zweite Quantisierung • Multireferenz Møller Plesset Störungstheorie (dynamische Korrelation)

Abbildung 9.1: Zusammenfassung der Eigenschaften und Grenzen der beiden hauptsächlich in dieser Arbeit angewandten, quantenchemischen Methoden.

Nach der Beschreibung der theoretischen Hintergründe, ist das erste wissenschaftliche Ziel dieser Arbeit, die photochemischen Eigenschaften und Unterschiede der schon experimentell eingesetzten Moleküle auf der Basis heterocyclischer Thiohydroxamisäure-*O*-estern

quantenchemisch zu beschreiben. Kapitel 4 befasst sich mit der Berechnung der Strukturen der Grundkörper von **1a** und **2a** sowie hauptsächlich mit der Beschreibung der senkrechten elektronischen Anregungsspektren. Hierzu wurden, in Zusammenarbeit mit der Arbeitsgruppe Hartung, kombinierte theoretische und experimentelle Untersuchungen zu den UV/vis spektroskopischen Eigenschaften der Grundkörper der Alkoxyradikalvorläufer auf Pyridinthion und Thiazolthion Basis durchgeführt. Die berechneten Grundzustandsstrukturen beider freien Säuren **1a-OH** und **2a-OH** sowie der *N*-(Methoxy) Derivate **1a-OMe** und **2a-OMe** wurden mit Röntgenkristallstrukturen bereits kristallisierter Derivate dieser Verbindungen verglichen. RI-BLYP Berechnungen mit den SVP Basissätzen sind ausreichend, um die wichtigsten strukturellen Eigenschaften dieser heterocyclischen Verbindungen zu beschreiben. RI-MP2/cc-pVTZ Berechnungen führten nur zu kompakteren Strukturen.

Im anschließenden Validierungsschritt wurden CASSCF, CASPT2, TD-DFT unter Anwendung verschiedener Funktionale, sowie der RI-CC2 Ansatz getestet, inwieweit sie in der Lage sind, die senkrechten elektronischen Übergänge in die ersten drei angeregten Singulettzustände von *N*-(Methoxy)-pyridin-2(1*H*)-thion (**1a-OMe**), *N*-(Methoxy)-thiazol-2(3*H*)-thion (**2a-OMe**), sowie der *N*-(Hydroxy) Derivate **1a-OH** und **2a-OH** zu beschreiben. Der „complete-active-space“ Ansatz in Kombination mit der Multistate-Variante der PT2 Störungstheorie (MS-CASPT2) beschreibt die experimentell gemessenen elektronischen Anregungsspektren aller Verbindungen sehr genau. Ein ähnliches Verhalten wurde für den RI-CC2 Ansatz gefunden. Allerdings werden die Anregungsenergien im Vergleich zu CASPT2 immer um 0.1 bis 0.3 eV zu hoch beschrieben. Die Ergebnisse der TD-DFT Berechnungen sind, im Gegensatz dazu, sehr empfindlich bezüglich der Wahl des Funktionals sowie des angeregten Zustandes, der beschrieben werden soll. Das reine BLYP Funktional unterschätzt die Anregungsenergien generell, wogegen die Anwendung des BHLYP Funktionals zu einer systematischen Überschätzung führt. Beckes drei Parameter Funktional (B3LYP) und das PBE0 Funktional liefern in den meisten Fällen Anregungsenergien, die den CASPT2 Berechnungen oder dem Experiment entsprechen. Eine Validierung der TD-DFT Ergebnisse durch einen Vergleich mit experimentellen Daten oder besseren *Ab-initio*-Berechnungen sollte immer durchgeführt werden.

Auf der Grundlage der CASPT2-Berechnungen wurden die spektroskopisch sichtbaren UV/vis-Banden beider Verbindungen dem $S_0 \rightarrow S_2$ Übergang zugeordnet. Dieser Übergang entspricht in beiden Fällen einer $\pi \rightarrow \pi^*$ Anregung in der Thiocarbonyleinheit der Thiohydroxamsäure-Gruppe. DFT-Berechnungen charakterisieren die beteiligten Orbitale als π_{CS} - und π_{ring}^* -Orbitale in **1a-OMe** und die π_{SCS}^{non} - und π_{SCS}^* -Orbitale in **2a-OMe**. Die experimentell beobachtete höhere Stabilität gegenüber Tageslicht im Falle der Thiazolthion-Verbindungen resultiert einfach aus der höheren Anregungsenergie in den photoaktiven S_2 -Zustand.

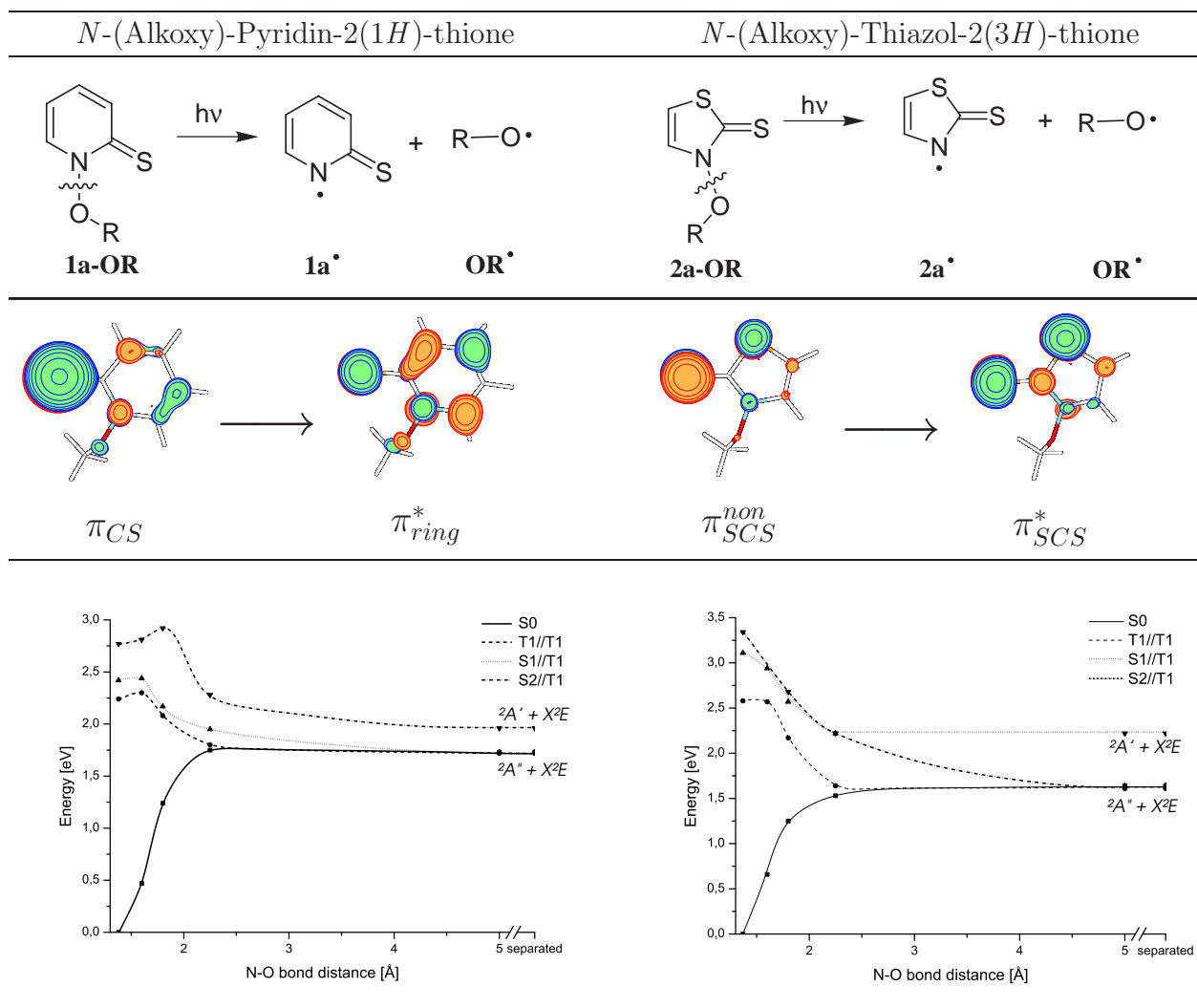


Abbildung 9.2: Vergleich der berechneten photochemischen Eigenschaften der beiden schon experimentell bekannten Alkoxyradikalvorläufer *N*-(Alkoxy)-pyridin-2(1*H*)-thion (**1a-OR**; linke Spalte) und *N*-(Alkoxy)-thiazol-2(3*H*)-thion (**2a-OR**; rechte Spalte).

In Kapitel 5 wird der Mechanismus der thermisch oder photochemisch induzierten N,O-Homolyse in *N*-(Methoxy)-pyridin-2(1*H*)-thion (**1a-OMe**) und *N*-(Methoxy)-thiazol-2(3*H*)-thion (**2a-OMe**) untersucht. Im Gegensatz zu den senkrechten Anregungsspektren liefert für den thermischen und photolytischen Bindungsdissoziationsprozess nur CASPT2 verlässliche Ergebnisse. Die durch UV-Licht induzierte N,O-Homolyse in den Thionen **1a-OMe** und **2a-OMe** beginnt im S_2 -Zustand, da Anregungen in diesen Zustand die einzigen mit einer messbaren Oszillatorstärke sind, d.h. der S_2 -Zustand ist der einzige der durch eine Bestrahlung mit UV Licht besetzt wird. Die N,O-Homolyse auf der Potentialfläche des S_2 -Zustandes würde, ohne Barriere im Falle von **2a-OMe**, beziehungsweise mit einer kleinen Barriere im Falle von **1a-OMe** verlaufen und zu den Sulfonyl Radikalen **1a•** oder **2a•** in ihrem ersten angeregten Zustand und dem Methoxyl Radikal in seinem Grundzustand führen.

Wegen einer zu erwarteten Relaxation vom S_2 -Zustand in den S_1 -Zustand wird dieser Reaktionsverlauf jedoch nicht auftreten. Im Fall der Thiazolthion Verbindung **2a-OMe** deuten die berechneten S_2 - und S_1 -Kurven auf eine konische Durchdringung der beiden Zustände hin, was zu einer sehr effektiven $S_2 \rightarrow S_1$ Relaxation führen sollte. Die Potentialflächen des S_1 - und S_2 -Zustandes von **1a-OMe** weisen kein solches Merkmal auf. Wegen der gehinderten Dissoziation im S_2 -Zustand^b wird eine langsamere $S_2 \rightarrow S_1$ -Relaxation, wie sie zum Beispiel von Kashas Regel vorhergesagt wird, erwartet. Für beide Thione **1a-OMe** und **2a-OMe** ist der S_1 -Zustand bezüglich der N,O Bindung repulsiv. Eine Relaxation der in den S_1 -Zustand angeregten Moleküle in den T_1 -Zustand ist über Spin-Orbit-Wechselwirkungen möglich. Der T_1 -Zustand führt zum tiefsten Dissoziationskanal, wobei für die nichtwechselwirkenden Fragmente der S_1 , sowie der T_1 beide dem entarteten 2E Grundzustand des Methoxyradikals entsprechen. Deshalb ist es für die nachfolgende Chemie nicht relevant, ob die Dissoziation auf der S_1 oder der T_1 Oberfläche stattfindet, da die Relaxation in den Grundzustand der Alkoxyradikale immer schneller sein sollte, als ihre chemischen Reaktionen.

Wegen des schnelleren Dissoziationsprozess im Falle der Thiazolthione ist anzunehmen, dass die Überschussenergie, die von der photochemischen Aktivierung der Moleküle herrührt, nur zu einem kleinen Teil auf das Lösungsmittel oder andere Freiheitsgrade der Fragmente übertragen wird. Für die *N*-(Alkoxy)-Pyridin-2(1*H*)-thione ist eine Energieübertragung auf das Lösungsmittel wesentlich wahrscheinlicher, da ihr S_2 -Zustand eine Barriere im Bezug auf die Dissoziation aufweist. Zusätzlich ist keine vermiedene Kreuzung zwischen dem S_2 und dem S_1 -Zustand gefunden worden, so dass auch der $S_2 \rightarrow S_1$ Relaxationsprozess deutlich langsamer verlaufen wird. Zu guter Letzt ist auch die maximal mögliche Überschussenergie der Fragmente geringer, die von **1a-OMe** erhalten werden. Dies resultiert aus einer kleineren senkrechten Anregungsenergie (Startpunkt der photochemischen Reaktion) und einer höheren thermischen Dissoziationsenergie im S_0 Grundzustand. Letztere bestimmt die energetische Lage der erhaltenen Radikale in ihrem Grundzustand. Die intrinsische chemische Reaktivität der freigesetzten Radikalfragmente wurde über isodesmische Wasserstoffabstraktionsreaktionen abgeschätzt. Es stellte sich jedoch heraus, dass der wichtigste Faktor für die Reaktivität der photochemischen Alkoxyradikalvorläufer ihre maximal mögliche Überschussenergie, sowie deren Übertragung auf das Lösungsmittel und andere Freiheitsgrade, während des Dissoziationsprozesses ist. Dass dieses wirklich der Fall ist, erkennt man an dem Radikalfragment **1b[•]**, das von dem, ebenfalls erfolgreich im Experiment eingesetzten Alkoxyradikalvorläufer *N*-(Methoxy)-Pyridin-2(1*H*)-on, freigesetzt wird und eine wesentlich höhere chemische Reaktivität aufweist, als die Fragmente **1a[•]** oder **2a[•]**. Im Gegensatz dazu weisen die berechneten N,O Bindungsdissoziationspfade Verläufe auf, die klar auf einen

^bBarriere zur Dissoziation ungefähr 11 kJ mol^{-1} (0.11 eV).

relativ langsamen Bindungsbruch hindeuten. Dies hilft die Überschussenergie, die durch die photochemische Aktivierung vorhanden ist, effektiv ins Lösungsmittel oder andere Freiheitsgrade zu übertragen. *N*-(Alkoxy) Derivate von **1b-OMe** sollten deshalb wie Derivate von *N*-(Methoxy)-Pyridin-2(1*H*)-thion (**1a-OMe**) als saubere photochemische Alkoxyradikalquelle dienen, was auch in der Tat experimentell gefunden wurde.

Die Berechnungen, die in den Kapiteln 4 und 5 vorgestellt wurden, liefern ein Modell für die theoretische Vorhersage der spektroskopischen Eigenschaften und des photochemischen Verhaltens von heterocyclischen Alkoxyradikalvorläufern. Das nächste Ziel der vorliegenden Arbeit besteht darin, die erhaltenen Kenntnisse über die Möglichkeiten zum Verständnis des photochemischen und photophysikalischen Charakteristiken solcher Verbindungen anzuwenden, um ihre Eigenschaften zu verbessern oder um neue Verbindungen vorzuschlagen, die ebenfalls in der photochemischen Alkoxyradikalchemie eingesetzt werden können.

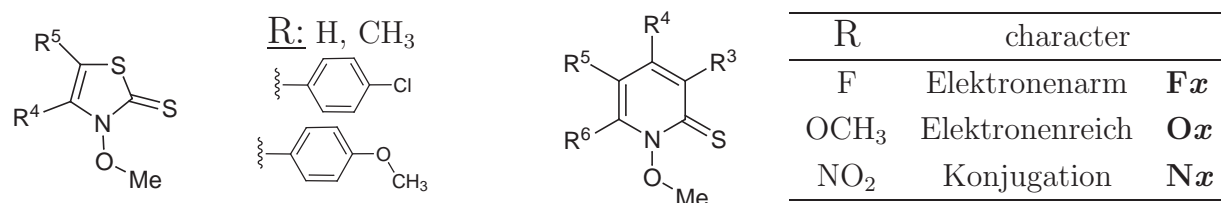


Abbildung 9.3: Die in Kapitel 6 dieser Arbeit untersuchten Substituenten an den zwei Heterocyclen, die die Anregungswellenlänge zur photochemischen Alkoxyradikalfreisetzung verändern sollen.

Kapitel 6 dieser Arbeit behandelt das Anpassen der Anregungswellenlänge der bekannten Pyridin-2(1*H*)-thion und Thiazol-2(3*H*)-thion Moleküle. In einer kombinierten theoretischen und experimentellen Studie wurden verschiedene C⁴ und C⁵ substituierte Derivate von **2a-OMe** synthetisiert, um ihre UV/vis Spektren aufzunehmen und systematisch den Effekt von CH₃ und Aryl Substituenten am Thiazolthion Heterocyclus zu erforschen. Um die experimentell beobachteten UV/vis Banden substituiertes Thiazol-2(3*H*)-thione elektronischen Übergängen zuzuordnen, wurden die Ergebnisse von zeitabhängigen DFT Berechnungen, unter Verwendung des B3LYP Funktionals, der TZVP Basissätze auf RI-BLYP/SVP optimierten Grundzustandsstrukturen, angewendet. Die UV/vis Spektren von 4 und 5 substituierten *N*-(Methoxy)-thiazol-2(3*H*)-thionen können, wie das Spektrum des Grundkörpers **2a-OMe**, interpretiert werden. Hier ist ebenfalls der spektroskopisch erlaubte $\pi_{SCS}^{non} \rightarrow \pi_{SCS}^*$ -Übergang für die beobachtete UV/vis-Bande und die photochemische Alkoxyradikalfreisetzung zuständig. Diese Berechnungen offenbarten allerdings die bekannten Probleme der zeitabhängigen Dichtefunktionaltheorie bei der Beschreibung elektronischer Übergänge, die einen größeren räumlichen Ladungstransfer beinhalten. Der bathochrome Einfluss eines Arylsubstituenten an der C⁵ Position des Thiazolthion-Fünfringes wurde von dem angewandten B3LYP Funktional wegen eines beträchtlichen Charge-Transfers-Effekts

vom Thiocarbonyl π_{SCS}^{non} -Orbital in das π_{SCS}^* -Orbital, das auch Dichte im aromatischen Ring des C⁵ Substituenten aufweist, überschätzt. Im Gegensatz hierzu, konnten RI-CC2 Berechnungen den experimentellen Rotshift von ungefähr 15 nm, im Falle eines 5-*p*-Methoxyphenyl (Anisyl) Substituenten, richtig reproduzieren.

N-(Alkoxy)-pyridin-2(1*H*)-thione (**1a-OR**) sind Alkoxyradikalvorläufer, die auf Grund ihrer Tageslichtempfindlichkeit schwieriger zu handhaben sind. Da diese Instabilität von einer breiten Absorptionsbande bei etwa 360 nm, die dem $\pi_{CS} \rightarrow \pi_{ring}^*$ Übergang zugeordnet wurde, herrührt, beschreibt der zweite Teil von Kapitel 6 die Identifikation eines Substitutionsmuster am Pyridinring, der eine Blauverschiebung dieser Bande zu ungefähr 350 nm induzieren soll. Zu diesem Zweck wurde die $\pi \rightarrow \pi^*$ Anregungen von substituierten *N*-(Methoxy)-pyridin-2(1*H*)-thionen auf TD-DFT und CASPT2 Niveau berechnet, da bis heute noch keine experimentellen UV/vis Daten zu substituierten Pyridinthionverbindungen vorliegen. Fluor stellt ein Modell für elektronenarme Substituenten dar, während eine Methoxygruppe ein Beispiel für elektronenreiche Substituenten ist. Die NO₂ Gruppe ist ein Modell für einen Substituenten, der mit dem π -Elektronensystem des Pyridinringes in Konjugation treten kann.

Die Berechnungen zeigen, dass elektronenarme und elektronenreiche Substituenten den gleichen Einfluss auf das elektronische Anregungsspektrum haben. Die stärkste hypsochrome Verschiebung im Falle einer Einfachfluorierung ist für *N*-(Methoxy)-6-fluorpyridin-2(1*H*)-thion mit 11 nm (CASPT2) vorhergesagt worden. Die Substituenteneffekte der Fluoratome auf die elektronischen Anregungen und auch auf die Orbitalenergien sind additiv. Folglich wird für *N*-(Methoxy)-3,4,6-Trifluorpyridin-2(1*H*)-thion eine Blauverschiebung von 24 nm vorhergesagt. Diese hypsochromen Verschiebungen kommen hauptsächlich daher, dass die π_{ring}^* -Orbitale weniger stabilisiert werden, als die π_{CS} -Orbitale. Die elektronenreiche OMe Gruppe scheint sogar zu noch stärkeren Blauverschiebungen der $\pi_{CS} \rightarrow \pi_{ring}^*$ Anregung zu führen (z.B. 22 nm bei *N*-(Methoxy)-3-Methoxypyridin-2(1*H*)-thion (**O3**)). Allerdings wird der Gesamteffekt wesentlich geringer ausfallen da der starke hypsochrome Effekt nur auftritt, wenn die Methoxygruppe in der Ebene des Pyridinringes liegt. Bei einer orthogonalen Anordnung wird dieser Effekt unterdrückt, so dass der Effekt für eine frei rotierende Methoxygruppe minimiert wird. Für eine Mehrfachmethoxylierung ist keine einfache Additivität der Substituenteneffekte festzustellen, da die sterischen Ansprüche der OMe Gruppen ihre optimale Orientierung verhindern. Der hypsochrome Effekt der Methoxygruppe hat ihren Ursprung in der stärkeren Destabilisierung des π_{ring}^* -Orbitals im Vergleich zu dem π_{CS} -Orbital. Als Modell für Substituenten, die zu mesomeren Effekten in der Lage sind, wurde die NO₂-Gruppe gewählt. Sie führt allerdings nur zu starken Rotverschiebungen (z.B. 160 nm in *N*-(Methoxy)-6-Nitropyridin-2(1*H*)-thion (**N6**)), die, wie im Falle der Methoxygruppe, wegen der Rotation abgeschwächt werden. Die Kopplung der beiden π -Systeme führt zu einem neuen π^* -Orbital, das energetisch deutlich unter dem π_{ring}^* -Orbital der unsubstituierten

ten Verbindung liegt. Eine Anwendung von Substituenten, die mit dem π -Elektronensystem des Heterocyclus konjugieren können, ist nicht in der Lage die Tageslichtempfindlichkeit zu verhindern. Sie können aber eingesetzt werden, wenn Vorläufersysteme benötigt werden die im sichtbaren Bereich des Spektrums absorbieren.

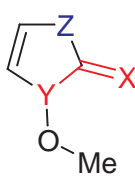
Z	Heterocyclus		X	Y	Funktionelle Gruppe
CH=CH	Pyridin (1)			S	N
S	Thiazol (2)		O	N	keton (b)
CH ₂	Pyrrol (3)		S	P	phosphonthion (c)
NH	Imidazol (4)				
O	Oxazol (5)				
PH	Phosphazol (6)				

Abbildung 9.4: Die systematischen Modifikationen des Heterocyclus und der funktionellen Gruppe, um neue vielversprechende photochemische Alkoxyradikalvorläufer zu erhalten.

Mit den Mitteln der Computational Chemistry ist es auch möglich neue, experimentell unbekannte Grundkörper für die Anwendung als photochemische Alkoxyradikalvorläufer vorzuschlagen, die die Vorteile beider schon angewandter Verbindungen vereinen. Kapitel 7 dieser Arbeit beschreibt hierzu ein computerunterstütztes Design neuer Alkoxyradikalvorläufer. Um die Vorteile der *N*-(Alkoxy)-Pyridin-2(1*H*)-thione und der *N*-(Alkoxy)-Thiazol-2(3*H*)-thione zu kombinieren, sollte die Radikalerzeugung mit Licht der Wellenlänge von ungefähr 350 nm initiiert werden, und es sollten wenige unerwünschte Nebenreaktionen während des Radikalbildungsprozesses auftreten, auch wenn keine Radikalfänger eingesetzt werden. Um die Eigenschaften neuer Testkandidaten theoretisch vorherzusagen wurde die Vorgehensweise gewählt, die schon erfolgreich die Unterschiede in den Eigenschaften von **1a-OMe** und **2a-OMe** erklären konnte, und zusätzlich auch an *N*-(Methoxy)-Pyridin-2(1*H*)-on (**1b-OMe**) getestet wurde. Dieser Test zeigte, dass das entwickelte Modell in der Tat die wichtigsten Fakten für die Vorhersage der Reaktivität beinhaltet.

Um neue Grundkörper zu finden, wurden 18 Testsysteme durch eine systematische Modifikation des Thiazolthion-Grundkörpers erhalten. Die Substitution des Thiazol Schwefelatoms mit einer CH₂ führt zum Pyrrol-Heterocyclus (**3**) und der Imidazolring (**4**) wird gebildet, wenn eine NH Gruppe eingeführt wird. Ein Sauerstoffatom anstatt des Schwefels führt zum Oxazol Heterocyclus (**5**). Die Substitution des Schwefel mit einer PH Einheit bildet den Phosphazolring (**6**). Weitere Variationen erhält man durch eine Modifikation der Thiohydroxamsäuregruppe. Das Ersetzen des Thiocarbonyl Schwefelatoms durch Sauerstoff führt zu den Hydroxamsäurederivaten **b**, wogegen das Ersetzen des Hydroxamsäure N Atoms durch Phosphor „Phosphothiohydroxamsäure“ Derivate **c** bildet.

Neue, vielversprechende Vorläufersysteme wurden durch ein Screening der ersten elek-

Molekül	eV / nm	f
1a	3.25 / 381	0.051
2a	3.99 / 310	0.134
3a	3.79 / 327	0.183
6a	3.57 / 348	0.139
1b	4.00 / 310	0.099
4c	3.00 / 414	0.118
5c	3.52 / 352	0.082

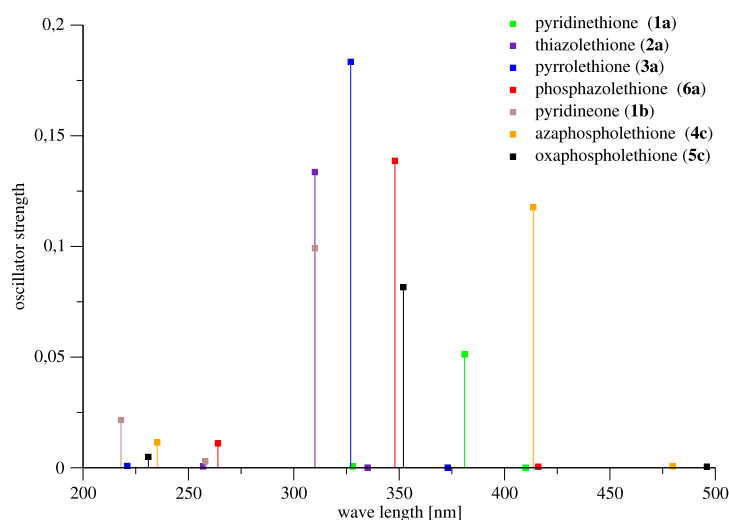


Abbildung 9.5: Die berechneten CASPT2 elektronischen Anregungsspektren der neuen vielversprechenden Vorläufermoleküle und der schon angewandten heterocyclischen Vorläufer-systeme.

tronischen Anregungen aller 18 Moleküle auf TD-DFT Niveau unter Verwendung des B3LYP Funktionals identifiziert. Der Einfluss eines polaren Lösungsmittels wurde ebenfalls abgeschätzt, stellte sich aber als nicht so wichtig für den sichtbaren $\pi \rightarrow \pi^*$ Übergang der interessanten Systeme heraus. Für die erhaltenen neuen, vielversprechenden Verbindungen *N*-(Methoxy)-(1,3)dihydro-pyrrole-2-thion (**3a**), *N*-(Methoxy)-(1,3)dihydro-[1,3]azaphosphole-2-thion (**6a**), *P*-(Methoxy)-(1,3)dihydro-[1,3]azaphosphole-2-thion (**4c**) und *P*-(Methoxy)-(1,3)dihydro-[1,3]oxaphosphole-2-thion (**5c**) wurden die senkrechten Anregungsenergien nochmals auf MS-CASPT2/cc-pVTZ//RI-MP2/cc-pVTZ Niveau berechnet, um Unsicherheiten des TD-DFT Ansatzes auszuschließen. Diese Berechnungen zeigten erneut die Probleme bei der Anwendung von TD-DFT. Während für die meisten untersuchten Verbindungen TD-DFT sehr gut ($\Delta E \leq 0.1$ eV) bis akzeptabel ($\Delta E < 0.25$ eV) mit den CASPT2 Werten übereinstimmt, überschätzt die zeitabhängige Dichtefunktionaltheorie die Anregungsenergie in **4c** um mehr als 50 nm (-0.5 eV). Dies schließt **4b** aufgrund einer erwarteten Tageslichtempfindlichkeit auch von der Liste der vielversprechenden neuen Vorläufermoleküle aus.

Für die verbleibenden drei neuen, vielversprechenden Systeme wurden die N,O oder P,O Bindungsdissoziationspfade im S_0 , T_1 und den zwei ersten angeregten Singulettzuständen berechnet. Während **5c** nicht in der Lage ist Alkoxyradikale photochemisch freizusetzen^c, scheinen eine methylierte Form^d **meth-6a** von *N*-(Methoxy)-(1,3)dihydro-[1,3]azaphosphole-2-thion (**6a**) und *N*-(Methoxy)-(1,3)dihydro-pyrrole-2-thion (**3a**) die vielversprechendsten

^cKeine der berechneten Potentialflächen zeigt einen repulsiven Verlauf bezüglich einer P,O Bindungsspaltung.

^dDie Methylierung des Phosphorzentrums ist nötig um eine Tautomerie zu vermeiden.

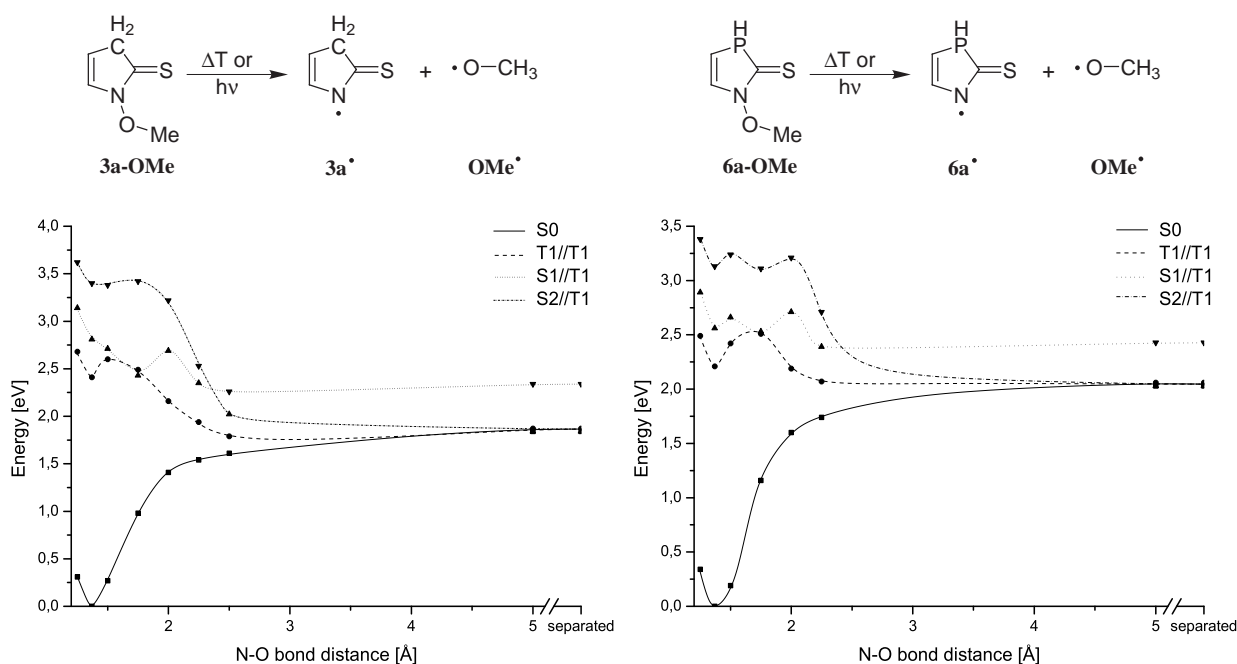


Abbildung 9.6: Die berechneten Bindungsdissoziationspfade im S₀, T₁ und den zwei ersten angeregten Singulettzuständen der zwei neuen vielversprechenden photochemischen Alkoxyradikalvorläufer *N*-(Methoxy)-(1,3)dihydro-pyrrole-2-thion (**3a**) und *N*-(Methoxy)-(1,3)dihydro-[1,3]azaphosphole-2-thion (**6a**).

neuen Kandidaten zu sein. Für **meth-6a** sagen die Berechnungen eine intensive Absorption bei ungefähr 350 nm voraus, während **3a** bei ungefähr 320 nm absorbieren sollte. Wegen der Menge an maximal möglicher Überschussenergie (188 kJ mol⁻¹ bei **3a** und 162 kJ mol⁻¹ bei **6a**), die zwischen den beiden Referenzsystemen **1a-OMe** und **2a-OMe** liegt, und aufgrund der Verläufe der Potentialflächen der N,O Bindungsdissoziationspfade, wird eine Reaktivität der Radikale **3a[•]** und **6a[•]** erwartet, die mehr dem Verhalten der Fragmente von der Homolyse der Pyridinthionverbindungen (**1a**) entsprechen sollte. Besonders für **6a** sollte eine Menge der Überschussenergie an das Lösungsmittel oder andere Freiheitsgrade abgeleitet werden, wesswegen auch eine Relaxation des angeregten Moleküls in den undissoziierten Grundzustand nicht ausgeschlossen werden kann.

Bibliography

- [1] Hartung, J.; Špehar, K.; Svoboda, I.; Fuess, H.; Arnone, M.; Engels, B. *Eur. J. Org. Chem* **2005**, pages 869–881.
- [2] Arnone, M.; Hartung, J.; Engels, B. *J. Phys. Chem. A* **2005**, *109*, 5943–5950.
- [3] Arnone, M.; Engels, B. *J. Phys. Chem. A* **2006**, *110*, 12330–12337.
- [4] Arnone, M.; Engels, B. *J. Phys. Chem. A* **2007**, *111*, 3161–3165.
- [5] Hartung, J.; Gottwald, T.; Špehar, K. *Synthesis* **2002**, pages 1469–1498.
- [6] Gray, P.; Williams, A. *Chem. Rev.* **1959**, *59*, 239–328.
- [7] Adam, W.; Hartung, J.; Okamoto, H.; Saha-Möller, C. R.; Špehar, K. *Photochem. Photobiol.* **2000**, *72*, 619–624.
- [8] Adam, W.; Hartung, J.; Okamoto, H.; Marquardt, S.; Nau, W. N.; Pischel, U.; Saha-Möller, C. R.; Špehar, K. *J. Org. Chem.* **2002**, *67*, 6041–6049.
- [9] Adam, W.; Grimm, G. N.; Marquardt, S.; Saha-Möller, C. R. *J. Am. Chem. Soc.* **1999**, *121*, 1179–1185.
- [10] Möller, M.; Adam, W.; Marquardt, S.; Saha-Möller, C. R.; Stopper, H. *Free Radical Biology & Medicine* **2005**, *39*, 437–482.
- [11] Aveline, B. M.; Redmond, R. W. *Photochem. Photobiol.* **1998**, *68*, 266–275.
- [12] Adam, W.; Grimm, G. N.; Saha-Möller, C. R. *Free Radical Biology & Medicine* **1998**, *24*, 234–238.
- [13] Borges, M.; Romao, A.; Matos, O.; Marzano, C.; Caffieri, S.; Becker, R. S.; Macanita, A. L. *Photochem. Photobiol.* **2002**, *75*, 97–106.
- [14] Hartung, J.; Hiller, M.; Schmidt, P. *Chem. Eur. J.* **2001**, *2*, 1014–1023.
- [15] Hartung, J. *Eur. J. Org. Chem* **2001**, pages 619–632.

- [16] Hartung, J.; Kneuer, R. *Tetrahedron: Asymmetry* **2003**, *14*, 3019–3031.
- [17] Hartung, J.; Kneuer, R.; Laug, S.; Schmitt, P.; Špehar, K.; Svoboda, I.; Fuess, H. *Eur. J. Org. Chem* **2003**, pages 4033–4052.
- [18] Hartung, J.; Kneuer, R. *Eur. J. Org. Chem* **2000**, pages 1677–1683.
- [19] Beckwith, A. L. J.; Hay, B. P. *J. Am. Chem. Soc.* **1988**, *110*, 4415–4416.
- [20] Hay, B. P.; Beckwith, A. L. J. *J. Org. Chem.* **1989**, *54*, 4330–4334.
- [21] Hartung, J.; Kneuer, R.; Schwarz, M.; Svoboda, I.; Fuess, H. *Eur. J. Org. Chem* **1999**, pages 97–106.
- [22] Barton, D. H. R.; Crich, D.; Kretzschmar, G. *J. Chem. Soc., Perkin Trans. 1* **1986**, pages 39–53.
- [23] Hartung, J.; Schwarz, M.; Svoboda, I.; Fuess, H.; Duarte, M. *Eur. J. Org. Chem* **1999**, pages 1275–1290.
- [24] Gross, E.; Dobson, J. F.; Petersilka, M. In *Topics in Current Chemistry*; Nalewajski, R. F., Ed.; Springer: Berlin, 1996; Vol. 181; pages 81–172.
- [25] Burke, K.; Gross, E. A guided tour of time-dependent density functional theory, In *Density Functionals: Theory and Applications*; Joubert, D., Ed.; Springer: Berlin, 1998; pages 1–31.
- [26] Runge, E.; Gross, E. K. U. *Phys. Rev. Lett.* **1984**, *52*, 997–1000.
- [27] Roos, B. O.; Wodmark, P.-O. *European Summerschool in Quantum Chemistry, Book 2*; Lund University: Schweden, 1999.
- [28] Roos, B. O. The complete active space self-consistent field method and its applications in electronic structure calculations, In *Advances in Chemical Physics; Ab Initio methodes in Quantum Chemistry - II*; Laweley, K., Ed.; John Wiley & Sons Ltd.: Chester, England, 1987; page 139.
- [29] Roos, B. O.; Taylor, P. R.; Siegbahn, P. E. M. *Chem. Phys.* **1980**, *48*, 157–173.
- [30] Andersson, K.; Malmqvist, P.-Å.; Roos, B. O. *J. Chem. Phys.* **1992**, *96*, 1218–1226.
- [31] Andersson, K.; Malmqvist, P.-Å.; Roos, B. O.; Sadley, A. J.; Wolinski, K. *J. Phys. Chem.* **1990**, *94*, 5483–5488.
- [32] Meschede, D. *Gerthsen Physik*; Springer: Berlin, 2004.

- [33] Klessinger, M.; Michl, J. *Excited states and photochemistry of organic molecules*; VCH Publishers, Inc.: Weinheim, 1994.
- [34] Graybeal, J. D. *Molecular Spectroscopy*; McGraw-Hill Book Co.: Singapore, 1988.
- [35] Grimme, S. Calculations of the electronic spectra of large molecules, In *Reviews in Computational Chemistry Vol. 20*; Lipkowitz, K., Ed.; John Wiley & Sons Ltd.: Chester, England, 2004; pages 153–218.
- [36] Dreuw, A.; Head-Gordon, M. *Chem. Rev.* **2005**, *105*, 4001–4037.
- [37] Hartung, J.; Hiller, M.; Schwarz, M.; Svoboda, I.; Fuess, H. *Liebigs Ann.* **1996**, pages 2091–2097.
- [38] Bond, A. D.; Feeder, N.; Teat, S. J.; Jones, W. *Tetrahedron* **2000**, *56*, 6617–6624.
- [39] Hartung, J.; Schwarz, M.; Svoboda, I.; Fuess, H. *Acta Crystallogr. Sect. C* **2003**, *59*, 682–684.
- [40] Finley, J.; Malmqvist, P.-Å.; Roos, B. O.; Serrano-Andrés, L. *Chem. Phys. Lett.* **1998**, *288*, 299–306.
- [41] Christiansen, O.; Koch, H.; Jørgensen, P. *Chem. Phys. Lett.* **1995**, *243*, 409–418.
- [42] Hätting, C.; Weigend, F. *J. Chem. Phys.* **2000**, *113*, 5154–5161.
- [43] Hätting, C.; Köhn, A. *J. Chem. Phys.* **2002**, *117*, 6939–6951.
- [44] Ballschmiter, K. *Angew. Chem.* **1992**, *104*, 501–528.
- [45] Eisenbrand, G.; Metzeler, M. *Toxikologie für Chemiker*; Georg-Thieme-Verlag: Stuttgart, 1994.
- [46] Jurkiewicz, B. A.; Buettner, G. R. *Photochem. Photobiol.* **1996**, *64*, 918–922.
- [47] Whittaker, M. M.; Whittaker, J. W. *J. Biol. Chem.* **1990**, *265*, 9610–9613.
- [48] Chaudhuri, P.; Hess, M.; Müller, J.; Hildenbrand, K.; Bill, E.; Weyhermüller, T.; Wieghardt, K. *J. Am. Chem. Soc.* **1999**, *121*, 9599–9610.
- [49] Norlund, P.; Sjöberg, B.-M.; Eklund, H. *Nature* **1990**, *345*, 593–598.
- [50] Stubbe, J.; van der Donk, W. A. *Chem. Rev.* **1998**, *98*, 705–762.
- [51] Wieland, H. *Ber. Dtsch. Chem. Ges.* **1911**, *44*, 2550–2556.
- [52] Höper, U.; Botschwina, P.; Köppel, H. *J. Chem. Phys.* **2000**, *112*, 4132–4142.

- [53] Tarczay, G.; Gopalakrishnan, S.; Miller, T. A. *J. Molec. Spectr.* **2003**, *220*, 276–290.
- [54] Ramond, T. M.; Davico, G. E.; Schwartz, R. L.; Lineberger, W. C. *J. Chem. Phys.* **2000**, *112*, 1158–1169.
- [55] Lee, J.; Oh, J.; Jin, S.-J.; Choi, J.-R.; Atwood, J. L.; Cha, J. K. *J. Org. Chem.* **1994**, *59*, 6955–6964.
- [56] Mićović, V. M.; Mamuzić, R. I.; Jeremić, D.; Mihailović, M. L. *Tetrahedron* **1964**, *20*, 2279–2287.
- [57] Clerici, A.; Minisci, F.; Ogawa, K.; Surzur, J.-M. *Tetrahedron Lett.* **1978**, *19*, 1149–1152.
- [58] Suginome, H.; Liu, C. F.; Furosaki, A. *Chem. Lett.* **1985**, *14*, 27–30.
- [59] Dowd, P.; Zhang, W. *Chem. Rev.* **1993**, *93*, 2091–2115.
- [60] Barton, D. H. R.; Chern, C.-Y.; Jaszberenyi, J. C. *Tetrahedron* **1995**, *51*, 1867–1886.
- [61] Barton, D. H. R.; Crich, D.; Motherwell, W. B. *Tetrahedron* **1985**, *41*, 3901–3924.
- [62] Hartung, J. In *Radicals in Organic Synthesis*; Renaud, P., Sibi, M. P., Eds., Vol. 2; Wiley-VCH: Weinheim, 2001; pages 425–439.
- [63] Buettner, G. R. In *General Aspects of the Chemistry of Radicals*; Alfassi, T., Ed.; Wiley: Chichester, 1999; pages 1–18.
- [64] Wilsey, S.; Dowd, P.; Houk, K. N. *J. Org. Chem.* **1999**, *64*, 8801–8811.
- [65] Walling, C.; Padwa, A. *J. Am. Chem. Soc.* **1963**, *85*, 1593–1597.
- [66] McMillen, D. F.; Golden, D. M. *Ann. Rev. Phys. Chem.* **1982**, *33*, 493–532.
- [67] Burkey, T. J.; Majewski, M.; Griller, D. *J. Am. Chem. Soc.* **1986**, *108*, 2218–2221.
- [68] Howard, J. A.; Scaiano, J. C. Oxyl Peroxyl und verwandte Radikale in Landolt-Börnstein Zahlenwerte und Funktionenaus Naturwissenschaft und Technik, In *Kinetische Daten von Radikalreaktionen*; Fischer, H., Ed., Vol. New Series Part D, Vol. 13; Springer: Berlin, 1984; pages 1–127.
- [69] Baldwin, J. E. *J. Chem. Soc., Chem. Commun.* **1976**, pages 734–736.
- [70] Harman, D. *J. Gerontol.* **1985**, *11*, 298–300.
- [71] Sohal, R. S. *Adv. Myochem.* **1989**, *2*, 21–34.

- [72] Sohal, R. S. *Aging Milano* **1993**, *5*, 3–17.
- [73] Blake, D. R.; Allen, R. E.; Lunec, J. *Br. Med. Bull* **1987**, *43*, 371–385.
- [74] Halliwell, B.; Gutteridge, J. M. *Free Radicals in Biology and Medicine*; Oxford University Press: Oxford, 1989.
- [75] Sies, H. *Oxidative Stress, Oxidants and Antioxidants*; Academic Press: New York, 1991.
- [76] Lim, P.; Wuenschell, G. E.; Holland, V.; Lee, D.-H.; Pfeifer, G. P.; Rodriguez, H.; Termini, J. *Biochemistry* **2004**, *43*, 15339–15348.
- [77] Walling, C. *Acc. Chem. Res.* **1975**, *8*, 125–131.
- [78] Filho, A. C. M.; Meneghini, R. *Biochim. Biophys. Acta* **1984**, *781*, 56–63.
- [79] Halliwell, B.; Gutteridge, J. M. C. *Biochem. J.* **1984**, *219*, 1–14.
- [80] Sies, H. *Angew. Chem.* **1986**, *98*, 1061–1075.
- [81] Steenken, S. *Chem. Rev.* **1989**, *89*, 503–520.
- [82] Pratviel, G.; Bernadou, J.; Meunier, B. *Angew. Chem.* **1995**, *107*, 819–845.
- [83] Jovanovic, S. V.; Simic, M. G. *J. Am. Chem. Soc.* **1986**, *108*, 5968–5972.
- [84] Hildenbrand, K.; Behrens, G.; Schulte-Frohlinde, D.; Herak, J. N. *J. Chem. Soc., Perkin Trans. 2* **1989**, pages 283–289.
- [85] Paillous, N.; Vicendo, P. *J. Photochem. Photobiol. B: Bio* **1993**, *20*, 203–209.
- [86] Dekant, W.; Vamvakas, S. *Toxikologie für Chemiker und Biologen*; Spektrum Akademischer Verlag: Heidelberg, 1994.
- [87] von Sonntag, C.; Schuchmann, H.-P. *Angew. Chem.* **1991**, *103*, 1255–1279.
- [88] Marchaj, A.; Kelley, D. G.; Bakac, A.; Espenson, J. H. *J. Phys. Chem.* **1991**, *95*, 4440–4441.
- [89] von Sonntag, C. *The Chemical basis of Radiation Biology*; Taylor and Francis: Philadelphia, 1987.
- [90] von Sonntag, C.; Schuchmann, H.-P. *J. Phys. Chem.* **1979**, *83*, 780–784.
- [91] Boivin, J.; Crépon, E.; Zard, S. Z. *Tetrahedron Lett.* **1990**, *31*, 6869–6872.

- [92] Aveline, B. M.; Kochevar, I. E.; Redmond, R. W. *J. Am. Chem. Soc.* **1995**, *117*, 9699–9708.
- [93] Aveline, B. M.; Kochevar, I. E.; Redmond, R. W. *J. Am. Chem. Soc.* **1996**, *118*, 10113–10123.
- [94] Schellman, J. A. *Chem. Rev.* **1975**, *75*, 323–331.
- [95] Horspool, W.; Armesto, D. *Organic Photochemistry: a Comprehensive Treatment*; Ellis Horwood Limited: Chichester, West Sussex, 1992.
- [96] Turro, N. J. *Modern Molecular Photochemistry*; University Science Books: Sausalito, 1991.
- [97] Berova, N.; Nakanishi, K.; Woody, R. W. *Circular Dichroism, Principles and Applications*; Wiley-VCH: Weinheim, 2000.
- [98] Helgaker, T.; Jørgensen, P. J.; Olsen, J. *Molecular Electronic-Structure Theory*; John Wiley & Sons Ltd.: Chichester, England, 2000.
- [99] Engels, B.; Hanrath, M. *DIESEL-MRCI 1997*, University of Bonn, Germany.
- [100] Azizi, Z.; Roos, B. O.; Veryazov, V. *Phys. Chem. Chem. Phys.* **2006**, *8*, 2727–2732.
- [101] Jensen, F. *Introduction to Computational Chemistry*; John Wiley & Sons Ltd.: Chichester, England, 1999.
- [102] Del Bene, J. E.; Ditchfield, R.; Pople, J. A. *J. Chem. Phys.* **1971**, *55*, 2236–2241.
- [103] Comeau, D. C.; Bartlett, R. J. *Chem. Phys. Lett.* **1993**, *207*, 414–423.
- [104] Koch, W.; Holthausen, M. C. *A Chemist's Guide to Density Functional Theory*; Wiley-VCH: Weinheim, 2000.
- [105] Gross, E. K. U.; Kohn, W. *Phys. Rev. Lett.* **1985**, *55*, 2850–2852.
- [106] Petersilka, M.; Gossmann, U. J.; Gross, E. K. U. *Phys. Rev. Lett.* **1996**, *76*, 1212–1215.
- [107] Appel, H.; Gross, E. K. U.; Burke, K. *Phys. Rev. Lett.* **2003**, *90*, 043005.
- [108] Petersilka, M.; Gross, E. K. U.; Burke, K. *Int. J. Quant. Chem.* **2000**, *80*, 534–554.
- [109] Grimme, S.; Parac, M. *ChemPhysChem.* **2003**, *3*, 292–295.
- [110] Dreuw, A.; Weisman, J. A.; Head-Gordon, M. *J. Chem. Phys.* **2003**, *119*, 2943–2946.
- [111] Dreuw, A.; Head-Gordon, M. *J. Am. Chem. Soc.* **2004**, *126*, 4007–4016.

- [112] Grimme, S.; Parac, M. *Chem. Phys.* **1975**, *75*, 323–331.
- [113] Cai, Z.-L.; Sendt, K.; Reimers, J. R. *J. Chem. Phys.* **2002**, *117*, 5543–5549.
- [114] Casida, M. E.; Salahub, D. R. *J. Chem. Phys.* **2000**, *113*, 8918–8935.
- [115] Vosko, S. J.; Wilk, L.; Nusair, M. *Can. J. Phys.* **1980**, *58*, 1200–1211.
- [116] Burke, K.; Perdew, J.; Ernzerhof, M. *Int. J. Quant. Chem.* **1997**, *61*, 287.
- [117] Koopmans, T. *Physica* **1934**, *1*, 104–113.
- [118] Becke, A. D. *J. Chem. Phys.* **1993**, *98*, 5648–5652.
- [119] Lee, C.; Yang, W.; Parr, R. G. *Phys. Rev. B* **1988**, *37*, 785–789.
- [120] Perdew, J. P.; Ernzerhof, M.; Burke, K. *J. Chem. Phys.* **1996**, *105*, 9982–9985.
- [121] Perdew, J. P.; Burke, K.; Ernzerhof, M. *Phys. Rev. Lett.* **1996**, *77*, 3865–3868.
- [122] Vahtras, O.; Almlöf, J.; Feyereisen, W. *Chem. Phys. Lett.* **1993**, *213*, 514–518.
- [123] Eichkorn, K.; Treutler, O.; Öhm, H.; Häser, M.; Ahlrichs, R. *Chem. Phys. Lett.* **1995**, *242*, 652–660.
- [124] Bauernschmitt, R.; Häslers, M.; Treutler, O.; Ahlrichs, R. *Chem. Phys. Lett.* **1997**, *264*, 573–578.
- [125] TURBOMOLE.; Ahlrichs, R.; Bär, M.; Baron, H.-P.; Bauernschmitt, R.; Böcker, S.; Ehrig, M.; Eichkorn, K.; Elliott, S.; Haase, F.; Häser, M.; Horn, H.; Huber, C.; Huniar, U.; Kattannek, M.; Kölmel, C.; Kollwitz, M.; Ochsenfeld, C.; Öhm, H.; Schäfer, A.; Schneider, U.; Treutler, O.; von Arnim, M.; Weigend, F.; Weis, P.; Weiss, H. **since 1988**, *Quant. Chem. Group, University of Karlsruhe, Germany*.
- [126] Gaussian 03 (Revision A.1).; Frisch, M. J.; Trucks, G. W.; Schlegel, H. B.; Scuseria, G. E.; Robb, M. A.; Cheeseman, J. R.; Montgomery, J. A.; Jr.; Vreven, T.; Kudin, K. N.; Burant, J. C.; Millam, J. M.; Iyengar, S. S.; Tomasi, J.; Barone, V.; Mennucci, B.; Cossi, M.; Scalmani, G.; Rega, N.; Petersson, G. A.; Nakatsuji, H.; Hada, M.; Ehara, M.; Toyota, K.; Fukuda, R.; Hasegawa, J.; Ishida, M.; Nakajima, T.; Honda, Y.; Kitao, O.; Nakai, H.; Klene, M.; Li, X.; Knox, J. E.; Hratchian, H. P.; Cross, J. B.; Adamo, C.; Jaramillo, J.; Gomperts, R.; Stratmann, R. E.; Yazyev, O.; Austin, A. J.; Cammi, R.; Pomelli, C.; Ochterski, J. W.; Ayala, P. Y.; Morokuma, K.; Voth, G. A.; Salvador, P.; Dannenberg, J. J.; Zakrzewski, V. G.; Dapprich, S.; Daniels, A. D.; Strain, M. C.; Farkas, O.; Malick, D. K.; Rabuck, A. D.; Raghavachari, K.; Foresman, J. B.; Ortiz, J. V.; Cui, Q.; Baboul, A. G.; Clifford, S.; Cioslowski, J.;

- Stefanov, B. B.; Liu, G.; Liashenko, A.; Piskorz, P.; Komaromi, I.; Martin, R. L.; Fox, D. J.; Keith, T.; Al-Laham, M. A.; Peng, C. Y.; Nanayakkara, A.; Challacombe, M.; Gill, P. M. W.; Johnson, B.; Chen, W.; Wong, M. W.; Gonzalez, C.; Pople, J. A. **2003**, *Gaussian, Inc.*, Pittsburgh, PA.
- [127] Becke, A. D. *Phys. Rev. A* **1988**, *38*, 3098–3100.
- [128] Perdew, J. P.; Chevary, J. A.; Volskoo, S. H.; Jackson, K. A.; Pederson, M. R.; Singh, D. J.; Fiolhais, C. *Phys. Rev. B* **1992**, *46*, 6671–6687.
- [129] MOLCAS Version 5.; Andersson, K.; Barysz, M.; Bernhardsson, A.; Blomberg, M. R. A.; Cooper, D. L.; Fleig, T.; Fülcher, C. M.; de Graaf, C.; Hess, B. A.; Karlström, G.; Lindh, R.; Malmqvist, P.-Å.; Neogrady, P.; Olsen, J.; Roos, B. O.; Sadley, A. J.; Schütz, M.; Schimmelpfennig, B.; Seijo, L.; Serrano-andrés, L.; Siegbahn, P. E. M.; Stålring, J.; Thorsteinsson, T.; Veryazov, V.; Widmark, P.-O. **2000**, *Lund University*, Sweden.
- [130] Levy, B.; Berthier, G. *Int. J. Quant. Chem.* **1968**, *2*, 307–319.
- [131] Malmqvist, P.-A.; Roos, B. O. *Chem. Phys. Lett.* **1989**, *155*, 189–194.
- [132] Hartung, J.; Gallou, F. J. *Org. Chem.* **1995**, *60*, 6706–6716.
- [133] Hartung, J.; Gottwald, T.; Špehar, K. *Synlett* **2003**, pages 227–229.
- [134] Maciejewski, A.; Steer, R. P. *Chem. Rev.* **1993**, *93*, 67–98.
- [135] Albini, A.; Alpegiani, M. *Chem. Rev.* **1984**, *84*, 43–71.
- [136] Tatchen, J.; Waletzke, M.; Marian, C.; Grimme, S. *Chem. Phys.* **2001**, *264*, 245–254.
- [137] Coyle, J. D. *Tetrahedron* **1985**, *41*, 5393–5425.
- [138] Moule, D. C.; Lim, E. C. *J. Phys. Chem. A* **2002**, *106*, 3072–3076.
- [139] Steer, R. P.; Ramamurthy, V. *Acc. Chem. Res.* **1988**, *21*, 380–386.
- [140] de Mayo, P. *Acc. Chem. Res.* **1976**, *9*, 52–59.
- [141] Turro, N. J.; Ramamurthy, V.; Cherry, W.; Farneth, W. *Chem. Rev.* **1978**, *78*, 125–145.
- [142] Petiau, M.; Fabian, J. *J. Mol. Struct (Theochem)* **2001**, *538*, 253–260.
- [143] Christiansen, O.; Koch, H.; Jørgensen, P.; Olsen, J. *Chem. Phys. Lett.* **1995**, *244*, 75–82.

- [144] Christiansen, O.; Koch, H.; Jørgensen, P.; Helgaker, T. *Chem. Phys. Lett.* **1996**, *263*, 530–539.
- [145] Fliegl, H.; Köhn, A.; Hätting, C.; Ahlrichs, R. *J. Am. Chem. Soc.* **2004**, *125*, 9821–9827.
- [146] Rappoport, D.; Furche, F. *J. Chem. Phys.* **2005**, *122*, 064105.
- [147] Schäfer, A.; Horn, H.; Ahlrichs, R. *J. Chem. Phys.* **1992**, *97*, 2571–2577.
- [148] Eichkorn, K.; Treutler, O.; Öhm, H.; Häser, M.; Ahlrichs, R. *Chem. Phys. Lett.* **1995**, *240*, 283–290.
- [149] Weigend, F.; Hätting, C.; Köhn, A. *J. Chem. Phys.* **2002**, *116*, 3175–3183.
- [150] Woon, D.; T.H. Dunning, J. *J. Chem. Phys.* **1993**, *98*, 1358–1371.
- [151] T.H. Dunning, J. *J. Chem. Phys.* **1989**, *90*, 1007–1023.
- [152] Andersson, K. *Theor. Chem. Acc.* **1995**, *91*, 31–46.
- [153] Schäfer, A.; Huber, C.; Ahlrichs, R. *J. Chem. Phys.* **1992**, *100*, 5829–5835.
- [154] Becke, A. *J. Chem. Phys.* **1992**, *98*, 1372–1377.
- [155] G.Schaftenaar.; Noordik, J. *J. Comput.-Aided Mol. Design* **2000**, *14*, 123–134.
- [156] Aveline, B. M.; Kochevar, I. E.; Redmond, R. W. *J. Am. Chem. Soc.* **1996**, *118*, 10124–10133.
- [157] F.Furche.; Ahlrichs, R. *J. Chem. Phys.* **2002**, *117*, 7433–7447.
- [158] Schinke, R. *Photodissociation Dynamics*; Cambridge University Press, 1993.
- [159] Ellen, C. G.; Crim, F. F. *Ann. Rev. Phys. Chem.* **2006**, *57*, 273–302.
- [160] Williams, J. M.; Hall, W. H. *J. Chem. Phys.* **1968**, *49*, 4467–4477.
- [161] Kasha, M. *Disc. Faraday Soc.* **1950**, *9*, 14–19.
- [162] Adam, W.; Marquardt, S.; Kemmer, D.; Saha-Möller, C. R.; Schreier, P. *Photochem. Photobiol. Sci.* **2002**, *1*, 609–612.
- [163] Adam, W.; Marquardt, S.; Kemmer, D.; Saha-Möller, C. R.; Schreier, P. *Org. Lett* **2002**, *4*(2), 225–228.
- [164] Farnworth, E. R.; King, G. W.; Moule, D. C. *Chem. Phys.* **1973**, *1*, 82–88.

Lebenslauf

Persönliches

Name	Mario Roberto Arnone
Geburtsdatum	05.01.1975
Geburtsort	Schrozberg
Adresse	Wenzelstraße 10 97084 Würzburg

Schulausbildung

1980 – 1984	Grundschule an der GHRS Schrozberg
1984 – 1991	Realschule an der GHRS Schrozberg
1991	Abschluss Mittlere Reife
1991 – 1994	Ernährungswissenschaftliches Gymnasium am Haus- und Landwirtschaftlichen Berufschulzentrum, Schwäbisch Hall
1994	Abschluss: allgemeinen Hochschulreife (1,5)

Wehrdienst

August – Oktober 1994	Grundausbildung bei der Luftwaffe in Germersheim
November 1994 – Juli 1995	Flugabwehrraketenbediener bei der 1. Staffel der FlaRak-Gruppe 23 in Manching

Studium

November 1995 – August 2001	Chemiestudium an der bayrischen Julius-Maximilians-Universität in Würzburg
November 2000 – August 2001	Anfertigung der Diplomarbeit im AK Engels Thema: „Theoretische Studien zur Reaktivität von Alkoxyradikalvorläufern auf Thiohydroxamsäure-O-ester-Basis“
August 2001	Abschluss: Diplom-Chemiker Univ. (sehr gut)
Oktober 2001 – Juni 2007	Promotion im Arbeitskreis Engels Thema: „Theoretical Characterisation and Optimisation of Photochemical Alkoxy Radical Precursors“

Publikationen

- J. Hartung, K. Špehar, I. Svoboda, H. Fuess, M. Arnone, B. Engels
4- and 4,5-substituted N-Methoxythiazole-2(3H)-thiones - Preparation, UV/Vis Spectra, and Assignment of Electronic Transitions in Comparison to N-Methoxypyridine-2(1H)-thione using Time-Dependent Density Functional Theory Calculations.
Eur. J. Org. Chem. **2005**, 869–881.
- M. Arnone, J. Hartung, B. Engels
On the Homolytic Cleavage of the N,O Bond in N-(Methoxy)pyridine-2(1H)-thione and N-(Methoxy)thiazole-2(3H)-thione in Thermally and Photochemically Induced Reactions: A Theoretical Study. *J. Phys. Chem. A* **2005**, 109, 2943–2950.
- F. Diwischek, M. Arnone, B. Engels, U. Holzgrabe
Studies on the Stereochemistry of 1,2,6-trimethyl-4-piperidone.
Tetrahedron **2005**, 61, 6993–7001.
- M. Arnone, B. Engels
Computer-Aided Design of Promising Photochemical Alkoxy Radical Precursors.
J. Phys. Chem. A **2006**, 110, 12330–12337.
- M. Christl, M. Braun, H. Fischer, S. Groetsch, G. Müller, D. Leusser, S. Deuerlein, D. Stalke, M. Arnone, B. Engels
The Stereochemical Course of the Generation and Interception of a Six-Membered Cyclic Allene: 3 δ^2 -1H-Naphthalene (2,3-Didehydro-1,2-dihydronaphthalene).
Eur. J. Org. Chem. **2006**, 5045–5058.
- M. Arnone, B. Engels
Rational Design of substituted N-alkoxypyridine-2(1H)-thiones with increased stability against daylight.
J. Phys. Chem. A **2007**, 111, 3161–3165.

ERKLÄRUNG

Hiermit erkläre ich, Mario Arnone, geboren am 05.01.1975 in Schrozberg, eidesstattlich diese Arbeit mit dem Titel

“Theoretical Characterisation and Optimisation of
Photochemical Alkoxy Radical Precursors”

selbstständig verfasst und keine anderen als die angegebenen Quellen und Hilfsmittel benutzt zu haben.

Ich erkläre außerdem, dass diese Dissertation weder in gleicher oder in anderer Form bereits in einem anderen Prüfungsverfahren vorgelegen hat.

Ich habe früher, außer den mit dem Zulassungsgesuch urkundlich vorgelegten Graden, keine weiteren akademischen Grade erworben oder zu erwerben versucht.

Würzburg, 14. Juni 2007

.....

